

UNIVERSITY OF VALENCIA
FACULTY OF CHEMISTRY
DEPARTMENT OF ANALYTICAL CHEMISTRY



VNIVERSITAT D VALÈNCIA

 Facultat de Química



PhD Thesis

**(NANO)MATERIALS: SENSORS AND LIQUID
CHROMATOGRAPHY**

Thesis presented to obtain the PhD degree in Chemistry under the “Programa de Doctorado en Química con Mención de Excelencia (R.D. 99/2011)”

Ana Isabel Argente García

Supervisors:

Prof. Dr. Pilar Campíns Falcó

Prof. Dr. Yolanda Moliner Martínez

Valencia, June 2018

Departament de Química Analítica

Dña. Pilar Campins Falcó, Profesora Catedrática, y Dña. Yolanda Moliner Martínez, Profesora Ayudante Doctor, ambas del Departamento de Química Analítica de la Universidad de Valencia,

CERTIFICAN

Que la presente memoria, titulada “*(Nano)materials: sensors and liquid chromatography*”, constituye la Tesis Doctoral de Ana Isabel Argente García para optar al grado de Doctora en Química, y que ha sido realizada en los laboratorios del Departamento de Química Analítica de la Universidad de Valencia, bajo su dirección y supervisión.

Y para que así conste a los efectos oportunos, firman el presente certificado en Valencia, a 1 de Junio de 2018.

Fdo. Dra. Pilar Campins Falcó

Directora de Tesis

Fdo. Yolanda Moliner Martínez

Codirectora de Tesis

This thesis has been completed thanks to a PhD research grant (FPU13/5220) funded by the Ministry of Education, Culture and Sports of Spain (MECD) in the Analytical Chemistry Department of the University of Valencia. A research stay of three months in IMS Laboratoire of the University of Bordeaux (Talence, Bordeaux) was carried out supported by MECD.



VNIVERSITAT [Q*] DE VALÈNCIA Facultat de Química



université
de BORDEAUX

Sí no conozco una cosa, la investigaré.

(Louis Pasteur)

AGRADECIMIENTOS

Tras estos años de trabajo, el esfuerzo ha tenido recompensa dando como resultado esta Tesis.

En este camino recorrido me han acompañado personas a las que quiero agradecer el tiempo que me han dedicado.

GRACIAS a Pilar por haberme ofrecido la oportunidad de trabajar en este grupo y dedicar tu tiempo en enseñarme todos tus conocimientos. De ti he aprendido que con esfuerzo y dedicación se pueden alcanzar los objetivos que te propongas.

GRACIAS a Yolanda por haberme enseñado tanto a nivel profesional como personal. Me gustaría darte las gracias por tu comprensión, ánimos y valiosos consejos dados con la serenidad y el cariño que te caracterizan. Sabes que te admiro como científica, pero sobre todo como persona. Gracias por no dejarme caer cuando tropezaba con las piedras de este camino, gracias por estar siempre ahí.

GRACIAS a Carmen, Rosa y Jorge, por haberme ofrecido vuestra ayuda en cada momento que la he necesitado. Gracias por hacer fácil este trabajo, ha sido un placer compartir estos años con vosotros.

Los 5 habéis conseguido crear un grupo puntero de investigación en el que predomina algo tan importante como una buena atmósfera de trabajo.

GRACIAS a Hélene Débeda y todos los componentes del grupo de investigación PRIMS por permitirme realizar mi estancia doctoral en el Laboratorio IMS de la Universidad de Burdeos y hacerme sentir tan cómoda.

GRACIAS también a Marcela, compañera de piso y amiga. Quiero darte las gracias por hacerme sentir como en casa cuando estaba lejos de mi familia. Me ha encantado conocerte, siempre serás mi mon amour.

GRACIAS a todos mis compañeros doctorandos del grupo MINTOTA (Lusine, Sara, Lorenzo, Rodrigo, Xavi, Neus, Henry, María y Pasu) por todas las experiencias compartidas. Ha sido una experiencia muy enriquecedora haber podido aprender de cada uno de vosotros. Quiero dar un especial agradecimiento a mis "chaticos". GRACIAS María y Pascu, por ofrecerme vuestra amistad, por haber aguantado mis indignaciones con bailes de conga, por criticar mis modelitos, por nuestras pruebas de sonido y mil historietas más. Gracias por acompañarme y ayudarme tanto dentro como fuera del laboratorio, pero sobre todo por compartir tantas

risas y lágrimas. No puedo describir con palabras lo agradecida que os estoy. “Espero que nunca se corte la cordeta”. María, gracias por ser mi guía y amiga. Me encanta nuestra loca complicidad. Siempre estaré muy agradecida por tu ayuda y tiempo que me ha permitido llegar al final del camino.

También me gustaría extender los agradecimientos a los miembros del Departamento de Química Analítica y en especial a los compañeros de doctorado por las comidas, cenas y congresos compartidos.

GRACIAS a Amparo, Eli, Omar y Duarte por haberos encontrado en el camino. Espero que el tiempo potencie nuestra amistad.

GRACIAS a Miguel, Oreto, Belinda y Jesús, por haber sido mis compañeros de carrera y poder agradecerlos ahora vuestra amistad.

Gracias a Alejandro por todas las experiencias compartidas con el cariño que te caracteriza. A M^a Carmen y Lorena por haber sido mi segunda familia todos estos años. Gracias por haberme cuidado tan bien.

Gracias a Rodrigo por haber sido y seguir siendo mi mejor amigo. Gracias por hacerme reír en cada una de nuestras quedadas. Estés donde estés yo seguiré a tu lado ofreciéndote el mismo cariño. Gracias por todos estos años.

Gracias a Pep por enseñarme tu capacidad de disfrutar del presente, recordarme a estar agradecida, amenizar este período con tus chistes, bailes y conversaciones patunas, pero sobretodo por pagar el plus. Por esto y más, gracias.

GRACIAS a mis padres, Alpidia y Heliodoro, por su apoyo incondicional. Gracias por los valores que me habéis inculcado, por protegerme y cuidarme. Me siento muy orgullosa y afortunada de tener unos padres como vosotros, os quiero. GRACIAS a mi hermano, Soraya y Jannis por vuestra admiración en todo lo que hago y ofrecerme vuestra ayuda siempre que la necesito.

GRACIAS A TODOS LOS QUE ME HABÉIS ACOMPAÑADO EN ESTE CAMINO.

RESUMEN

RESUMEN

El progreso de la Química Analítica está gobernado por la implantación de nuevas tecnologías así como el desarrollo de nuevos (nano)materiales y los cambios sociales. Gracias al avance tecnológico, los métodos clásicos están siendo reemplazados por nuevas herramientas e instrumentación que reducen el tiempo de análisis y mejoran las figuras de mérito de los procedimientos analíticos. En este contexto, el avance informático está permitiendo llevar a cabo una automatización, miniaturización y simplificación tanto en los sistemas de análisis como en el tratamiento de datos.

La irrupción de nuevos (nano)materiales es otro punto importante a tener en cuenta en la evolución de la Química Analítica. De hecho, el estudio de (nano)materiales para mejorar las técnicas existentes y/o desarrollar nuevas técnicas es un área de investigación en pleno crecimiento. Por ello, el principal objetivo de esta Tesis ha sido la investigación de (nano)materiales para su aplicación a técnicas de detección, extracción y separación. La meta que pretende alcanzar la Química Analítica Verde es el desarrollo de metodologías analíticas sostenibles que garanticen el mantenimiento del medio ambiente para las generaciones futuras. Así, las estrategias analíticas empleadas en esta Tesis han tenido presente para su desarrollo los principios de sostenibilidad.

A pesar del progreso en instrumentación analítica, la preparación de la muestra sigue siendo una etapa crítica del proceso analítico. Para conseguir una respuesta analítica adecuada se requieren diferentes operaciones de extracción, concentración, purificación y/o transformación del compuesto de interés. Dentro de la etapa de preparación de muestra, las técnicas de extracción juegan un papel importante. El analito es transferido desde la matriz hacia la fase extractante con la que interacciona, por lo que la elección del material que actúa como extractante es uno de los parámetros clave. La investigación de nuevos materiales y estrategias de extracción para mejorar la selectividad y eficiencias de extracción es un campo de investigación emergente hoy en día. La extracción de los analitos puede llevarse a cabo a través de la extracción en fase líquida (*LPE, Liquid Phase Extraction*) o en fase sólida (*SPE, Solid Phase Extraction*). Estas técnicas permiten además preconcentrar y aislar los analitos de otros componentes antes de aplicar una técnica de detección. La SPE es más utilizada que la LPE debido al menor consumo de disolvente que requiere. Esta técnica es ampliamente utilizada en la

preparación de muestras biológicas, farmacéuticas, medioambientales y alimentarias. La SPE no sólo se puede llevar a cabo con matrices líquidas sino también sólidas, como es el caso de la dispersión de la matriz en fase sólida (*MSPD, Matrix Solid Phase Dispersion*). Así, el proceso analítico es considerablemente simplificado, reduciendo el consumo de muestra y disolventes, además de no requerir instrumentación de elevado coste. Debido a las ventajas de la MSPD, es una técnica empleada en diversos campos como el medioambiental, toxicológico y alimentario. La selectividad y eficiencia de esta técnica depende principalmente del material extractante y del disolvente empleado. En cuanto a los materiales, el C₁₈ y C₈ son los más utilizados para la retención de analitos lipofílicos, como es el caso de esta Tesis.

Teniendo en cuenta los principios de la Química Analítica Verde, las técnicas convencionales (SPE y LPE) se han ido sustituyendo por técnicas miniaturizadas y automatizadas que permiten reducir el consumo de disolventes/reactivos y la generación de residuos, además de mejorar la selectividad y preconcentración en un menor tiempo de análisis. En este sentido, la microextracción en fase sólida (*SPME, Solid Phase MicroExtraction*), introducida por Arthur y Pawliszyn en 1990, se propuso como alternativa miniaturizada a la SPE. Inicialmente, la SPME se desarrolló mediante una fibra recubierta en su superficie externa con una fase extractante polimérica. Esta técnica presentaba ventajas como la reducción de disolventes y el tiempo de extracción. Sin embargo, presentaba limitaciones como la fragilidad de la fibra, baja capacidad de extracción, sangrado del recubrimiento de la fibra y dificultad de acoplamiento a cromatografía líquida (*LC, Liquid Chromatography*). Para superar estas limitaciones, se propuso como alternativa la microextracción en fase sólida en tubo (*IT-SPME, In-tube Solid Phase MicroExtraction*). En 1997, Eisert y Pawliszyn desarrollaron la primera IT-SPME acoplada en línea con cromatografía líquida de alta resolución (*HPLC, High Performance Liquid Chromatography*). La IT-SPME se basa en el uso de un capilar de sílica fundida empacado o recubierto en su superficie interna con una fase extractante. Cuando la muestra circula a través del capilar, los analitos son extraídos y concentrados mediante interacción con el recubrimiento interno del capilar. Después, los analitos son desorbidos mediante un disolvente apropiado, el cual puede ser recogido para su posterior procesamiento (desorción estática) o puede ser transferido hacia el sistema analítico mediante un flujo de disolvente (desorción dinámica). Aunque la IT-SPME se ha utilizado generalmente en combinación con cromatografía de gases (*GC, Gas Chromatography*),

recientemente es más utilizada con la LC. La IT-SPME se ha desarrollado principalmente desarrollada con el objetivo de extender la SPE hacia el camino de la automatización y acomplamiento en línea con un sistema cromatográfico. De este modo se llevan a cabo la limpieza, preconcentración, separación y detección de los analitos en un único paso. Además, esta técnica miniaturizada puede ser considerada una técnica respetuosa con el medio ambiente gracias a la reducción de disolventes, residuos, energía y costes, mejorando parámetros analíticos como la sensibilidad, precisión y exactitud.

La IT-SPME es una técnica versátil que puede llevarse a cabo en diferentes tipos de configuración:

- (i) Modalidad de carga/expulsión: la columna capilar se inserta entre la aguja y el bucle de un inyector automático programable. A continuación, una fracción de la muestra es aspirada y expulsada repetidamente a través de la columna capilar hasta alcanzar el equilibrio. Finalmente, se desorben los analitos y se transfieren a la columna analítica mediante un disolvente (modo estático) o mediante el flujo de fase móvil (modo dinámico).
- (ii) Modalidad de circulación o IT-SPME en válvula: una columna capilar es empleada como bucle de inyección del sistema cromatográfico. Los analitos son retenidos en el capilar durante la carga de la muestra y después son transferidos a la columna analítica mediante el cambio de posición de la válvula a inyección.

Otra tendencia que suscita especial interés en la Química Analítica actual es el desarrollo de nuevos dispositivos para análisis in-situ. Los métodos que permiten un análisis in-situ en tiempo real incluyen potenciales ventajas como la miniaturización del tratamiento de muestra y la consiguiente reducción del tiempo y costes de análisis. Además, el riesgo de contaminación o degradación de la muestra durante el transporte al laboratorio es eliminado.

Algunos de los aspectos a tener en cuenta a la hora de elegir un método de análisis in-situ son la disponibilidad de recursos y personal cualificado. En ciertas ocasiones, los sistemas complejos que proporcionan un alto rendimiento analítico pueden ser inadecuados debido a la necesidad de personal especializado y equipos caros. Gracias a las posibilidades que ofrecen los sensores in-situ, son aplicados en un amplio rango de campos como el medioambiental, industrial,

médico, forense y seguridad. A pesar de que las publicaciones sobre métodos analíticos siguen siendo principalmente dedicadas a métodos cromatográficos, los sensores ópticos y electromecánicos que permiten realizar medidas in-situ están adquiriendo una mayor importancia.

Entre los diferentes tipos de sensores ópticos destacan los colorimétricos, ya que su cambio de color en presencia del analito puede detectarse fácilmente a simple vista. Estos sensores se basan en un cambio de color a través de una reacción química entre un cromóforo y el compuesto de interés. Los colores resultantes están relacionados con la concentración de analito. Por tanto, se puede llevar a cabo un análisis cualitativo mediante inspección visual y un análisis cuantitativo mediante medida de absorbancia por reflectancia difusa y/o valores del color de una fotografía.

En base a los progresos tecnológicos, el análisis de imagen mediante teléfonos móviles es una alternativa emergente para propósitos cuantitativos. Para ello, se toma una imagen digital mediante un dispositivo electrónico comercial, como puede ser un teléfono móvil o un escáner, y los colores de la imagen son convertidos en valores numéricos mediante programas de imágenes como Adobe®Photoshop, GNU Image Manipulation Program (GIMP) and ImageJ. En función del método que representa los colores, se encuentran diferentes modelos de color: rojo-verde-azul (*RGB, red-green-blue*), cian-magenta-amarillo-negro (CMYK, cyan-magenta-yellow-black), tonalidad de saturación (HSV, hue-saturation-value) y luminancia-color (CIELAB). El modo RGB es usado en muchos trabajos, por eso ha sido seleccionado en la presente Tesis. En este modo, los colores son creados por una mezcla de colores basada en rojo, verde y azul. Aunque los métodos basados en teléfonos móviles han abierto una poderosa alternativa a los equipos convencionales de medida, se deben tener en cuenta una serie de parámetros relacionados con la imagen. Uno de los parámetros más influyentes son las condiciones luminosas bajo las que se captura la fotografía. Con el objetivo de corregir las variaciones de luz, se han propuesto diferentes opciones como integrar el teléfono móvil en una caja oscura a medida, tomar áreas de referencia, incorporar una fuente de luz con los parámetros de la cámara fijos y usar un escáner para adquirir la fotografía.

En algunos ensayos colorimétricos, el cambio de color se lleva a cabo en disolución. Sin embargo, el cambio de color en otros ensayos se lleva a cabo mediante un soporte sólido donde los reactivos colorimétricos son inmovilizados.

Los dispositivos sólidos evitan problemas de manipulación y estabilidad de los reactivos derivatizantes en disolución. Algunos de los materiales propuestos como soportes sólidos para el diseño de sensores in-situ son los polímeros, papel y sílice. El papel despierta gran interés para el desarrollo de sensores debido a su bajo coste, versatilidad, abundancia, simplicidad y compatibilidad. Además, la amplia variedad de papeles disponibles en el mercado permite la elección de un papel óptimo para cada tipo de ensayo. Por otra parte, el polidimetilsiloxano (*PDMS, polydimethylsiloxane*) es el polímero más usado como soporte encapsulante de diferentes especies como por ejemplo, reactivos colorimétricos, quantum dots y nanopartículas (NPs).

Continuando con los sensores in-situ, los sensores electromecánicos, y particularmente los sistemas microelectromecánicos (*MEMS, microelectromechanical systems*), han recibido especial atención. Los MEMS son utilizados en campos tan diversos como la automoción, electrónica, diagnóstico clínico, comunicación y control medioambiental. Una de las estructuras más destacadas dentro de los MEMS son las micropalanca en forma de T, donde una parte está unida a una base y la otra queda suspendida. Estos sistemas son ampliamente estudiados como sensores para la detección de gases debido a sus ventajas como sensibilidad, miniaturización y bajo precio. Debido a su pequeña escala, pequeños cambios físicos o mecánicos debido a la interacción del analito es suficiente para ser detectado, por lo que son altamente sensibles.

Para poder utilizar las micropalanca como sensores, deben ser funcionalizadas en su superficie superior mediante una capa de material que tenga afinidad por el analito. La interacción de los compuestos de interés con la puede ser física o química. Estas micropalanca pueden trabajar en dos modos diferentes. En modo estático, la interacción de los analitos con la capa sensible genera una tensión superficial, resultando en una desviación de la micropalanca. En modo dinámico, la micropalanca entra en resonancia y la interacción de los analitos con la capa sensible causa un desplazamiento de esa frecuencia de resonancia asociada al cambio de masa. El modo estático se puede llevar a cabo en diferentes medios, comúnmente en líquidos. Sin embargo, el modo dinámico se usa en medio gas debido a que en medio líquido surgen amortiguaciones de las oscilaciones debido a la alta viscosidad del medio. Las micropalanca que trabajan en modo dinámico se utilizan como sensores gravimétricos sensibles y rápidos.

Se requiere un sistema de lectura para monitorizar la flexión o los cambios en la frecuencia de resonancia de la micropalanca. Los sensores electromecánicos pueden clasificarse en los siguientes tipos en función del principio de detección: capacitivo, óptico, piezorresistivo y piezoeléctrico. Para el modo dinámico, las micropalancas piezoeléctricas son las más adecuadas por ventajas como rápida respuesta, alta sensibilidad a escala miniaturizada y bajo coste. Estos sensores consisten en una capa piezoeléctrica entre dos electrodos de oro. Las formulaciones de $\text{PbZr}_x\text{Ti}_{1-x}\text{O}_3$ son el material más ampliamente utilizado para sensores piezoeléctricos. Este material exhibe propiedades piezoeléctricas después de su polarización ya que se produce el alineamiento de sus dominios conduciendo a una polarización remanente.

Existen dos efectos piezoeléctricos. El efecto piezoeléctrico directo consiste en la generación de un campo eléctrico cuando se aplica una tensión mecánica, mientras que el efecto piezoeléctrico inverso sucede cuando el material sujeto a un campo eléctrico causa una tensión mecánica. En el caso de las micropalancas piezoeléctricas resonantes, experimentan un efecto piezoeléctrico inverso mediante la aplicación de un campo eléctrico para alcanzar la resonancia, pero la detección se lleva a cabo mediante cambios de frecuencia debido a la interacción del analito a través del efecto directo. Entre las diferentes técnicas para la fabricación de estos sensores, la técnica de impresión serigráfica junto con el método de la capa de sacrificio permite la fabricación de MEMS piezoeléctricos a bajo coste, obteniendo una buena reproducibilidad y resolución.

De acuerdo con lo comentado, se observan dos tendencias en la Química Analítica durante los últimos años que se basan en la necesidad de simplificar las metodologías analíticas. Por una parte, existe una tendencia hacia la automatización del tratamiento de la muestra con el objetivo de reducir la manipulación de la muestra y por tanto el tiempo de análisis. En relación con esto, también se buscan técnicas miniaturizadas que permitan disminuir el consumo de disolventes y la generación de residuos, además de mejorar parámetros como la sensibilidad. Por otra parte, hay un creciente interés en el desarrollo de sensores para el análisis in-situ, muchos de ellos basados en el análisis de imagen digital. Algunos de los beneficios que ofrecen estos sensores son la simplicidad, rapidez y análisis en tiempo real, sin necesidad de personal altamente cualificado.

Ambas tendencias están asociadas a la necesidad de desarrollar metodologías sostenibles, como destaca la Química Analítica Verde. El desarrollo de estas metodologías que se enmarcan dentro de las tendencias actuales de la Química Analítica se rige por el uso de nuevos (nano)materiales. Por eso, el principal objetivo de esta Tesis ha sido el estudio de (nano)materiales para mejorar metodologías analíticas existentes, así como también desarrollar nuevas metodologías analíticas con alto rendimiento en términos de operación y sostenibilidad. Concretamente, esta tesis se ha focalizado en el estudio de (nano)materiales para su aplicación en técnicas de extracción, separación y detección para llevar a cabo la estimación de diferentes compuestos en campos tan diversos como el forense, medioambiente, industria y medicina. Los materiales investigados se han clasificado en tres grupos: basados en sílica, basados en carbono y basados en metal.

Los objetivos específicos de esta Tesis se han organizado en función de las aplicaciones analíticas de los materiales estudiados:

1. Desarrollo de metodologías analíticas basadas en IT-SPME acoplada en línea con cromatografía líquida miniaturizada, como es la cromatografía líquida capilar (*CapLC, capillary liquid chromatography*), consiguiendo así automatizar y miniaturizar el proceso. Para abordar este objetivo, el polímero PDMS, un material basado en sílica, se ha evaluado como fase extractante de IT-SPME para su aplicación en la determinación de compuestos de interés medioambiental, industrial y forense en diferentes tipos de matrices: (i) Di(2-etilhexil)ftalato (*DEHP, Di(2-ethylhexyl)phthalate*) en sedimentos y agua, (ii) Cloruro de benzalconio (*BAK, benzalkonium chloride*) en formulaciones industriales y (iii) Difenilamina (*DPA, diphenylamine*) en manos de un tirador. En el mismo contexto, se han evaluado los nanotubos de carbono (*CNTs, carbon nanotubes*), que son uno de los materiales basados en carbono más populares, para la funcionalización de capilares basados en PDMS y así mejorar las eficiencias de extracción en el análisis de drogas de tipo anfetamínicas en fluido oral.
2. Desarrollo de una herramienta analítica basada en la MSPD empleando el material basado en sílica C_{18} para la dispersión, preconcentración y derivatización de anfetaminas en matriz de pelo. Esta técnica también ha sido utilizada en el tratamiento de sedimentos para la extracción de DEHP. En el mismo contexto de preparación de muestra, se ha evaluado un nuevo *metal-*

organic framework (MOF) de Cu (II) 3D tripeptídico (Gly-L-His-Gly) como fase quiral en SPE para la separación enantioselectiva de metanfetamina y efedrina.

3. Diseño de sensores colorimétricos basados en el encapsulamiento de cromóforos dentro de PDMS como soporte sólido para llevar a cabo el análisis in-situ de compuestos de interés en la industria (estimación de caseína en efluentes de la industria láctea y control del biocida N-(3-aminopropil)-N-dodecil-1,3- propandiamina, ADP, en formulaciones industriales de detergentes) y control policial (estimación de anfetamina y ketamina en muestras ilegales de droga). También se ha desarrollado otro tipo de sensor colorimétrico basado en la inmovilización de nanopartículas de plata (AgNPs) en una membrana de nailon. Este nanomaterial metálico se ha estudiado para diseñar un kit clínico con el que poder detectar compuestos sulfúricos volátiles en el aliento, los cuales son responsables de la halitosis que puede estar relacionada con enfermedades como la periodontitis o gingivitis. Diferentes parámetros que afectan a la respuesta analítica han sido estudiados. Además, se ha investigado el análisis mediante imagen digital para simplificar y abaratar el análisis.

Las técnicas empleadas a lo largo de esta tesis pueden clasificarse en tres grupos: espectroscópicas, cromatográficas y microscópicas.

Las metodologías llevadas a cabo para desarrollar los tratamientos de muestra fuera de línea como la SPE y la MSPD se detallan a continuación. Para la separación enantiomérica de metanfetamina y efedrina con el MOF peptídico, se rellena un cartucho de SPE con Cu(GHG) y se hace pasar a través una mezcla racémica. Para su identificación quiral, se lleva a cabo su derivatización y procesado en el sistema cromatográfico.

Para la MSPD, un cartucho de SPE se rellena con la muestra de pelo mezclada con la fase extractante C_{18} y seguidamente los analitos son derivatizados y desorbidos con el reactivo de derivatización para su posterior procesado en el sistema cromatográfico.

En cuanto al tratamiento de muestra en línea llevado a cabo en esta Tesis, IT-SPME en válvula, consiste en sustituir el bucle de acero inoxidable de la válvula de inyección por un segmento de columna capilar de GC, generalmente basado en PDMS. La muestra o disolución de trabajo se procesa manualmente mediante la

válvula en posición de carga quedando los analitos adsorbidos. Seguidamente son desorbidos y transferidos a la columna analítica mediante la fase móvil al cambiar la válvula a posición de inyección.

La fabricación de los sensores poliméricos ha consistido en encapsular los reactivos colorimétricos (NQS o $\text{Co}(\text{SCN})_2$) en una matriz basada en PDMS. Para ello, el agente gelificante se adiciona en una proporción 1:10 respecto de la base polimérica. En el caso de los sensores de NQS, también se adicionan tetraetilortosilicato (TEOS) y nanopartículas de sílice (SiO_2NPs). Después de homogeneizar la dispersión, la mezcla se vierte en moldes y se deja gelificar en la estufa a 30 °C. Estos sensores se ponen en contacto con la muestra basificada (calentada para el caso sólo de la caseína) y tras 10 min de reacción, los sensores que han cambiado de color son extraídos para medir la señal analítica.

Para la fabricación del sensor basado en AgNPs, se sitúa una membrana de nailon en un portafiltros acoplado a una jeringa y se hace pasar una dispersión de AgNPs (20 nm) de modo que queden atrapadas. Este sensor se cuelga en una botella de dilución estática donde se ha adicionado ácido fosfórico. Una vez cerrada la botella, se adiciona la disolución de Trabajo para generar H_2S y se deja bajo agitación durante 10 min. A continuación, el sensor se extrae de la botella y se procede a la medida de la señal analítica.

El análisis cuantitativo de estos sensores coloreados se lleva a cabo mediante medida de absorbancia por reflectancia difusa y/o medida del valor rojo, verde y azul a través de una imagen digital obtenida mediante dispositivos de captura de imágenes como un teléfono móvil.

Para la fabricación de los MEMS, concretamente micropalancas y discos piezoeléctricos, se emplea la técnica de impresión serigráfica en combinación con el método de la capa de sacrificio. En primer lugar se fabrica el material piezoeléctrico con composición 97 % en peso de $\text{PbZr}_{0.52}\text{Ti}_{0.48}\text{O}_3$ y 3 % de LBCu (≈ 25 wt % Li_2CO_3 , 40 wt % Bi_2O_3 , 35 wt % CuO) para ayudar a la sinterización. Esta mezcla tras ser homogeneizada con etanol en un mezclador en espiral se deja secar, se mezcla con un aglutinante comercial en un 14 % en peso y finalmente se lleva a un molino de tres rodillos para que adquiera las propiedades reológicas requeridas. A continuación se lleva a cabo la impresión de los sensores por deposición sucesiva de cada capa. Una vez impresos, cada capa se deja secar en la estufa para eliminar los disolventes. Posteriormente, los sensores se prensan

isostáticamente para mejorar la densificación y después se sinterizan en un horno que llega a los 900 °C donde se elimina la capa de sacrificio. Finalmente los sensores son polarizados y funcionalizados mediante deposición de una dispersión acuosa de sílica mesoporosa. Para evaluar el potencial como sensor de gases, la micropalanca se introduce en una cámara conectada a un analizador de impedancia que lleva a cabo la lectura en tiempo real. Los vapores del analito se generan y controlan gracias a un generador de vapor. El principio de funcionamiento consiste en inducir una vibración a la micropalanca hasta alcanzar el estado de resonancia. Debido a que la frecuencia de resonancia es sensible a la masa, se produce un desplazamiento de la frecuencia (vibración 31-longitudinal) asociado al cambio de masa cuando el analito se adhiere permitiendo así su detección.

En conclusión, las aplicaciones de los (nano)materiales estudiados en esta tesis se han centrado en dos de las actuales tendencias de la Química Analítica:

- (i) Técnicas de tratamiento de muestra y de separación miniaturizadas
- (ii) Sensores para análisis in-situ

Uno de los puntos más importantes de las técnicas para el tratamiento de muestra es el uso de un adecuado material extractante. En esta Tesis, el C₁₈ ha sido evaluado como fase en MSPD para la disrupción, limpieza y derivatización de anfetaminas en pelo. Este método ha permitido una estimación sencilla y rápida de anfetamina, metanfetamina, efedrina y metilendioximetanfetamina en pelo, con límite de detección (*LOD, limit of detection*) de 0.25–0.75 ng mg⁻¹. La MSPD se considera una alternativa a los métodos clásicos que consisten en múltiples pasos, ya que el proceso analítico se simplifica y el consumo de muestra y disolvente se reduce. Por otra parte, el MOF peptídico Cu(GHG) ha sido estudiado como material quiral en SPE para la separación enantioselectiva de metanfetamina y efedrina. Dicho MOF ha sido capaz de separar >50 % de (+)-Efedrina de una mezcla racémica. Este es un resultado prometedor teniendo en cuenta la limitada disponibilidad de cartuchos de SPE para separaciones quirales que hay en el mercado.

En base a los principios de la Química Analítica Verde, se ha utilizado una técnica de fácil miniaturización y automatización como es la IT-SPME en válvula, donde el PDMS ha jugado un papel importante como fase extractante. En esta

Tesis se ha propuesto la combinación de IT-SPME-CapLC con detector de fila de diodos y fluorescencia para estimar DEHP, BAK y DPA.

La determinación de DEHP en sedimentos y agua mediante la combinación de MSPD usando C_{18} y IT-SPME-CapLC usando un capilar basado en PDMS₉₅ se ha llevado a cabo satisfactoriamente en menos de 20 min. Los LODs obtenidos han sido adecuados para control de calidad medioambiental ($90\text{-}270\ \mu\text{g kg}^{-1}$). Además la reducción del consumo de muestra y disolventes, así como también de los pasos de extracción evitan el riesgo de contaminación.

Se ha demostrado la versatilidad de IT-SPME-CapLC con capilares basados en PDMS₆₅ para el análisis de homólogos de BAK en mezclas de biocidas. El método propuesto ha mostrado que se requiere la evaluación del efecto matriz para analizar BAK en mezclas de biocidas. Diferentes efectos han sido observados en función del tipo de co-biocida presente, relación co-biocida/BAK homólogo y de cantidad total de surfactante, posiblemente por la formación de mezcla de micelas. En todos los casos, la respuesta del homólogo C_{12} se ha visto más afectada que la del homólogo C_{14} . Por lo que el método propuesto se puede considerar una vía de bajo coste para controlar procesos industriales donde el BAK es un producto indeseado en una formulación.

También se ha llevado a cabo una satisfactoria estimación de DPA mediante IT-SPME-CapLC usando un capilar de PDMS₆₅. La utilidad del método propuesto ha sido probado para estimar DPA muestreada de las manos de tiradores mediante un hisopo de algodón y extracción mediante vórtex. El método propuesto permite obtener información de interés judicial en una investigación forense.

Con el objetivo de mejorar la capacidad de extracción de la IT-SPME, se han utilizado CNTs para funcionalizar capilares de PDMS. Gracias a la alta relación superficie-volumen de estos nanomateriales, se incrementa la eficiencia de extracción, lo que permite extender la IT-SPME a problemas analíticos donde el volumen de muestra está limitado como es el caso de la saliva. La presencia de CNTs mejora la eficiencia de extracción y los perfiles cromatográficos, resultando en una opción interesante para el análisis de anfetaminas en saliva. El método propuesto resulta muy simple y económico, además de proporcionar adecuada selectividad, precisión y sensibilidad a niveles de concentración de $\mu\text{g mL}^{-1}$ (LODs = $0.5\text{-}0.8\ \mu\text{g mL}^{-1}$).

Es importante destacar los satisfactorios parámetros analíticos y satisfactoria aplicación a muestras que se han obtenido mediante IT-SPME-CapLC en los trabajos descritos en esta Tesis. Estos resultados han demostrado la idoneidad del método IT-SPME-CapLC para detectar los analitos presentes en diferentes tipos de matrices.

El segundo enfoque de esta tesis ha sido el desarrollo de sensores colorimétricos que permiten un análisis in-situ.

Los sensores fabricados en se han basado por una parte en el encrustamiento de reactivos colorimétricos (NQS y $\text{Co}(\text{SCN})_2$) en una matriz de PDMS, y por otra parte, en la inmovilización de AgNPs en un soporte de nailon. En ambos casos, el analito interacciona con el cromóforo o las AgNPs del sensor cambiando así de color. El análisis semicuantitativo se lleva a cabo mediante inspección visual y el cuantitativo mediante la medida de absorbancia por reflectancia difusa o y/o medida de valores de color de una imagen digital. También se han estudiado micropalancas piezoeléctricas como sensores in-situ.

En esta Tesis, los sensores se han desarrollado para la determinación de caseína en aguas residuales de industrias lácteas, ADP en productos industriales, drogas de tipo anfetamínico y ketamina en drogas ilícitas en formato pastilla o polvo, así como también, la detección de compuestos sulfúricos volátiles en aliento.

Para la estimación de caseína se ha desarrollado un sensor de PDMS/TEOS/SiO₂NPs/NQS con satisfactorio LOD= 15 mg L⁻¹. El método propuesto supera una de las principales limitaciones del método convencional en disolución con ácido biocínico, la degradación del reactivo. Teniendo en cuenta las ventajas de rapidez, sencillez, portabilidad y estabilidad que presenta este sensor, se considera una potencial herramienta para su aplicación en el control in-situ de la cantidad de caseína en efluentes de industrias lácteas.

Para la estimación del biocida ADP en formulaciones industriales, se ha desarrollado un sensor basado en PDMS/TEOS/SiO₂NPs/NQS con satisfactorio LOD de 0.018 % en peso. Este sensor permite llevar cabo un análisis sostenible, económico y rápido para el control de ADP, lo que sugiere buenas perspectivas para su implantación a nivel industrial.

Para la estimación de drogas ilegales, se han desarrollado dos tipos de sensores poliméricos. Un kit colorimétrico basado en un sensor de PDMS/TEOS/SiO₂NPs/NQS para la identificación y determinación in-situ de drogas de tipo anfetamínico y otro basado en un sensor de PDMS/Co(SCN)₂ para la estimación de ketamina. Satisfactorios LOD fueron obtenidos para esta aplicación (0.002-0.005 g mL⁻¹ y 30 µg para los tipo anfetamínicos y ketamina, respectivamente). Ambos kits son herramientas muy útiles para el cribado instantáneo de las drogas ilícitas más utilizadas en las pruebas en carretera debido a su simplicidad, rapidez, estabilidad y portabilidad, a un coste muy bajo. De modo que los tiempos de demora podrían minimizarse a través de esta prueba en campo.

Con respecto al sensor basado en AgNP, los compuestos sulfúricos volátiles se han detectado satisfactoriamente con LOD de 45 ppb (v/v, µL m⁻³). Este sensor pasivo no requiere una fuente de energía externa y, por lo tanto, el coste de energía es cero. Sus ventajas tales como estabilidad, simplicidad, rapidez (10 min) y bajo coste lo convierten en una potencial kit clínico para el control del mal aliento, así como en atmósferas o áreas cerradas.

Finalmente, las micropalanca piezoeléctricas has sido evaluadas como sensores de gas. Se han estudiado nuevos procedimientos de fabricación, diseño y composición. Las mejores propiedades electromecánicas se han conseguido con 0.75% de Li₂O₃, 1.2% de Bi₂O₃ y 1.05% de composición de CuO ($K_{eff} \approx 33.5\%$ para la vibración planar de los discos). El uso de un material comercial polimérico para la capa de sacrificio ha permitido simplificar el procedimiento de fabricación debido a que éste es eliminado durante la sinterización. También se ha funcionalizado exitosamente mediante deposición de una dispersión de sílica mesoporosa tipo MCF (*Mesoporous Cellullar Foam*) en la capa superior del electrodo de oro. La baja sensibilidad (0.1 Hz ppm⁻¹) obtenida para la humedad sugiere una potencial aplicabilidad como sensor de compuestos orgánicos volátiles para fines ambientales.

Es decir, los sensores in-situ propuestos en esta Tesis pueden ser considerados como una alternativa sostenible y eficaz a los métodos instrumentales convencionales. La inmovilización de reactivos o nanopartículas en un soporte sólido evita la necesidad de preparar disoluciones que resultan ser inestables y no se requieren equipos de elevado coste.

La importancia de los (nano)materiales para desarrollar metodologías analíticas ha quedado demostrada:

- 1. El PDMS es un excelente material extractante y encapsulante de colorantes gracias a sus coeficientes de partición, permeación y transparencia.*
- 2. El C₁₈ es ampliamente usado como material abrasivo en MSPD debido a su hidrofobicidad y fácil empacado.*
- 3. La sílica mesoporosa MCF es un material con una potencial aplicabilidad como capa sensible en micropalanca resonantes gracias a su gran área superficial.*
- 4. Los CNTs en las columnas capilares para IT-SPME mejoran las eficiencias de extracción y la resolución para analitos que interaccionan a través de interacciones π - π .*
- 5. El MOF peptídico Cu(GHG) es un material adecuado para el reconocimiento enantioselectivo de drogas quirales como la efedrina debido a su interacción preferente por uno de los enantiómeros a través de puentes de H adicionales o más fuertes.*
- 6. Las AgNPs son materiales muy sensibles para el diseño de sensores in-situ en soporte de nailon.*

ABSTRACT

ABSTRACT

The research on materials and new strategies to improve sample pretreatment and/or instrumental techniques has attracted great attention in the current developments of Analytical Chemistry. This Thesis presents interesting uses of (nano)materials to improve or develop sensing, extraction and separation techniques. The recent goal in Analytical Chemistry is the development of ecofriendly methodologies. In order to achieve this aim, analytical strategies focused on green aspects have been carried out: (i) miniaturized sample pretreatment and separation techniques and (ii) in-situ sensors. The materials studied in this Thesis have been organized in silicon-based (PDMS, C₁₈ and MCF), carbon-based (MWCNTs and SWCNTs) and metallic-based (MOF and AgNPs).

The versatile properties and low cost of PDMS has promoted its use as extractive phase in SPME and support for sensing devices has grown in importance. PDMS has been studied as extractive phase in IT-SPME-Cap-LC for estimating DEHP, BAK and DPA at trace levels in several matrices of environmental, industrial and forensic interest. The potential use of CNTs as extractive phase has been widely reported. Thus, CNTs have been studied to functionalize capillary columns for IT-SPME. Due to the enhancement on extraction efficiency and chromatographic profiles, CNTs have proved to be a reliable alternative to conventional phases in IT-SPME for estimating amphetamines in oral fluids. The proposed IT-SPME approach coupled to CapLC integrates on-line extraction, preconcentration and separation, reducing the sample treatment steps.

Another important application of PDMS is its use as embedding material of dyes for developing optical sensors for in-situ analysis. In this context, colorimetric sensors for on-site estimation of amino compounds such as casein, a biocide, amphetamine-like compounds and ketamine have been developed.

Moreover, a sensor based on AgNPs has been also developed as clinical kit for the in-situ and real time detection of volatile sulfur compounds, which are related to oral malodour. AgNPs are highly sensitive materials for their application as plasmonic sensor.

A new application of the material C₁₈ has been carried out. Thanks to the retentive capacity for amphetamine compounds, and thus, the capacity of C₁₈ to disrupt as well as to clean-up the sample, this material has been successfully evaluated as dispersant phase for MSPD. This approach integrates matrix disruption, clean-up and derivatization to simplify sample preparation for the determination of amphetamines in hair.

A potential applicability of MCF silica as sensing layer for resonant piezoelectric microcantilevers has been tested. In addition, an alternative fabrication procedure by using a polymeric commercial material for the sacrificial layer has been developed. Thus, the fabrication procedure is simplified due to sacrificial layer is removed during the firing step.

To our knowledge, the first example of a MOF capable of separating chiral polar drugs by using SPE has been studied in this Thesis. A chiral Cu(II) 3D MOF based on the tripeptide Gly-L-His-Gly has been used as extractive phase for the enantioselective separation of ephedrine.

The potential applicability of the materials studied has been demonstrated by the determination of several target compounds in different matrices. The proposed methodologies have reported improvements in terms of cost, rapidity, simplicity and sensitivity, besides protecting the operator and the environment.

INDEX

INDEX

CHAPTER 1. INTRODUCTION	1
1.1 RECENT TRENDS IN ANALYTICAL CHEMISTRY	3
1.2 MINIATURIZED SYSTEMS.....	6
1.2.1 Miniaturized sample pretreatment techniques.....	6
1.2.1.1 IT-SPME configurations.....	10
1.2.1.2 Trends in extractive phases	12
1.2.2 Miniaturized separation techniques	14
1.2.3 Figures of merit of the online IT-SPME-LC	18
1.3 IN-SITU DEVICES.....	19
1.3.1 Optical sensors.....	24
1.3.2 Electromechanical sensors.....	29
1.4 (NANO)MATERIALS AND APPLICATIONS.....	35
1.4.1 Si-based materials	36
1.4.1.1 PDMS.....	36
1.4.1.2 Bondesil C ₁₈	39
1.4.1.3 Mesoporous silica	40
1.4.2 C-based materials.....	42
1.4.3 Metallic-based materials.....	44
1.4.3.1 AgNPs and AuNPs.....	44
1.4.3.2 MOFs	49
1.5 ANALYTES AND ANALYTICAL TECHNIQUES	50
1.5.1 Phthalates	50
1.5.2 Biocides	52
1.5.2.1 Benzalkonium chloride (BAK).....	53
1.5.2.2 ADP.....	55
1.5.3 Casein.....	55

1.5.4 Drugs	57
1.5.4.1 Amphetamine-like designed drugs	57
1.5.4.2 Ketamine	61
1.5.6 Volatile sulfure compounds (VSCs)	64
CHAPTER 2. OBJECTIVES	67
CHAPTER 3. METHODOLOGY	77
3.1 CHEMICALS AND REAGENTS	79
3.2 INSTRUMENTATION	82
3.2.1 Spectroscopic techniques	82
3.2.1.1 UV-Vis spectrophotometry	82
3.2.1.2 Infrared spectroscopy	83
3.2.1.3 RAMAN spectroscopy	84
3.2.1.4 Electro-mechanical Impedance spectroscopy	85
3.2.2 Chromatographic techniques.....	86
3.2.2.1 HPLC–FLD	86
3.2.2.2 CapLC–DAD	87
3.2.2.3 CapLC–FLD.....	89
3.2.3 Microscopic techniques	90
3.2.3.1 Light microscopy	90
3.2.3.2 Scanning electronic miscroscopy (SEM).....	91
3.2.3.3 Surface profiler microscopy	91
3.3 SAMPLE PRETREATMENT TECHNIQUES	92
3.3.1 Off-line sample pretreatment techniques	92
3.3.1.1 SPE.....	92
3.3.1.2 Vortex-assited extraction (VAE)	93
3.3.1.3 Ultrasound-assisted extraction (UAE).....	93
3.3.1.4 MSPD.....	94
3.3.2 On-line extraction techniques.....	96

3.3.2.1 In-valve IT-SPME	96
3.4 FABRICATION OF SENSORS	97
3.4.1 PDMS/TEOS/SiO ₂ NPs-NQS sensors (Patent 201300436)	97
3.4.2 PDMS-Co(SCN) ₂ sensors	98
3.4.3 AgNPs-based sensors (Patent 201600440)	100
3.4.4 Screen-printed piezoelectric MEMS	100
3.5 PROCEDURES AND EXPERIMENTAL CONDITIONS	106
3.5.1 Chromatographic conditions	106
3.5.2 IT-SPME conditions	108
3.5.3 Derivatization procedures	109
3.5.4 Response of polymeric sensors	110
3.5.5 Response of AgNPs based sensors	112
3.5.6 Response of screen-printed sensors	113
3.6 SAMPLES	114
3.6.1 ENVIRONMENTAL SAMPLES	114
3.6.1.1 Sediments	114
3.6.1.2 Water	114
3.6.2 BIOLOGICAL SAMPLES	115
3.6.2.1 Oral fluid	115
3.6.2.2 Hair	115
3.6.2.3 Breath	116
3.6.3 INDUSTRIAL SAMPLES	116
3.6.4 FORENSIC SAMPLES	117
3.6.4.1 Street drug samples	117
3.6.4.2 Shooter hands	117
CHAPTER 4. RESULTS AND DISCUSSION	119
4.1 Si-BASED MATERIAL	121
4.1.1 PDMS AS EXTRACTIVE PHASE FOR IT-SPME	121

4.1.1.1 A cost-effective method for estimating DEHP in coastal sediments by IT-SPME-CapLC.....	122
4.1.1.2 IT-SPME-CapLC method for BAK determination as a component or contaminant in mixtures of biocides.....	130
4.1.1.3 A new method for estimating DPA in GSRs as a new tool for identifying both, inorganic and organic ones, in the same sample	141
4.1.2 PDMS AS SUPPORTING MATERIAL FOR SENSORS DEVELOPING.....	159
4.1.2.1 PDMS sensor containing NQS as unique dispositive for the estimation of casein in effluents from dairy industries	160
4.1.2.2 A solid device based on doped hybrid composites for controlling the dosage of ADP in industrial formulations	171
4.1.2.3 A solid colorimetric sensor for the analysis of amphetamine-like street samples	185
4.1.2.4 A passive solid sensor for in-situ colorimetric estimation of the presence of ketamine in illicit drug samples	196
4.1.3 C ₁₈ AS PHASE FOR MSPD	208
4.1.3.1 Determination of amphetamines in hair by integrating sample disruption, clean-up and solid phase derivatization	208
4.1.4 Mesoporous silica as sensing layer for MEMS	222
4.2 C-BASED MATERIAL.....	237
4.2.1 Application of CNTs modified coatings for the determination of amphetamines by IT-SPME-CapLC	237
4.3 METALLIC-BASED MATERIALS	252
4.3.1 MOF.....	252
4.3.1.1 Peptide MOF for enantioselective separation of chiral drugs	252
4.3.2 AgNPs and AuNPs.....	265
4.3.2.1 Colorimetric sensor based on silver nanoparticles for detecting volatile sulfur compounds	265
CHAPTER 5. GENERAL CONCLUSIONS	275
REFERENCES	285

ANNEX.....	337
A1. Abbreviations.....	339
A2. Figure list	345
A3. Table list.....	361
A4. PhD contributions to publications	367

CHAPTER 1. INTRODUCTION

The development of Analytical Chemistry is governed by the implementation of new technologies and internet, the development of (nano)materials and the social changes produced in the last years. Thanks to technological progress, the tendency is that classical methods are being replaced with new tools and instruments reducing the time analysis and improving the figures of merit of the analytical procedures. In addition, the advance in computing is supporting the automatization, miniaturization and simplification of systems and data treatment. The miniaturization of instruments is a key point since the small scale is giving rise to more sustainable methods thanks to the reduction of solvents, reagents and wastes. This is the starting point to develop portable instruments for in-situ analysis. In the same direction, it should be note the use of new analytical responses as the image analysis by smartphones. Their responses have opened alternative tools providing real-time measurements for in-situ analysis. The irruption of new (nano)materials is another break point in the global evolution of Analytical Chemistry. Indeed, the study of (nano)materials to enhance the existing techniques and develop new techniques remains a growing area of research.

1.1 RECENT TRENDS IN ANALYTICAL CHEMISTRY

From the concern about environmental issues such as chemical pollution and resource depletion, Green Chemistry emerges in 1990's. This chemical area is foccused on the development of environmental friendly technologies in order to reduce or eliminate the use and generation of hazardous substances. Paul Anastas and John Warner developed the following list of twelve principles guides the practice of Green chemistry (*Anastas, P.T. et al., 1998*):

1. **Prevention:** it is better to prevent waste than to treat or clean up waste after it is created.
2. **Atom Economy:** synthetic methods should be designed to maximize the incorporation of all materials used in the process into the final product.
3. **Less Hazardous Chemical Syntheses:** wherever practicable, synthetic methods should be designed to use and generate substances that possess little or no toxicity to human health and the environment.

4. **Designing Safer Chemicals**: chemical products should be designed to affect their desired function while minimizing their toxicity.
5. **Safer Solvents and Auxiliaries**: the use of auxiliary substances (e.g., solvents, separation agents, etc.) should be made unnecessary wherever possible and innocuous when used.
6. **Design for Energy Efficiency**: energy requirements of chemical processes should be recognized for their environmental and economic impacts and should be minimized. If possible, synthetic methods should be conducted at ambient temperature and pressure.
7. **Use of Renewable Feedstocks**: a raw material or feedstock should be renewable rather than depleting whenever technically and economically practicable.
8. **Reduce Derivatives**: unnecessary derivatization (use of blocking groups, protection/ deprotection, temporary modification of physical/chemical processes) should be minimized or avoided if possible, because such steps require additional reagents and can generate waste.
9. **Catalysis**: catalytic reagents (as selective as possible) are superior to stoichiometric reagents.
10. **Design for Degradation**: chemical products should be designed so that at the end of their function they break down into innocuous degradation products and do not persist in the environment.
11. **Real-time analysis for Pollution Prevention**: analytical methodologies need to be further developed to allow for real-time, in-process monitoring and control prior to the formation of hazardous substances.
12. **Inherently Safer Chemistry for Accident Prevention**: substances and the form of a substance used in a chemical process should be chosen to minimize the potential for chemical accidents, including releases, explosions, and fires.

The application of these principles to Green Analytical Chemistry entailed a revision in order to fulfill the requirements and characteristics of Analytical Chemistry. In this context, concise guidelines in the form of Green Analytical Chemistry principles were reported to be helpful in greening analytical laboratory (*Gałaszka, A. et al., 2013*):

1. Direct analytical techniques should be applied to avoid sample treatment.
2. Integration of analytical processes and operations to reduce the consumption of reagents and energy.
3. Reduction in generated amounts of wastes and proper management of wastes.
4. Energy saving.
5. Automated and miniaturized methods should be selected.
6. Reagents obtained from renewable source should be preferred.
7. Safety for operator should be increased.
8. In situ measurements should be performed.
9. Derivatization should be avoided.
10. Minimal size and number of samples are goals.
11. Multi-analyte or multi-parameter methods are preferred versus methods using one analyte at a time.
12. Eliminate or replace toxic reagents.

Therefore, the goal of Green Analytical Chemistry is the development or improvement of analytical methodologies to reduce the negative impacts on health and environment. As a consequence of the principles of the Green Analytical Chemistry, the current trends in analytical chemistry are focused on the development of new techniques amenable to miniaturization and automatization, as well as in-situ analysis.

Hence, the general aim of this Thesis is the investigation of (nano)materials for their application in miniaturized systems, particularly for extraction and separation techniques, and in-situ devices in order to achieve the new challenges of the analytical chemistry.

1.2 MINIATURIZED SYSTEMS

Despite of the progress in analytical instrumentation, sample preparation is still a critical step. In order to obtain a reliable analytical response, many operations are required to extract, concentrate, purify and/or transform the analyte. Within the sample preparation, extraction techniques play an important role since the analytes are transferred from the matrix to an extractive phase. Although an efficient extraction depends on each extraction technique, the most important point is the use of a suitable extractive phase. In this sense, the research of new extractive strategies and new materials to improve the extraction efficiencies and selectivity is an emerging field as will explain later.

1.2.1 Miniaturized sample pretreatment techniques

The extraction of the analytes from different matrices can be carried out through liquid-phase extraction (LPE) or through solid-phase extraction (SPE). However, in the last decades, the use of SPE is preferred mainly due to the pressure to decrease organic solvent usage which encouraged the requirements for solvent-free procedures. SPE has been widely used for the preparation of biological, pharmaceutical, environmental and food samples (*Lindsey et al., 2001; Picó, Y. et al., 1994, 2007; Ridgway, K. et al., 2007*). This technique is based on the interaction of analytes dissolved in a liquid with a solid sorbent through which the sample passes. The result is the separation between desired and undesired components from the sample. The portion that passes through the sorbent is collected or discarded, depending on whether it contains the analytes or impurities. In the case that the analytes are retained on the sorbent, they can be removed by rinsing with an adequate eluent for their collection (*Figure 1*). SPE is a powerful technique used to pre-concentrate and isolate the analytes prior to the determination technique.

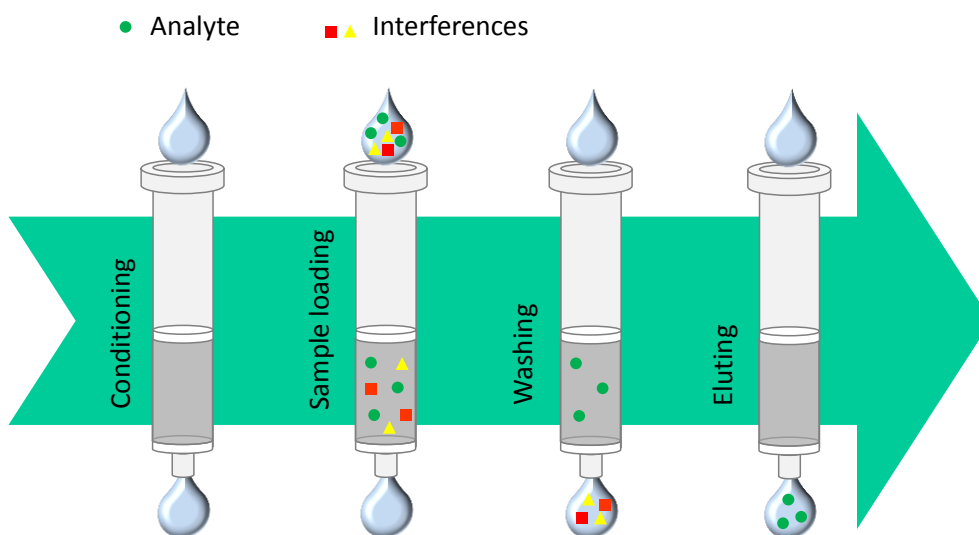


Figure 1. Scheme of the SPE procedure.

SPE is not only carried out in liquid matrix but also in solid matrix, this is the case of matrix solid phase dispersion (MSPD) (Barker, S.A., 2007; García-López, M. et al., 2008; Moliner-Martínez, Y. et al., 2012a). This technique involves the grinding of a portion of the sample with an abrasive solid material. The grinding process disrupts the sample structure and disperses it over the surface of the extractive material. The blend is then packed into a pre-fritted SPE tube, and finally the analytes are selectively desorbed with an appropriate solvent. The analytical process is considerably simplified, and typical problems encountered when using other treatments (e.g. emulsion formation) are avoided. This technique also reduces sample and solvents consumption and does not need special instrumentation. Due to the inherent advantages, MSPD is widely applied in the environmental and toxicological fields as well as in food analysis (Capriotti, A.L. et al., 2010; Míguez-Framil, M. et al., 2010; Freitas, S.S. et al., 2018; Souza, I.D. et al., 2018). The selectivity and efficiency of MSPD is mainly dependent on the sorbent and extractive solvent used. As regards the sorbents, most reported methods used reversed phase SPE materials, such as C_{18} and C_8 phases for the dispersion and retention of lipophilic analytes, whereas silica and alumina particles are the normal phase sorbents most frequently used. More recently, sorbents such as graphene (Liu, Q. et al., 2011; Li, C. et al., 2014; Peng, L.Q. et al.,

2017), polymeric materials (Wang, T. et al., 2011 and 2018) and metal-organic frameworks (MOFs) (Santos Barreto, A. et al., 2018) have been reported.

According to the principles of Green Analytical Chemistry, many of the research contributions in analytical chemistry have been focused on the development of easy and ecofriendly techniques. Consequently, traditional extraction techniques such as SPE, LPE and others are being gradually replaced by techniques amenable to miniaturization and automatization that provide the reduction of solvent/reagent consumption and waste generation (Belay, K., 2016), and also the improvement on selectivity and preconcentration in lower times. Many attempts have been carried out in this sense; one of them is the solid phase microextraction (SPME) as miniaturized alternative to SPE introduced by Arthur and Pawliszyn in 1990 (Arthur, C.L. and Pawliszyn, J., 1990).

Initially, SPME was developed using silica fiber coated on its outer surface with a polymeric extractive phase, mainly polydimethylsiloxane (PDMS), which is inside a device, similar to a syringe with needle (fiber-SPME). The needle protecting the fiber is retracted and the fiber is immersed in the sample solution or the headspace of sample for the adsorption of the analytes on the polymer coating. After equilibrium is reached, the fiber is withdrawn and transferred into the chromatograph for desorption and analysis of analytes. This new technique eliminated the problems related with SPE remaining the advantages; elimination of solvents, reduction of blanks values and reduction of extraction time.

Despite the advantages of fiber-SPME, this technique showed some limitations such as fiber fragility, low extraction capability, bleeding from coatings of fiber and also difficult coupling to liquid chromatography. To overcome the limitations of fiber-SPME, in-tube solid phase microextraction (IT-SPME) was proposed as an alternative. In 1997, Eisert and Pawliszyn (Eisert, R. and Pawliszyn, J., 1997) developed the first on-line IT-SPME copupled to High Performance Liquid Chromatography (HPLC) system. IT-SPME is based on the use of a fused-silica capillary tube packed or coated on its inner surface with an extractive phase. When the sample is passed through the capillary, the analytes are extracted and concentrated by adsorption/absorption into the internally coating of the capillary. After that, the extracted analytes are desorbed by filling the capillary with a proper solvent, which can be collected for further processing (static desorption) or can be transferred to the analytical instrument by means of a solvent stream (dynamic desorption). Static mode is usually applied when analytes have strong

interactions with the extractive phase and cannot be desorbed easily by the mobile phase. Although this technique has been used in combination with gas chromatography (GC) (Aguilar, C. et al., 2000; Globig, D. and Weickhardt, C., 2005), liquid chromatography (LC) is by far the most used system in IT-SPME-based assays (Andrade, M.A. and Lancas, F.M., 2017; Fernández-Amado, M. et al., 2017; Kataota, H., 2002; Mei, M. and Huang, X., 2017; Wang, R. et al., 2018). IT-SPME has been also coupled with other analytical instruments such as direct analysis in real time mass spectrometry (DART-MS) (Wang, X. et al., 2014) and hybrid generation atomic absorption spectrometry (HG-AAS) (Asiabi, H. et al., 2016a) for on-line conditioning. IT-SPME has been mainly developed to extend the SPME towards the path of automatization and on-line coupling to analytical instrumentation. Cleaning, preconcentration, separation and detection of analytes are carried out at the same step. In addition, this miniaturized technique can be consider an environmental friendly technique due to the reduction of solvents and wastes, energy, and so costs, maintaining or improving the reliability of the analytical performance parameters, such as sensitivity, precision and accuracy (Turner, C., 2013). From the advantages mentioned, IT-SPME has managed a widespread acceptance as preferential technique for many applications, illustrated by the increasing number of citations since its discovery (Figure 2).

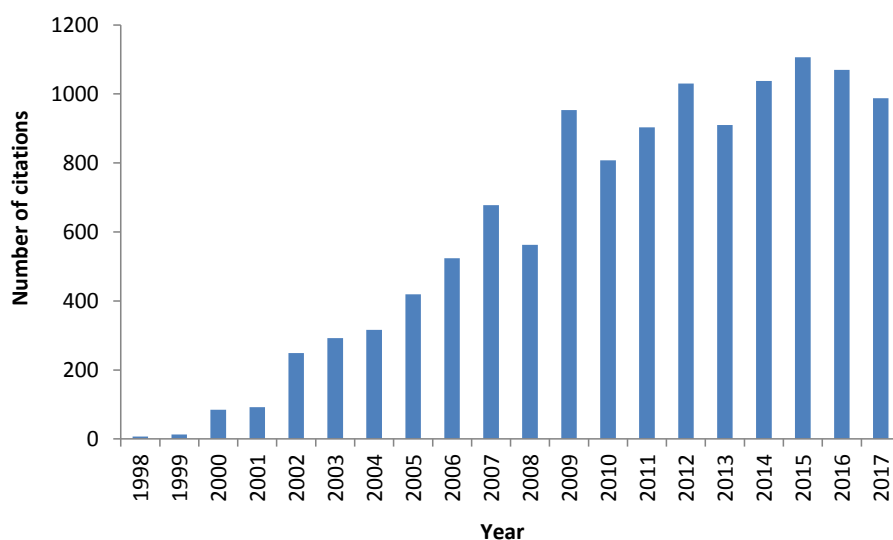


Figure 2. Evolution of the number of citations on Web of Science for matching the search items "IT-SPME" OR "In-tube SPME" OR "In-tube solid phase microextraction".

Among the different modalities to perform SPME, IT-SPME is a versatile technique that can be effected with several configurations. The on-line configuration combines extraction and separation/detection in one step, therefore the process can be automated (*Moliner-Martínez, Y. et al., 2015*). IT-SPME involves the on-line coupling of the extraction to a LC system. There are two main modes to carry out this coupling, known as draw/eject and flow-through modes (*Figure 3*).

1.2.1.1 IT-SPME configurations

a) Draw/eject IT-SPME

The sample is repeatedly aspirated and dispensed through the extractive capillary a number of cycles until partition equilibrium between analytes and extractive phase is reached or until the amount of analyte extracted is enough. For this purpose, a programmed autosampler is required (*Cháfer-Pélicas, C. et al., 2008; Chaves, A.R. et al., 2011; Mizuno, K. and Kataoka, H., 2015; Saito, K. et al., 2012; Zhang, S. et al., 2010*). The extractive capillary is placed between the needle and the loop of an autosampler. The extracted analytes are statically desorbed from the capillary coating by filling the capillary with an appropriate solvent and then transferred to the chromatographic column. Alternatively, extracted analytes can be desorbed and transported to the analytical column by mobile-phase flow (*Figure 3A*). In this mode, cleaning and conditioning of the capillary between runs is required. For this, many systems incorporate an additional pump for transferring, cleaning and conditioning.

b) In flow-through IT-SPME

The sample is passed through the extractive capillary (one time) to retain the analytes. Next, the retained analytes are desorbed and transferred to the chromatographic column by delivering the appropriate solvent, statically or dynamically. In this case, conditioning, loading, cleaning and transferring operations can be carried out manually or automatically. Different setups can be used. The simplest setup named in-valve IT-SPME (*Figure 3B*) entails the replacement of the loop of an injection valve by the extractive capillary (*Jornet-Martínez, N. et al., 2015a; Li, Y. and Xu, H., 2015; Wang, S. et al., 2015*). The analytes are extracted during sample loading, and transferred to the separative

column with the mobile phase by changing the valve position to inject position. Another setup consists of two valves (*Figure 3C*). The extracted analytes can be desorbed and transferred from the capillary of first valve to the injection loop of the second valve by means of an auxiliary pump. Next, the plug of solvent in the loop with the desorbed analytes is sent to the chromatographic column with the mobile phase by changing the valve position from load to inject (*Masià, A. et al., 2013*).

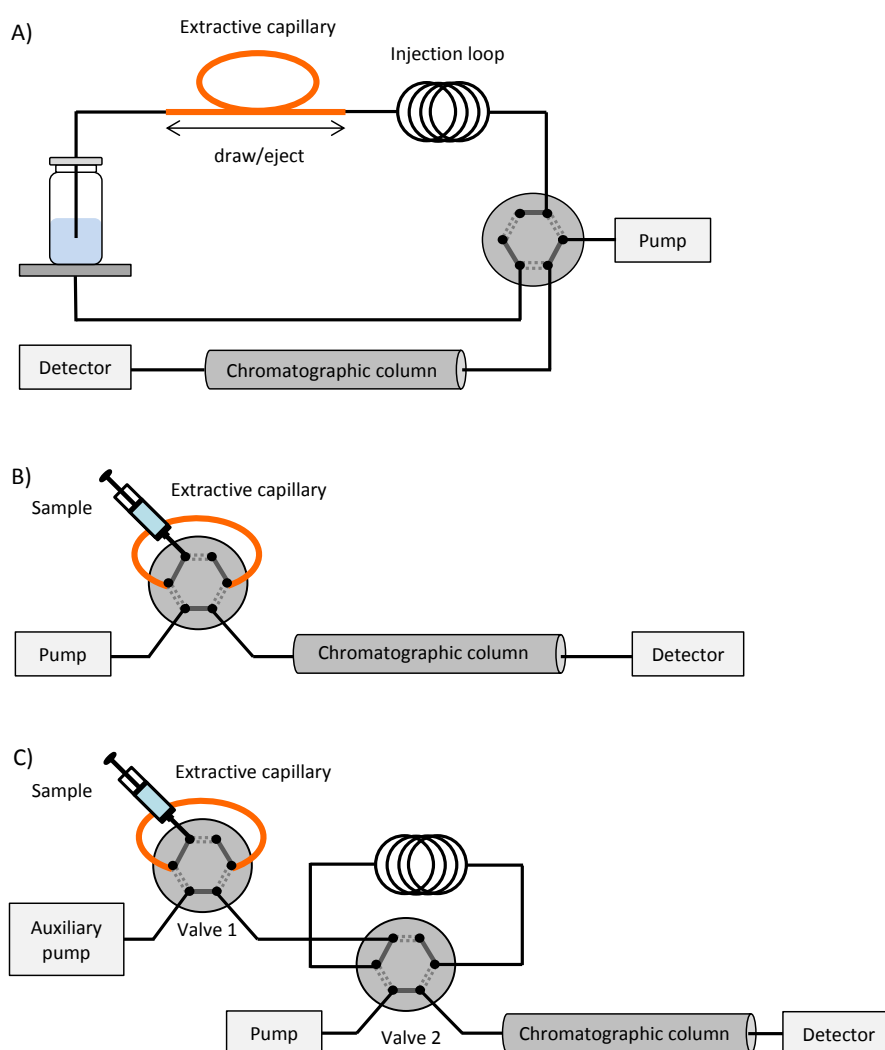


Figure 3. Schematic representation of configurations used for IT-SPME-LC: A) draw/eject cycle mode, B) flow-through in-valve IT-SPME and C) flow-through with an additional pumping system.

In the draw/eject system, the extraction efficiency can be enhanced by increasing the number of cycles, so relatively high recoveries can be reached. Although extraction recoveries in flow-through systems are lower than in draw/eject approach, the amount of analytes extracted can be increased by increasing the sample volume loaded into the capillary. Due to this fact, flow/through configuration is suited for the analysis of water samples, where volumes up to 2-4 mL can be passed through the extractive capillary without causing its deterioration or clogging. Satisfactory selectivity has been reported for many organic pollutants in environmental waters (Wu, J.C. and Pawliszyn, J., 2001; Cháfer-Pélicas, C. et al., 2008; Aufartová, J. et al., 2012).

In this Thesis, the in-valve IT-SPME modalities has been studied to determine contaminants in coastal sediments and water, biocides in industrial mixtures, organic gunshot compound deposited on hands and amphetamine compounds in oral fluid.

1.2.1.2 Trends in extractive phases

The extraction, cleanup and preconcentration is related to the interactions between the analytes and the extractive phase (hydrogen bonding, acid-base, π - π , dipole-dipole, dipole-induced-dipole and dispersion forces), and so depend on several parameters of capillary column such as coating type and thickness, and length and internal diameter (Moliner-Martínez, Y. et al., 2015a). With the aim to improve the performance, the study of new materials for its application as extractive phases is an expanding field of research. Typically, segments of commercial capillary columns such as those used in GC have been employed as extractive capillaries, taking advantage of the fact a variety of extractive phases are available for compounds of different polarities. *Figure 4* summarizes the percentages of studies about materials used as extractive phases in the last five years. The extractive phases mainly employed to perform IT-SPME can be divided into silicon-based (Si-based) and carbon-based (C-based). Diphenyl-modified PDMS has been deeply researched, although dimethylsiloxane and cyanomethyl silicones are reported in the literature (Campins-Falcó, P. et al., 2008, 2009, 2010; Cháfer-Pericás, C. et al., 2006, 2007; Fernández-Amado, J. et al., 2016; Hakobyan, L. et al., 2018; Jornet-Martínez, N. et al., 2014a, 2015a; Masià, A. et al., 2013; Moliner-Martínez, Y. et al., 2010, 2011, 2015b; Muñoz-Ortuño, M. et al., 2012; Pla-Tolós, J. et al., 2015, 2016a; Prieto-Blanco, M.C. et al., 2008, 2011, 2012,

2013a, 2013b; Vitta, Y. et al., 2010). With regard to C-based sorbents, polyethyleneglycol (PEG) (Gou, Y. and Pawliszyn, J., 2000), divinylbenzene (Kataoka, H. et al., 2009; Nonaka, Y. et al., 2009; Saito, K. et al., 2010) and carbon-(nano)materials-based such as graphene, carbon nanotubes (CNTs) and fibres (Li, Y. and Xu, H., 2015; Liu, X.-Y. et al., 2008; Moliner-Martínez, Y. et al., 2015b; Wang, X. et al., 2013; Zhang, W.P. et al., 2013) are the most widely studied. Si-based sorbents have been mainly used for environmental, food and industrial products analysis, while C-based sorbents have been proposed for biological and food sample analysis. Extraction efficiency provided by some conventional capillary coatings is limited due to low loading capacity, stability and slow diffusion of the analytes from the sample to the coating. Hence, the main challenges in microextraction-based techniques, particularly IT-SPME, are the improvement on selectivity, sensitivity, stability and extraction time. As a consequence, the study of new extractive phases is a subject matter that arouses great interest. In this regard, a wide range of sorbents are documented in the literature, including polypyrrole (Mullet et al., 2002; Wang, S. et al., 2015; Wu, J.C. and Pawliszyn, J. 2001), magnetic nanoparticles (NPs) (González-Fuenzalida, R.A. et al., 2014; Manbohi, A. and Ahmadi, S.H., 2015; Moliner-Martínez, Y. et al., 2012b, 2014a; Shamsayei, M. et al. 2018), antibodies-based (Chaves, A.R. et al., 2011, 2013; Xu, B. et al., 2015; Ying, L.-L. et al., 2017), molecular imprinted polymers (MIPs) (Asiabi, H. et al., 2016b; Chaves, A.R. and Queiroz, M.E.U., 2013b; Souza, I.D. et al., 2016; Zarejousheghani, M. et al., 2013), MOFs (Shih, Y.H. et al., 2016; Zhang, J. et al., 2015), silver-nanostructures (Sun, M. et al., 2015) and monolithic capillary columns (Wang, T. et al., 2016; Wu, F. et al., 2016; Zheng, M.-M. et al. 2009). Among these materials, C-based nanomaterials are the most widely used as extractive phases in IT-SPME. Thereby, the application of C-based nanomaterials will be further discussed in detail. In addition, the application of external sources such as magnetism, electrical fields and thermal energy have been also tested to enhance the affinity of analytes towards the extractive phases (Mei, M. et al., 2016; Moliner-Martínez, Y. et al., 2012b). These approaches have been effected in the flow-through modality due to the easy implement of equipment to provide magnetic, electric or thermal field that provide this modality.

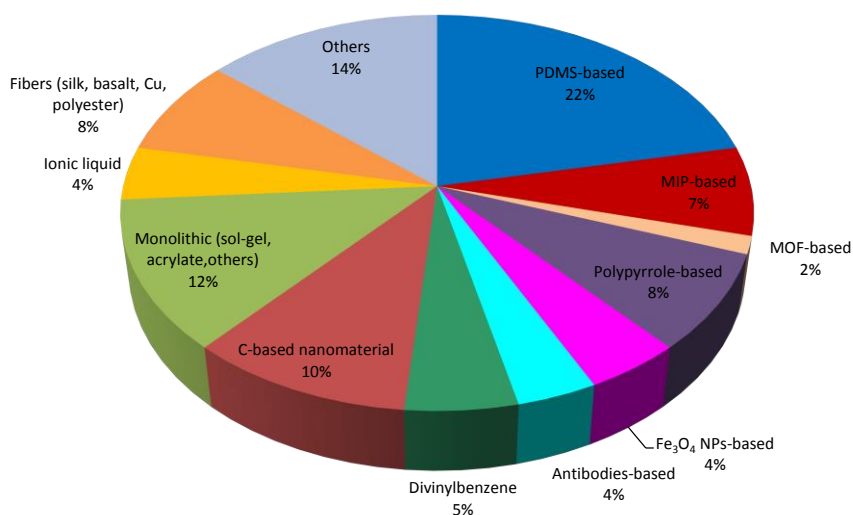


Figure 4. Percentage of studies using several materials as extractive phases for the last five years. Data from Web of Science matching the search terms “IT-SPME” OR “In-tube solid phase microextraction” OR “In-tube SPME”.

1.2.2 Miniaturized separation techniques

Another challenge of the Analytical Chemistry, as regards chromatographic techniques, has been the reduction of mobile phase flow to microliters (μL) or nanoliters (nL) per time. In this context, IT-SPME coupled to miniaturized chromatographic techniques has received special attention. IT-SPME on-line combined with conventional LC is well-documented. Many references have applied IT-SPME-HPLC with Ultraviolet-Visible (UV-Vis) detector (Campíns-Falcó, P. et al, 2008; Li, T. et al., 2009; Prieto-Blanco, M.C. et al, 2009a; Wang, T.T et al., 2015), fluorescence detector (FLD) (Campíns-Falcó, P. et al 2009; Prieto-Blanco, M.C. et al, 2008; Zhang, J. et al., 2015) or mass spectrometry (MS) (Kataoka, H. et al., 2009; Tan, F. et al., 2015; Zheng, M.-M. et al., 2009 and 2010) for the analysis of biological, food, environmental or industrial samples. However, current trends focused on the miniaturization have triggered the development of IT-SPME coupling to chromatographic techniques with reduced dimensions (i.e. capillary liquid chromatography, Cap-LC, and liquid nanochromatography, nano-LC). The operational parameters and dimensions used in several miniaturized designs of IT-SPME-LC are shown in Table 1. The direct combination of IT-SPME with the

chromatographic flow path of CapLC does not cause extra band broadening. Nevertheless, the on-line connection to chromatographic systems that operate at lower flow rates such as NanoLC requires a specific interface by using two interconnected valves as injection setup.

Table 1. Operative values for IT-SPME-CapLC and IT-SPME-NanoLC.

Operative value	IT-SPME-Cap-LC	IT-SPME-Nano-LC
Extractive capillary i.d. (μm)	100-320	≤ 100
Extractive capillary length (cm)	14-100	≤ 15
Chromatographic column (μm)	100-500	10-100
Chromatographic column length (cm)	35-150	5-15
Flow ($\mu\text{L min}^{-1}$)	4-20	0.2-1

Coupling on-line IT-SPME to the miniaturized chromatographic system deserves some attention because improvements on efficiencies and sensitivity, as well as, reduction of solvent consumption can be achieved. In this field, the Miniaturization and Total Methods of Analysis (MINTOTA) research group, where this Thesis have been worked out, is specialized in IT-SPME coupled to HPLC and miniaturized LC (Cap-LC and nano-LC). This is evidence by more than 30 works published about this topic in international reviews since 2006. *Table 2* shows some examples of IT-SPME coupling to LC that use different extractive capillaries reported during the last 5 years for several applications.

Table 2. Summary of Applications of IT-SPME described in the literature between 2013 and 2018.

Technique	Extractive capillary	Analyte	Matrix	Reference
IT-SPME-CapLC-DAD-MS	PDMS ₆₅ and nitrile	Homologues of benzalkonium chloride	Industrial samples and washes water	Prieto-Blanco, M.C. et al., 2013a
IT-SPME-CapLC-DAD-MS	PDMS ₆₅	aldehydes	Water	Prieto-Blanco, M.C. et al., 2013b
IT-SPME-UHPLC-MS/MS	PDMS ₉₅	Atrazine, chlorfeniphos, chlorpyrifos, DEHP, diuron, isoproturon, simazine, terbuthylazine and trifluralin	Waste water, influents, effluents, river water and coastal water	Masià, A., et al., 2013
Magnetic IT-SPME-CapLC-DAD	Fe ₃ O ₄ -SiO ₂	Chlorfeniphos and chlorpyrifos	Waste water	Moliner-Martínez, Y., et al., 2014
IT-SPME-CapLC-DAD	PDMS ₉₅	Di(2-ethylhexyl) (DEHP), diethyl (DEP), dibutyl (DBP) and mono-ethylhexyl (MEHP) phthalates	Coast water	Jornet-Martínez, N. et al., 2014
Magnetic IT-SPME-CapLC-DAD	Fe ₃ O ₄ -SiO ₂	Atrazine, terbuthylazine and simazine	Water	Gonzalez-Fuenzalida, R.A. et al., 2014
IT-SPME-CapLC-DAD	PDMS ₉₅	DEHP, DEP, DBP and MEHP	Urine	Jornet-Martínez, N. et al., 2015a
IT-SPME-CapLC-DAD	PDMS ₉₅	Monochloramine	Tap and swimming pool water	Pla-Tolós, J. et al., 2015
IT-SPME-CapLC-DAD	PDMS ₉₅ and PDMS ₆₅ modified with carboxylated single and multiwall carbon nanotubes (c-SWCNTs and c-MWCNTs)	Triazines and degradation products	Water	Moliner-Martínez, Y., et al., 2015
IT-SPME-CapLC-DAD	PDMS ₉₅ and PDMS ₆₅ modified with c-SWCNTs and c-MWCNTs	Triazines and PAHS	Water	Jornet-Martínez, N. et al., 2015b
IT-SPME-LC-MS/MS	Carboxen 1006 PLOT	8-Hydroxy-2'-deoxyguanosine	Urine	Kataoka, H. et al., 2016
IT-SPME-HPLC-UV	Poly(ether ether ketone) (PEEK) and poly(acrylamine-ethyleneglycoldimethacrylate) monolith	Protoberberine alkaloids	Rat plasma	Ling, X. et al., 2016
IT-SPME-LC-UV	Stainless steel tube coated with graphene/polyaniline	Aldehydes	Human exhaled breath	Wang, S. et al., 2015

Continuation Table 2. Summary of Applications of IT-SPME described in the literature between 2013 and 2018.

Technique	Extractive capillary	Analyte	Matrix	Reference
IT-SPME-CapLC-MS	PDMS ₈₅	Carbonyl compounds	Aqueous fraction particulate matter (PM _{2.5})	Prieto-Balanco, M.C. et al., 2013b
IT-SPME-LC-FLD	PEEK tube coated with zeolitic imidazolate framework	PAHs	Water and soil	Zhang, J. et al., 2015
IT-SPME-LC-UV	PEEK tube coated with nanostructured silver	PAHs	River and rain water	Sun, M. et al., 2015
IT-SPME-LC-DAD	Polytetrafluoroethylene tube coated with a polydopamine/dialdehyde starch/chitosan	Hexanal and 2-butanone	Blood	Wu, S. et al., 2016
IT-SPME-CapLC-DAD	PDMS ₈₅	AgNPs	Water	Gonzalez-Fuenzalida, R.A. et al., 2016a
IT-SPME-LC-DAD-FLD	PDMS ₉₅	PAHs	Rain water	Fernández-Amado, M, et al., 2016
Magnetic-IT-SPME-LC-UV	Stainless steel tube packed with sodium dodecyl sulfate coated Fe ₃ O ₄ NPs	Moxifloxacin	Urine	Bu, Y. et al 2016
IT-SPME-CapLC-DAD	PDMS ₈₅	Irgarol-1051 and diuron	Water	Pla-Tolós, J. et al. 2016a
IT-SPME-NanoLC-DAD	Silica capillary coated with SiO ₂ /PEG-spherical Fe ₃ O ₄	Diclofenac	River water	Gonzalez-Fuenzalida, R.A. et al., 2016b
IT-SPME-NanoLC-DAD	TEOS-MTEOS-SiO ₂ NPs	Polar triazines and their degradation products	Wastewater	Serra-Mora, P. Et al., 2017
IT-SPME-HPLC-DAD	Rt® -S-BOND	Phthalates and their degradation products	Atmospheric particulate matter	Fernández-Amado, M. et al., 2017
IT-SPME-CapLC-DAD	PDMS ₈₅ , PDMS ₈₀ and PDMS ₅	Meropenem	Endotracheal tubes	Hakobyan, L. et al., 2018
IT-SPME-HPLC-DAD	Basalt fiber functionalized with AuNPs	PAHs	Water	Feng, J. et al., 2018
Magnetism-enhanced monolith-based IT-SPME-HPLC-DAD	Monolith doped with magnetic Fe ₃ O ₂ -SiO ₂ NPs	Organic UV filters	Water	Mei, M. and Huan, X. 2017
IT-SPME-CG-FID	MOF-CJ3	Aromatic positional isomers	-	Fang, Z.-L. et al 2013

1.2.3 Figures of merit of the online IT-SPME-LC

By online IT-SPME-LC, high sensitivity and no matrix effects can be achieved in less than 30 min, in the majority of procedures. *Table 3* shows a summary of the analytical parameters obtained for different applications of IT-SPME-LC. The environmental impact of an analytical procedure has been traditionally categorized with qualitative parameters, but the establishment of a quantitative environmental performance indicator, as the carbon footprint, is mandatory (*Moliner-Martínez, Y. et al., 2015a*). Carbon footprint represents the amount of greenhouse gases emissions produced by an activity, expressed as KgCO₂eq. Carbon footprint can be calculated by the following equation:

$$\text{KgCO}_2\text{eq} = \Sigma(\text{electricity consumed, KWh}) \times \text{emission factor for electricity, KgCO}_2/\text{KWh}$$

Where the electricity consumed can be obtained from the electrical company or from the technical data of apparatus, and the emission factor converts the electrical activity data in emission values, depending on the season, time and supplier. Recently, our group has calculated the carbon footprint to evaluate the environmental performance of an analytical method (*Pla-Tolós, J. et al., 2016*). The environmentally friendliness of IT-SMPE has been demonstrated by carbon footprint, which depends on injection system (automatic or manual), extraction setup (one or two pumps), separation technique (conventional or miniaturized chromatograph) and detector (optical, electrochemical, mass spectrometry, etc.). Values from 1.1 to 3.0 KgCO₂eq can be obtained for different modalities of on-line IT-SPME (data calculated using diode array detection, DAD, and a reference emission factor of 0.247 KgCO₂/ KWh) (*Moliner-Martínez, Y. et al., 2015b*). However, off-line extraction technique exhibit carbon footprint one order of magnitude higher due to the use of additional instrumentation (ultrasound, evaporator, etc.). These results show the potential of online IT-SPME in Green Analytical Chemistry.

Table 3. Summary of analytical parameters (precision, limits of detection (LODs) and recoveries) for different applications of IT-SPME.

Application	Separation/Detection	Precision	LODs	Recoveries
Environmental analysis	HPLC-FLD	<20	0.005-400 ng L ^{-1*}	72-110
	HPLC-UV	<10	0.001-200 µg L ⁻¹	70-120
	LC-MS	<10	2-5 µg L ⁻¹	88-105
	LC-MS/MS	<7	0.5-5 ng L ⁻¹	82-112
	CapLC-DAD	<19	8-5000 ng L ⁻¹	81-120
Clinical analysis	HPLC-FLD	<13	8-15 µg L ⁻¹	-
	HPLC-UV	<7	0.01-0.1 µg L ⁻¹	70-108
	LC-MS	<11	9-1000 ng L ⁻¹	75-113
	LC-MS/MS	<8	3 ng L ⁻¹	92
	CapLC-DAD	<20	0.05-1.5 µg L ⁻¹	50-90
Food analysis	HPLC-FLD	<8	0.3-5 ng L ⁻¹	-
	HPLC-UV	<7	0.02-21 µg L ⁻¹	80-110
	HPLC-MS	<11	0.01-20 µg L ⁻¹	80-88
Industrial analysis	CapLC-DAD	<18	6-30 µg L ⁻¹	117
	NanoLC-DAD	<4	1 µg L ⁻¹	50

*up to 2 µg L⁻¹ for the determination of PAH₅ in soil and dust (Zhang, W. et al., 2014).

1.3 IN-SITU DEVICES

Another trend in current Analytical Chemistry is the development of new devices for in-situ analysis, which means at the same place where the target compound is present. The progress in technology, (nano)materials and society have attracted attention for methods that allow measurements in real time and on site. These methods entail potential benefits including the minimization of sample treatment and the subsequent reduction of time and costs (Nightingale, A.M. et al., 2015; Pandey, S.K. et al., 2012). Additionally, the risk of contamination or degradation of sample during its transport to the laboratory can be avoided. Well known in-situ sensors are today marketed, for example glucometer, pregnancy test, alcohol breathalyzer or test drug kit. Besides, it is important to remark that not trained personnel are usually required due to the easy-to-use of these sensors. Thanks to the great possibilities offered by in-situ sensors, they are applied to wide range of fields such as environmental, health, industrial, medical, forensic and security. Some examples of in-situ sensors are given in Table 4.

Table 4. Summary of *in-situ* sensors described in the literature between 2013 and 2018.

Assay format	Matrix	Analyte	LODs	Reference
Molecularly imprinted photonic hydrogels	Human urine and saliva	Ketamine	10 $\mu\text{g mL}^{-1}$ by UV-vis spectrophotometer and 1 ng mL^{-1} by naked eye.	Meng, L. et al, 2013
Inkjet-Printed array paper-based dye-encapsulating polymer nanoparticles		Volatile amines	-	Soga, T. et al., 2013
Methyltriethoxysilane/PDMS-OH ormosil coating doped with rose anthocyanin dye	Indoor air	Formaldehyde	0.06 ppm	Meng, Q. et al., 2014
Poly(ethylene glycol)-terminated and perfluoroalkyl-terminated alkanethiols modified gold nanoparticles	Water	Perfluorinated compounds	0.1 $\mu\text{g L}^{-1}$	Niu, H. Et al, 2014
Aptamer-AuNPs conjugates	Mimicking samples	Cocaine	0.2 mg mL^{-1}	Smith, J.E. et al., 2014
Primary amine-functionalized polyaniiline nanothin film	Air	Formaldehyde	400 ppb	Srinives, S. et al., 2014
Sol gel based Nano scaled ZnO quantum dots	Water	Cu^{2+}	7.68×10^{-7} M	Wang, F. et al., 2014
Paper microfluidic with FeCl_3 , Ninhydrin, Scott's Morris and Froehde's reagents	Drugs	ketamine, cocaine, morphine, MDMA, MET, codeine, thebaine, EP	2.7-11 μg (visually)	Musile, G. et al., 2015
Cobalt tetrathiocyanate@NS support	Water	Ketamine	0.01 mg mL^{-1}	Maddah, B. t al., 2015
PDMS/thymo/nitroprusside	Waters and PM_{10} aqueous extract	Ammonium	0.4 mg L^{-1} , 0.1-1.5 mg L^{-1}	Prieto-Blanco, M.C. et al., 2015
2[[[2aminophenyl]imino]methyl]-4,6-di-tert-butylphenol encapsulated in polymeric ethyl cellulose	Water	Cu^{2+}	3.3×10^{-13} M	Kacmaz, S. et al., 2015

Continuation Table 4. Summary of *in-situ* sensors described in the literature between 2013 and 2018.

Assay format	Matrix	Analyte	LODs	Reference
N,N-dimethyl-phenylenediamine/FeCl ₃ on paper	Water and atmospheres	Hydrogen sulphide	0.5 mg L ⁻¹	Campins-Falcó, P. et al., 2016
Platinum NPs and 3,3',5,5'-tetramethylbenzidine (TMB) paper-based	Water and fish	Hg ²⁺	0.01 µM	Chen, W. et al., 2016
PDMS/TEOS/NQS or ETH'4001	Atmosphere and fish degradation	Aliphatic amine and ammonia	1 mg m ⁻³ ; 3-30 mg m ⁻³	Jornet-Martínez, N. et al., 2016a
Zein-alkaline phosphatase	Water, saline and pesticides	Phosphate, alkaline phosphatase, chlorpyrifos	0.2 mg L ⁻¹ ; 0.5-5 mg L ⁻¹	Jornet-Martínez, N. et al., 2016b
PDMS/TMB/enzymes	Commercial products	Hydrogen peroxide	0.04 mg L ⁻¹ ; 0.142-2.448 mg L ⁻¹	Pla-Tolós, J. et al., 2016b
Patterned microfluidic paper-based of trichlorosilane	Human blood	Glucose	13 mg dL ⁻¹	Lam, T. Et al., 2017
Smartphone-based portable system—Bionic e-Eye	Mussel extracts	Marine toxins	0.0075-0.0096 ppb	Su, K. et al., 2017
Silver nitrate paper-based	Water	As	1.1 ng mL ⁻¹	Pena-Pereira, F., et al., 2018
Optical-fiber-based aptasensor coated with aptamer-modified gold nanorods	Grape juice	Mycotoxin, ochratoxin A	12.0 pM	Lee, B. et al., 2018
Graphene quantum dot-luminol-AgNP nanocomposites with luminol,	Human serum	Glucose	8 µM	Salehnia, F., et al., 2018
Graphene sheet-nanoribbon/nickel nanoparticles hybrid material modified electrode	Human serum	Glucose	2.5 nM	Jothi, L. et al., 2018
Portable electrochemiluminescence biosensor with the screen-printed electrode	Biological	Abrin	0.1 ng mL ⁻¹	Liu, S. et al., 2018

Figure 5 shows the different modalities of analytical processes based on the way in which they are carried out. In off-line process, the sample is transported to the laboratory for its analysis, whereas in-situ analysis can be carried out by introduction the device at sampling place (in-line) or can be carried out in fixed station close to sampling place (on-line). In addition, in-situ devices can be classified as passive or active in function of the sampling type. Active devices require an energy source for sampling (e.g. pump). Whereas, passive devices not required energy consumption because sampling is carried out by diffusion.

In this Thesis we have focused on the development of passive sensors for on-line analysis.

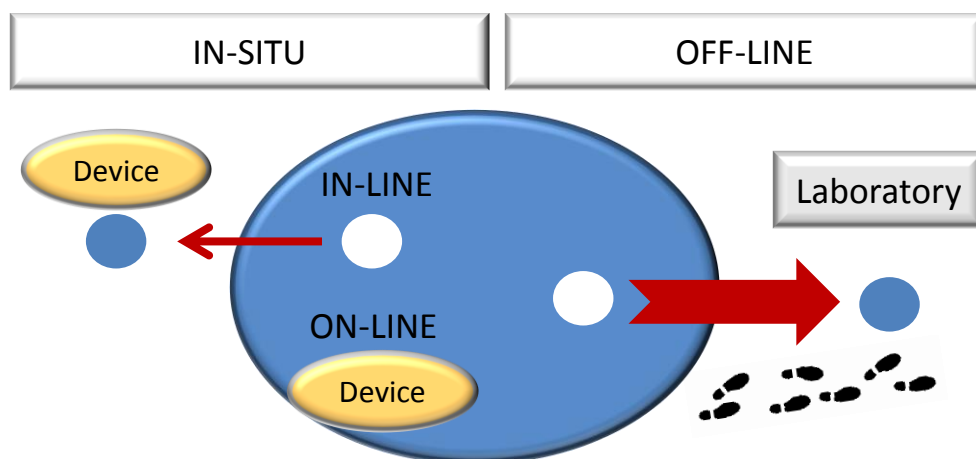


Figure 5. Schematic representation of in-line, on-line and off-line analytical methods and their relationship with in-situ analysis.

Table 5 outlines the current methods for in-situ analysis, which can be divided in monitoring stations, portable instruments, electromechanical devices and optical devices (Jornet-Martínez, N. et al., 2017). The availability of resource and skilled personnel, and also the monitoring purposes are some of factors to take into account when choosing one of these methods. In some cases, complex systems that provide high analytical performance can be unsuitable due to their requirement of qualified personnel and expensive equipment.

Table 5. Summary of characteristics of some current methods for in situ analysis.

Method	Type	Advantages	Disadvantages
Monitoring station	-Air -Water	-High precision -High accuracy -High sensitivity -Multiple analysis	-High energy consumption -Expensive -High carbon footprint -Specialized operator
Portable instruments	-Spectrophotometer -Fluorimeter -Infrared -Chromatography	-Low energy consumption -Moderate accuracy -Portability	-Cost -Specialized operator
Electrochemical and electromechanical devices	-Amperometric -Voltamperometric -Conductimetric -Potenciometric	-Low energy consumption -Sensitivity -Low specialized operator	-Low stability -Moderate/low accuracy
Optical devices	-Colorimetric -Fluorescence -Luminiscence	-Low cost -Low/non energy consumption -Easy to use -No training personnel -Portable -Rapid	-Moderate sensitivity -Low accuracy

Although the number of publications about analytical methods up to nowadays remains mainly dedicated to chromatographic methods, optical, electrochemical and electromechanical sensors are taking on greater importance because real time and on site measurements can be accomplished. It should be highlight that the number of citations dealing with the in-situ analysis is growing during the last years (See *Figure 6*). Although there are references prior to the XXI century, the figure has been referenced since 1998 with the aim of comparing the evolution of the two main techniques on which this thesis has focused, which are IT-SPME and in-situ sensors.

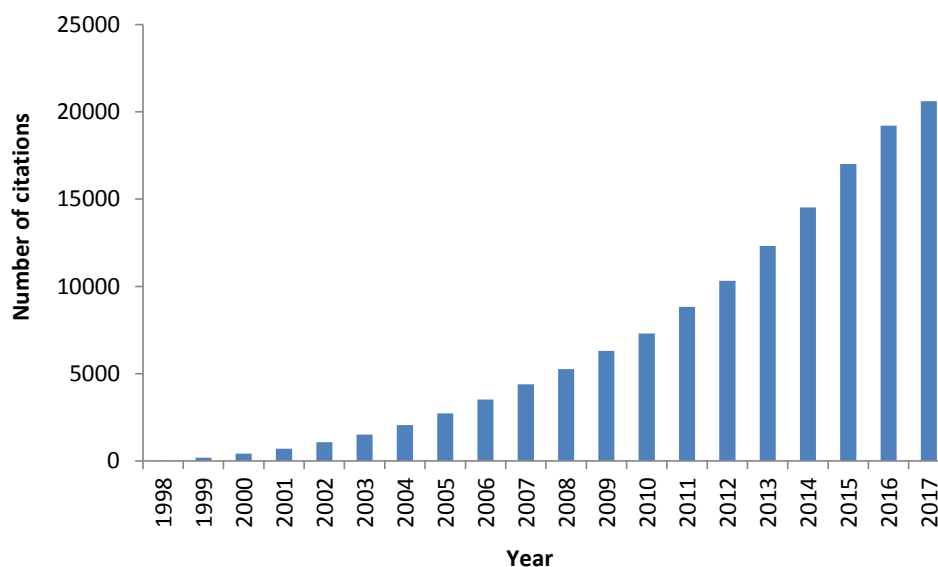


Figure 6. Number of citations on Web of Science for matching the following search term “in-situ analysis” AND “sensors” in the 1998-2017 period.

From all the methods shown in Table 5, this thesis pays special attention to optical and electromechanical sensors due to their interesting characteristics such as portability and low-cost.

1.3.1 Optical sensors

Among the different optical sensors, colorimetric devices are highlighted because their color change in presence of the analyte can be easily detected by naked eyes. These sensors are based on a color change through a chemical reaction between a chromophore and the target compound. The resulting intensity colors are related to the concentration of analyte. Thereby, a qualitative determination can be carried out by visual inspection, but a quantitative determination can also be done by absorbance or diffuse reflectance (DR) measurements (Jornet-Martínez, N. et al., 2016a; Prieto-Blanco, M.C. et al., 2015). Following current trends in technology, image analysis by mobile phones is an emerging alternative for quantification purposes (Capitán-Vallvey, L.F. et al., 2017; Ogirala, T. et al., 2017; Roda, A. et al., 2016; Su, K. et al., 2015, 2017;

Vashist, S.K. et al., 2015). Figure 7 reveals the growing trend to use smartphone as analysis instruments (Web of science for matching the following search terms: “Smartphone sensor” or “smartphone reader” or “Smartphone photometer”).

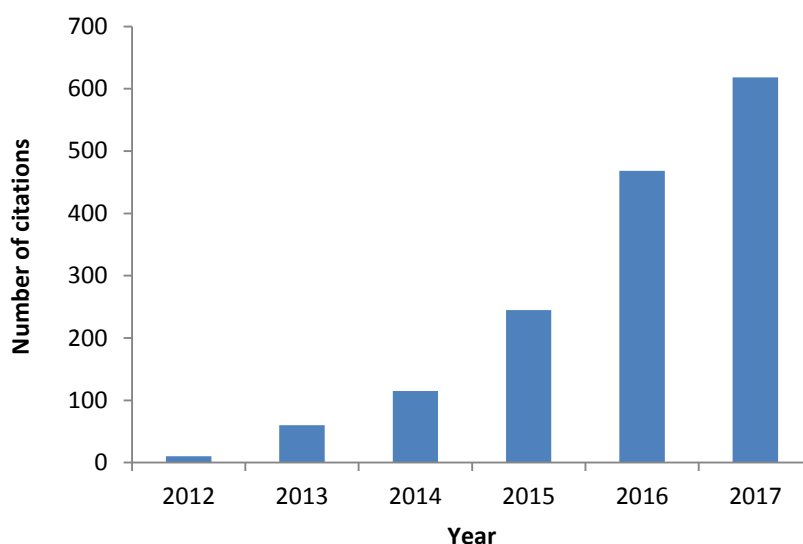


Figure 7. Number of citations on Web of Science for matching the following search term “smartphone sensor” OR “smartphone reader” OR “smartphone photometr” in the 2012-2017 period.

For image analysis, a digital image (DI) of colorimetric assay is firstly taken by consumer electronic device (e.g., scanner and smartphone) and after that, its colors are converted into numeric values, which depend on the color model used, by image softwares such as Adobe®Photoshop, GNU Image Manipulation Program (GIMP) (Pla-Tolós, J. et al., 2016) and ImageJ. Different color models can be found according to the method to represent the colors (Capitán-Vallvey, L.F. et al., 2015): red-green-blue (RGB), cyan-magenta-yellow-black (CMYK), hue-saturation-value (HSV) and luminance-color change from red to green and yellow to blue (CIELAB). RGB color mode is used in many works (Chen, Y. et al., 2015; Pla-Tolós, J. et al., 2018), as well as in this Thesis to perform the quantification of analyte. In this model, colors are created from the mixture of red, green and blue colors and their intensities can be expanded from 0 to 255, where black color has 0 value and white color has 255 value. Although smartphone-based assays have opened up a powerful alternative to conventional equipment, a set of parameters relating to

image should be taken into account. One of the most influential parameter on DI is the lighting conditions under which the image is captured (*Chaplan, C.A. et al., 2014*). In order to correct intensity variations of light, several options have been proposed in the literature such as integrating the smartphone with a custom-made dark box (*Hosur, O. et al., 2017; Su, K. et al., 2017; Vashist, S.K. et al., 2014*) taking reference areas to normalize (*Jia, M.Y. et al., 2015*), incorporating light source with fixed camera parameters (*Oncescu, V. et al., 2013*) and using scanner to take pictures (*Alkasir, R.S.J. et al., 2012; Christodouleas, D.C., et al., 2015; Gabrielson, J. et al., 2002*).

Several colorimetric devices can be found in the literature. **Devices for delivery reagents** are based on the immobilization of derivatizing reagents in solid supports, mainly polymers and paper. In this kind of device, the reagent diffuses from the support to the solution, where is the analyte, and so the derivatization reaction occurs. An example of this is reported by Prieto-Blanco et al., 2015, where thymol and nitroprusside are embedded into PDMS for determining ammonium in waters. Also, Pla-Tolós, J. et al., 2016 embedded 3,3',5,5'-tetramethylbenzidine (TMB) and horseradish peroxidase enzyme (HRP) into PDMS-tetraethylortosilicate (TEOS)-silicon dioxide NPs (SiO₂NPs) for determining hydrogen peroxide in commercial products. Conversely in **solid sensors**, the chromophore reagent is immobilized into solid support and the analyte diffuses from the sample matrix to the sensor in order to react with the reagent. Our research group has developed a paper-based sensor for hydrogen sulphide determination both water and air (*Pla-Tolós, J. et al., 2016c*). Additionally, other optical sensor based on sodium 1,2-naphthoquinone-4-sulfonate (NQS) embedded in PDMS matrix have been designed for several applications such as discrimination of volatile amines (*Jornet-Martínez, N. et al., 2016*), determine casein in effluents from dairy industries (*Section 4.1.2.1 of this Thesis*) and analysis of a biocide in industrial formulations (*Section 4.1.2.2 of this Thesis*). NQS/PDMS-based sensor has also been used to develop a test kit for amphetamine-like drugs (*Section 4.1.2.3 of this Thesis*). **Test kit** generally contains a testing solution with reagents and/or buffer and its color change when the sample is added. In this context, colorimetric kits for chlorine and pH estimation in swimming pools, as well as kits for forensic applications are frequently used (*Commercial Pool Test Kits*). Along this line, test strips have also given rise to remarkable applications in the biomedical, food and environmental fields (*Ngom, B. et al., 2010*). The most known test strip is the pregnancy test (*Leuvering, J.H.W. et al., 1980*). **Test strips** involve chromophores

or biological components immobilized on a paper strip. The advantages of these strips are the speed, specificity and low-cost. Nevertheless, the results obtained by test strips are qualitative, and so quantification cannot be carried out (*Chin, C.D. et al., 2007*). On the other hand, there are microfluidic platforms in which sample flows by capillary along a channel on paper, where reagents are pre-deposited, and color change when sample reach the reagent and interact with it. **Microfluidic platforms** allow the opportunity to analyze multiple compounds on the same platform by creating different reaction zones (*López-Ruiz, N. et al., 2014*). For air analysis, **colorimetric tubes** are active monitoring devices. These tubes contain an impregnated material with a chromophore through which the air passes manually or by a battery-operated pump, producing a color change in presence of the analyte (*Coffey, C.C. et al., 2010*). Besides the requirement of a pump, the unespecificity is the main limitation of colorimetric tubes. Other optical sensors are the **colorimetric arrays**. They are based on chemical dyes adsorbed on a support, providing a characteristic pattern of response when they are exposed to a mixture of analytes. The sensing mechanism for volatile compound relies on optical or optoelectronic noses, this means molecular recognition of patterns of response rather than specific recognition of enzymes lock-and-key. In the literature, we can find application examples of colorimetric arrays for the analysis of bacteria (*Lim, S.H. et al., 2014*), explosives (*Kangas, M.J. et al., 2016*), soft drinks (*Zhang, C. et al., 2007*) and volatile organic compounds (VOCs) (*Janzen, M.C. et al., 2006*).

More recently, the use of metallic NPs (MNPs) as a new alternative of reagents to carry out colorimetric tests has caused the development of **plasmonic sensors**. MNPs such as silver nanoparticles (AgNPs) and gold nanoparticles (AuNPs) have color in the visible region due to localized surface plasmon resonance, whereas their aggregates analyte-induced exhibit different color (*Stewart, M.E. et al., 2008*). Hence, the gradual optical changes can be measured by absorbance or DR for quantification purposes. Due to advantages like high-sensitivity and selectivity offered by AuNPs and AgNPs as plasmonic sensors, they are widely used for food (*Caelen, I. et al, 2004*), medicine (*Masson, J.F., 2017*) and environmental analysis (*Mauriz, E. et al., 2006*). The characteristic properties of MNPs are related to their synthesis and functionalization. In most cases, functionalization of NPs is necessary (*Chai, F. et al., 2010; Chen, Y.-C. et al., 2013*), although the use of pseudo-naked AuNPs have been managed to increase sensitivity (*Jornet-Martínez, N. et al., 2014*).

In some colorimetric assays, the color change can be carried out in solution (Hatamie, A. et al., 2014; Jose, D.A. et al., 2007), whereas in other assays, the color change takes place in/on solid support where the colorimetric reagents are immobilized (Chen, Y. et al., 2015; Endo, T. et al., 2007; Jornet-Martínez, N. et al., 2016a; Peters, K.L. et al., 2015; Pla-Tolós, J. et al. 2016b, 2016c, 2018). Compared to the solution assays, solid devices overcome undeniable limitations concerning stability of chromophores and management. Polymers, paper, silica and glass are some of materials proposed as solid support for designing in-situ sensors. Table 6 exposes the properties of some substrates reviewed in the literature.

Table 6. Features of different type of solid supports.

Features	Silica	Glass	PDMS	Paper
Surface/volume ratio	Low	Low	Low	High
Flexibility	No	No	Yes	Yes
Fluid flow	Forced	Forced	Diffusion	Capillarity
Humidity effect	No	No	No	Yes
Biocompatibility	Yes	Yes	Yes	Yes
Biodegradability	No	No	Yes	Yes
Easy availability	No	No	No	Yes
Easy handling	No	No	Medium	Yes
Homogeneity	Yes	Yes	Yes	No
Cost	High	Medium	Low	Low

The paper has raised considerable interest for developing in-situ devices owing to its low-cost, versatility, abundance, simplicity as well as chemical compatibility. Moreover, the huge variety of papers in the market allows the selection of the optimal paper for each kind of assay (Liana, D.D. et al., 2012). Paper-based sensors have become a sensing platform for many application areas including environmental monitoring (Chang, J. et al., 2016; Sicard, C. et al., 2015), quality control (Saraz, J.A.O. et al., 2015) and clinical diagnosis (Zhao, W. et al., 2008). On the other hand, PDMS is the most used polymer as support for embedding several species such as chromogenic reagents, quantum dots and NPs (Campins-Falcó, P. et al., 2016; Prieto-Blanco, M.C. et al., 2015). Another polymer used is polyvinylchloride (PVC), for example, a colorimetric sensor based on dicyclohexylamine entrapped in PVC matrix plasticized with dioctylphthalate is

described for trinitrotoluene sensing (Ercag, E. et al., 2009). Glass is also used as substrate, a glass dipstick device with the reagent aza-boro-dipirromethane is reported to detect nitrites ions in natural water resources (Adarsh, N. et al., 2013).

From all these materials, paper and PDMS have been selected in this Thesis as supporting materials for developing in-situ sensors due to their advantages that will be assessed below.

1.3.2 Electromechanical sensors

According to the trends in exploring sensors for in-situ analysis, electromechanical sensors, and microelectromechanical systems (MEMS) in particular, have received intensive attention. Since their development in 1970, MEMS have expanded substantially. MEMS are considered successful devices widespread used in such diverse fields as automotive, aerospace, consumer electronics, point-of-care diagnostics, communication and industrial and environmental control (Boisen, A. et al., 2011; Guo, Y. et al., 2017; Khalid, N. et al., 2017; Sheikhaieh, A. et al., 2017). Microcantilever-type is the most ubiquitous structure in the field of MEMS (Bouchaala, A. et al., 2016), mainly for gas detection (Boudjiet, M.-T. et al., 2015) due to their advantages such as high sensitivity, integration into a circuit, miniaturization, in-situ detection, low-price and large scale array construction (Chaudhary, M. and Gupta, A., 2009; Li, X. and Lee, D.W., 2015).

The structure of a microcantilever is based on a dividing board, which is anchored at one end and the rest is suspended. As their name suggests, the dimensions of these sensors can be from micrometers up to a few millimeters. At such a small scale, small physical or mechanical changes due to analyte interaction achieve high sensitivity. To perform it as a sensor, the top surface of cantilever is coated with a sensing layer of a material, commonly known as functionalized layer, which has the affinity towards the analyte. The interaction between the target molecules and the functionalized layer can be physical or chemical. Depending on the material of the sensing layer, cantilevers can be used in several sensing applications. *Figure 8* shows the structure of the sensor aforescribed.

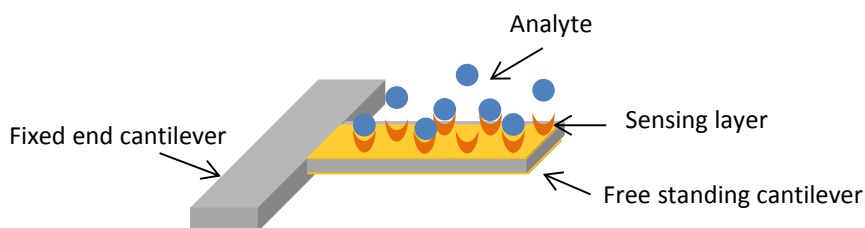


Figure 8. Microcantilever-based sensor

As can be seen in *Figure 9*, microcantilevers can operate in two modes (*Gopinath, P.G., 2014*). In **static mode**, the sorption of the analytes onto sensitive coating generates the surface stress, resulting in a deflection of the microcantilever due to interaction forces. In the **dynamic mode**, the cantilever is excited into resonance and the sorption of the analytes into the sensitive coating caused a shift in the resonant frequency associated to the change mass. Indeed, the resonance frequency depends on the mass, geometry and mechanical properties of the cantilever.

The static mode operation can be performed in several environments, commonly in liquid-based applications. Nevertheless, the dynamic mode is used in gas media due to the difficulty of this operation in liquid, arising from the damping of the microcantilever oscillations due to the high viscosity of the liquid media (*Chaudhary, M. and Gupta, A., 2009*). Under dynamic mode, resonant microcantilever is used as gravimetric-type sensor with high sensitivity and fast response (*Zhang, H.-Y. et al., 2012*).

In this Thesis, resonant microcantilever has been used as gravimetric-type chemical sensor through direct readout of frequency shift that is induced by mass-adsorption.

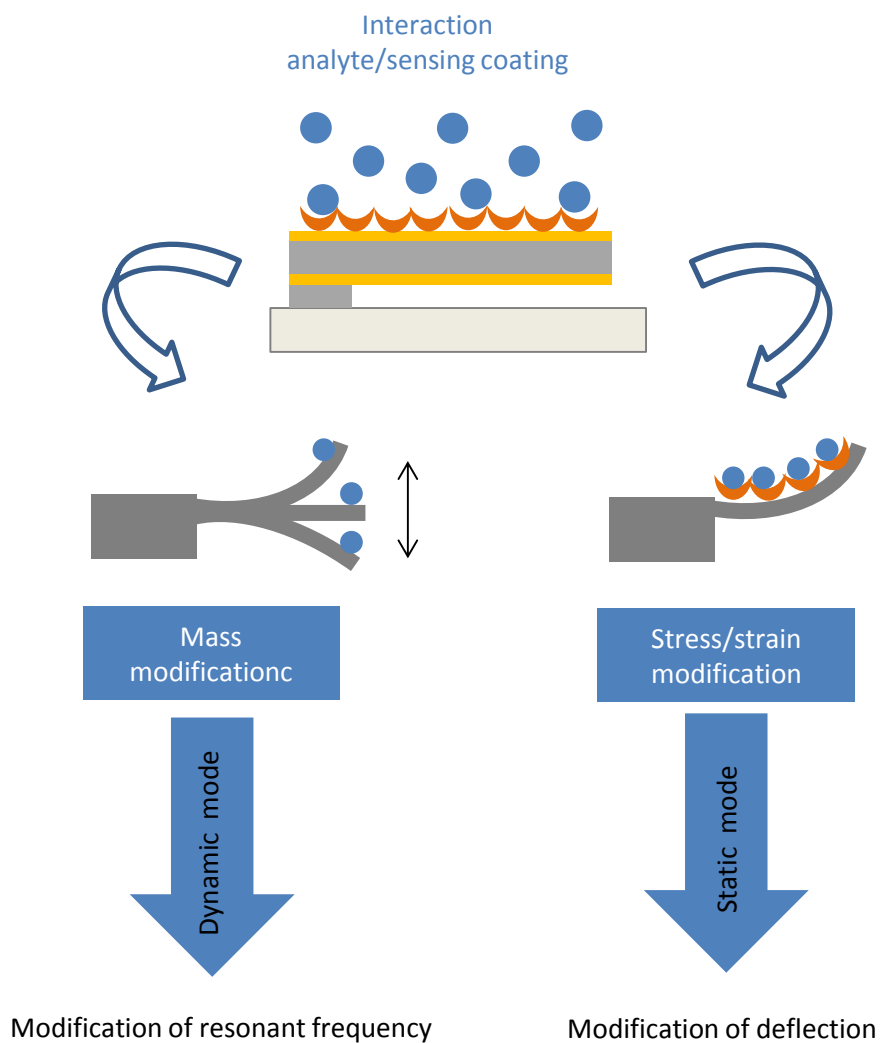

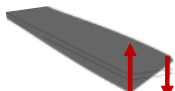




Figure 9. Principle of micro-cantilever-based sensors for chemical detection: static and dynamic mode.

There are four resonant modes for a parallelepipedal microcantilever. Analytical expressions of each mode in terms of the simple harmonic oscillator model are illustrated in *Table 7*. For each type of vibration, there are also different modes of vibration that occur for different frequencies.

Table 7. Summary of cantilever resonant modes in terms of the simple harmonic oscillator model, where L is the length, t is the thickness, E is the Young's modulus, w is the width, λ_n is the eigenvalue (n is a positive integer) and m is the cantilever mass.

Mode	Resonant Frequency	Spring Constant (k_i)	Mode scheme
Transverse	$\frac{\lambda_n^2}{2\pi} \sqrt{\frac{k_{Tr}}{m}}$	$\frac{Ew^3t}{12L^3}$	
Torsional	$\frac{2n-1}{4} \sqrt{\frac{k_{To}}{m}}$	$\frac{Ew^3t}{12L^3}$	
Lateral	$\frac{\lambda_n^2}{2\pi} \sqrt{\frac{k_{La}}{m}}$	$\frac{Ew^3t}{12L^3}$	
Longitudinal	$\frac{2n-1}{4} \sqrt{\frac{k_{Lo}}{m}}$	$\frac{Ewt}{L}$	

where i = Transverse (Tr), Torsional (To), Lateral (La), or Longitudinal (Lo) modes

A readout system for monitoring the bending or changes in resonance frequency induced on the cantilever is required. Based on the sensing principle, electromechanical sensors can be classified into the following main types: capacitive, optical, piezoresistive and piezoelectric (Chaudhary, M. and Gupta, A., 2009). Among these sensors, piezoelectric method is better suited for the dynamic mode presenting advantageous features such as rapid response, high resolution, integration of actuation and detection in miniaturized scale and low cost (Clément, P. et al., 2016).

One part of this Thesis has been focused on the development of resonant piezoelectric microcantilevers for gas detection.

Piezoelectric microcantilever consists of a piezoelectric layer between gold electrode layers inducing transient charge due to cantilever movement. Piezoelectric materials can be natural and man-made such as ceramics, polymers and composites. Ceramics-based are physically strong, chemically inert, and relatively inexpensive to manufacture. Within ceramics, formulations of lead

zirconate titanate, known as PZT ($\text{PbZr}_x\text{Ti}_{1-x}\text{O}_3$), are the most widely used material for piezoelectric sensors (Debéda, H. and Lucat, C., 2014; Debéda, H., et al., 2015) due to their benefit properties of high sensitivity and operating temperatures, as well as satisfactory electromechanical coupling and piezoelectric constants. These materials exhibit the piezoelectric properties after poling it because the alignment of domains lead to a remanent polarization (Figure 10a). Indeed, there are two piezoelectric effects. **Direct piezoelectric effect** consists of an electric field generation when mechanical stress is applied (Figure 10b and c), whereas **converse piezoelectric effect** happens when the material is subjected to an electrical field which causes a mechanical strain (Figure 10d and e). In the case of resonant piezoelectric microcantilevers, they are driven via converse effect by applying electric field to achieve the resonance but the sensing is performed by frequency changes due to analyte interaction through the direct effect.

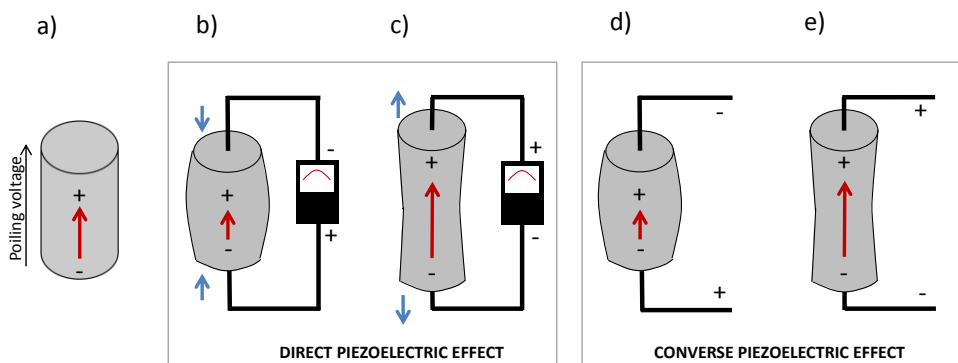


Figure 10. Summary of piezoelectric effect a) after polarization, b) output voltage of same polarity as material due to a compressive stress, c) output voltage of opposite polarity as material due to a tensile stress, d) applied voltage of same polarity as material produce a contraction of material and e) applied voltage of opposite polarity as material produce an expansion of material.

Previous works have shown that screen-printed cantilevers based on PZT are an alternative technology to the traditional silicon micromachining for gas sensors (Debéda, H. et al., 2013). Among different technologies, screen-printing is one of the most cheap, fast, flexible and simple technology that offers good resolution and repeatability. It is based on an additional process, overcoming a lot of steps required in the conventional process. The print cycle is schematized in Figure 11.

All these features show that screen-printed piezoelectric microcantilevers are good candidates for gas sensing applications.

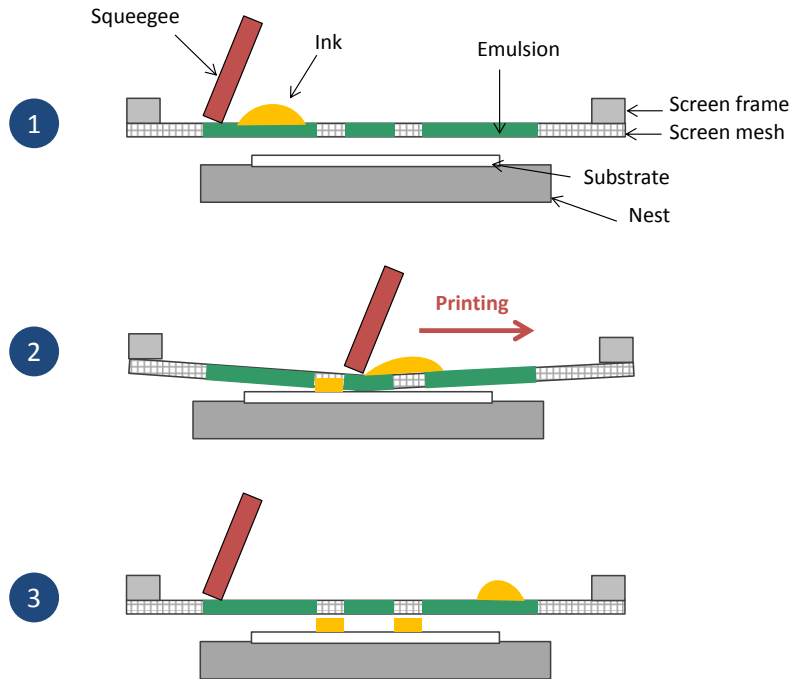


Figure 11. Print cycle of the screen-printing procedure. The screen is located just above the substrate (1). Then, the mesh of the screen is brought into line contact with the squeegee and scanned across the screen (2). The mesh should peel away from the surface immediately behind the squeegee, leaving all the ink that was in the mesh deposited onto the printing surface (3).

The selection of the material for the sensitive layer is very important in the gas sensor development. This material should be sensitive, selective, stable and short time of response, allowing the reversible sorption/desorption of target compounds. *Table 8* summarizes several works of resonant sensors coated with different materials to detect gases. Advanced sensing materials include polymers (Betts, T.A. et al., 2000; Débeda, H. et al., 2013), nanorods (Kilinc, N. et al., 2014), CNTs (Clément, P. et al., 2016) and MOFs (Xu, T. et al., 2016). Compared to the aforementioned materials, mesoporous materials feature higher specific surface area and porosity (up to $1500 \text{ m}^2 \text{ g}^{-1}$) (Wan, Y. and Zhao, D. Y., 2007). In this

context, mesoporous silicas are good candidates to provide more sensing sites for gas adsorption (Bao, Y.Y. et al., 2018; Stassi, S. et al., 2015; Xu, P.C. et al., 2014). Specifically in this Thesis, a resonant PZT microcantilever coated with mesoporous silica as sensing layer has been tested for gas detection.

Table 8. Summary of resonant microcantilevers coated with different sensitive layers reported.

Sensing layer	Analyte	LOD	References
polyethyleneoxide, polyethylenevinylacetate, polyvinylalcohol	Hexane, Octane, Toluene, Benzene, Acetone, Ethanol	-	Dong, Y. et al., 2010
Polyetherurethane	Toluene	80 ppm	Debéda, H. et al., 2013
ZnO nanotubes ZnO nanorods	Diethylamine	10 ppm	Kilinc, N. et al., 2014
Zeolite	2-nitrotoluene	0.1 ppm	García-Romeo, D. et al., 2014
MOF (HKUST-1)	Xylene	0.4 ppm	Xu, T. et al., 2016
Functionalized-CNTs	Benzene	1 ppm	Clément, P. et al., 2016
Functionalized mesoporous silica	Aniline and acetic acid	≈ppm	Bao, Y.Y. et al., 2018

1.4 (NANO)MATERIALS AND APPLICATIONS

(Nano)materials and their applications are an important part in several research fields and in particular in Analytical Chemistry. Indeed, the Analytical nanotechnology is considered a breakpoint in the Analytical Chemistry field. Special attention has been paid to the study of (nano)materials for improving or developing techniques to give rise numerous analytical applications. Nowadays, there are a wide variety of (nano)materials that can be used to improve the performance of analytical process. The materials studied in the present Thesis have been organized in three groups depending on the building framework: Si-based, C-based and metallic-based materials. Specifically, PDMS, mesoporous silica and C₁₈ as Si-based materials, CNTs as C-based materials and AgNPs and MOF as metallic materials. The selection of these materials is due to their notable use in Analytical Chemistry, which are the 66% of all the materials used (data from

Web of Science). Within these classifications, some materials can be also organized as function of the scale of size such as the nanomaterials. In our case, AgNPs, CNTs and mesoporous silica have specific properties due to their nanometric size and so they can also be classified as nanomaterials.

1.4.1 Si-based materials

1.4.1.1 PDMS

PDMS is an organosilicon compound based on units of $\text{Si}(\text{CH}_3)_2\text{O}$ (See Figure 12). This polymer is one of the most used in several fields due to its optical clarity, chemical inertness, biocompatibility, non-bioaccumulable, non-toxic, flexibility, thermal stability, low cost and easy of processing (Dittrich, P. S. and Manz, A., 2006; Lee, J.N. et al., 2003; Löttersy, J.C. et al., 1997; Nazari, A.M. et al., 2016; Stankova, N.E. et al., 2015).

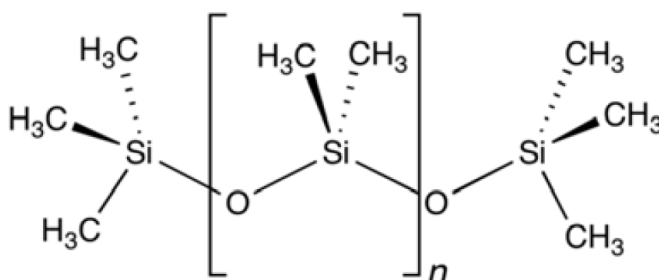


Figure 12. Chemical structure of PDMS.

This thesis is mainly focused in two different applications of PDMS: (a) as extractive phase for in-valve IT-SPME coupled on-line to different systems, mainly miniaturized liquid chromatography and (b) as polymeric matrix to develop in-situ sensing devices.

a) PDMS as extractive phase

PDMS is the most commonly used polymer as extractive phase for GC commercial capillary columns. It is crosslinked and chemically bonded as coating on the inner surface of capillary. In the market, there are GC capillary columns with several percentages of PDMS, usually from 95 to 50%. PDMS-based capillaries can be applied in IT-SPME thanks to inherent hydrophobicity (Bodas, D. and Khan-Malek, C., 2007) of PDMS, together with its other interesting properties. This hydrophobicity does not enable aqueous solvents to penetrate and to swell the polymer, allowing the extraction of analytes from aqueous media or other hydrophilic solvents frequently used in analytical chemistry. Under these conditions, analytes from the solvents are transported to the PDMS where the extraction takes place. Satisfactory results are reported by using capillary columns based on PDMS coupled to LC systems (Campins-Falcó, P. et al., 2010; Seethapathy, S. and Górecki, T., 2012). The weak point of PDMS used in IT-SPME is the commonly low extraction efficiencies achieved. As a consequence, a current research trend is focused on the improvement of extraction efficiencies, selectivity and stability either by functionalization of capillaries or by the synthesis of new (nano)materials. In this way, nanostructured coatings appear as an interesting alternative to improve the extraction efficiency (See section 4.2.1 of this Thesis). As can be observed in Figure 13, the evolution of citations about PDMS as extractive phase evidences the continuous interest in this polymer during the last five years.

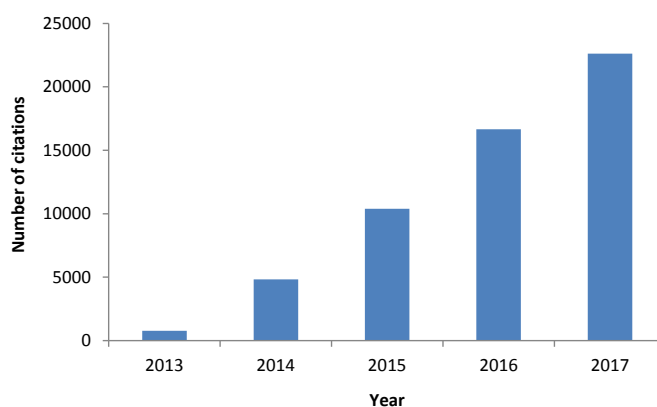


Figure 13. Number of citations on Web of Science for matching the following search terms: “PDMS” OR “Polydimethylsiloxane” AND “extractive phase” between 2013 and 2017 (March 2018).

b) PDMS as support for sensing devices

Another of the multiple applications of the PDMS derived from its benefit properties is the development of colorimetric sensors, both in air and water. That is why some authors have used PDMS as supporting material for embedding chromophores into the polymeric matrix. In this respect, *Table 9* presents several works in which PDMS has been used as supporting material in sensing devices. Working in the same direction, MINTOTA group have developed a patent based on a passive sensor where the chromophores NQS or 4-N,N-dioctylamino-4'-trifluoroacetylazobenzene (ETH^T4001) are immobilized into PDMS for in-situ detection of amines in atmospheres (*Campins-Falcó, P. et al., 2016*). From this patent, PDMS-based matrix has been evaluated as encapsulant of dyes, specifically NQS and Co(SCN)₂, for developing sensors that allow in-situ detection of analytes as diverse as a biocide in industrial products, casein in effluents from dairy industries and amphetamine-like compounds and ketamine in street drugs.

Table 9. Examples of PDMS-based colorimetric sensors reported in the literature between 2010-2018.

Device	Matrix	Analyte	Analytical signal	Reference
CdSe/CdS-QDs embedded in PDMS	Atmosphere	Hydrogen sulfide	- Fluorescence quenching - Visual color change	Xu, H. et al., 2010.
PDMS-6-(4'-methoxyphenoxy)-5,12-naphthacenequinone	Atmosphere	n-Butylamine	- Visual color change	Park, I.S. et al., 2012.
Methyltriethoxysilane /PDMS-OH ormosil coating doped with rose anthocyanin	Indoor air	Formaldehyde	- UV-Vis absorbance - Visual color change - Atomic Force microscopy	Meng, Q. et al., 2014.
PDMS-Thymol/Nitroprusside	Water	Ammonium	- UV-Vis absorbance	Prieto-Blanco, M.C. et al., 2015
NQS or ETH ^T 4001 embedded in PDMS/TEOS	Atmosphere	Ammonia Aliphatic amines	-UV-Vis absorbance (reflectance mode) -Visual color change	Campins-Falcó, P. et al., 2016.
PDMS-TEOS-SiO ₂ NPs-TMB-HRP	Commercial product	Hydrogen peroxide	- UV-Vis absorbance	Pla-Tolós, J. Et al., 2016 b.
PDMS-TEOS-SiO ₂ NPs-TMB-HRP-Glucose oxidase	Human serum	Glucose	- Image analysis (color intensity) - UV-Vis absorbance	Pla-Tolós, J. Et al., 2018.

Even though the favorable properties of PDMS, its use for sensors in aqueous samples with polar compounds is difficult because of its hydrophobicity. To overcome this limitation, hydrophilic compounds such as tetraethyl orthosilicate can be added to increase the hydrophilicity (Campins-Flcó, P. et al., 2016; Jornet-Martínez, N. et al., 2016a). Copolymerization reactions between polymeric fraction (PDMS) and silicon alcoxide, specifically TEOS, give, as a result, a hybrid material in which both PDMS (organic fraction) and TEOS (inorganic fraction) take part in the mixed network (Tamayo, A. and Rubio, J., 2010). Chemical-physical treatments by UV/ozone (Ma, K. et al., 2011) or oxygen plasma (Tan, F. et al., 2010) which required expensive equipment and tedious steps can be replaced by the easy copolymerization between PDMS and TEOS in order to achieve hydrophilicity. Moreover, this polymeric mixture is usually cracked when the network is gelled. In order to prevent the cracks, SiO₂NPs can be added in the polymeric mixture. Li et al., 2013 have already performed the incorporation of SiO₂NPs into the coating sol and concluded that NPs cause an increase of pore size that prevents the cracking.

In fact, hybrid PDMS/TEOS/SiO₂NPs material has been studied for developing the sensors based on NQS in this Thesis.

1.4.1.2 Bondesil C₁₈

Bondesil C₁₈ phase is based on a hydrocarbon of 18 carbon atoms which is chemically bonded to silica (Figure 14). Silica particles are available in many shapes (regular spherical or irregular), sizes (0.9-10 μm and larger), porosities (as large as 1000 Å), and is either fully porous or they have a solid core by design. Since the surface of the silica is covered with hydrocarbons, the polarity of the material is very low. As is well known, this material has been widely used as adsorbent phase. The popularity of a C₁₈ stationary phase is that it offers a simple hydrophobic interaction. Due to its hydrophobicity and easy packing, the main use of C₁₈ is in a reverse phase chromatography, as well as in treatment samples techniques. It should be remembered the main characteristics of bondesil C₁₈ such as wide pH range stability, reproducible, high throughput, easy packing in columns (capillary, stainless steel, peek and glass) that have made it a very popular material.

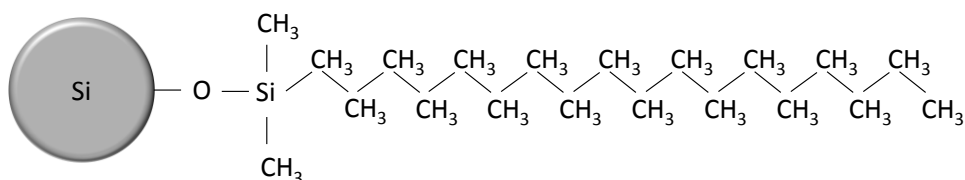


Figure 14. Chemical structure of bondesil C₁₈.

Bondesil C₁₈ is typically used as abrasive solid material for MSPD which is used for the analysis of solid and semisolid samples. Many times a chemical derivatization of analytes retained onto the sorbent is required. This methodology offers clear advantages over derivatizations carried out in liquid phase, such as the improvement of the reaction rates and the simplification of the overall derivatization procedure. A solid phase derivatization approach could be combined with MSPD by using C₁₈.

In the present thesis, we have evaluated for the first time the possibility of use bondesil C₁₈ material for combining MSPD and the solid phase derivatization technique as an alternative to simplify sample preparation for the determination of amphetamines in hair. In addition, C₁₈ has been also employed as dispersant phase in MSPD for the determination of a phtalate in sediments.

1.4.1.3 Mesoporous silica

Mesoporous silica materials have received considerable attention due to their excellent features such as ordered pore structure, high surface area, large pore volume, tunable mesostructure, narrow pore size distribution and their possible synthesis in a wide range of morphologies, as for instance spheres, rods, discs, among others (Dou, B. et al., 2011; Kosuge, K. et al., 2007; Qin, Y., 2013). Since the size of pore can be varied from 2 to 50 nm, mesoporous silica is considered a nanomaterial. From 2016, almost 8000 publications have dealt with mesoporous silica (data from Web of Science searching mesoporous silica as topic). Indeed, this material is employed in a wide range of application areas. These include its use as adsorbent for environmentally hazardous (Hamdi, K. et al., 2016), catalysis (Liu, C.C et al., 2018; Tsai, C.H. et al., 2018), drug delivery

(Gary-Bobo, M. et al., 2012; Saroj, S. and Rajput, S.J., 2018; Wang, L.Y. et al., 2018) and electronics (Yamben, S.D. et al., 2017). In this case, we will focus on its capacity as adsorbents. Many works reported the great potential of mesoporous silicas as adsorbents for VOCs (Dou, B., et al., 2011; Hamdi, K. et al., 2016; Hung, C. and Bai, H., 2008). Following this context, mesoporous silica has been used in resonant microcantilevers to enhance the sensing performance. Their huge surface area allows the adsorption of more molecules and thus, higher mass-adding is leded inducing a higher frequency-shift sensing signal. Various types of mesoporous silica are well documented in the literature (SBA-15, SBA-16, MCM-41, MCM-48, KIT-6, MCF, etc). *Table 10* shows the main characteristics of the most common mesoporous silica types.

Table 10. Characteristics of SBA-15, MCM-41 and MCF-types mesoporous silica. MCM: Mobile Composition of Matter, SBA: Santa Barbara Amorphous, MCF: Mesoporous Cellular Foam (Beck, J. S. et al., 1992; Kruk, M. et al., 2000; Selvam, P. et al., 2001).

Characteristics	MCM-41	SBA-15	MCF
Pore geometry	hexagonal	round	spherical
Internal structure	2-D hexagonal array	2-D hexagonal array	3-D mesocellular foam
Pore diameter (nm)	1.5-10	4-30	22-42
Pore volume (cm ³ g ⁻¹)	0.84	1.06	1.6
Surface area (m ² g ⁻¹)	>1000	680	445-618

Among mesoporous silica material, MCM-41 and SBA-15 are considered the most common adsorbents studied for VOCs (Gibson, L. T., 2014). MCF silica is another most recently type of mesostructured material studied that have attracted a great deal of attention. MCF is a three-dimensional material with ultra-large mesopores (up to 50 nm) that are hydrothermally robust. In terms of structure, MCF is composed of spherical cells interconnected by window pores with a narrow size distribution (≈ 10 nm) (Li, Q. et al., 2010; On, D.T. and Kaliaguine, S., 2003; Schmidt-Winkel, P. et al., 1999). Due to its 3D system based on cellular form with larger pores than MCM-41 or SBA-15 and so, showing enhanced adsorption, MCF seems to be an interesting candidate to be used as sensing layer of resonant microcantilevers.

The aim of this thesis has been to investigate the ability of MCF silica as sensing material for microcantilever development.

1.4.2 C-based materials

Among the different varieties of C-based nanomaterials described for analytical purposes, carbon nanotubes have been the most widely used in several applications. In this thesis, we will focus on carbon nanotubes due to their outstanding properties.

CNTs are based on sheets of carbon atoms organized in a hexagonal pattern (graphite lamella) rolled up either on a single tube (SWCNTs) or concentric SWCNTs held together by van der Waals forces (MWCNTs). MWCNTs can range from one outer and one inner tube (double-walled nanotube) up to more than 100 tubes. The lengths of CNTs can varied from a few hundred nanometers to several microns. With regard to the outer diameters, SWCNTs have diameters range from 1 to 10 nm while diameters of MWCNTs ranged from 5 to a few hundred nm. The surface areas of CNTs can vary from 150 to 1500 m² g⁻¹. In general, MWCNTs presents superior adsorption capacity than SWCNTs. Thus, CNTs characteristics depend on the different factors such as lengths, diameters and number of layers.

From the discovery of CNTs in 1991 (*Iijima, S., 1991*), a new era in materials science and nanotechnology has been opened. During the last five years, more than 85.500 publications reported the use of CNTs in a wide variety of applications in electronic devices, drug carriers, electrochemical and biological sensors, among many others (*Bin, L. et al., 2018; Ghrera, A.S. et al., 2018; Pérez-López, B. and Merkoçi, A., 2011; Wu, Z.X. et al., 2018*). Due to the high surface-to-volume ratio of CNTs, they are considered attractive sorbents for extraction and microextraction techniques, increasing the extraction efficiencies. CNTs have been extensively tested as sorbents for SPE and fiber SPME because they can interact with a variety of compounds through different mechanisms such as hydrogen bonding, π - π stacking interactions, electrostatic and van der Waals forces, and hydrophobic interactions (*Bahzadi, M. et al., 2013; Feng, X. et al., 2014; Kueseng, P. and Pawliszyn, J., 2013; Liang, X. et al., 2014; Ravelo-Pérez, L.M. et al., 2010; Song, X.Y. et al., 2014; Xu, J. et al., 2013; Zhang, B.-T., 2013*).

In the first application of CNTs as SPME sorbent, MWCNTs coatings were prepared by dipping silica fibers into a suspension of MWCNTs in dimethylformamide (Wang, J-X. et al., 2006). The fibers were used for the

extraction of polybrominated diphenyl ethers in water and milk samples by immersing them directly into the samples. Then, the fibers were inserted into a GC injector at 295 °C for desorption of the analytes. Considerable enhancement factors in the responses compared to typical coatings such as PDMS and activated carbon were achieved. Additionally, the surface of CNTs can be modified by changing their polarity or functionalizing in order to improve the sensitivity and selectivity of the extraction process (Pyrzynska, K., 2011; Valcarcel, M. et al., 2008). In this context, acidic oxidation of CNTs leads to the introduction of carboxylic groups in the surface which enhances the retention efficiency for charged or polar compounds at proper pHs. Liu et al. immobilized –COOH functionalized MWCNTs onto the external surface of a fused silica fiber using epoxy resin glue. The fibre was then inserted into a polyether ether ketone (PEEK) tube which was used as the injection loop in an in-valve IT-SPME configuration. The proposed device was applied to the extraction of aniline compounds from water (Liu, X.-Y. et al., 2008). Although there are many works using CNTs as adsorbent material for SPME, the use of CNTs for IT-SPME is still a challenge. Indeed, a few examples of CNTs functionalized capillary columns for IT-SPME are described in the literature. In recent studies, the use of different PDMS-based capillary columns modified covalently with CNTs has been reported. *Figure 15* shows a MWCNTs coating capillary, as an example. The new coatings provided high efficiencies for the extraction of some pollutants from water samples (Jornet-Martínez, N. et al., 2015b; Moliner-Martínez, Y. et al., 2015b).

In the present thesis, the extraction capabilities of CNTs modified PDMS-based capillaries for amphetamines have been explored in order to extend the IT-SPME methodology to drug analysis in oral fluid. To our knowledge CNTs modified coating have never been used for the extraction of drugs by in-valve IT-SPME.

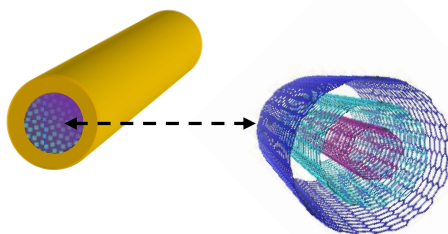


Figure 15. Schematic representation of MWCNTs coating.

1.4.3 Metallic-based materials

1.4.3.1 AgNPs and AuNPs

When a metallic NP is excited by light with higher wavelength than NP size, the conduction electrons on the metal surface undergo a collective oscillation with electromagnetic wave frequency but confined in the nanometric size. As a consequence of oscillations of electric charges, scattering of the incident light is produced (*Figure 16*). Thus, a new absorbance band known as Surface Plasmon Resonance band (SPR) is observed in the UV-vis spectrum. The characteristics of this band depend on several parameters of NPs such as shape, size and dielectric constant. At nanometric scale, the movement of electrons is confined and color is result from the absorption and scattering of light instead of the free movement of electrons and metallic color originated from the reflection of light at macroscopic scale.

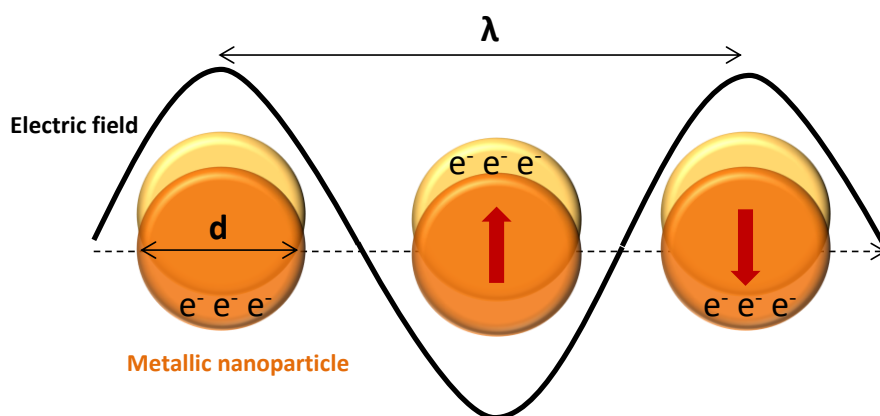


Figure 16. Illustration of the excitation of localized SPR where electrons in the metal nanoparticle are driven into oscillation due to coupling with incident light; d is the diameter of sphere and λ is the wavelength of the light.

AgNPs and AuNPs are extraordinarily efficient at absorbing and scattering light and, unlike many dyes, their color depends on the size and the shape of the particle. *Figure 17* shows an example of surface plasmon band of spherical AgNPs of 15-20 nm and their characteristic color (used in this Thesis). The peak wavelength and width and the effect of secondary peaks due to secondary resonances yield a

unique spectral fingerprint for a plasmonic nanoparticle with specific size and shape.

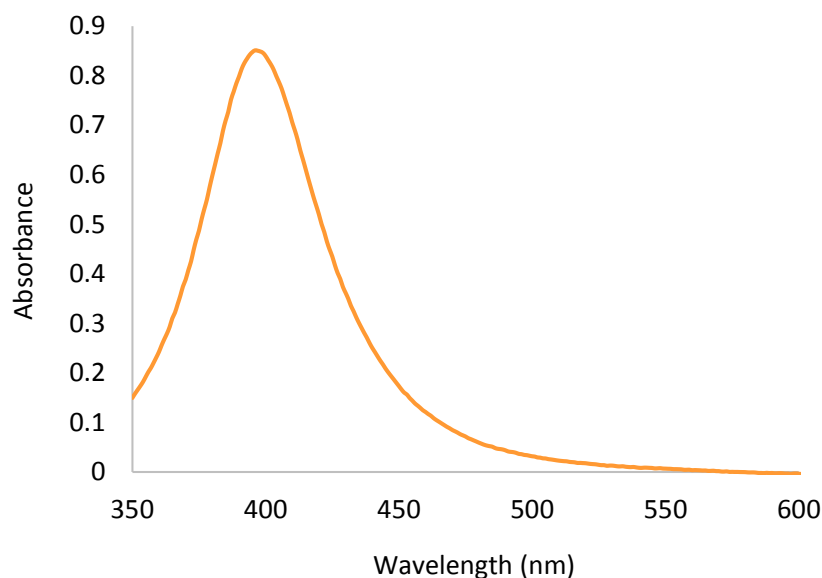


Figure 17. Surface plasmon band of spherical AgNPs of 15-20 nm.

AgNPs are relevant materials; around 66000 articles of AgNPs have been published from 2007 in several fields of science (data from Web of Science, researching “AgNPs” OR “silver nanoparticles” in the title). *Figure 18* shows the impact of this topic in our society in the last years.

AgNPs are used in numerous fields owing to their unique properties:

- Nanometric size and high surface area.
- Functionalizable surfaces.
- Sensitivity to physical-chemical changes.
- Stability in aqueous media.
- Biocompatibility.
- Antibacterial.
- High electrical conductivity.
- Low sintering temperature.

From these optical, electrical, thermal and biological properties, AgNPs have become one of the most widely marketed nanomaterials for several applications, including medical devices, food, antibacterial agents, household, healthcare, optical sensors, cosmetics, orthopedics, drug delivery and industry purposes (Bala, R. et al., 2018; Nowack, N. et al., 2011; Zhang, X.F. et al., 2016).

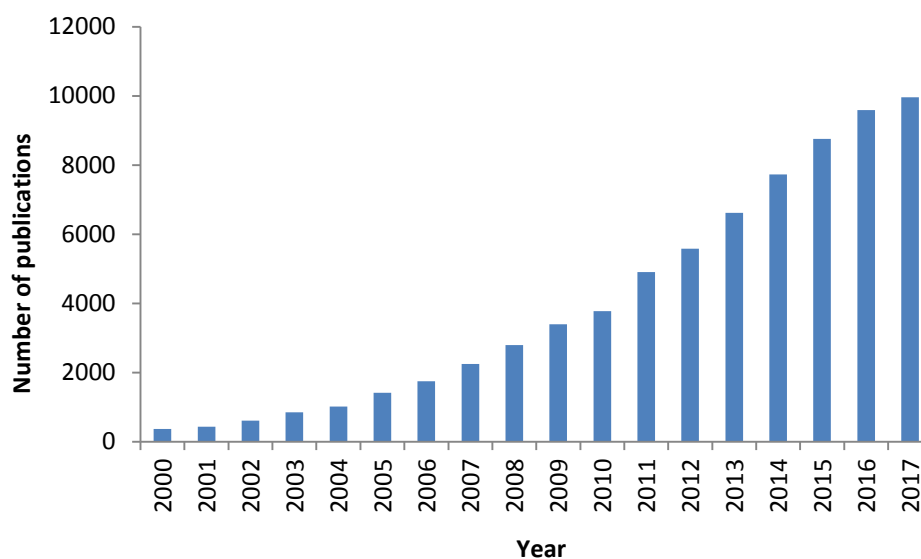


Figure 18. Evolution of number of citations about AgNPs from the year 2008 in the web of science by searching “AgNPs” OR “Silver nanoparticles” in the field of “Title”.

Although AgNPs are exploited for various applications, we will focus on their potential application as sensors. Thanks to the novel optical properties before mentioned, AgNPs are considered suitable materials for the development of (bio)sensors (Jornet-Martínez, N. et al., 2014; Ma, X.-M. et al., 2018; Saha, K. et al., 2012). From the discovery of the SPR in 1980, the interest in using the optical properties of NPs to detect several chemical compounds has grown considerably. Table 11 evidences the huge number of publications where AgNPs have been applied as colorimetric sensors of different analytes based on their SPR band.

Table 11. Selected examples of plasmonic assays.

Assay	Analyte	Matrix	LOD	Reference
AgNPs in solution	Melamine	Raw milk	0.01-1.26 mg L ⁻¹	Ma, Y. et al., 2011.
AuNPs on paper	Mercury (II)	Water	50 nM	Chen, G.H. et al., 2014.
TMB-H ₂ O ₂ system catalyzed-bare AuNPs	Sulfide	Water	80 nM	Deng, H.-H. et al., 2014.
Antiaggregation of AuNPs	Hydrogen Sulphide	Air	0.5 ppm (v/v)	Zhang, Z. et al., 2014
AuNPs in solution	Spermine	Urine	15 ng L ⁻¹	Jornet-Martínez, N. et al., 2015a.
AuNPs-aptamers	MAMP MDMA	Water	10 ⁻⁴ M 5 mM	Yarbakht, M. and Nikkhah, M., 2016.
Anti-aggregation of AgNPs	Manganese (II)	Water	20 nM	He, Y. and Zhang, X., 2016.
Citrate-capped silver nanoparticles	Creatinine	Urine	53.4 nM	Alula, M.T. et al., 2018
Sucrose capped gold nanoparticles	Vitamins B1 and B6	Rice	8 ng mL ⁻¹ for B1 and 15 ng mL ⁻¹ for B6	Shrivastava, K. et al., 2018.

The analytical signal of the plasmonic sensors is based on changes in the SPR band. In presence of the analyte, the monodisperse solution of AgNPs (≈ 400 nm) changes from yellow to brownish due to an aggregation of these NPs (≈ 500 nm). Different colors are observed according to their dispersion/aggregation state. As a consequence, the SPR band is shifted to longer wavelengths and broadened when the analyte is present (*Figure 19*).

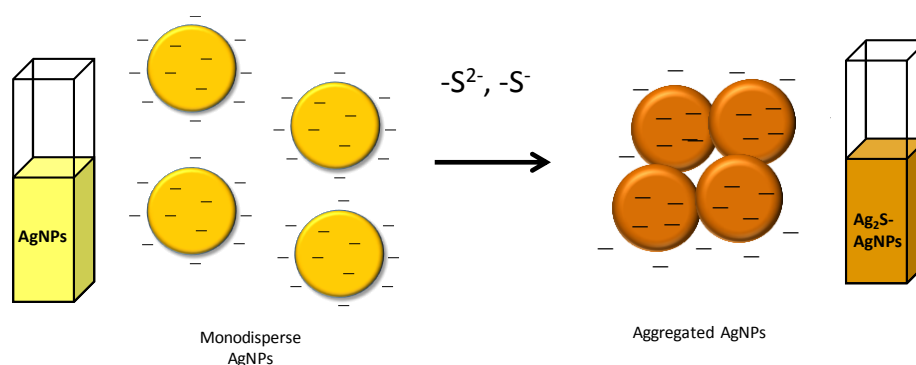


Figure 19. Schematic picture of the AgNPs aggregation in presence of sulphure compounds (See Section 4.3.2.1).

These changes on the SPR band can be monitored by UV-Vis spectroscopy allowing a rapid colorimetric detection of analytes. Moreover, the quantification of analyte concentration can also be carried out observing the band changes because the aggregation of NPs is a function of the analyte concentration. The main advantage of the nano-plasmonic sensors is their high sensitivity from nanomolar up to picomolar levels. In fact, nano-plasmonic sensors offer a viable detection technique in some medical diagnostics where the concentration of biomarkers secreted is usually very low. Additionally, it is remarkable the simplicity by visual inspection without expensive equipment and energy sources.

Although AgNPs are not as widely used as AuNPs, considerable efforts are being directed toward the development of new plasmonic sensors for different applications. Most works about plasmonic sensors have been concerned with using AuNPs instead of AgNPs due to the difficulty of AgNPs synthesis. However, AgNPs have specific characteristics which are advantages such as higher molar extinction coefficient increasing sensitivity when using absorption spectroscopy.

In this Thesis, a plasmonic sensor based on AgNPs immobilized on nylon has been developed to detect sulphur compounds from breath which are responsible of oral malodour.

1.4.3.2 MOFs

Self-assembled structures of metal oxide cations and organic electron donor linkers are the basis of MOFs. These compounds are crystalline materials built from the interconnection of metal ions or clusters and organic linkers to produce porous architectures. *Figure 20* shows an example of MOF compound with its porous (*Figure 20A*) and crystalline (*Figure 20B*) characteristic structure.

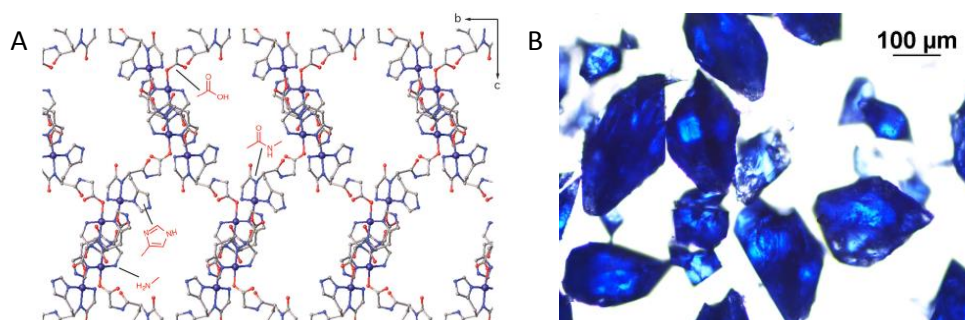


Figure 20. A) Porous structure and B) Crystalline structure of Cu(GHG) MOF.

MOFs are nanostructured materials increasingly used in sample preparation because they present surface areas in the $1000\text{-}10400\text{ m}^2\text{ g}^{-1}$ range. They also offer excellent thermal stability. Examples of the utility of MOFs-based coatings for fiber SPME have been reported for the extraction of benzene homologues from air samples (*Chang, N. et al., 2012*) or alkanes from fuel and biological samples by the head space SPME (HS-SPME) approach (*Cui, X-Y. et al., 2009*), among others. Besides other applications like catalysis or sensing, the unlimited structural/chemical flexibility of MOFs enables rational tailoring of the chemical function and pore dimensions for more efficient and selective separation of gases (*Nugent, P. et al., 2013*), hydrocarbons (*Blonch, E. et al., 2012; Cadiau, A. et al., 2016*) or aromatic compounds (*Warren, J. E. et al., 2014*). In this context, the separation of chiral molecules is also very relevant.

Compared to classical adsorbents like zeolites or activated carbons, MOFs are arguably more promising candidates for chiral separation. They can be more easily engineered to deploy a periodic array of chiral channels that are accessible to guest sorption and can be modified in size, shape, and chemical function to optimize mass-transfer rates and chiral recognition. However, the application of

MOFs in enantioselective separation is still limited by the small number of homochiral phases available (Duerinck, T. and Denayer, J. F. M., 2015; Kutzscher, C. et al., 2016). These are typically prepared either by using chiral templates that drive enantiomeric resolution, by postsynthetic linker exchange for partial grafting of chiral linkers in the metal struts at the expense of accessible porosity, or by direct synthesis from enantiopure linkers. This last route is compatible with the use of naturally occurring chiral linkers like camphoric and tartaric acid, amino acids (aa's) or oligopeptides. Among these, peptides are well suited to producing functional, chiral MOFs whose robustness, chemical stability, and porous response can be effectively modulated by suitable choice of aa's in the peptidic sequence (Katsoulidis, A. P. et al., 2014; Martí-Gastaldo, C. et al., 2012, 2014; Rabone, J. et al., 2010). The broad choice of side-chain groups available from proteinogenic aa's can be also used to engineer the chiral pockets in their structure with specific functions. Due to their crystalline nature, peptide MOFs are also well suited for theoretical modeling of the enantiomer interactions in a confined space, which is important to accelerate screening of materials already available and guide the design of more efficient systems.

This thesis reports the ability of a chiral Cu(II) three-dimensional (3D) MOF based on the tripeptide Gly-L-His- Gly (GHG) for the separation of chiral drugs.

1.5 ANALYTES AND ANALYTICAL TECHNIQUES

The materials investigated during this Thesis have been applied to develop analytical methodologies in order to determine compounds related to fields as diverse as health, environment, industry and forensic control. The characteristics of these diverse analytes as well as the interest of their determination are detailed. In addition, a bibliographic review of the documented methods for their analysis is included.

1.5.1 Phthalates

Phthalates are esters of phthalic acid. They are synthetic compounds widely used as plasticizers in plastic, rubber, cellulose, and styrene production to increase their flexibility, strength, optical clarity and resistance. These compounds are present in many consumer products such as food preservatives, children toys

cosmetics, medical equipment, flooring, organic solvents, personal care products, detergents, packaging, adhesives, paper coating, lacquers, and insecticides, among other products (Biedermann-Brem, S. et al., 2008; Gonzalez-Castro, M. I. et al., 2011; Green, R. et al., 2005; Schettler, T., 2006). Due to the phthalates are not chemically bound in the polymer matrix, they can leach into the environment (Chaler, R. et al., 2004; Muñoz-Ortuño, M. et al., 2012; Net, S. et al., 2015). For this reason, phthalates are nowadays considered as ubiquitous environmental pollutants. Indeed, the United States Environmental Protection Agency (USEPA) and the European Union (EU) have established limits of certain phthalates in drinking and natural waters (Directive 2008/105/EC; USEPA, 1991). This is the case of di(2-ethylhexyl)phthalate (DEHP), which is the most widespread phthalate produced and used (Figure 21).

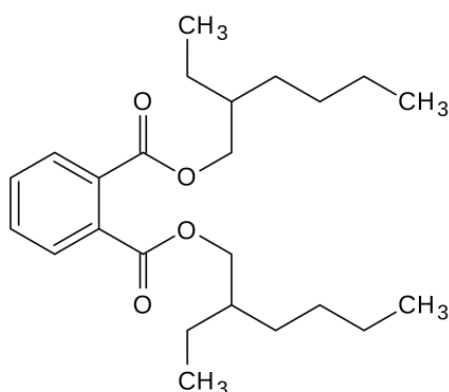


Figure 21. Structure of the phthalate analyzed in this thesis, DEHP.

DEHP is commonly found in drinking water, and it is also the most persistent phthalate found in wastewaters (Alatríste-Mondragón, F. et al., 2003). The maximum annual average concentration established for DEHP by Directive 2008/105/CE in surface waters is 1.3 g L^{-1} , whereas the USEPA has set the maximum concentration level for this compound in water systems at 6 g L^{-1} . It is important to note that DEHP have been classified as very dangerous substance in EU regulation on chemicals (REACH Regulation (CE) n. 1907/2006).

Owing to the low solubility and highly hydrophobic nature of DEHP, it is preferentially absorbed and/or adsorbed to the organic matter suspended in

water as well as to the organic fraction of soils and sediments. Furthermore, DEHP tends to bio-accumulate in fats, and a considerable transfer of this compound from sediments to aquatic organisms may occur (Huang, P.-C. et al., 2008). Therefore, the development of simple and sensitive methods for the determination of DEHP in sediments is of great interest for the characterization of aquatic ecosystems.

Due to the low concentration of DEHP in environmental matrices, extensive sample preparation is often obligatory to reach the required sensitivity. Several extraction methods have been proposed like Soxhlet, ultrasonic extraction, SPE or LPE with high sample, solvent and energy consumption (Hui, I. et al., 2010; Huang, P.-C. et al., 2008; Wen, X. L. et al.; 2008; Yuan, S.-Y. et al., 2010). In addition, special efforts are necessary during sample manipulation to prevent contamination by DEHP, as this compound is present in packages, solvents, or glassware (Frankhauser-Noti, A. and Grob, K., 2007). Obviously, elimination or simplification of the sample preparation would reduce the risk of contamination. As discussed above, simplified and miniaturized analytical methods which reduce the sample handling as well as the consumption of sample and reagents are an interesting alternative. In this sense, in-valve IT-SPME has been used as reliable technique for the enrichment of traces of DEHP from water samples or extracts obtained after the treatment of solid samples to be analyzed by LC. A further improvement of the sensitivity can be achieved by coupling IT-SPME to capillary LC (Campíns-Falco, P. et al., 2010; Cháfer-Pélicas, C. Et al., 2008; Muñoz-Ortuño, et al., 2012).

In this thesis, the analysis of DEHP in sediment and water samples have been effected by a new method based on MSPD and on-line IT-SPMECapLC-DAD, with the subsequent reduction of sample, organic solvent, and energy consumption and no evaporation step required in comparison with other methods.

1.5.2 Biocides

According to Directive 98/8/EC of the European Parliament and of the Council Official Journal of the European Communities, biocidal products are defined as active substances and preparations containing one or more active substances, put up in the form in which they are supplied to the user, intended to destroy, deter, render harmless, prevent the action of, or otherwise exert a

controlling effect on any harmful organism by chemical or biological means. These products are present in detergents used in many areas such as food industry, household, institutions and hospitals (Ash, M. and Ash, I., 2004), for disinfecting or preserving. Patents about cleaning products including compounds like the biocide N-(3-aminopropyl)-N-dodecyl-1,3-propanediamine (ADP), trimethyl-tetradecyl-ammonium chloride (TMTDAC) (See Figure 22), and quaternary ammonium compounds (QACs) mixtures have been published (Tezel, U., 2009). However, their use can pose risks to humans, animals and the environment owing to their intrinsic properties. In fact, the use of these agents is subject to regulations. Therefore, quantification of biocides is mandatory in two scenarios, in industrial formulations and waste samples for monitoring environmental impacts. This Thesis is focused on two widely used biocides listed below.

1.5.2. 1 Benzalkonium chloride (BAK)

The main active ingredients of biocide formulations are QACs or sodium hypochlorite (Biondi, C.A.M., 2011). The QACs are most effective against microorganisms at neutral or slightly alkaline pH and become virtually inactive below pH 3.5. They are incompatible with anionic detergents, demonstrating a high degree of binding to non-ionic surfactants. The (bio)available QAC concentration reaches a maximum at the critical micellar concentration (CMC). Any agent or factor that decreases the CMC also diminishes the available QAC concentration, and so the biocidal activity. It was demonstrated that anions decrease the CMC of QACs by reducing the polarity of the head and in turn increase the hydrophobicity of the overall molecule as they form ion pairs with the QACs.

QACs with high CMCs are more mobile in engineered and natural systems but also more toxic than the ones with lower CMCs. The combination of these two facts brings out a detrimental environmental impact associated with QACs, that is, QACs which are more mobile and (bio)available are more toxic. This information may be used in the selection of mixtures of QACs in industrial applications by assessing the trade off between sanitation efficiency and their impact on the treatment of QAC-bearing wastewaters. The most employed QAC is BAK, which has activity against yeast, fungi and positive and negative Gram bacteria. BAK is classed as a Category III antiseptic active ingredient by the United States Food and Drug Administration, meaning "available data are insufficient to classify as safe

and effective and further testing is required". BAK (See Figure 22) is a mixture of homologues of the alkylbenzyl dimethylammonium chlorides with predominance of the alkyl chain of 12 carbon atoms C₁₂-BAK (CMC 3.80 mM), followed in a minor proportion by the chain of 14 carbon atoms C₁₄-BAK (CMC 1.70 mM).

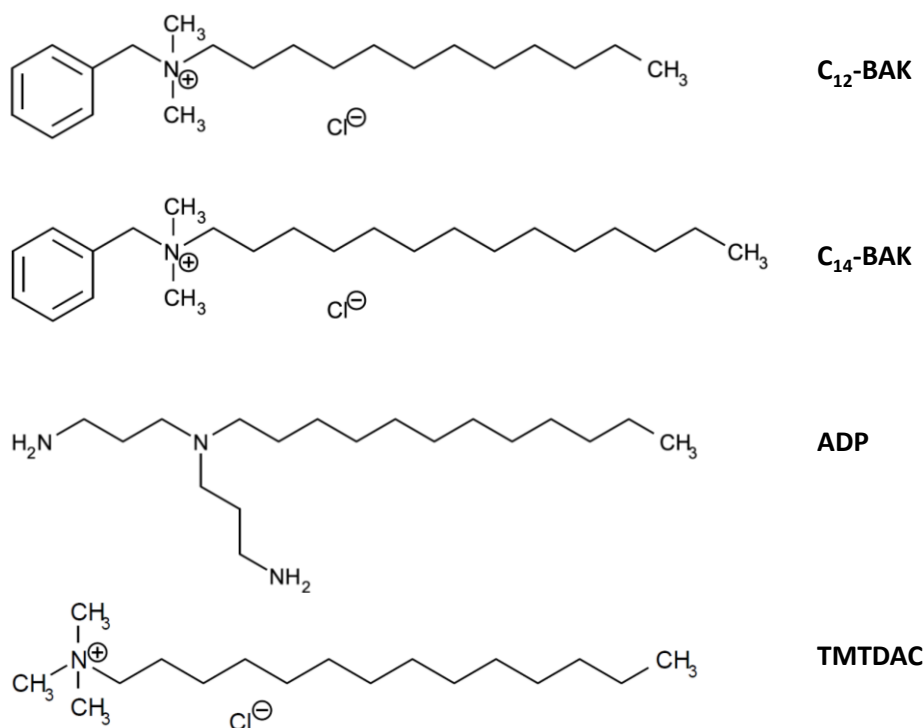


Figure 22. Structure of several biocides studied in this Thesis.

Several methods for BAK determination in industrial production (Prieto-Blanco, M.C. et al., 1999; 2009b; 2013a) and environmental monitoring are documented (Bassarab, P. et al., 2011; Boyacı, e. et al., 2014; Chen, Y. et al., 2012; Martínez-Carballo, E. et al., 2007; Peng, X.-T. et al., 2011). Specific problems related with their surfactant nature have been reported in some works (Prieto-Blanco, M.C. et al., 2012). The chemistry of surfactants is different from that of other analytes due to the formation of direct/reversed micelles or monomers that may cause specific matrix effects. The mixtures of surfactants in biocide formulations are one of the complex cases in which new parameters should be considered for establishing analytical procedures. In most methods of the

literature, the conditions are optimized from standard solutions containing a similar amount of all surfactants studied or for developing their determination in water samples. However, the matrix effect for samples, in which one of the surfactants (in this case BAK) is a minor component or impurity, is not covered for these methods.

Thus, the present Thesis establishes the parameters under which matrix effects may occur in formulations containing BAK as minor component and other co-biocides and provides new strategies of analysis combining on-line IT-SPME/CapLC. For commercial formulation, this method allows the control of BAK as potential impurity when different formulations are made in the same production plant or when the cleaning of an installation requires biocides.

1.5.2.2 ADP

Another effective biocide is the ADP, a polyamine with an alkyl chain of 12 carbon atoms (*See Figure 22*). This compound is used to formulate several commercialized disinfectants due to its activity against enveloped viruses and positive and negative Gram bacteria. Some authors have described episodes of allergic contact dermatitis due to the ADP (*Schliemann, S. et al., 2010*). Analytical techniques such as NMR spectroscopy, LC coupled MS and acid–base titration have been employed in the literature for the characterization and quantification of ADP (*Mondin, A. et al., 2014*). Also, derivatization techniques can be used thanks to the primary amine groups of this biocide.

Due to one of the trends in analytical chemistry is to develop in-situ sensors, a colorimetric sensor based on NQS/TEOS/ SiO₂NPs embedded into PDMS has been developed in this Thesis for controlling ADP dosage in industrial formulations.

1.5.3 Casein

Casein is the major protein component of milk, comprising about 80% of the total milk protein. It is made up of different proteins, including α S1-, α S2-, β -, and κ -casein, which together with calcium phosphate form aggregates, known as casein micelles. These proteins, have a primary amino acid sequence (*See Figure*

23) different from each other and occupy different positions in micelle performing specific functions (Steinhauer, T. et al., 2014).

The cleaning procedures are important in dairy industries to ensure the hygiene in food processing lines by completely removing the organic or inorganic materials and bacteria from the surfaces. In these industries, a cleaning in place (CIP) process is used for cleaning and disinfection of circuits, tanks, pasteurizers and packing, filling and metering equipments. In this process, large amounts of wastewaters mainly composed of diluted milk, which is based on fat, protein (mainly casein), calcium and lactose, are generated. These effluents may cause serious environmental problems, without the appropriate treatment. Indeed, the organic matter load of these wastewaters enables the reproduction of microorganisms producing significant changes in the biological oxygen demand. Therefore, the dairy industry should treat its effluents efficiently and effectively before disposal into public drainage. Considering these aspects, a method for the determination of the main components such as the casein in these effluents is still needed to control these effluents.

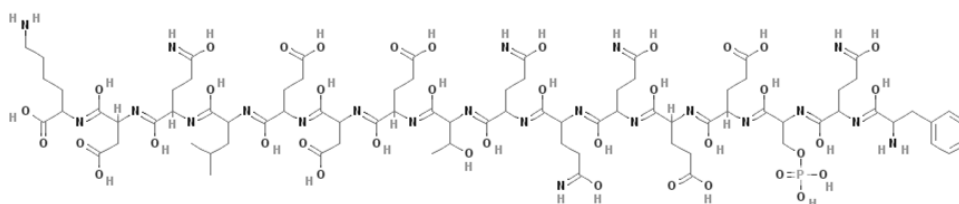


Figure 23. Structure of casein (data from PubChem).

There are different methods proposed in the literature for the determination of proteins. The most traditional method is the Kjeldahl method (Lynch, J.M. et al., 1998), followed by colorimetric and spectrophotometric methods (Chutipongtanate, S. et al., 2012) such as Biuret (Oftedal, O.T. et al., 2014), Bradford (Aminian, M. et al., 2013; Kamizake, N.K.K. et al., 2003), Lowry (Kusunoki, H. et al., 2012), Ninhydrin (Drochioiu, G. et al., 2006) and bicinchoninic acid (BCA) (Kralj, J.G. et al., 2014). More selective methods, such as chromatographic techniques with different detectors (Pierri, G. Et al., 2013; Ramirez-Palomino, P. et al., 2014) or immunoassay test (ELISA Kit) (Stumr, F. et al.,

2010) have also been described for the determination of casein in food. Most of these methods are not in situ analysis and require long analysis time.

In response to the aforementioned demand of in-situ analysis, casein from dairy effluents has been estimated in this Thesis by in-situ sensor based on the entrapment of NQS/TEOS/SiO₂NPs in PDMS.

1.5.4 Drugs

1.5.4.1 Amphetamine-like designed drugs

The consumption, production and commercialization of illicit synthetic drugs remain a serious problem in many countries. Amphetamine-type drugs have become popular drugs of abuse because they are powerful stimulants of the central nervous system. *Figure 24* shows the structure of these compounds, based on an aromatic group linked to an aliphatic amine, primary and secondary amine for amphetamine (AMP) and methamphetamine (MAMP), respectively, and an additional methylenedioxy group in the case of 3,4-methylenedioxyamphetamine (MDA) and 3,4-methylenedioxymethamphetamine (MDMA).

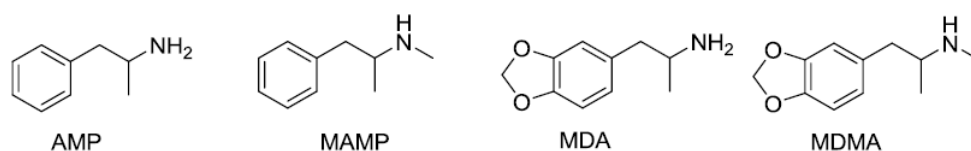


Figure 24. Structure of the amphetamine-like drugs studied in this Thesis.

Although AMP has been traditionally the most used compound, there are recent signs of the increasing availability of MAMP. Under the generic name “ecstasy” a wide variety of illicit tablets are sold in which MDMA is usually the active substance, but they may also contain other methylenedioxyated amphetamines such as MDA and 3,4- methylenedioxyethylamphetamine (MDEA) (Freudenmann, R.W., Spitzer, M., 2004). According to official investigations, the confiscated amounts of amphetamines and ecstasy samples have increased in recent years (European Drug Report, 2017; Vidal Giné, C. et al., 2016). The identification and quantification of amphetamine-like drugs in illicit tablets have

been described using several methods such as capillary electrophoresis (*Piette, V. and Parmentier, F., 2002*), infrared spectroscopy (*Schneider, R.C. and Kovar, K.A., 2003*), GC (*El-Haj, B.M. et al., 2013*) and LC (*Cháfer-Pericas, C. et al., 2004; Herráez-Hernández, R. et al., 2001*). However, these methods require strict laboratory conditions and trained personnel. The development of suitable assays for instant detection of the most frequently used drugs in roadside drug testing would facilitate to take legal actions quickly. Uncertainty and delay times could be also minimized through the development of workplace screening tests. Therefore, there is an increasing interest in the development of affordable, easy-to-use and handheld devices for the detection and identification of these illicit substances in the field.

Fast detection of illicit drugs has been reported using portable ion mobility (*Verkouteren, J.R. and Staymates, J.L., 2010*), Fourier transform infrared (FTIR) (*Tsujikawa, K. et al., 2008*) and Raman spectrometers (*Weyerman, C. et al., 2011*). It is important to note that street drugs are usually modified with excipients (i.e. adulterants or diluents) because they are typically sold by weight. Adulterants are added to mimic the effects of the active substance in order to increase its perceived quality, whereas diluents are simply added to increase the bulk and, consequently, the profits of the drug dealer. Owing to the wide range of excipients and their proportions in illicit preparations, the utility of spectral libraries available is limited hindering the characterization of some street samples. Moreover, these spectrometers are expensive and trained personnel may be required to interpret the results.

The employment of colorimetric tests such as Marquis, Mandelin, Mecke and Simon's tests can be an inexpensive and fast alternative for on-site screening of suspected illicit substances. However, some of these tests are hazardous; for example, the Marquis and the Mandelin reagents involve concentrated sulfuric acid. Also the reagent solutions may be instable and solutions have to be prepared daily. For on-site control tests, the employment of solid sensors is generally considered a more convenient alternative.

From previous works, a solid sensor based on NQS/TEOS/SiO₂NPs embedded into PDMS has been developed in this Thesis for the in-situ screening of amphetamine-like compounds (AMP, MAMP, MDMA, MDA).

On the other hand, these substances are frequently detected in biological samples such as blood, urine, oral fluid, sweat and hair samples (Wada, M. *et al.*, 2010). Immunoassays are generally used for screening tests, whereas chromatographic methods are required for quantitative purposes. Usually, LC methods entail previous chemical derivatization to convert the analytes into highly detectable products due to the poor sensitivity achieved with typical LC detectors. In this respect, a variety of methods have been proposed using different reagents (Cháfer-Pericás, C. *ET AL.*, 2004; Herráez-Hernández, R. *et al.*, 2002; Tomita, M. *et al.*, 2007). According to the results obtained in previous studies, fluorogenic reagent 9-Fluorenylmethyl chloroformate (FMOC) has been selected for derivatization in this Thesis (Cháfer-Pericás, C. *et al.*, 2004). Although there are several methods available for drugs in plasma and urine samples, there is an increasing interest in the analysis of alternative biological matrices such oral fluid or hair (Baciu, T. *et al.*, 2015; Lledo-Fernandez, C. and Banks, C.E., 2011; Vogliardi, S. *et al.*, 2015; Wada, M. *et al.*, 2010).

Oral fluid has gained popularity as an alternative to urine and blood for the investigation of illicit drug consumption because sample collection is non-invasive and it can be done under supervision. The main difficulty encountered in the analysis of these fluids is the low amount of sample available and the low concentration of analyte present in the sample. Thus, a selective and sensitive method is required such as in-valve IT-SPME-CapLC. In addition, the extraction capability of the capillary coating is the key factor to extend the applicability of in-valve IT-SPME to drug analysis in oral fluid whose volume is limited.

In the present thesis, CNTs modified coating of capillary column has been evaluated for the extraction of AMP, MAMP and ephedrine (EP) derivatives in oral fluid by in-valve IT-SPME coupled online to CapLC-FLD.

Another biological sample of growing importance in the investigation of illicit amphetamines consumption is the hair. Besides being a non-invasive collection, hair can be used to establish long intake history of abusers. In addition, the risk of sample adulteration and/or deterioration during storage and transportation is minimized. Consequently, an increasing number of methods are being developed to identify and quantify amphetamines in hair samples. However, the isolation of amphetamines from hair continues to be a critical step of the analysis. Successful examples for the extraction of amphetamines from hair by microwave (Chang, Y.J. *et al.*, 2014) and ultrasound (Zhu, K.Y. *et al.*, 2012) have been reported. MSPD has

emerged as an attractive approach for the isolation of drugs from hair (Míguez-Framil, M et al., 2010, 2011, 2013).

In the present thesis, we have evaluated for the first time the possibility of combining MSPD and the solid phase derivatization technique as an alternative to simplify sample preparation for the determination of drugs such as AMP, MAMP, EP and MDMA in hair, which integrates sample disruption, analyte isolation and derivatization.

A large number of drug compounds are often dosed as racemic mixtures. Enantiomers generally display different pharmacological and/or toxicological properties which can lead to a loss in activity or even to undesired side reactions. This is the case of MAMP and EP, which are chiral compounds used as recreational drugs, but also as components in pharmaceutical preparations of therapeutic use as bronchodilators and respiratory stimulants. Both compounds possess a chiral center and exist as a pair of enantiomers (See Figure 25) which may differ in their pharmacological activity as well as in their metabolic and pharmacokinetic characteristics. Separation of MAMP or EP enantiomers is frequently required in clinical, forensic, and toxicology laboratories. In this context, the discovery of chiral adsorbents that permit rapid separation of individual enantiomers is of utmost importance in the early stages of drug research in the pharmaceutical industry. This type of separation relies on chiral recognition rather than shape/size selectivity. Hence, preferential interaction of one of the enantiomers with the adsorbent must lead to the formation of a transient diastereomeric adsorbate, whose free energy shall be sufficiently different for enantiomeric separation to take place.

In this Thesis, a chiral Cu(II) 3D MOF based on the tripeptide GHG for the enantioselective separation of MAMP and EP is reported.

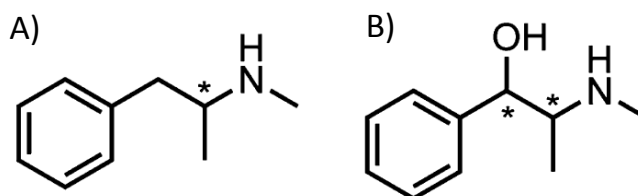


Figure 25. Structures of chiral A) MAMP and B) EP.

1.5.4.2 Ketamine

Ketamine is an anesthetic drug widely prescribed for human and animal use. It is also used as an analgesic in the treatment of certain diseases. *Figure 26* illustrates the structure of ketamine. Since its introduction in the market, this compound is increasingly used for recreational purposes, probably because it can be produced at low cost and has a relatively favorable safety profile, although at high doses it can cause severe dysfunctions. Its main effects associated with recreational use are diminishing of attention and learning ability, floating sensations, loss of memory, and distortion of time and space (*Giorgetti, R. et al., 2015*).

Today, the consumption of ketamine for recreational purposes has become a major problem, especially among young people. Moreover, as ketamine is colorless, tasteless and odorless it can be added to drinks or illicit drug preparations, which facilitates sexual assaults (*Demoranville, T. and Verkouteren, J.R., 2013*). There is also an increasing concern about the role of ketamine in traffic accidents (*Waddell-Smith, R.J.H., 2007*). The United Nations Office on Drugs and Crime (UNODC) and the European Monitoring Centre for Drugs and Drug Addiction (EMCDDA) have included this drug in their respective lists of new psychoactive substances (*Smith, J.P. et al., 2015*). For these reasons ketamine has become a controlled substance in most countries, and there is an increasing demand of tests for the rapid identification of suspected samples at the sites of trafficking and consumption, as well as for roadside tests (*Gjerde, H. et al., 2016; Vidal Giné, C. Et al., 2016*).

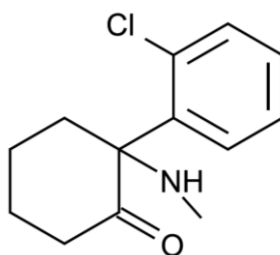


Figure 26. Structure of ketamine.

In spite of the high level of sensitivity, accuracy and specificity of chromatographic methods, they are not suitable for on-site analysis because the instrumentation is complex, and strict laboratory conditions and trained personnel are required. So far, only a few portable chromatographs are commercially available and they do not allow high speed high resolution separations (*Sharma, S. et al., 2015; Smith, P.A. et al., 2012*). Different assays with portable instrumentation have been proposed for ketamine detection such as IMS (*Demoranville, T. and Verkouteren, J.R., 2013*) and deep UV-Vis reflected optical fiber sensors (*Li, Q. et al., 2012*). Nevertheless, because of their simplicity, colorimetric test are the option preferred for a rapid preliminary on-site detection of ketamine in suspected samples; positive findings are then derived to the laboratory for confirmatory chromatographic analysis.

Different reagents have been proposed for presumptive colorimetric tests, such as the Mandelin reagent (ammonium metavanadate in concentrated sulphuric acid), which produces reddish-orange derivative in the presence of ketamine that can be distinguished from the colors originated by other drugs, or the Janovsky reagent (a mixture of m-dinitrobenzene and potassium hydroxide in ethanol) which forms with ketamine a brown-purple precipitate. Another reagent used for presumptive detection of ketamine is cobalt (II) thiocyanate (Co(SCN)_2). Under basic conditions, this reagent produces an insoluble purplish blue derivative with ketamine (Morris test) (*Morris, J.A., 2007*). A modification of the test has been reported by Maddah et al. based on the immobilization of the Co(SCN)_2 reagent onto silica NPs (*Maddah, B. et al., 2015*). A portion of the developed material is added to a solution of the suspected sample in a spot plate, so that the formation of a purple precipitate is indicative of the presence of ketamine. The same reagent was used by Musile et al. in a paper-based microfluidic device for the presumptive detection of different drugs, including ketamine (*Musile, G. et al., 2015*). On-site colorimetric detection of illicit drugs by solid sensors is a popular alternative because the manipulation of solutions is minimized and they can be operated by unskilled personnel, as aforementioned.

Thereby, a colorimetric sensor for ketamine estimation has been developed in this Thesis based on the entrapment of Co(SCN)_2 onto PDMS. Experimental parameters have been optimized.

1.5.5 Diphenylamine (DPA)

An important component of gun propellants is the DPA. *Figure 27* shows the DPA structure. This organic compound is used as a stabilizer in order to deter the decomposition of the explosive products nitrocellulose and nitroglycerine, which are present in some smokeless powders used as propellant (*Burleson, G. L. et al., 2009; Laza, D. et al., 2007*). Thus, this stabilizer remains on the shooter body, mainly onto the index fingers and thumbs of the hands, after discharge a firearm and it may be used as an indicator of gunshot residues (GSRs). A suspect in firearm-related crime can be successfully identified if GSRs are reliably analyzed.

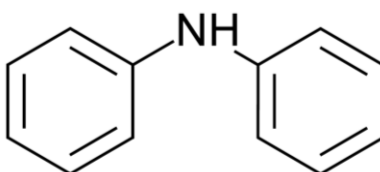


Figure 27. Structure of DPA.

Several techniques have been described for the DPA estimation such as LC (*Laza, D. et al., 2007; Mei, H. et al., 2016*), GC (*Tarifa, A. and Almirall, J. R., 2015*) and capillary electrophoresis (*Bernal Morales, E. et al., 2004*). Although MS coupled to GC or LC offers suitable sensitivity, the chromatographic techniques present issues. Thermal degradation of DPA can occur by GC and the wide range of polarities of compounds present in GSRs can limit the LC. Many works have successfully identified DPA by using MS without any chromatographic system such as tandem MS (*Tong, Y. et al., 2001*), desorption electrospray ionization-MS (*Morelato, M. et al., 2012*), nanoelectrospray ionization MS (*Scherperel, G. et al., 2009*) and IMS (*Arndt, J. et al., 2012*).

In addition, the analysis of inorganic gunshot residues (IGSRs) combined with the organic gunshot residue (OGSR) analysis, such as DPA, may strength the probative value of forensic sample. IGSRs are usually spherical particles mainly composed of barium (Ba), lead (Pb) and tin (Sb) (*Tarifa, A. and Almirall, J. R., 2015*). Other metallic elements such as calcium (Ca), aluminium (Al), copper (Cu), iron (Fe), zinc (Zn), nickel (Ni), silicon (Si), and potassium (K) can also be found. The presence of these metallic particles has been traditionally confirmed by

electronic microscopy coupled to Energy Dispersion X-ray (EDX) detector (*Bailey, M. J. et al., 2009; Dalby, O. et al., 2010*). However, the analysis of IGSRs has limitations. False positive results can be produced from inorganic particles derived from environmental and occupational sources (*Farokhcheh, A. and Alizadeh, N. et al., 2013; Grima, M. et al., 2012*). Moreover, the commercial growth of lead and other toxic metals free ammunition can also produce false negative results when only IGSR are analysed (*Oommen, Z. and Pierce, S. M., 2006*). The issues related to false positives and negatives can be overcome by combining IGSR and OGSR analysis.

The present Thesis reports the detection of DPA from shooter hands by IT-SPME-Cap-LC-DAD with easy sampling by cotton swab and vortex-assisted extraction. A complementary analysis of IGSRs has been carried out in order to confirm the presence of gunshot residues on shooter hands.

1.5.6 Volatile sulfure compounds (VSCs)

VSCs such as hydrogen sulphide (H₂S), methyl mercaptan (CH₃SH) and dimethyl sulphide (CH₃)₂S in breath are the main responsible for oral malodor (*Hunter, C.M. et al., 2005*). They are produced by various oral bacterial species that degrade and metabolize sulfur-containing amino acids. This symptom is one of the most common problems to people in their day to day life and interpersonal relations. In addition, halitosis can be related to different diseases, as for example, periodontitis and gingivitis (*Amou, T. et al., 2014*). According to several studies reported (*Alagirisamy, N. et al., 2010; Bolle, C.M. and Beikler, T., 2012*), levels <100-200 µL m⁻³ of VSCs are normal, while levels >300-400 µL m⁻³ would be due to a persistent oral odor and severe halitosis. These VSCs are considered suitable biomarkers for breath quality evaluation (*Tangerman, A. and Winkel, E.G., 2007*). Thus, the quantitative analysis of sulfide compounds from the breath allows the evaluation of the efficiency of therapeutic treatment on halitosis (*Suarez, F.L. et al., 2000*).

GC is the most commonly used method for the detection of VSCs (*Wardencki, W., 2000*) due to its sensitivity and precision. However, GC is expensive and requires special knowledge for operation. Instead of GC, several portable and easy to use breath clinics have been proposed including HalimeterTM and Oral

Chroma™ (Salako, N.O. and Philip, L., 2011; Tangerman, A. et al., 2008). Electromechanical sensors based on the absorption of sulfur on semiconductor metal oxide or conductive polymer producing an electrical signal have been also proposed (Pandey, S.K et al., 2012). Nevertheless, many electromechanical sensors present problems of stability to environmental factors. Optical sensors have advantages in terms of applicability easy-functionality and low-cost, allowing in situ detection with zero energy cost. Several optical sensors have been described in the literature for sulphure compounds detection. Bismuth-paper based sensor has been proposed as colorimetric sensor for testing human bad breath (Rosolina, S. M. et al., 2016). The detection of H₂S in air has been also carried out by bubbling the air through AgNPs solution and measuring UV-Vis spectra (Zhang, Z. et al., 2014). In the same way, another work has used colloidal AgNPs in solution to detect organo-sulfur compounds generated during onion deterioration (Sachdev, D. et al., 2016). Although NPs in solution allow satisfactory sensitivity, the development of solid sensor is an interesting alternative as in-situ clinical kit.

In this Thesis, a rapid and portable AgNPs paper-based sensor has been developed to detect H₂S, SH⁻, S²⁻ at μL m⁻³ levels as a potential enabler for oral malodour.

CHAPTER 2. OBJECTIVES

During the last years, the need to simplify analytical methodologies has prompted a thorough review of the fundamental pillars upon which the conventional analytical techniques have been built. From the revision of the literature in analytical chemistry, there is a tendency aiming to automate the pretreatment of the sample in order to reduce the manipulation of sample as well as the time of analysis. Related to this, miniaturized techniques for carrying out the extraction, separation and detection are also being sought to decrease the solvent consumption and waste generation, besides enhancing the sensitivity.

On the other hand, there is also a growing interest in developing sensors for in-situ determinations, most of them based on image analysis and bearing in mind the internet. Some of the benefits of these sensors are the simplicity, speed and on-site analysis without highly trained personnel requirement and in some case with connectivity. Both trends are associated to the emerge of Green Analytical Chemistry which highlights the need to develop ecofriendly methodologies. The development of these sustainable methodologies, which are framed within the current trends in analytical chemistry, is governed by the use of new (nano)materials.

Thus, the main aim of this Thesis is to propose new (nano)materials for the improvement of the existing analytical methods, as well as the development of new analytical methods and tools with high-throughput in terms of operation and sustainability. Specifically, this Thesis is focused on the study of (nano)materials for their application in extraction, separation and detection techniques. These materials have been classified in three groups, metallic based, Si-based and C-based materials. Listed below are the three specific objectives in which the Thesis has been divided based on the applications of the investigated materials.

1. Development of analytical methodologies based on IT-SPME on-line coupled to CapLC to achieve the features of miniaturization and automatization. To address this objective, the polymer polydimethylsiloxane, a silicone-based material, has been evaluated as extractive phase of IT-SPME for its application in the determination of compounds of environmental, industrial and forensic interest in different types of matrices, such as (i) DEHP in sediments, (ii) BAK in industrial formulations and (iii) DPA on shooter hands. In the same context, PDMS coating functionalized with CNTs (SWCNTs and MWCNTs), one of the most popular C-based materials, have been evaluated

for enhancing the extraction efficiencies in the analysis of AMP-like drugs in oral fluids. For carrying out these methodologies, the analytical performance and the application to real samples has been evaluated.

2. Development of analytical tool based on MSPD using the C-based material C₁₈ as dispersant phase for the disruption, preconcentration and derivatization of amphetamines from hair matrix. This technique has been also used in the treatment of sediments for the extraction of DEHP. MSPD is considered an alternative to classical multi-step methods for sample treatment. The analytical process is considerably simplified; it reduces sample and solvents consumption and it does not need special instrumentation. Moreover, MSPD is well-suited for miniaturization. In the context of sample treatment, a novel chiral Cu(II) 3D MOF based on tripeptide GHG has been evaluated as chiral phase in SPE for the enantioselective separation of MAMP and EP.
3. Design of colorimetric sensors based on the embedding of derivatizing reagents into PDMS as solid support for the in-situ analysis of compounds of interest in industrial (e.g. casein estimation in effluents from dairy industries and biocide control in industry formulations) and police control fields (e.g. amphetamine-type and ketamine estimation in illicit street drugs). Another type of colorimetric sensor based on the immobilization of AgNPs on nylon membrane has been developed. This nanosized metallic-based material can be used as clinical kit since it allows the detection of sulfide compounds from breath, which are responsible of halitosis. Several parameters that affect the analytical response and stability have been tested, as well as the analytical performance has been evaluated. In addition, the benefits that offer the DI analysis have been also tested.

It should be marked that the three objectives of this Thesis have been carried out taking into account the principles of Analytical Chemistry. The objectives presented above have become possible thanks to the pre-doctoral scholarships:

- FPU13/05220 *Ayudas para la formación de profesorado universitario*, Spanish Ministry of Education, Culture and Sports, 4 years.
- EST16/00962 *Ayudas a la movilidad para estancias breves y traslados temporales - Programa Estatal de Promoción del Talento y su Empleabilidad*,

Spanish Ministry of Education, Culture and Sports. Internship in IMS Laboratoire of University of Bordeaux, 3 months.

In addition, the results of the present Thesis are part of the following research projects granted to MINTOTA research group of the Analytical Chemistry Department at the University of Valencia.

- CTQ 2011-26760 Project, granted by Spanish Ministry of Economy and competitiveness - *Proyectos de Investigación Fundamental no Orientada, "Nuevas estrategias de análisis en técnicas cromatográficas miniaturizadas que incorporan la microextracción en fase sólida en tubo con nuevos (nano)materiales"*, 2011-2014.
- PROMETEO 2012/045 Project, granted by Generalitat Valenciana - *Programa Prometeo para grupos de investigación de Excelencia, "Desarrollo de nuevas estrategias para el diseño de dispositivo de análisis in situ"*, 2012-2015.
- CTQ2014-53916-P Project, granted by Spanish Ministry of Economy and competitiveness and EU from FEDER - *Programa Estatal de Fomento de la Investigación Científica y Técnica de Excelencia Subprograma Estatal de Generación de Conocimiento, "Desarrollo de nuevas estrategias para el diseño de técnicas de cromatografía líquida miniaturizada en línea: nanopartículas, contaminación secundaria"*, 2015-2017.
- OTR2015-15329ASESO, University of Valencia - ITENE Company contract to study smart inks field, *"Estudios de viraje de distintas etiquetas frente a dos variables, el tiempo y la concentración de H₂S"*.
- PROMETEO 2016/109 Project, granted by Generalitat Valenciana - Programa Prometeo para grupos de investigación de Excelencia, *"Desarrollo de nuevas estrategias para el diseño de dispositivos de análisis in situ: nano y biomateriales"*, 2016-2019.

Thanks to both scholarship and projects, ten scientific papers (one of them submitted), one book chapter and one patent have been resulted from this PhD Thesis. The corresponding impact factors from the Journal of Citation Reports are shown in each paper.

- I. M. Muñoz-Ortuño, **A. Argente-García**, Y. Moliner-Martínez, J. Verdú-Andrés, R. Herráez-Hernández, M.T. Picher, P. Campíns-Falcó, *A cost-effective method*

- for estimating di (2-ethylhexyl) phthalate in sediments*, Journal of Chromatography A. 1324 (2014) 57-62. Impact factor (JCR 2018): 3.981.
- II. M. Muñoz-Ortuño, **A. Argente-García**, Y. Moliner-Martínez, C. Molins-Legua, P. Campíns-Falcó, *Polydimethylsiloxane composites containing 1,2-naphthoquinone 4-sulphonate as unique dispositive for estimation of casein in effluents from dairy industries*, Analytica Chimica Acta. 873 (2015) 31-37. Impact factor (JCR 2018): 4.950.
- III. **A. Argente-García**, M. Muñoz-Ortuño, C. Molins-Legua, Y. Moliner-Martínez, P. Campíns-Falcó, *A solid device based on doped hybrid composites for controlling the dosage of the biocide N-(3-aminopropyl)-N-dodecyl-1,3-propanediamine in industrial formulations*, Talanta. 147 (2016) 147-154. Impact factor (JCR 2018): 4.162.
- IV. M.C. Prieto-Blanco, **A. Argente-García**, P. Campíns-Falcó, *A capillary liquid chromatography method for benzalkonium chloride determination as a component or contaminant in mixtures of biocides*, Journal of Chromatography A, 1431 (2016) 176-183. Impact factor (JCR 2018): 3.981.
- V. **A. Argente-García**, Y. Moliner-Martínez, E. López-García, P. Campíns-Falcó, R. Herráez-Hernández, *Application of Carbon Nanotubes Modified Coatings for the Determination of Amphetamines by In-Tube Solid-Phase Microextraction and Capillary Liquid Chromatography*, Chromatography, 3 (2016) 7-21.
- VI. **A. Argente-García**, Y. Moliner-Martínez, P. Campíns-Falcó, J. Verdú-Andrés, R. Herráez-Hernández, *Determination of amphetamines in hair by integrating sample disruption, clean-up and solid phase derivatization*, Journal of Chromatography A. 1447 (2016) 47-56. Impact factor (JCR 2018): 3.981.
- VII. **A. Argente-García**, N. Jornet-Martínez, C. Molins-Legua, Y. Moliner-Martínez, P. Campíns-Falcó, *A solid colorimetric sensor for the analysis of amphetamine-like street samples*, Analytica Chimica Acta. 943 (2016) 123-130. Impact factor (JCR 2018): 4.950.
- VIII. J. Navarro-Sánchez, **A. Argente-García**, Y. Moliner-Martínez, D. Roca-Sanjuán, Dmytro Antypov, P. Campíns-Falcó, Matthew J. Rosseinsky, C. Martí-Gastaldo, *Peptide Metal–Organic Framework for Enantioselective Separation*

of *Chiral Drugs*, Journal of the American Chemical Society. 139 (2017) 4292-4297. Impact factor (JCR 2018): 13.858.

- IX. **A. Argente-García**, N. Jornet-Martínez, R. Herráez-Hernández, P. Campíns-Falcó, *A passive solid sensor for in-situ colorimetric estimation of the presence of ketamine in illicit drug samples*, Sensors and Actuators B. 253 (2017) 1137-1144. Impact factor (JCR 2018): 5.401.
- X. **A. Argente-García**, L. Hakobyan, C. Guillem, P. Campíns-Falcó, *A new method for estimating diphenylamine in gunshot residues as a new tool for identifying both, inorganic and organic ones, in the same sample*. Submitted
- XI. Y. Moliner-Martínez, **A. Argente-García**, R. Herráez-Hernández, J. Verdú-Andrés, C. Molins-Legua, P. Campíns-Falcó, *Environmental Applications of Instrumental Chemical Analysis, Determination of organic pollutants in environmental samples*, Part II, **Chapter 14**, Mahmood Barbuooti. Apple Academic Press. CRCpress, a Taylor & Francis Group, 471-532, 2015, ISBN 9781771880619.
- XII. **A. Argente-García**, N. Jornet-Martínez, C. Molins-Legua, Y. Moliner-Martínez, J. Verdú-Andrés, R. Herráez-Hernández, P. Campíns-Falcó, *Sensor colorimétrico basado en nanopartículas de plata para la determinación de compuestos volátiles de sulfuro*, **Patent 201600440**, Presentation data: 24/05/2016.

Below are listed the International and National Conferences where several works carried out during the Thesis have been presented.

- I. **A. Argente-García**, Y. Moliner-Martínez, M. Muñoz-Otruño, J. Verdú-Andrés, R. Herráez-Hernández y P. Campíns-Falcó, *Capillary liquid chromatography coupled to in-tube solid-phase microextraction for estimating Di(-ethylhexyl) phthalate in different matrices*, Poster, 3rd SCARCE International Conference: Bridging toxicants, stressors and risk-based management under water scarcity, Valencia (Spain), 2012.
- II. N. Jornet-Martínez, M. Muñoz-Ortuño, Y. Moliner-Martínez, R. Herráez-Hernández, **A. Argente-García**, P. Campíns-Falcó, *Cost effective methodology as analytics tools for DEHP and their degradation products in*

- waters*, Poster, 4th Scarce. Towards a better understanding of the links between stressors, hazard assessment and ecosystem services under water scarcity, Cádiz (Spain), 2013.
- III. M. Muñoz-Ortuño, **A. Argente-García**, R. Herráez-Hernández, Y. Moliner-Martínez, C. Molins-Legua, J. Verdú-Andres, P. Campíns-Falcó, *NQS based optical sensor for on site real time determination of casein in effluents from dairy industries*, Poster, Extech2014. 16th International symposium on advances in extraction technologies, Creta (Greece), 2014.
- IV. Y. Moliner-Martínez, **A. Argente-García**, M. Muñoz-Ortuño, R. Herráez-Hernández, J. Verdú-Andrés, C. Molins-Legua and P. Campíns-Falcó, *Development of an in-situ sensor for estimating biocide amine (Bis(3-aminopropyl) dodecylamine) in detergents for food industry*, Poster, Extech2014. 16th International symposium on advances in extraction technologies, Creta (Greece), 2014.
- V. Y. Moliner-Martínez, **A. Argente-García**, M. Muñoz-Ortuño, P. Serra-Mora and P. Campíns-Falcó, *A new approach for in-tube solid-phase microextraction-nano-LC coupling: evaluation of carbon nanotubes based adsorbent phases for environmental analysis*, Poster, 30th International Symposium on Chromatography, Salzburg (Austria), 2014.
- VI. **A. Argente-García**, S. Aparicio-Antón, Y. Moliner-Martínez, C. Molins-Legua, J. Verdú-Andrés and P. Campíns-Falcó, *Determination of Irgarol in coastal waters of the Region of Valencia by in-tube solid phase microextraction coupled to capillary liquid chromatography*, Assistance and poster, Final SCARCE International Conference. River Conservation under Water Scarcity, Tarragona (Spain), 2014.
- VII. **A. Argente-García**, M.C. Prieto-Blanco, M. Muñoz-Ortuño, M. Hurtado-Jiménez, Y. Moliner-Martínez y P. Campíns-Falcó, *Analysis of benzalkonium chloride in biocidal formulation producing matrix effect by using in-tube solid-phase microextraction*, Assistance and poster, HPLC2015. 42nd International Symposium on high performance liquid-phase separations and related techniques, Geneva (Switzerland), 2015.
- VIII. **A. Argente-García**, N. Jornet-Martínez, B. Marí-Boluda, R. Herráez-Hernández, C. Guillem-Villar y P. Campíns-Falcó, *Determination of*







- diphenylamine deposited onto shooter hands by using in-tube solid-phase microextraction coupled to capillary liquid chromatography*, Assistance and poster, HPLC2015. 42nd International Symposium on high performance liquid-phase separations and related techniques, Geneva (Switzerland), 2015.
- IX. C. Molins-Legua, Y. Moliner-Martínez, N. Jornet-Martínez, **A. Argente-García**, J. Pla-Tolos, P. Campins-Falcó, *NQS doped PDMS composite as an alternative environmental observation technology: application to estimate NH₃ emissions from animal production industries*, Poster, XXSEQA 2016, Santiago de Compostela (Spain), 2015.
- X. **A. Argente-García**, N. Jornet-Martínez, Y. Moliner-Martínez, R. Herráez-Hernández, y P. Campíns-Falcó, *Colorimetric kit based on SiO₂ Nanoparticles modified PDMS-TEOS composite for on-site screening of illicit drugs*, Assistance and poster, Workshop NYNA2015. Nanociencia and analytical nanotechnology, Salamanca (Spain), 2015.
- XI. P. Campíns-Falcó, Y. Moliner-Martínez, C. Molins-Legua, R.Herráez-Hernández, P. Serra-Mora, **A. Argente-García**, *New strategies for designing on-line miniaturized liquid chromatography techniques by coupling in-tube solid phase microextraction*, Oral communication, Extech & ISSS: 18th International symposium on advances in extraction technologies and 22nd international symposium on separation sciences, Torun (Polonia), 2016.
- XII. **A. Argente-García**, N. Jornet-Martínez, J. Pla-Tolos, C. Molins-Legua and P. Campíns-Falcó, *Sensitive colorimetric sensor based on silver nanoparticles for sulphur compound detection in water*, Assistance and poster, NET-SCARCE International Conference, Rivers Under Water Scarcity, Threats and Challenges, Barcelona (Spain), 2016.
- XIII. Y. Moliner-Martinez, **A. Argente-García**, J. Pla-Tolos, P. Serra-Mora, L. Hakobyan and P. Campins-Falcó, *Evaluation of in-tube solid phase microextraction coupled to capillary LC with mass spectrometry for the estimation of irgarol-1051 and its polar transformation products in water samples*, Assistance and poster, NET-SCARCE International Conference, Rivers Under Water Scarcity, Barcelona (Spain), 2016.




- XIV. **A. Argente-García**, L. Hakobyan, Y. Moliner-Martínez and P. Campíns-Falcó, *Optimization of sampling and treatment of forensic samples for fast and sensitive estimation of diphenylamine using on-line in-tube solid phase microextraction coupled to capillary liquid chromatography*, Assistance and poster, 2nd Caparica Christmas Conference on Sample Treatment, Caparica (Portugal), 2016.
- XV. **A. Argente-García**, Y. Moliner-Martínez, P. Campíns-Falcó, J. Verdú-Andrés, R. Herráez-Hernández, *Matrix solid phase dispersion integrating sample disruption, clean-up and solid phase derivatization for amphetamine analysis in hair*, Assistance and poster, ExTech2017, 19th International Symposium on Advances in Extraction Technologies, Spain (Santiago de Compostela), 2017.
- XVI. C. Molins-Legua, N. Jornet-Martínez, **A. Argente-García**, Y. Moliner-Martínez, J. Verdú-Andrés, R. Herráez-Hernández, P. Campíns-Falcó, *Immobilization of noble nanoparticles on solid supports: application to detection of sulphur compounds*, Oral communication, ExTech2017, 19th International Symposium on Advances in Extraction Technologies, Spain (Santiago de Compostela), 2017.
- XVII. **A. Argente-García**, N. Jornet-Martínez, R. Herráez-Hernández, P. Campíns-Falcó, *A colorimetric sensor for the on-site detection and quantification of ketamine in illicit drug samples*, Poster, XXI SEQA, Spain (Valencia), 2017.
- XVIII. Y. Moliner-Martínez, J. Navarro-Sanchez, **A. Argente-García**, D. Roca-Sanjuan, D. Antypov, P. Campíns-Falcó, M. J. Rosseinsky, C. Martí-Gastaldo, *Peptide Metal-Organic frameworks as chiral solid-phase extraction sorbents for enantioselective separations of chiral drugs*, Oral presentation, ISSS 2017 23rd International Symposium on Separation Sciences, Austria (Vienna), 2017.
- XIX. J. Navarro-Sanchez, **A. Argente-García**, Y. Moliner-Martínez, D. Roca-Sanjuan, D. Antypov, P. Campíns-Falcó, M. J. Rosseinsky, C. Martí-Gastaldo, *Peptide Metal-Organic for enantioselective separations of chiral drugs*, Poster, International Symposium on composites of metal and covalent organic frameworks: fundamental designs and applications, Granada (Spain), 2017.

CHAPTER 3. METHODOLOGY

3.1 CHEMICALS AND REAGENTS

The chemicals and reagents (analytical grade) employed in this Thesis are summarized in *Table 12*. Commercial suppliers and GHS (Globally Harmonized System of classification and labeling of chemicals) hazard pictograms are also included. The pictograms classify the chemical products by the standardized symbols according to European Union.

Table 12. Summary of reagents and chemicals used in this Thesis, with their suppliers and GHS pictograms, where  = Flammable (GHS02);  = Corrosive (GHS05);  = Toxic (GHS06);  = Harmful (GHS07);  = Health hazard (GHS08);  = Environmental hazard (GHS09).

Chemical/Reagent	Supplier						
Acetone	Merck	X			X		
Acetonitrile	Romil	X			X		
Acetylsalicylic acid	Sigma						
3-Aminopropyltriethoxysilane	Aldrich		X		X	X	
Amphetamine sulfate	Aldrich	X		X			
Ammonium acetate	Panreac				X		
Arginine	Sigma-Aldrich				X		
Bicinchoninic acid disodium salt hydrate	Sigma-Aldrich					X	
Bismuth (III) oxide	Alfa Aesar				X		
Bondesil C ₁₈ (40, 50 μm)	Varian/ Phenomenex						
Caffeine	Guinama			X	X	X	
Cannabinol	Sigma-Aldrich					X	
Cannabidiol	Sigma-Aldrich			X	X	X	
Cocaine hydrochloride	Sigma-Aldrich			X	X	X	
Cobalt (II) thiocyanate	Sigma-Aldrich				X		X
Copper (II) acetate	Sigma-Aldrich		X	X	X		X
Copper (II) oxide	Sigma-Aldrich				X		X
Copper (II) sulfate pentahydrate	Merck				X		
1, 3-Dicyclohexylcarbodiimide	Sigma-Aldrich		X	X	X		
Di (2-ethylhexyl) phtalate	Aldrich			X			
Dimethylformamide	Scharlau	X			X	X	
Dimethyl sulphide	Sigma-Aldrich	X	X	X	X		
Diphenylamine	Sigma-Aldrich			X		X	X
Ephedrine hydrochloride	Sigma-Aldrich				X	X	
Ethanol	Scharlau	X					

Florisil	Aldrich				X		
9-Fluorenylmethyl chloroformate	Sigma		X		X		
Glacial acetic acid	Merck	X	X		X	X	
Glycerol	Sigma				X		
Glucose anhydrous	Scharlau						
Glutaraldehyde	Sigma-Aldrich		X		X	X	X
Gold nanoparticles ^a	Sigma-Aldrich						
Hydrochloric acid	Scharlau		X		X		
Ibuprofen	Sigma-Aldrich				X	X	X
Levamisole hydrochloride	Fluka				X		
Leucine	Sigma-Aldrich						
Lithium carbonate	Alfa Aesar		X		X		
Lysine	Sigma-Aldrich						
Magnesium sulfate	Probus				X		
Maltose-1-hydrate	Panreac						
Mannitol	Scharlau						
Methanol	Scharlau	X		X		X	
Methamphetamine hydrochloride	Sigma-Aldrich						
3,4-Methylenedioxyamphetamine	Sigma-Aldrich			X	X		
3,4-Methylenedioxymetamphetamine	Sigma-Aldrich			X	X		
Methyl mercaptan	Sigma-Aldrich	X		X	X	X	
Multiwall carbon nanotubes	Sigma-Aldrich					X	
N-Benzyl-N-dodecyl-N,N-dimethylammonium chloride	Sigma-Aldrich		X		X		X
N-benzyl-N-tetradecyl-N,N-dimethylammonium chloride	Sigma-Aldrich		X		X		X
Nitric Acid	Panreac		X				
n-Hexane	Scharlau	X			X	X	X
Paracetamol	Guinama				X		
Polydimethylsiloxane Sylgard®184 Kit	Dow corning						
Phosphoric acid	Sigma-Aldrich		X	X	X	X	
Potassium sodium tartrate tetrahydrate	Scharlau		X				
Procaine hydrochloride	Sigma-Aldrich			X	X		
Proline	Sigma-Aldrich				X		
PZT	Ferroperm Piezoceramics Meggit				X	X	X
Saccharose	Guinama						
Silica gel (70-230 mesh)	Aldrich						
Silicon dioxide nanoparticles	Sigma-Aldrich				X		

(5-15 nm)							
Silver nanoparticles (20, 40 and 60 nm) ^b	Sigma-Aldrich						
Single-wall carbon nanotubes	Sigma-Aldrich					X	
Scopolamine hydrobromide	Sigma-Aldrich			X	X	X	
Sodium carbonate	Panreac				X		
Sodium chloride	Probus						
Sodium dihydrogen phosphate monohydrate	Merck				X		
Sodium hydrogencarbonate	Probus				X		
Sodium hydroxide	Panreac		X		X		
Sodium 1,2-naftoquinone-4-sulphonate	Sigma-Aldrich				X		
Sodium sulfide	Sigma-Aldrich		X	X	X		X
Starch	Probus						
Sulfuric acid	Scharlau		X	X		X	
Tetraethyl orthosilicate	Sigma-Aldrich	X			X		
Trimethyl-tetradecyl ammonium chloride	Sigma-Aldrich		X		X		X
Tripeptide H-Gly-L-His-Gly-OH	Bachem®						
Ketamine hydrochloride	Sigma-Aldrich				X		

^a stabilized suspension in 0.1 mM phosphate buffered saline (PBS)

^b 0.02 mg mL⁻¹ in aqueous buffer, contains sodium citrate as stabilizer

LONZABAC, BAK and DECTODICE were supplied by BetelgeuxS.L. Company (Gandía, Spain). Protective coat 244-T polymer, gold paste 8336 and dielectric composite 4702 were purchased from ESL Europe.

3.2 INSTRUMENTATION

The development of the experimental procedure of this Thesis has been carried out by using several instruments and materials:

- Ultrasonic bath Sonitech (TerraTech, Spain)
- Magnetic stirrer (450 W) (Sstuart Scientific)
- Crison microPH 2000 pH-meter (Crison Instruments, Spain)
- Nanopure II water system (Barnstead, UK)
- ZX3 vortex mixer (VELP Scientifica, Italy)
- Thermostat LT200 (Hagh Lange United for water quality, Sapin)
- Nylon membranes (0.45 and 0.22 μm) (Teknokroma, Spain)
- Polypropylene SPE tube (3 mL) (Supelco, USA)
- Polyethylene frits (20 μm porosity) (Supelco, USA)
- Double-sided carbon adhesive tape (8 mm wide x 0.16 mm thick x 1 cm long) (Ted Pella Inc. Redding, US)
- Tape lift kit (Sirchie Finger Print Laboratories, USA)
- Plastic well-plates (Sharlau, Spain)
- Ricoh Aficio MP2550 PCL6 multifunctional printer
- Nikon CoolPix S2600 digital camera (14 megapixels and 5xwide optical zoom)
- Bond Elut C₁₈ 100 mg cartridges (Varian,USA)

The analytical techniques used along this Thesis can be classified into three groups: spectroscopic, chromatographic and microscopic. The sample pretreatment techniques and sensor fabrication will be explained separately.

3.2.1 Spectroscopic techniques

3.2.1.1 UV-Vis spectrophotometry

Spectrophotometric measurements were carried out using a Cary 60 Fiber Optic UV-Vis spectrophotometer (Agilent Technologies, USA). This spectrophotometer is fitted with a remote fiber optic DR accessory from Harrick Scientific Products (Pleasantville, NY) for DR measurements of solid sensors. Data were recorded and processed using a Cary WinUV software (Agilent Technologies

Products, Australia). The spectral range measured was from 200-1000 nm (*Figure 28*).



Figure 28. A) Cary 60 Fiber Optic UV-Vis spectrophotometer and B) Remote fiber optic DR accessory.

3.2.1.2 Infrared spectroscopy

Fourier-transform infrared-attenuated total reflectance (FTIR-ATR) measurements were performed on an Agilent Cary 630 FTIR spectrophotometer fitted with a diamond ATR accessory (Agilent Technologies, Böblingen, Germany). Spectra were recorded in the frequency range of 4000-600 cm^{-1} at a resolution of 4 cm^{-1} . A background scan was made against the air, and 8 scans were averaged for each measurement. For data collection and processing, MicroLab FTIR and ResolutionPro software (Agilent Technologies) were used, respectively (*Figure 29*). FTIR Nicolet 5700 spectrometer in the 4000-400 cm^{-1} range from ground crystals diluted in a KBr pellet was used for the Cu(GHG) characterization.



Figure 29. Cary 630 FTIR-ATR spectrophotometer.

3.2.1.3 RAMAN spectroscopy

Raman measurements for AgNPs sensors characterization were done using Raman spectrometer Horiba-MTB (a Perkin Elmer Raman Station 400). For the laser at 785 nm, 50% of its power was applied with acquisition time of 60 s and 2 accumulations, objective x10 and grating 600 g mm^{-1} (Figure 30).



Figure 30. Horiba-MTB RAMAN spectrophotometer.

3.2.1.4 Electromechanical Impedance spectroscopy

Electromechanical characterization of screen-printed MEMS was carried out with the impedance analyzer (Agilent E5061B) of *Figure 31*, in the range from 5 Hz to 3 GHz. The planar and the first 31-longitudinal vibration mode were measured for the disks and cantilevers, respectively. During the humidity test, the conductance of the first 31-longitudinal mode was monitored.



Figure 31. Impedancemeter HP4194A.

Table 13 summarizes the spectrometric techniques and experimental details used for the several purposes of this Thesis.

Table 13. Spectrometric techniques and experimental details used in the present Thesis.

Technique	Experimental details	Purpose	Section		
UV-Vis reflectance	200-1000 nm range	Quantification of casein, ADP, amphetamine-type drugs and ketamine by PDMS-based sensor	4.1.2.1 4.1.2.2 4.1.2.3 4.1.2.4		
		Quantification of VSCs by AgNPs-based nylon sensor	4.3.2.1		
		UV-Vis absorbance	200-1000 nm range	BCA assay	4.1.2.1
		C_{18} solid support derivatization as validating method for ADP detection	4.1.2.2		
		Study of NQS stability in solution.	4.1.2.2		

UV-Vis absorbance	300-800 nm	Colorimetric detection of sulphur compounds in solution by AgNPs.	4.3.2.1
FTIR	4000-600 cm ⁻¹ (ATR)	Sediment and illicit drug samples characterization	4.1.1.1 4.1.2.3
	4000-400 cm ⁻¹	Cu(GHG) characterization	4.3.1.1
RAMAN	785 nm laser; 60 s acquisition time; 2 accumulations, x10;600 g/mm	AgNPs-sensor characterization	4.3.2.1
Impedance	5 Hz to 3 GHz	MEMS characterization and humidity test.	4.1.4.1

3.2.2 Chromatographic techniques

HPLC and CapLC have been used. The miniaturized system was coupled to IT-SPME in order to extract and pre-concentrate the analytes before their separation and detection. The detectors employed were a FLD for both systems and a DAD for the CapLC.

3.2.2.1 HPLC–FLD

HPLC-FLD was employed in two methods to determine amphetamine compounds. For one hand, drug chiral separation was carried out by a chromatographic system consisted of a quaternary pump (Jasco, PU-2089 Plus, Tokyo, Japan), a six port injection valve equipped with a 20 µL stainless steel sample injector loop (Rheodyne 7725), and a FLD (Jasco FP-2020 Plus, Tokyo, Japan). The detector was coupled to a data system (Jasco ChromNAV Chromatography Data System, Jasco Corporation, Tokyo, Japan) for data acquisition and calculation (Figure 32A). On the other hand, HPLC-FLD was used to validate the results obtained for estimating amphetamine compounds by PDMS-based sensor (*See Section 4.1.2.3*). In this case, the chromatographic system consisted of a quaternary pump (Hewlett-Packard 1050 Series, Palo Alto, CA, USA), a high-pressure six-port injection valve (Rheodyne Model 7000) and a FLD (Hewlett-Packard, 1046 Series). The detector was linked to a data system (Hewlett-Packard, HPLC ChemStation) for data acquisition and calculation (*Figure 32B*). In

both cases, the analytical signal was recorded at excitation and emission wavelengths of 264 nm and 313 nm, respectively.

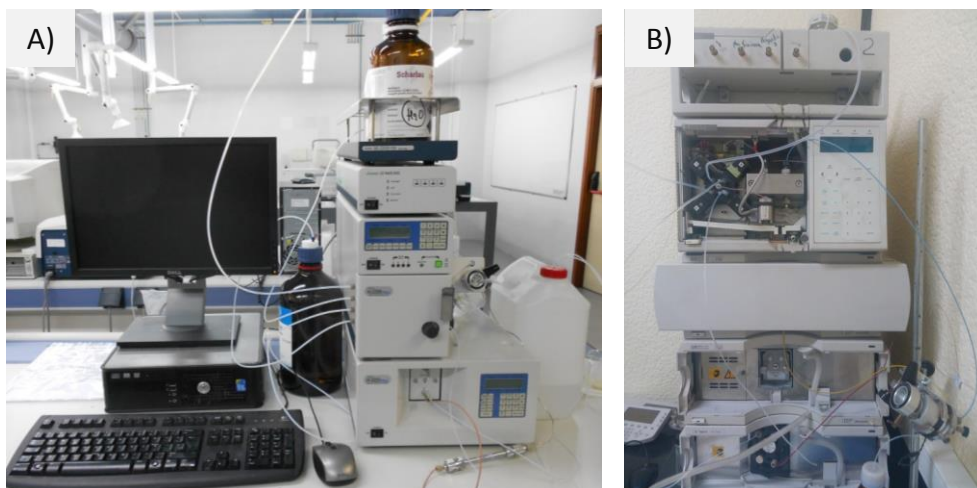


Figure 32. HPLC-FLD System A) Jasco and B) Hewlett-Packard.

3.2.2.2 CapLC-DAD

Depending on the analytes, two different equipments were employed. For the analysis of DEHP, the chromatographic system consisted of an isocratic capillary pump (Jasco Corporation micro 21PU-01, Tokio, Japón), a high-pressure six-port injection valve (7725 Reodyne, Rohnert Park, CA, USA) and UV-Vis DAD (Agilent, 1200 series, Waldbronn, Alemania) equipped with a 80 nL flow cell (Figure 33).



Figure 33. CapLC-DAD system for isocratic mode.

For the study of BAK and DPA, the chromatographic system consisted of a binary capillary pump (Agilent 1100 series, Waldbronn, Alemania), an on-line degasser, a high-pressure six-port valve (7725 Reodhyne) and a DAD (Agilent, 1260 Series) equipped with a 80-nL flow cell and linked to a data system (Agilent, HPLC ChemStation) (Figure 34).

In both systems, the detector was linked to a data system (Agilent, HPLC ChemStation) for data acquisition and calculation. The analytical signal was recorded from 190 to 400 nm.



Figure 34. CapLC system with binary capillary pump.

3.2.2.3 CapLC-FLD

The comparison of the extractive phase of IT-SPME to estimate amphetamine-like compounds was carried out by CapLC system. It consisted of an isocratic capillary pump (Micro 21PU-01, Jasco, Tokyo, Japan), a six-port injection valve (7725 Reodyne, Rohnert Park, CA, USA), a LC-Net II/ADC interface and a FLD (Micro 21FP-01, Jasco Corporation, Tokyo, Japan). The detector was coupled to a data system (Jasco ChromNAV Chromatography Data System, Jasco Corporation, Tokyo, Japan) for data acquisition and calculation. The analytical signal was recorded at excitation and emission wavelengths of 285 nm and 320 nm, respectively (*Figure 35*).



Figure 35. CapLC-FLD system in isocratic mode.

In *Table 14* are summarized the separation and detection techniques used in this Thesis, as well as their application.

Table 14. Summary of the chromatographic techniques used in this Thesis.

Separation technique	Detection technique	Analyte	Matrix	Section
HPLC	FLD	AMP, MAMP, EP, MDMA	Hair	4.1.3.1
		AMP, MAMP, MDA, MDMA	Illicit street drugs	4.1.2.3
CapLC	DAD	DEHP	Sediment and water	4.1.1.1
		BAK	Biocide mixture	4.1.1.2
		DPA	Hands	4.1.1.3
		(±)-MET, (±)-EP	-	4.3.1.1
CapLC	FLD	AMP, MET, EP	Oral fluid	4.2.1
		(±)-MET, (±)-EP	-	4.3.1.1

3.2.3 Microscopic techniques

3.2.3.1 Light microscopy

Microscopic images were taken with a Nikon microscope ECLIPSE E200LED MV Series (Nikon Corporation, Tokyo, Japan) under bright-field illumination with three objective lens (10x, 50x, 100x). For acquiring the images a Nis-Elements 4.20.02 software (Nikon) was used (Figure 36).

**Figure 36.** Nikon microscope.

3.2.3.2 Scanning electronic microscopy (SEM)

Two microscopes were employed in this Thesis: HITACHI-S4100 equipment for the characterization of AgNPs based sensors; and Philips XL30 ESEM with EDAX system incorporated into the microscope for elemental analysis of GSRs. Both microscopes operated at 20 kV. Samples were coated with Au/Pd for electron conduction (*Figure 37*).

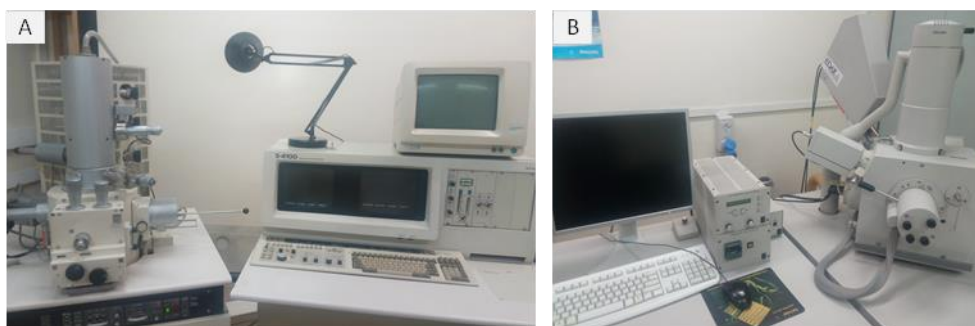


Figure 37. SEM A) Hitachi S-4100 and B) Philips XL 30 ESEM.

3.2.3.3 Surface profiler microscopy

The profile analysis of the microelectromecalical systems was carried out with the surface profilometer Veeco Dektak 150 Surface Profiler before firing (*Figure 38*).

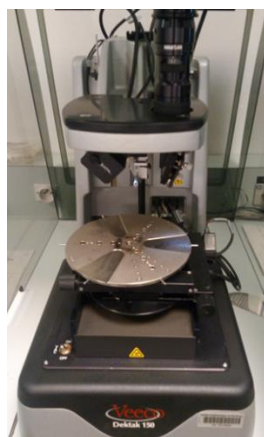


Figure 38. Dektak 150 profilometer.

3.3 SAMPLE PRETREATMENT TECHNIQUES

In the present Thesis, off-line and on-line sample pretreatment techniques have been studied. For the details of optimization, see the *Chapter of Results and discussion*.

3.3.1 Off-line sample pretreatment techniques

3.3.1.1 SPE

SPE was employed to evaluate the chiral capacity of Cu(GHG) MOF. For this aim, a SPE cartridge (polypropylene SPE tube, 1 mL, Supelco, USA) was filled with 50 mg of Cu(GHG) with upper and lower polyethylene frits (20 μm pore size, Supelco). For enantioselective separation of (\pm)-EP and (\pm)-MAMP, a racemic mixture of enantiomers (200 $\mu\text{g mL}^{-1}$ of each enantiomer) in 1 mL of ethanol:hexane (1:4) was passed through the cartridge by gravity (approximately 4 min of contact time). Eluted solution was collected and evaporated to dryness using nitrogen. Then, the extract was dissolved in 1 mL of water and derivatized following the procedure described in *Section 3.5.3* for chiral identification by HPLC (See *Figure 39*).

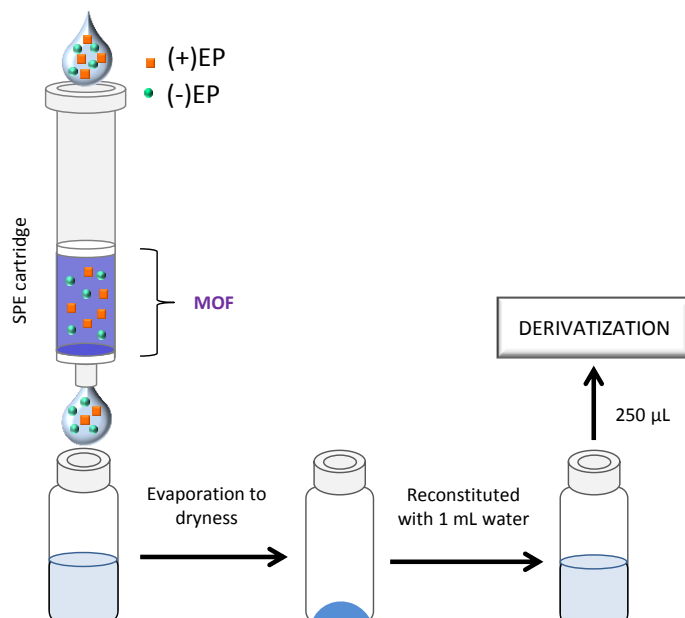


Figure 39. Scheme of the experimental setup used for SPE enantioseparation.

3.3.1.2 Vortex-assisted extraction (VAE)

For the detection of DPA from hands, firstly the analytes were extracted by scrubbing the hand with one tip of a cotton swab. In order to obtain the standard solutions, a volume of DPA solution was deposited on a glass slide, then the solvent was evaporated to dryness at room temperature and the solid DPA was collected carefully by scrubbing the glass slide with a cotton swab. After sample collection, the tip was placed into a storage vial containing 2 mL of water, so that the cotton was totally wetted. Next, DPA was extracted from the swab under vortex condition for 20 seconds at room temperature. Finally, the swab was discarded, and 1800 μL of the solution was loaded into the IT-SPME capillary. Several solvents, samplers and extraction techniques were tested in order to find the proper sampling procedure. The procedure of DPA extraction is shown in *Figure 40*.

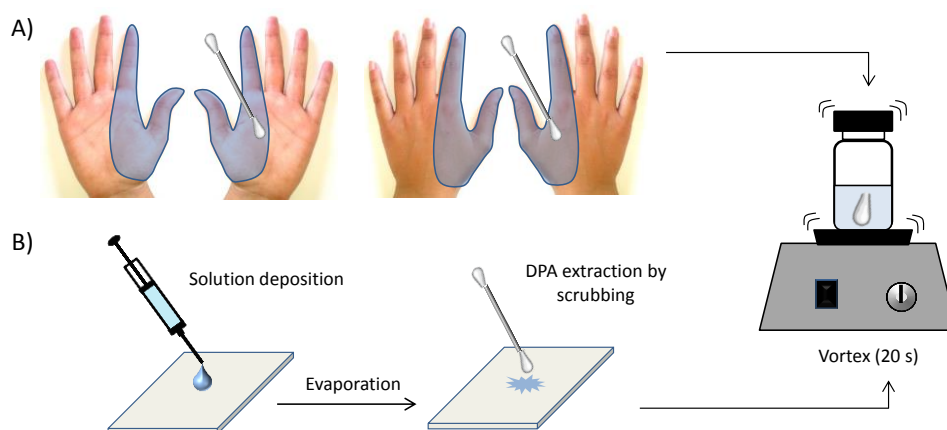


Figure 40. Scheme of A) Sampling by scrubbing the shooter hand with a cotton swab B) Standard solution preparation, for the VAE.

3.3.1.3 Ultrasound-assisted extraction (UAE)

For the estimation of amphetamine-type drugs in human hair, UAE by using alkaline digestion was carried out. For this purpose, 10 mg of hair samples were accurately weighted and placed into 2-mL glass vials containing 500 μL of 1 M NaOH. The vials were then sealed and introduced into an ultrasonic bath for 5 min to remove the analytes from the sample matrix. A portion of 250 μL of the obtained extracts was then removed and transferred to another vial, and

neutralized by adding 250 μL of 1 M HCl. The neutralized extracts were then derivatized with FMOC (*See Section 3.5.3 for details*), so neutralization was necessary because FMOC is not stable under highly basic pHs.

3.3.1.4 MSPD

This technique was carried out for the estimation of DEHP in sediments and the determination of amphetamine compounds in hair samples (*See 4.1.1.1 and 4.1.3.1 Sections*). For this aim, accurately weighted sample (0.1 - 0.3 g of sediment and 0.025 g of hair) was placed in a glass mortar and blended with 0.4 g of C_{18} by a pestle for 5 min (other dispersants such as silica and florisil were also tested). The resulting blend was then transferred to a polypropylene SPE tube (3 mL) with a polyethylene frit (20 μm) (Supelco, USA) placed at the bottom. Another frit was then placed at the top of the tube with the aid of a syringe plunger. Next, the analytes were desorbed with acetonitrile (1.2 and 1.5 mL for sediments and hair, respectively) by applying positive pressure and collected into glass vial.

For the DEHP estimation, the desorbed analytes were diluted with 2.6 mL of Milli-Q water and finally, the extract obtained (3 mL) was processed in the chromatographic system. C_{18} phase used for MSPD of sediments was previously cleaned by UAE. For this purpose, portions of 2.5 g of the C_{18} were placed into a pre-fritted glass SPE tube (6 mL) with polyethylene frits (20 μm). The tube was rinsed with 3 mL of acetonitrile. Once the solvent reached the exit by gravity, the tube was plugged with a PVC cap and introduced into an ultrasonic bath until the level of water in the bath was above the extraction solvent level inside the tube. Next, sonication was applied for 5 min. Then, the tube was removed from the bath, PVC cap was removed, and acetonitrile was flushed out by vacuum. The ultrasonic extraction process was repeated with 3 mL of 0.01 M NaOH prepared in water, 3 mL of 0.01 M phosphate buffer of pH 7.0, and 3 mL of water. Finally, the sorbent was dried with air.

In the case of drug estimation, before the desorption step, 2 mL of carbonate buffer was flushed through the tube by applying positive pressure in order to remove unwanted compounds, and then the blend was dried by passing air. Previously to the MSPD, hair samples were treated (*See Section 3.6.2.2*). Different MSPD/derivatization methods were tested: MSPD/solution derivatization and

Integrated MSPD/solid support derivatization. *Figure 41* depicts the scheme of several MSPD procedures developed in this Thesis.

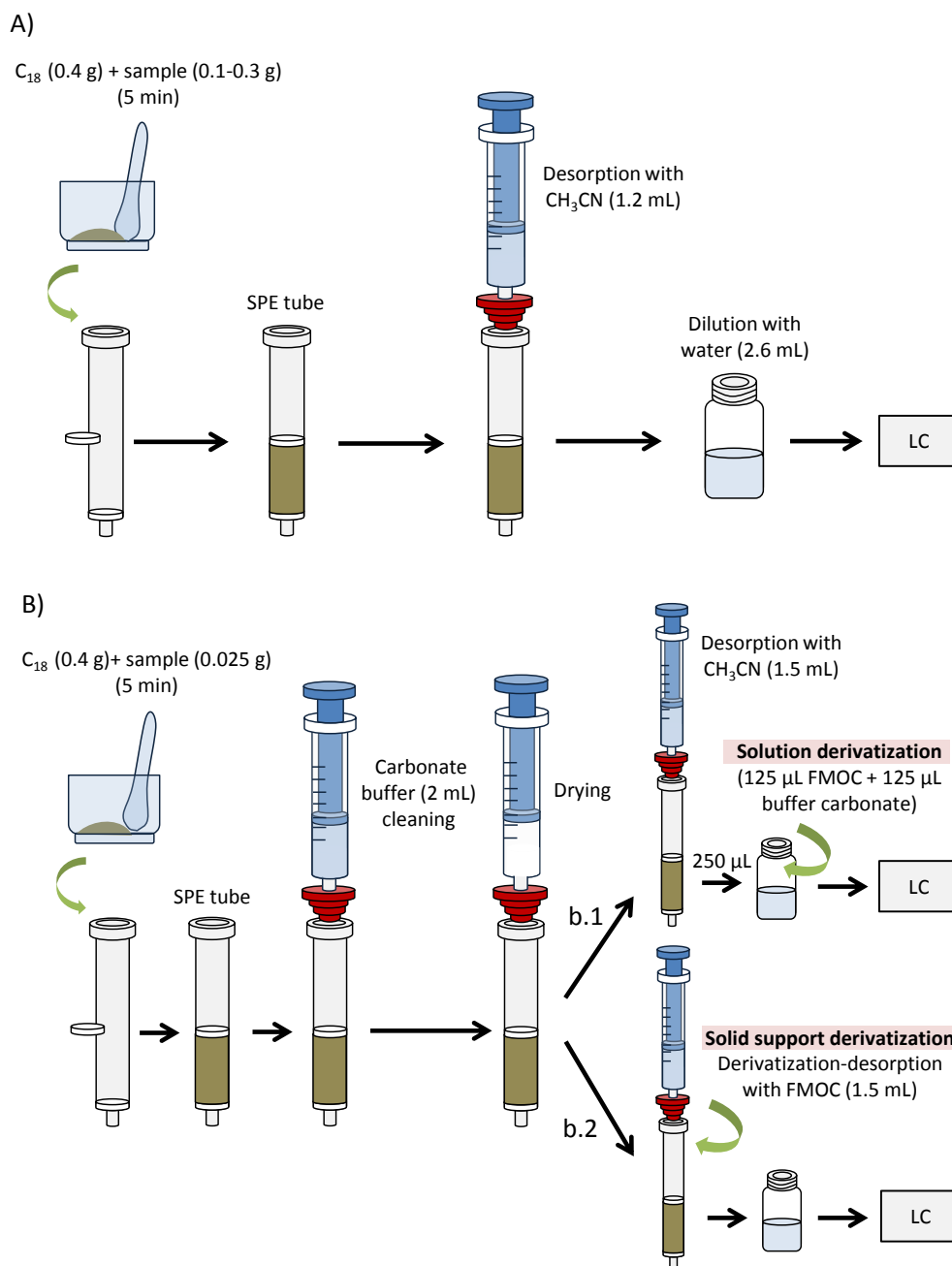


Figure 41. Scheme of A) MSPD for DEHP determination in sediments, B) MSPD/solution derivatization (b.1) and Integrated MSPD/solid support derivatization (b.2) for amphetamines estimation in hair.

3.3.2 On-line extraction techniques

3.3.2.1 In-valve IT-SPME

For in-valve IT-SPME procedure, the stainless steel loop of the conventional six port injection valve was replaced by a segment of open tubular capillary columns of GC. Several PDMS-based extractive phases with different dimensions were used depending on the analytes. The capillary columns were connected to the valve by using 2.5 cm sleeves of 1/16 in. PEEK tubing and 1/16 in PEEK nuts and ferrules. Aliquots of the solutions (samples and/or working solutions) were manually processed into the extractive capillary, in load valve position, by means of a 100-1000 μL precision syringes. Finally, the valve was manually rotated to the injection position, so the analytes were desorbed from the extractive capillary coating with the mobile-phase and transferred to the analytical column for their separation and detection. In-valve IT-SPME integrates the on-line cleaning, extraction and preconcentration of the analytes from the matrix in one single step. *Figure 42* shows the schematic diagram of in-valve IT-SPME coupled to CapLC or HPLC-FLD system with the valve positions.

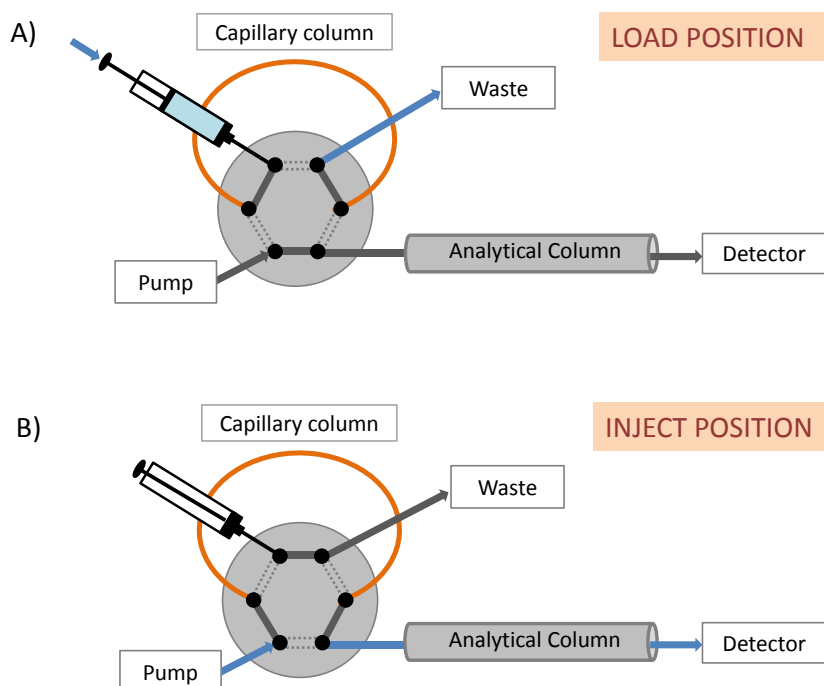


Figure 42. In-valve IT-SPME-LC with six port valve A) In load position B) In inject position.

3.4 FABRICATION OF SENSORS

3.4.1 PDMS/TEOS/SiO₂NPs-NQS sensors (Patent 201300436)

Different sensing devices have been studied. *Table 15* summarizes the sensors developed. The sensors highlighted in blue were the optimum sensors used in each work of this Thesis.

Table 15. Composition, size and curing time of the developed sensors. Optimum sensor highlighted in blue.

PDMS:TEOS* weight ratio	Ethanol (%, w/w)	NQS (%, w/w)	SiO ₂ NPs (%, w/w)	Size (diameter; thickness, mm)	Cure time (hours)	Section
50:50	-	0.05	0.1	15; 1	8	4.1.2.1
50:50	-	0.1	0.1	15; 1	8	
50:50	-	0.2	0.1	15; 1	8	
50:50	-	0.2	1	15; 1	8	
50:50	-	0.2	-	15; 1	-	
40:60	-	0.2	0.1	15; 1	>8	
70:30	-	0.1	0.1	3; 1	<8	4.1.2.2
50:50	-	0.1	-	3; 1	-	
50:50	-	0.1	0.1	3; 1	8	
50:50	-	0.1	1	3; 1	8	
50:50	-	0.05	0.1	3; 1	8	
50:50	-	0.2	0.1	3; 1	8	
40:60	-	0.1	0.1	3; 1	>8	4.1.2.3
100:0	3.6	0.1	0.1	2; 1 (square)	4	
50:50	-	0.1	0.1	8; 1	8	
50:50	-	0.1	0.1	3; 1	8	
40:60	-	0.1	0.1	3; 1	> 8	

*Large amounts of TEOS (>80%) were also tested but resulted in difficult gelation process.

PDMS-based sensors were prepared by the following procedure; the NQS reagent was dissolved in ethanol under ultrasonic condition, and this solution was added to the PDMS base. The mixture was stirred vigorously at room temperature for 15 min to get homogeneous dispersion. Then, PDMS curing agent was added at a weight ratio of 1:10 to the PDMS base, and stirred for 15 min at room

temperature. Finally, amounts of the resulting mixture were deposited on plastic molds and cured at room temperature for 2 days.

PDMS/TEOS-based sensors were prepared following a similar procedure, but the NQS and SiO₂-NPs were dispersed in TEOS (instead of ethanol) under ultrasonic condition for 10 min. The resulting dispersion was added to the PDMS base under vigorous magnetic stirring for 15 min at room temperature to get homogeneous dispersion. Then PDMS curing agent was added with a weight ratio of 1:10 to PDMS base and was stirred for 15 min at room temperature. Finally, the mixture was poured on molds, and then cured at 30 °C for days or hours, depending on its composition (*Table 15*). All the sensors were stored dry in polyethylene bags at room temperature until use. *Figure 43* shows the procedure of the PDMS/TEOS/SiO₂NPs-NQS sensors fabrication.

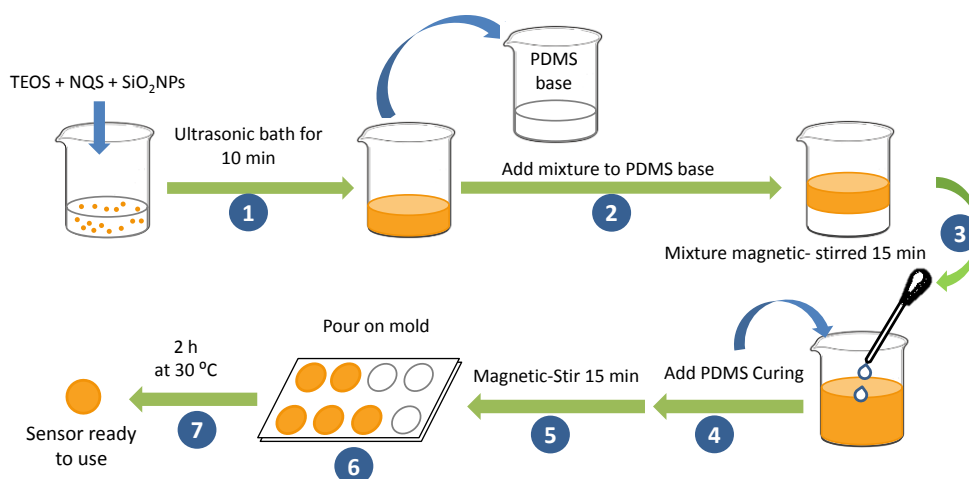


Figure 43. Procedure of PDMS/TEOS/SiO₂NPs-NQS sensors fabrication.

3.4.2 PDMS-Co(SCN)₂ sensors

According to previous studies, the best approach to prepare PDMS-based sensors is to mix a solution of the reagent in an organic solvent such as acetone or methanol with the PDMS base and the curing agent. However, all attempts made in preliminary experiments with solutions of Co(SCN)₂ failed because no gelification was observed even after several days of curing. For this reason, in the present study the bulk solid reagent was directly embedded into the polymer. The

reagent was previously ground in a glassmortar in order to obtain suitable homogeneity. PDMS-based sensors were prepared by mixing the appropriate amounts of Co(SCN)_2 , PDMS base and curing agent. After curing, the sensors were removed from the plates (6 mm of diameter) and stored in polyethylene bags at ambient temperature until use (Figure 44).

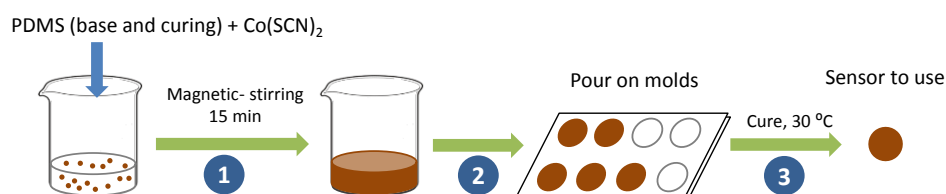


Figure 44. Procedure of PDMS- Co(SCN)_2 sensors fabrication.

As the PDMS is a hydrophobic material, the addition of TEOS to facilitate the diffusion of the analyte molecules from the solution to the sensors was also tested. PDMS-TEOS sensors were prepared by dispersing the solid Co(SCN)_2 reagent in the appropriate amount of TEOS under ultrasonic conditions for 10 min; then, the resulting dispersion was added to the PDMS base-curing agent mixture. In all cases the resulting reagent/polymerization mixtures were vigorously stirred for 15 min. Finally, this mixture was placed in well polystyrene plates and cured at 35 °C inside an oven for 8 hours. Different sensor compositions were assayed (see Table 16). The sensors highlighted in blue are the optimum sensors used.

Table 16. Compositions of the different PDMS- Co(SCN)_2 tested sensors.

Co(SCN)_2 (% w/w)	PDMS (% w/w) (base + curing agent) ^a	TEOS (% w/w)
0.1	99.9	-
0.3	99.7	-
0.6	99.4	-
0.9	99.1	-
0.3	91.4	8.3
0.3	49.85	49.85

^a For a 10:1 base:curing agent ratio

3.4.3 AgNPs-based sensors (Patent 201600440)

A nylon membrane (0.45 μm) was placed into a filter holder which is coupled to a syringe. Then, 200 μL of citrate-AgNPs dispersion of 20 nm (0.02 mg mL^{-1} in aqueous buffer, containing sodium citrate as stabilizer) was loaded into a syringe and it was passed through the membrane. AgNPs were trapped and the membrane became coloured. The surplus dispersion was passed through the membrane in order to retain the maximum AgNPs. A retention of 60 % of AgNPs ($0.0024 \pm 0.0002 \text{ mg}$) was obtained. The sensing membranes were stored by parafilm in the dark at room temperature.

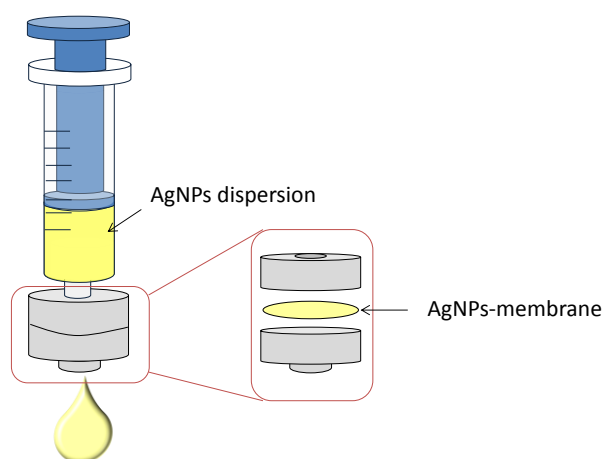


Figure 45. Procedure of the AgNPS immobilization on nylon membrane.

3.4.4 Screen-printed piezoelectric MEMS

Resonant piezoelectric MEMS composed of a PZT layer between two gold electrodes were fabricated on a substrate by combining screen-printing technology and the sacrificial layer method. This technique included different steps:

a) Ink fabrication

The gold ink (ESL8836) and sacrificial ink (ESL protective coat 244-T polymer) are commercially available (ElectroScience Laboratories, UK). However, the PZT

ink was prepared at the IMS laboratory. This ink was composed of 97 wt % of commercial piezoelectric PZT ($\text{PbZr}_{0.52}\text{Ti}_{0.48}\text{O}_3$) powder (PZ26, Ferroperm, Denmark) and 3 wt % of LBCu (≈ 25 wt % Li_2CO_3 , 40 wt % Bi_2O_3 , 35 wt % CuO) as sintering aid. The piezoelectric powder PZT:LBCu (40 g) in ethanol (60 mL) was firstly rotated during 18 h in a Turbula mixer with 8 zircon balls (5 mm) (*Figure 46A*). The homogenized powder was afterwards dried in an oven at 60 °C (4 days). Then, the piezoelectric paste was prepared by blending the PZT:LBCu powder (86%, w/w) with the organic binder ESL400 (ElectroScience Laboratories) (14%, w/w) in order to achieve good viscosity. After manual mixing in a mortar, the dispersion was optimized during 5 min using a three-roll mill (EXAKT 80S) to fulfill the required rheological properties (*Figure 46B*).

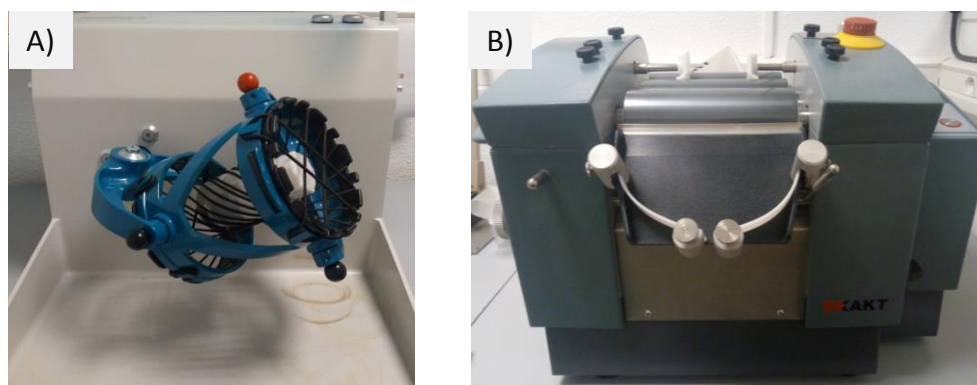


Figure 46. A) Turbula mixer and B) three-roll mill (EXAKT 80S).

b) Screen fabrication

Two kinds of screens were used: a steel stencil for printing PZT layers (*Figure 47A*) and a screen based on a piece of stainless steel mesh for printing gold, sacrificial or dielectric layers (*Figure 47B*), both screens are stretched over a frame. A stencil on the mesh was formed by blocking off parts of the screen by a mask with the pattern in the negative image of the design to be printed; that is, the open spaces are where the ink will appear on the substrate. For preparing the mesh screen, a photosensible and water soluble emulsion was firstly deposited on the mesh. Next, a mask with the pattern selected (*Figure 47C*) is placed on the emulsion and the selected pattern was formed by the screen copy unit Variocop S (*Figure 47D*).

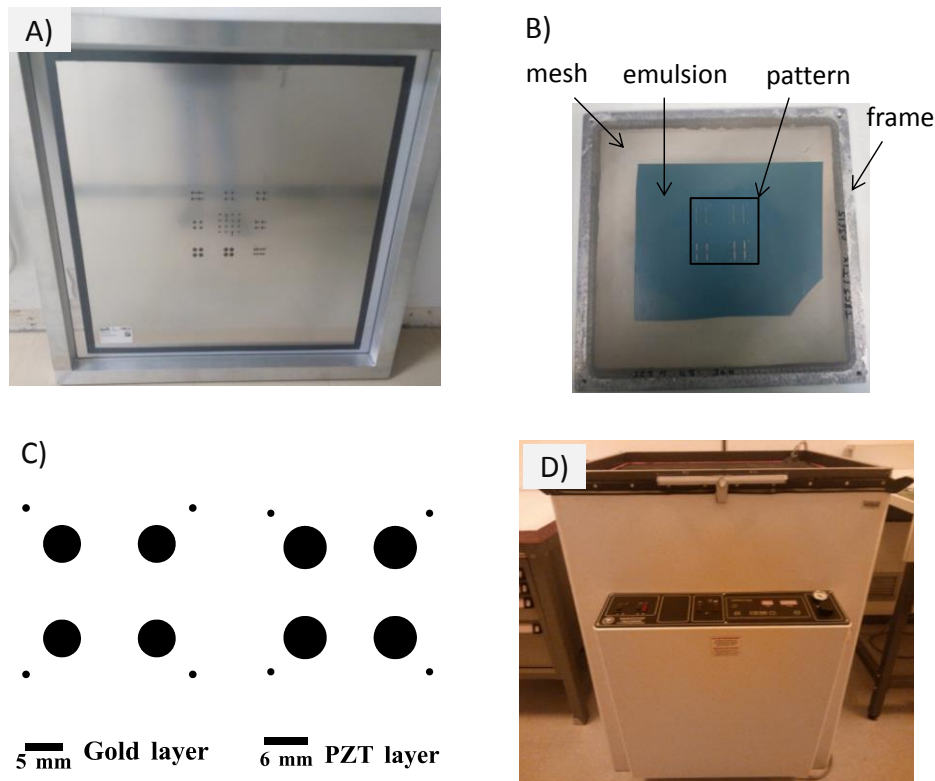


Figure 47. A) Stencil for PZT printing; B) Screen with emulsion with patterns on mesh for gold, sacrificial and dielectric printings; C) Mask with pattern of disks and fiducials for revealing; D) Screen copy unit Variocop S for insolation.

As can be seen in *Figure 48*, which shows the mesh revelation procedure, the soluble photosensible emulsion turned insoluble in water when it is exposed to UV light ($\lambda=350$ nm). However, the zones with the black pattern were not irradiated remaining soluble and so, the emulsion was removed by water allowing open spaces where the ink passes to the substrate.

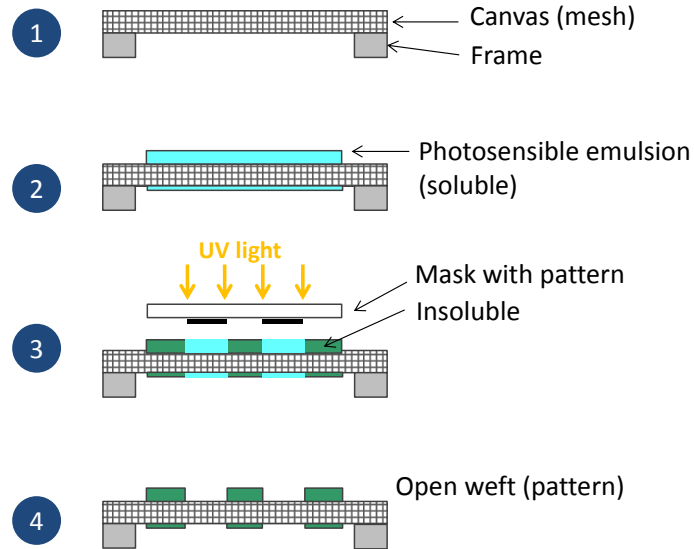


Figure 48. Procedure of mesh revelation.

Table 17 shows the different materials and screens used for the step deposition to fabricate sensors by screen-printing technique.

Table 17. Summary of materials and screen characteristics used to fabricate disks and cantilevers

Layer	Material	Screen thickness (μm)		Shime board (μm)
		Photoresist	Mesh	
Sacrificial layer	ESL protective coat 244-T polymer (ESL Erope)	50	70	250
Bottom electrode	ESL 8336 gold paste (ESL Erope)	15	325	300
Top electrode	ESL 8336 gold paste (ESL Erope)	15	325	400
PZT	PZT paste prepared in Laboratory	150 (steel stencil)		300
Anchor pad	PZT paste or glass-ceramic paste 4702 overglaze	50	70	300

c) Screen-printing:

The fabrication process by the DEK Horizon 03iX screen printing platform (ASM, Switzerland) consists of the successive deposition of each pattern for printing each layer (*Figure 49*).

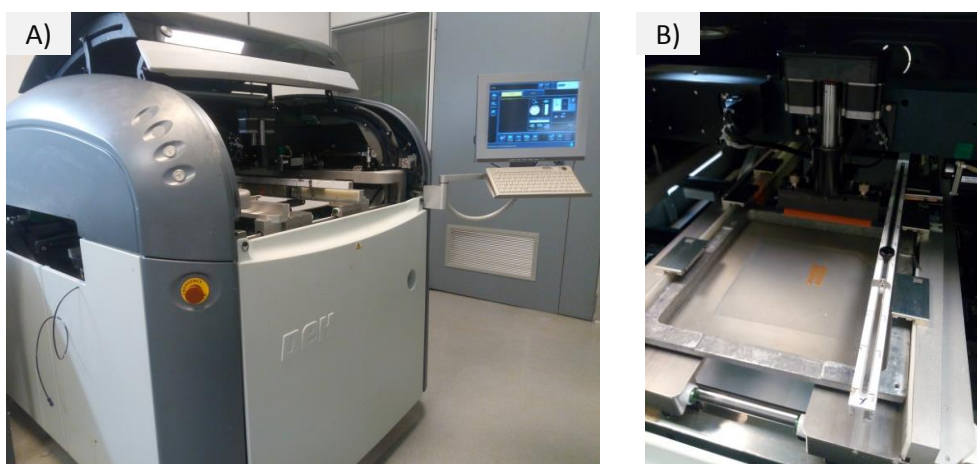


Figure 49. A) Overall view of DEK Horizon 03iX screen printing platform and B) view of the print cycle.

d) Drying

Once printed, each layer was dried at 120 °C for 15-30 min, depending on the layer, in an oven to remove the solvents of the ink. In case of the piezoelectric layer, a specific drying of 1 °C min⁻¹ up to 120 °C before its maintaining 30 min at this temperature was carried out in order to limit cracks or holes.

e) Pressing

Subsequently, the dried sensors were isostatically pressed at 40 MPa for 4 minutes at 65 °C (Exxelia Temex Parc Industriel, Pessac, France) to improve the sensor densification before firing.

f) Firing

Afterwards, the sensors were fired in an AET Technologies furnace (*Figure 50A*). Taking into account the temperatures of organic binder elimination ($30 < T(^{\circ}\text{C}) < 350$), sacrificial layer elimination ($450\text{ }^{\circ}\text{C}$), LBCu eutectic fusion ($600\text{ }^{\circ}\text{C}$) and PbO evaporation ($920\text{ }^{\circ}\text{C}$), the temperature programme used to prevent cracks and deformations is shown in *Figure 50B*. The temperature increased from $50\text{ }^{\circ}\text{C}$ to $250\text{ }^{\circ}\text{C}$ for 5 min; then, it was increased to $450\text{ }^{\circ}\text{C}$ with heating rate of $1^{\circ}\text{C min}^{-1}$ for a slow elimination of organic binder and sacrificial layer; next temperature was increased up to $900\text{ }^{\circ}\text{C}$ with heating rate of $40\text{ }^{\circ}\text{C min}^{-1}$ and this temperature was holding for 2 hours to sinter PZT; and finally, sensors were cooled down to room temperature at $40\text{ }^{\circ}\text{C/min}$ (*Figure 50B*). After firing, sensors were released from substates.

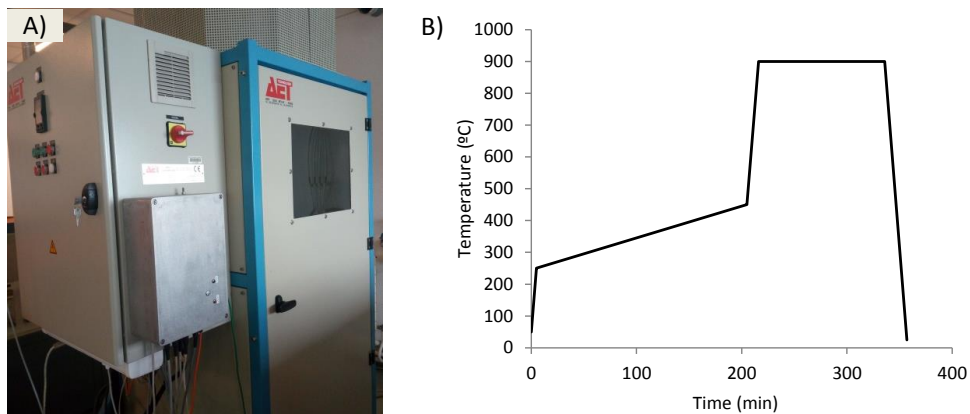


Figure 50. A) Furnace and B) Time-temperature profile in the firing process.

g) Polarization

Before polarization, platinum wires of $50.8\text{ }\mu\text{m}$ diameter (Alfa Aesar, Ward hill) were glued on the center of the gold electrodes and bonded to tin-plated copper tubes (Schneider Electric DZ5CE) using an epoxy-silver paste (ESL1901, ElectroScience); then they were cured for 1 h at $120\text{ }^{\circ}\text{C}$. Afterthat, the sensors were poled to reach the piezoelectric behavior by AET Technologies polarizing (*Figure 51*). Firstly, vacuum was generated inside the polarization chamber under 0.1 mbar of pressure to remove ambient humidity and prevent electric arc discharges at high voltages. Next, the samples were polarized under nitrogen

atmosphere (avoiding material spoilage) at 280 °C, just below the Curie temperature (284 °C) of PZT. A maximum electric field of 55 kV·cm⁻¹ is increasingly applied while the leakage current intensity is monitored below 5 μA. Then the system was cooled down while reaching and keeping constant the maximum electric field.



Figure 51. Polarization equipment AET.

The process described above was applied for the fabrication of two types of MEMS, disks and cantilevers.

h) Functionalization

Cantilevers were coated with mesoporous silica as sensitive coating to perform detection of gas. For this purpose, mesoporous silica MCF (1.60 cm³ g⁻¹ volume pore) was dispersed in water (100 mg mL⁻¹) under ultrasonic condition. The dispersion was then deposited on the top gold electrode by drop-casting with a microdispenser and finally, the solvent was evaporated at room temperature.

3.5 PROCEDURES AND EXPERIMENTAL CONDITIONS

3.5.1 Chromatographic conditions

Table 18 summarized the chromatographic conditions for each procedure developed in this Thesis. All solvents were filtered through 0.45 mm nylon membranes (Teknokroma) before use.

Table 18. Main characteristics of the chromatographic works described in this Thesis.

Analyte	Sample	Method	IT-SPME capillary	Analytical column	Mobil phase	Elution	Flow	Sample injection volume	λ (nm)	Section
DEHP	Sediment Water	CapLC-DAD	PDMS ₉₅	Zorbax SB C ₁₈ (35 mm x 0.5 mm, 5 μ m, Agilent)	CH ₃ CN:H ₂ O 95:5	Isocratic	10 μ L min ⁻¹	3 mL ACN:water, 1:3.25 v/v (+ 50 μ L water)	230	4.1.1.1
BAK	Biocide mixture	CapLC-DAD	PDMS ₆₅	Inertsil CN-3 (150 mm x 0.5 mm, 3 μ m, Sugelabor) Zorbax C ₁₈ (35 mm x 0.5 mm, 5 μ m, Agilent)	CH ₃ CN:Acetate buffer 85:15 65:35	Isocratic	10-20 μ L min ⁻¹	100-1000 μ L (+ 34 μ L methanol:water, 40:60)	212	4.1.1.2
DPA	Hands	CapLC-DAD	PDMS ₉₅ PDMS ₉₀ PDMS ₆₅ PDMS ₅₀ PEG	Zorbax SB C ₁₈ (150 mm x 0.5 mm, 3.5 μ m, Agilent)	CH ₃ CN:H ₂ O 70:30 (0-12 min) 100:0 (12-16 min) 70:30 (16-20 min)	Gradient	10 μ L min ⁻¹	1800 μ L (+ 120 μ L water)	280	4.1.1.3
AMP MAMP EP MDMA	Hair	HPLC-FLD	-	Lichrospher 100 RP18 (125 mm x 4 mm, 5 μ m, Merck)	CH ₃ CN:H ₂ O 60:40 (0-12 min) 80:20 (12-16 min)	Gradient	1 mL min ⁻¹	20 μ L	264 ($\lambda_{\text{excitation}}$) 313 ($\lambda_{\text{emission}}$)	4.1.3.1
AMP MAMP MDA MDMA	Illicit street drugs	HPLC-FLD	-	Lichrospher 100 RP18 (125 mm x 4 mm, 5 μ m, Merck)	CH ₃ CN:H ₂ O 60:40 (0-12 min) 80:20 (12-16 min)	Gradient	1 mL min ⁻¹	20 μ L	264 ($\lambda_{\text{excitation}}$) 313 ($\lambda_{\text{emission}}$)	4.1.3.3
Ketamine	Illicit street drugs	CapLC-DAD	-	Zorbax SB C ₁₈ (150 mm x 0.5 mm i.d., 5 μ m, Agilent)	CH ₃ CN:H ₂ O 90:10	Isocratic	8 μ L min ⁻¹	20 μ L	230	4.1.2.4
AMP MAMP EP	Oral fluid	CapLC-FLD	PDMS ₉₅ ; PDMS ₆₅ c-SWCNTs-PDMS ₉₅ c-SWCNTs-PDMS ₆₅ c-MWCNTs-PDMS ₆₅	Zorbax SB C ₁₈ (35 mm x 0.5 mm, 3.5 μ m, Agilent)	CH ₃ CN:H ₂ O 50:50 70:30	Isocratic	20 μ L min ⁻¹	20-50 μ L (+ 20 μ L water)	285 ($\lambda_{\text{excitation}}$) 320 ($\lambda_{\text{emission}}$)	4.2.1
(±)-MAMP (±)-EP	-	CapLC-DAD ^a HPLC-FLD ^b	-	Zorbax C ₁₈ column (35 mm x 0.5 mm i.d., 5 μ m, Agilent) ^a Hypersil ODS-C ₁₈ (250 mm x 4 mm i.d., 5 μ m, ThermoFisher) ^b	CH ₃ CN:H ₂ O 60:40	Isocratic	15 μ L min ⁻¹ ^a 0.5 mL min ⁻¹ ^b	20 μ L	264 ^a 264 ($\lambda_{\text{excitation}}$) ^b 313 ($\lambda_{\text{emission}}$) ^b	4.3.1.1

^aPDMS₉₅: commercial TRB-5 (95% Dimethyl-5% diphenyl polysiloxane); PDMS₉₀: commercial TRB-20 (80% Dimethyl-20% diphenyl polysiloxane); PDMS₆₅: commercial TRB-35 (65% Dimethyl-35% diphenyl polysiloxane); PDMS₅₀: commercial TRB-50 (50% Dimethyl-50% diphenyl polysiloxane)

As can be seen, the main differences between HPLC and Cap-LC are the inner diameter dimensions of analytical columns and the flow rates of mobile phase. The i.d. of CapLC analytical columns and HPLC columns used in this Thesis were 0.5 mm and 4 mm, respectively. Flow rates for CapLC and HPLC were 10-20 $\mu\text{L min}^{-1}$ and 0.5-1 mL min^{-1} , respectively.

3.5.2 IT-SPME conditions

Different PDMS-based commercial capillary columns modified with CNTs were investigated for the determination of amphetamine compounds in *Section 4.2.1*. The functionalization of the capillary columns for IT-SPME was carried out by following the procedure described in (*Jornet-Martínez, N. et al., 2015*). CNTs were carboxylated prior to their immobilization on the capillary column. To carboxylate SWCNTs, 5 mL of $\text{H}_2\text{SO}_4:\text{HNO}_3$ (3:1) were added to 0.025 g of SWNTs and ultrasonicated for 90 min (50 W, 60 Hz). Next, this suspension was diluted with 500 mL of water and filtered through a cellulose acetate filter (0.45 μm). Finally, c-SWNTs were washed with 1 M HCl and left to dry at room temperature. To carboxylate MWCNTs, 80 mL of a mixture of sulfuric and nitric acids (3:1, v/v) were added to 0.02 g of MWCNTs and ultrasonicated for 5 h (50 W, 60 Hz). Then, this mixture was diluted with water (1.5 L), filtered and washed with water. The following step was immobilization of c-CNTs on the inner surface of the PDMS capillary columns. Firstly, the PDMS capillary columns were activated by passing successively 2 M NaOH (24 h), water (5 min), (3-aminopropyl)triethoxysilane (APTS) (2%, v/v) of in anhydrous acetone (15 min), water (5min), methanol (5 min) to eliminated APTS excess and glutaraldehyde (10%, v/v) prepared in 50 mM borate buffer of pH 9.0 (10 min). Then, suspensions of c-CNTs (5 mg mL^{-1}) prepared in dimethylformamide (4.5 mL) containing 1,3-dicyclohexylcarbodiimide (DCC) (0.5 mg) were passed through the activated capillaries for 30 min in order to immobilize the c-CNTs into the PDMS-based coating. Finally, unreacted c-CNTs were eliminated by flushing water through the capillaries. The total time required for preparation of the capillaries after activation of the PDMS phase was about 2 h.

3.5.3 Derivatization procedures

The determination of amphetamines by LC entailed a previous chemical derivatization step to enhance the sensitivity. In this Thesis, the fluorogenic reagent FMOC was selected (Figure 52).

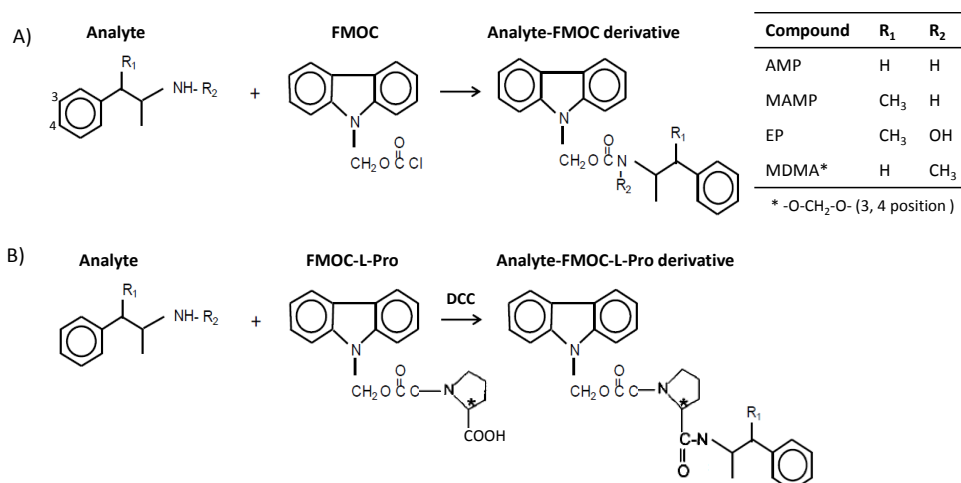


Figure 52. Scheme of the reaction between amphetamines tested and A) FMOC B) FMOC-L-Proline and DCC.

For the derivatization in solution, aliquots of analyte solution were mixed with carbonate buffer solution and with derivatizing reagent solution of FMOC. After reaction time of 5 min, 20 μ L of the resulting solution was injected into the chromatograph. For quiral identification in solution (Section 4.3.1), 125 μ L of FMOC-L-proline and 125 μ L of DCC were mixed for 5 min and added to 250 μ L of hydrogencarbonate buffer. The resulting solution was allowed to react for 2 min and then was injected (20 μ L) into the chromatographic system. For the derivatization in solid support (Section 4.1.3.1), 1.5 mL of FMOC was transferred to the SPE tubes containing the sorbet-sample blends by applying positive pressure, and after 2-3 min of contact time the resulting solution was flushed out the tubes and collected into glass vials. Unless otherwise stated, the extract (20 μ L) was injected after 5 min (counted from the addition of the reagent to the tube). The FMOC solutions were prepared daily by dissolving the pure compound in acetonitrile. The hydrogencarbonate buffer was prepared by dissolving the

appropriate amount of sodium hydrogencarbonate in water, then adjusting the pH to 10.0 with a solution of sodium hydroxide (10%, w/v). *Table 19* illustrates several volumes and conditions of derivatization procedures carried out in this Thesis.

Table 19. Conditions for derivatization procedures of this Thesis.

Sample volume (μL)	Carbonate buffer	Derivatizing reagent	Section
250	125 μL ; 0.05 M; pH 10.5	125 μL FMOC (1 mM)	4.1.3.1
125	125 μL ; 0.01 M; pH 10	250 μL FMOC (1 mM)	4.1.2.3
125	125 μL ; 0.01 M; pH 10	250 μL FMOC (0.1 mM)	4.3.1.1
250	250 μL ; 4 %(m/v); pH 10	125 μL FMOC-L-proline (1 mM) + 125 μL DCC (10 mM)	4.3.1.1

3.5.4 Response of polymeric sensors

The experimental conditions for obtaining the response of polymeric sensors are shown in *Table 20*.

Table 20. Experimental conditions used in several works of this Thesis based on polymeric sensors.

Analyte	Matrix	Sensor	Reagents	Sample volume (μL)	Reaction time (min)	λ (nm)	Section
Caseine	Effluent	PDMS/TEOS/ SiO_2 NPs/NQS	NaOH	2.5	10	525	4.1.2.1
ADP	Industrial product	PDMS/TEOS/ SiO_2 NPs/NQS	Hydrogen carbonate buffer (8%, w/v, pH 11.0)	1	6	525 600	4.1.2.2
AMP MAMP MDA MDMA	Illicit street drug	PDMS/TEOS/ SiO_2 NPs/NQS	Hydrogen carbonate buffer (8%, w/v, pH 11.0)	1	10	525	4.1.2.3
Ketamine	Illicit street drug	PDMS- $\text{Co}(\text{SCN})_2$	NaOH (0.1Mm)	100	10	625	4.1.2.4

The estimation of casein by PDMS/TEOS/SiO₂NPs/NQS sensor, consisted of soaking the sensor into 2.5 mL of sample, basified to pH 12 with NaOH, and heating at 100 °C for 10 min. For estimating amphetamines and ADP biocide by PDMS/TEOS/SiO₂NPs/NQS sensor, 1 mL of sample in hydrogen carbonate buffer (8%, w/v, pH 11.0) was placed in a glass vial and then three sensors were added. After reaction time, sensors were removed from the vials and the analytical signal was measured. The quantitative analysis was carried out by absorbance measurements by DR and color measurements by DI (Figure 53).

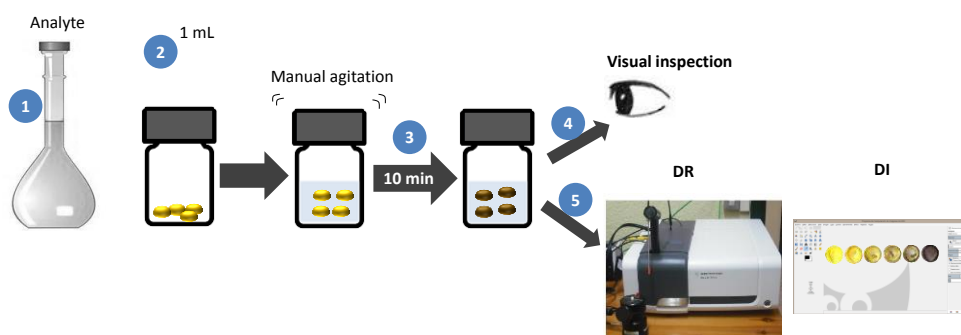


Figure 53. Procedure to obtain the colorimetric response of polymeric sensors.

In order to measure absorbance by DR, first, a back ground scan was made against a white paper and a blank was also measured. Then, the sensor after analyte reaction was placed under the camera of the DR accessory and the absorbance measurements were registered. For the color intensity measurements, firstly DI was obtained. In the caseine and biocide works, colored sensors were scanned with a conventional scanner, at a resolution of 300 dots per inch. For the amphetamine work, photographic images of the sensors were taken with a Nikon CoolPix S2600 digital camera with 14 megapixels and 5x wide optical zoom. The camera was programmed without flashlight and the object distance was 10 cm. Next, the images were imported into a computer, and their color differences were analyzed by the free image editor software GIMP (version 2.8). The color intensity was assessed using the color picker tool on GIMP, with an average of 35x35 pixels for the amphetamine and biocide determination and 50x50 pixels for caseine determination. An area composite of approximately 100x100 pixels (amphetamine and biocide determination) and 132x132 pixels (caseine determination) was selected using the ellipse select tool. The RGB color

mode was applied to transform the DI into numerical color values. Color difference patterns were obtained by calculating the difference of the red, green, and blue values at the center of scanned composites. The intensity of green color was selected due to higher signals.

For the estimation of ketamine by PDMS/Co(SCN)₂ sensor, aliquots of 100 μ L of sample were mixed with 100 μ L of 0.1 M sodium hydroxide in 2 mL glass vials. Then, sensors were immersed into the mixtures. After the reaction time, the sensors were removed from the vials and their colors were analyzed by visual inspection and monitored by recording their absorbance spectra by DR following the same procedure above mentioned.

3.5.5 Response of AgNPs based sensors

Firstly, the gaseous standard of VSCs was generated into a 2000 mL static dilution glass bottle under magnetic stirrer as *Figure 54* shows. The sensor was firstly hung by a thread into the static dilution bottle, then 100 μ L of phosphoric acid 85 % in order to facilitate volatilization was added. Once the bottle was closed, aliquots of standard solutions of the Na₂S between 0 – 100 μ L were injected by the bottom of this static dilution bottle and the mixture was stirred for 10 min. Afterthat, the sensor was removed from the bottle and was coated by glycerol. The analytical response was measured by DR and/or DI (RGB color analysis). The same protocol was followed for the analytes CH₃SH and (CH₃)₂S and also, to test interferences as ethanol, acetone and ammonia.

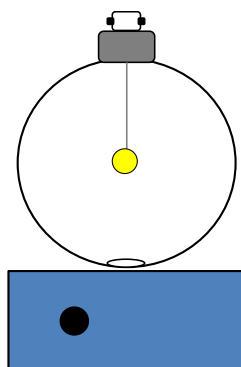


Figure 54. Sensor hanged up into static dilution bottle to generate gaseous standard.

3.5.6 Response of screen-printed sensors

Screen-printed piezoelectric cantilever coated with sensitive layer was used as gas sensor. To perform the test, the cantilever on alumina substrate was bonded on printed circuit board (PCB) support with platinum wires (150 μm diameter) using a silver paste. After drying the silver paste for 20 min at 120°C, the cantilever was placed in a gas chamber (35 mL) connected to an impedance analyzer (Figure 55A), which allowed the real-time reading. The detection configuration is based on a vapor generator (CALIBRAGE PUL 110) to generate and control the concentrations of the target vapor from a liquid contained in a heated bottle (Figure 55B). The vapor particles are transported by constant flow of nitrogen (100 mL min^{-1}) as a carrier gas. Thus, a sequence of target vapor concentrations was delivered on the sensor placed inside the chamber. Previously, a nitrogen flow was carried out for 450 min to ensure stability at room temperature. Moreover, a nitrogen flow was carried out between each concentration sequence as rinsing step. Humidity was used as model target vapor up to 2500 ppm for 10 min each concentration step. During the test, the resonance frequency shifts (at first 31-longitudinal mode) produced by the mass change due to the analyte sorption were measured by the impedance analyzer. All detections were carried out under the same conditions.

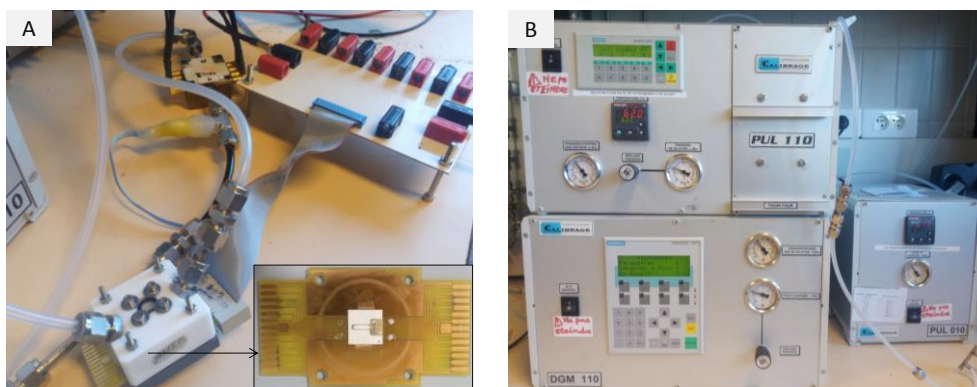


Figure 55. A) Gas chamber connected to impedancemeter and gas generator (Inset: top view of cantilever on alumina substrate bonded on PCB support and B) Vapor generator.

3.6 SAMPLES

In this Thesis, several kinds of samples have been analyzed, including environmental, biological, industrial and forensic samples. *Table 20* summarizes the samples and the analytes studied. All samples were analyzed in triplicate at room temperature.

3.6.1 ENVIRONMENTAL SAMPLES

Sediments and waters were analyzed as environmental samples to detect DEHP.

3.6.1.1 Sediments

Sediments were collected at different points along the coast of the Valencian Community (Spain) during 2012, from coast zone, transition zone and port. The coast sediments were collected from Sierra de Irta (Peñíscola) to Cabo de Cervera (Torrevieja). The sediments from transition zones were collected from Salinas de Santa Pola, Estany de Cullera and Riu Xúquer. The ports studied were Alicante, Castellón, Denia, Gandia, Sagunto and Valencia. All sediments were stored in plastic flasks, previously cleaned with acetonitrile, 2 L capacity. Samples collected were moved to the laboratory with coolers and were kept at 4 °C until analysis in glass flasks. Fortified samples (before MSPD treatment) were also processed.

3.6.1.2 Water

Two different water samples were analyzed. On the one hand, water samples collected at the same place that sediments were analyzed. The analyte evaluated was DEHP. The samples were stored in dark, in brown glass flasks at 4 °C until analysis. For the analysis, samples were previously centrifuged in glass tubes for 5 min at 45 rpm. Finally, aliquots of 4 mL were processed by IT-SPME-CapLC.

On the other hand, effluent water samples from dairy industry were analyzed by using PDMS/TEOS/SiO₂NPs/NQS sensors to determine casein. Water samples were provided by Betelgeux S.A (Gandia, Valencia, Spain). The dairy effluent samples analyzed were collected from a pilot plant aimed at the production of

cheese. The samples were collected at different stages of the CIP process. The CIP process consisted in four steps: (1) initial rinse with warm water, (2) rinse with a highly alkaline solution, (3) rinse with acidic solution, (4) heat disinfection with hot water. In some cases, the last step consists of chemical disinfection followed by hot water (*Dev Satyanarayan, S.R. et al., 2014*). Samples were stored at 4 °C until analysis. Before the analysis each sample was vigorously shaken. Finally the samples were alkalized and diluted if required.

3.6.2 BIOLOGICAL SAMPLES

In this Thesis, biological samples have been analyzed to determine amphetamine compounds in oral fluid and hair, and VSCs in breath.

3.6.2.1 Oral fluid

Owing to the high viscosity of oral fluid, its direct loading into the IT-SPME capillary was unsuitable, even after dilution with the buffer and FMOc solutions. For this reason, cotton swabs were used to collect oral fluid. In order to simplify the analytical procedure and to avoid excessive dilution of the analytes, the tip of the swab was directly immersed into vials containing the derivatization solution (250 µL of carbonate buffer and 250 µL of 0.1 mM FMOc). In such a way, the analytes were simultaneously extracted from the swabs and derivatized. After the reaction period (5 min), the swab was discarded and an aliquot of the resulting solutions was removed from the vials and processed by IT-SPME-CapLC. Drug-free oral fluid samples were obtained from volunteers after informed consent. Cotton swabs were purchased from a local market; the amount of cotton on each tip was of about 0.03 g.

3.6.2.2 Hair

Hair samples were collected from different volunteers. Portions of 1 g of hair were washed three times with 100 mL of water, and then twice with 100 mL of methanol in order to eliminate personal care products and other unwanted compounds that may be present.

According to the literature, drugs are firmly enclosed in the hair structure (Wada, M. *et al.*, 2010) and therefore, it was assumed that the conditioning step did not modify the amount of the analytes in the samples. After washing, the samples were dried in air. Dry samples were cut into 1–3 cm segments and then pulverized with ball mill (Fritsch, Oberstein, Germany) for 15 min. The resulting hair pieces (<1 mm) were kept in dark glass vials at room temperature until analysis.

3.6.2.3 Breath

Human oral breath was collected from ten volunteers by exhaling a mixture of mouth and alveolar air into Nalophan bags of 1L in a single expiration. Prior to collection, the sensor was hanged up into the bag. To spiked breath sample a suitable volume of Na₂S solution and acid ortophosphoric (85%) and stirred bar were introduced and mixed on the bottom of the bag. After 10 min of sampling the sensor was removed from the bag for visual inspection and its absorbance by DR was registered.

3.6.3 INDUSTRIAL SAMPLES

Three samples containing 4, 3 and 1.6% (w/v) of the ADP biocide were supplied by Betelgeux S.L (Gandía, Spain). Samples were diluted with water and aliquots of 1 mL were analyzed by PDMS/TEOS/SiO₂NPs/NQS sensors. For the recovery study, samples were spiked at concentrations from 0.3 to 1% (w/v). These samples were basic. In order to validate the results, samples were also analyzed by C₁₈ support derivatization.

On the other hand, two samples containing the ADP biocide and suspicious of containing BAK were also supplied by Betelgeux Company. Samples, called DECTOCIDE, which include 4.2% of ADP, as well as water, a non-ionic surfactant, phosphoric acid and other minor components, were tested by IT-SPME-CapLC. Standard addition curve was required to determine low concentrations of BAK in presence of ADP. For this purpose, samples were diluted to 720 µg mL⁻¹ in order to introduced about 30 µg mL⁻¹ of ADP into the system and moreover, the same concentration of 30 µg mL⁻¹ of BAK homologues were added on samples.

3.6.4 FORENSIC SAMPLES

3.6.4.1 Street drug samples

Illicit street samples, based on MDMA, MAMP, AMP, EP and ketamine were voluntarily donated by users who were previously informed of the aim of the study. The samples were finely powdered and homogenized thoroughly. For the analysis by PDMS/TEOS/SiO₂NPs/NQS sensors, accurately weighed portions of the powdered samples (≈ 2.5 mg) were transferred to glass vials containing 1 mL of buffer. For the analysis with PDMS-Co(SCN)₂ sensors, powdered samples (20-50 mg) were dissolved in the appropriate volume of nanopure water. Then, aliquots of 100 μ L of the resulting solutions were transferred to glass vials containing 100 μ L of 0.1 M NaOH and put into contact with the sensors. After the reaction time, the absorbance spectra of both sensors were registered. For the analysis of these samples by the reference LC method, portions of the samples were dissolved in the proper volume of water and filtered with 0.22 μ m nylon syringe filters. Next, aliquots of the resulting solutions were derivatized with the fluorogenic reagent FMOC (See Section 3.5.3 for derivatizing conditions), and injected (20 μ L) into the chromatograph. For characterization by FTIR-ATR, bulk powdered samples were placed in contact with the spectrophotometer ATR crystal, and then the spectra were registered.

3.6.4.2 Shooter hands

Test shots were carried out by police officers in an indoor range at Police Headquarters of Valencian Community (Valencia, Spain) under typical shooting practice conditions. The shots were fired with 9 mm Heckler & Koch pistols model USP Compact (Oberndorf/Neckar, Germany) which is the most commonly used firearms among police forces in Spain. Each volunteer police fired a total number of 25 shots (regulatory number of shots). Only one of these polices fired 12 shots because his pistol jammed. In order to avoid contamination, each police fired with his own firearm and did not touch other surfaces with the hands during the analysis. GSRs samples were collected from the shooter hands immediately after discharging the firearm. For each police, both hands right and left (palm and back) were sampled after shooting. Two techniques for GSRs collection from hands were carried out: swabbing and tape lifting. Swabbing was performed by

scrubbing the hand with one of the tips of a cotton swab. The tape lift kit consisted of a metal stub equipped with a carbon adhesive tape inserted in a plastic vial with a tightly fitted cap. For the sampling, the metal stub was passed over the surface of the hand. Once all the collected samples were placed back into their vials and capped, they were transported to the laboratory and were stored at room temperature awaiting analysis. A total of 21 hands were sampled by swab and 6 by tape. Additional swab samples from each volunteer police before test shots were also analyzed as blanks (hands were not previously washed). After sample collection, the DPA was extracted from cotton swab as *Section 3.3.1.2* described and 1800 μL of the solution was loaded into the IT-SPME capillary. *Table 21* presents all the samples and analytes analyzed in this Thesis.

Table 21. *Samples per analytes studied.*

Sample	Analyte	Section
Sediment Water	DEHP	4.1.1.1
Industrial biocide formulation	BAK, ADP	4.1.1.2 4.1.2.2
Hands	DPA	4.1.1.3
Effluent from dairy industry	Casein	4.1.2.1
Illicit street drugs (powder or pill)	AMP, MAMP, MDA, MDMA, Ketamine	4.1.2.3 4.1.2.4
Hair	AMP, MAMP, EP, MDMA	4.1.3.1
Oral fluid	AMP, MAMP, EP	4.2.1
Breath	Sulphur	4.3.2.1

CHAPTER 4. RESULTS AND DISCUSSION

4.1 Si-BASED MATERIAL

4.1.1 PDMS AS EXTRACTIVE PHASE FOR IT-SPME

IT-SPME is a sustainable extractive technique that follows the current trend of miniaturization in Analytical Chemistry. As mentioned in the *Introduction Chapter*, this miniaturized technique entails the reduction of sample handling, analysis time, sample consumption and waste generation. The automation of the analytical process can be achieved when IT-SPME is on-line coupled to chromatographic system. A further improvement of the sensitivity can be achieved by coupling IT-SPME to a miniaturized LC technique such as CapLC due to the decrease of the chromatographic dilution. Therefore, IT-SPME coupled to LC allows an automatized and miniaturized analysis with the required sensitivity. Due to IT-SPME is based on the affinity of analytes for the coating of a capillary column, the nature of the capillary coating is a key point. In this section, commercially PDMS-coated capillaries have been used to determine several analytes such as DEHP (*Section 4.1.1.1*), BAK (*Section 4.1.1.2*) and DPA (*Section 4.1.1.3*). However, the utility of conventional coatings is limited mainly due to the low extraction efficiencies. In order to improve the performance, CNTs have been studied as alternative coating nanomaterials for IT-SPME. As a practical application, capillary columns functionalized with CNTs have been tested to detect amphetamines in oral fluid (*Section 4.2.1*).

This section has been divided in four parts, as listed below:

1. IT-SPME on-line coupled to CapLC-DAD for estimating DEHP in coastal sediments previous pretreatment by MSPD.
2. Development of new strategies of analysis combining on-line analysis (IT-SPME-CapLC) and chromatographic conditions for BAK estimation in formulations with other co-biocides.
3. IT-SPME-CapLC method for estimating DPA with the previously optimization of the extraction procedure of DPA from hands. A complementary analysis of IGRs by SEM-EDX have been carried out. Comparison of several PDMS-based coatings.
4. Application of CNTs modified coatings for the determination of amphetamines by IT-SPME-CapLC. Comparison of several coatings, unmodified and modified by CNTs.

4.1.1.1 A cost-effective method for estimating DEHP in coastal sediments by IT-SPME-CapLC

DEHP is the most widespread phthalate produced and used. Owing to the low solubility and highly hydrophobic nature of DEHP, it is preferentially absorbed and/or adsorbed to the organic matter suspended in water as well as to the organic fraction of soils and sediments. Considerable transfer of this compound from sediments to aquatic organisms may occur (*Chaler, R. et al., 2004; Huang, P.-C. et al., 2008*). Therefore, the development of a method for the estimation of DEHP in sediments is of great interest for the characterization of aquatic ecosystems. In this work, MSPD and IT-SPME-CapL-DAD by using PDMS-based capillary have been proposed for estimating DEHP in sediments. Furthermore, FTIR-ATR has been used to characterize sediments.

Study of MSPD and IT-SPME-CapLC

DEHP is strongly retained into the PDMS-based coating of the extractive column used for IT-SPME owing to its high hydrophobicity. Therefore, a mobile phase with high elution strength has been necessary to desorb this compound from the extractive capillary in a reasonable time. According to previous studies, a mixture of acetonitrile:water (95:5, v/v) has been an adequate solvent for desorption of the analyte from the PDMS₉₅ capillary column and using a C₁₈ analytical column (*Muñoz-Ortuño, M. et al., 2012*). Replicates of solid phase blanks were processed in order to evaluate the DEHP contamination. Conditions selected as the best option for MSPD were as follows: 100–300 mg of sample, 400 mg of C₁₈ phase, and 1.2 mL of acetonitrile for analyte desorption. It should be noted that the final volume of the extracts collected after flushing the extraction tubes with 1.2 mL of acetonitrile was of about 0.8 mL. After, 2.6 mL of water was added. *Figure 56* shows the FTIR-ATR spectra obtained from sediment, MSPD mixture, and after-extracted MSPD mixture. The sediment spectra shows only the features of carbonates and clay materials, C-O absorption peaks in the frequency 1430 cm⁻¹ and Si-O at 1025 cm⁻¹, respectively. C-O bands are also present in the spectra corresponding to MSPD and after-extracted MSPD mixtures. As it can be observed, a small amount of matrix passed to the extract with acetonitrile because the spectra of the mixture after extraction present a smaller absorbance than that provided by the MSPD mixture.

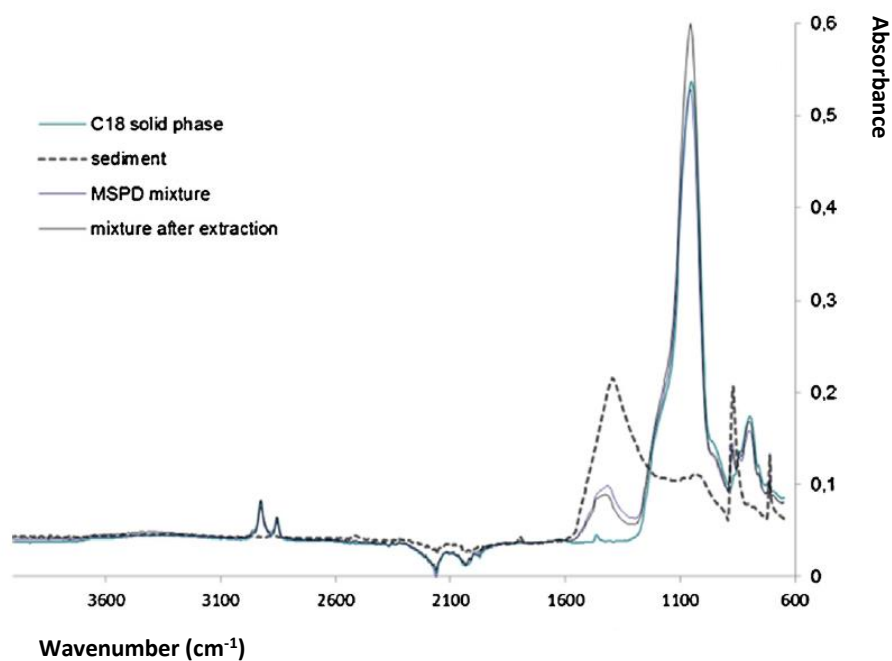


Figure 56. FTIR-ATR spectra obtained for C₁₈ used as solid phase in the MSPD procedure, sediment, MSPD mixture and MSPD mixture after extraction with acetonitrile.

Analytical parameters

Standard solutions of DEHP were prepared in water: acetonitrile (1:3.25, v/v) since the extraction solvent used for sediment samples after the MSPD was water-acetonitrile. The reliability of the procedure was also tested for sediments by obtaining relevant analytical parameters such as the limits of detection (LODs) and quantification (LOQs), and the linearity. A sediment without DEHP (i.e., with a content below LOD/3) was selected and amounts of DEHP were added for obtaining up to 200 $\mu\text{g L}^{-1}$ in the extracts, which were processed according MSPD and IT-SPME-CapLC-DAD. Adequate linearity was obtained as can be seen in *Table 22*.

Table 22. Some figures of merit to detect DEHP in sediments by MSPD and IT-SPME-Cap-LC-DAD.

$a \pm s_a$	$b \pm s_b$ ($\mu\text{g L}^{-1}$)	R^2	LOD ($\mu\text{g L}^{-1}$)	RSD (%)	Recovery (%) (n=8)
94 ± 120	65 ± 3	0.9969	8	5-10	80 ± 20

$a \pm s_a$: ordinate \pm standard deviation of ordinate, $b \pm s_b$: slope \pm standard deviation of slope, RSD: relative standard deviation

For sediment extracts, the LOD given in *Table 22* corresponds to the concentration of DEHP in the extracts loaded into the capillary that gave a peak height of three times the peak height of the blank. If 0.100 g of sediment was used, the achieved LOD was $270 \mu\text{g kg}^{-1}$, and when 0.300 g was employed, the LOD was $90 \mu\text{g kg}^{-1}$ for sediments. Similar values were obtained compared to methods with evaporation steps and higher amounts of samples. The LOQ was established as the concentrations that resulted in peak height ratios of ten, it was three times the LOD. The precision was evaluated by obtaining the intra and inter-day relative standard deviations (RSDs) for the spiked sediments processed. The results obtained were satisfactory, RSD values lower than 10 % in all cases were obtained. Recovery studies were carried out and no matrix effect were obtained (See *Table 22*). By way of example, *Figure 57* shows some chromatograms obtained for a sediment sample.

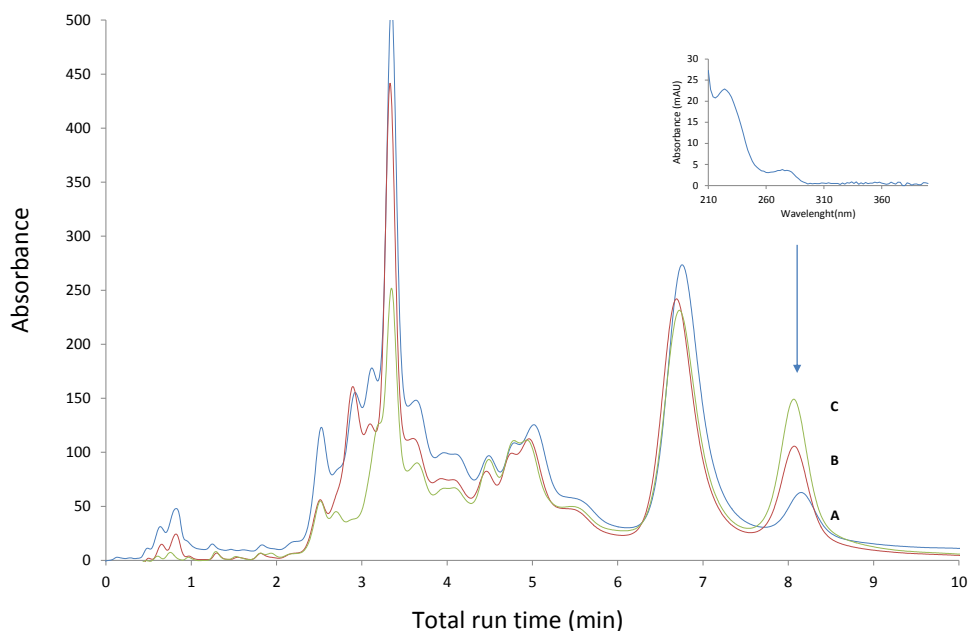


Figure 57. Chromatograms at 230 nm obtained for a sediment sample (A), sediment sample spiked with $47.62 \mu\text{g L}^{-1}$ (B), and $69.77 \mu\text{g L}^{-1}$ (C) of DEHP (concentrations in the extracts). The spikes were realized before MSPD treatment. Inset corresponds to DEHP spectrum.

Analysis of samples

The proposed conditions have been applied to analyze sediments samples collected at different points along the coast of the Valencian Community area (Spain) during 2012. The parameters used to establish the presence or absence of the analyte in each sample were the concordance between (i) the retention time and (ii) UV spectra of DEHP and the suspected peak in the chromatogram of the sample, and (iii) the comparison of the chromatograms obtained for the sample and after spiking the sample with known amounts of the analyte. Special efforts were necessary during sample manipulation to prevent contamination by DEHP, as significant amounts of this compound are present in packages, solvents, or glassware (Frankhauser-Noti and A., Grob, K., 2007).

Obviously, elimination or simplification of the sample preparation would reduce the risk of contamination. In general, solvents must be assayed previously,

because most of them contain DEHP, increasing blank signal and therefore, affecting the determination of the analyte of interest. Several kinds of blanks and fortified samples have been employed in order to test the presence or absence of bias error. Solid phase blanks have been prepared as samples, but without adding it. Standards in solution can be used for processing samples provided solid phase blanks do not present a matrix effect. Solvent blanks and cleaning blanks have been also tested. In order to estimate the percentages of DEHP recovered by MSPD, samples providing a signal for DEHP similar to that of solid phase blanks have been fortified both before MSPD treatment and after the elution process, at measured levels between 20 and 100 $\mu\text{g L}^{-1}$ of DEHP. Recoveries as those given in *Table 22* have been obtained. In addition, between 0.3 and 0.1 g of a sample spiked with 50 $\mu\text{g L}^{-1}$ (measured concentration) have been processed and the signals obtained for DEHP were in accordance with the amount of DEHP processed by the method in a 95 % of the value obtained for 0.1 g. The sediments have been also characterized by FTIR-ATR. *Table 23* shows the particle size of the sediments assayed (See also *Figure 58*).

Table 23. Comparison of the composition of the three kind of sediment assayed according to size of particle after sieving.

Particle size (nm)	Coast sample	Transition sample	Port sample
>0.4	1.05	27.75	3.94
0.4	4.82	17.31	3.3
0.3	23.68	13.51	13.3
0.2	66.37	15.2	50.2
0.1	2.75	23.62	25.96
Lost in process	1.33	2.61	3.24

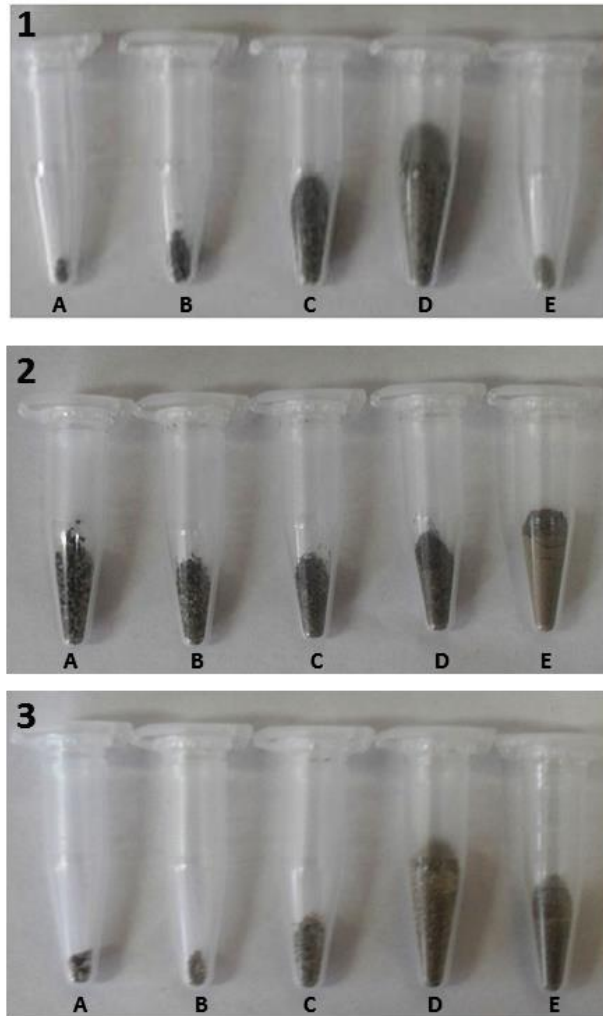


Figure 58. Photographs of the proportions according to particle sizes (A, B, C, D, and E corresponding to bigger than 0.4, 0.4, 0.3, 0.2, and 0.1 mm, respectively) for different types of sediments: (1) sediment sample obtained from coast zone, (2) sediment sample obtained from transition zone, and (3) sediment sample obtained from a port zone.

Figure 59 shows the absorbance ratios Si-O/C-O of sediments studied. Three kinds of sediments were analyzed: coast, transition, and port zones with different particle size composition and also absorbance ratios Si-O/C-O as can be seen in this figure.

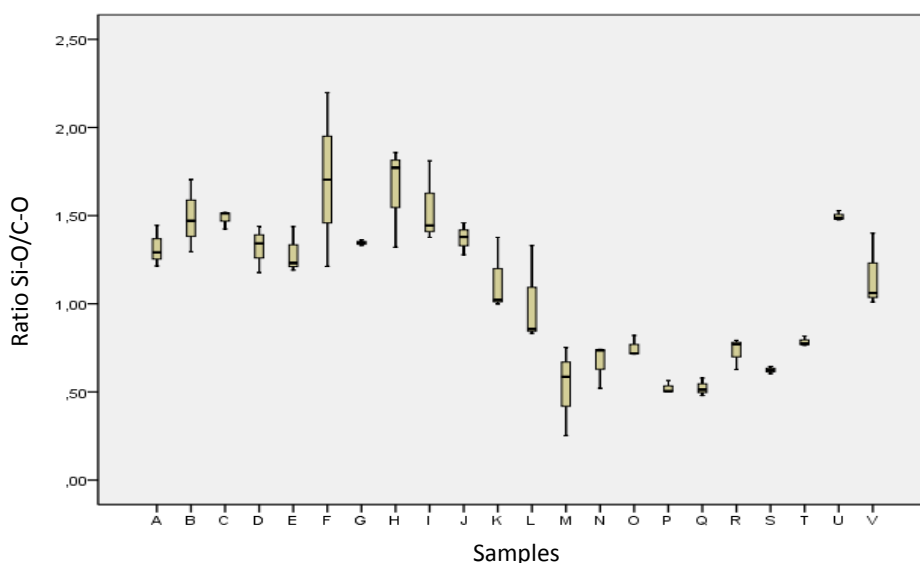


Figure 59. Absorbance ratio Si-O/C-O for the sediments assayed (see also Figure 58 and Table 23).

DEHP was detected only in one of the sediments analyzed (See Figure 57, photograph 3 of Figure 58 and sample F of Figure 59), being the LOD $90 \mu\text{g kg}^{-1}$ (0.300 g was used of sediment as sample taken). Chromatogram A in Figure 57 presented an analytical signal for DEHP three times higher than that shown for solid phase blanks. The concentration found in positive sample was in accordance with the values reported in reference (Lin, Z.P. *et al.*, 2003). The results obtained for the water samples sampled in the same place than sediments provided mean concentrations of DEHP below or near LOD achieved in water analysis ($0.25 \mu\text{g L}^{-1}$) and were similar for all samples analyzed. The mean concentration of DEHP was lower than the Environmental Quality Standards (EQS) value, fixed in $1.3 \mu\text{g L}^{-1}$ (Directive 2008/105/EC). The water mass in contact with the positive value found for the sediment contained a value of $0.25 \mu\text{g L}^{-1}$ of DEHP. The EQS is the allowable concentration of pollutant in water, sediment or biota, that should not exceeded for human and environmental protection. The directive 2008/105/EC proposes to apply EQS of priority substances for sediment and/or biota where they tend to accumulate, giving information for long-term trend analysis of those priority substances.

Conclusions

In this work, the possibility to combine the MSPD with IT-SPME-CapLC based on PDMS-based capillary for determining DEHP in sediment samples has been studied. The proposed procedure is cost effective and allows the identification and quantification of DEHP at $\mu\text{g L}^{-1}$ level concentrations to control environmental quality. Moreover, the considerable reduction on the amounts of sample and chemicals in reference to other procedures proposed in the literature, can also reduce the risk of DEHP overestimation due to background contamination.

4.1.1.2 IT-SPME-CapLC method for BAK determination as a component or contaminant in mixtures of biocides.

BAK is one of the most employed QAC in biocide formulations. In many cases, this compound can be present as pollution when different formulations are made in the same production plant or when the cleaning of an installation requires the use of this biocide. The complex chemistry of the surfactants makes necessary an evaluation of matrix effects that depends on kind of biocides, ratio between biocides and also total amount of surfactants. Thereby, a suitable method to control BAK in mixtures of biocides is required. Thus, this work establishes the parameters under which matrix effects may occur in formulations containing BAK as a minor component or impurity and other biocides, including a tertiary amine like ADP and TMTDAC. New strategies based on on-line analysis (IT-SPME/CapLC) by using PDMS-based capillaries for BAK estimation have been proposed.

Optimization of chromatographic separation of C₁₂-BAK and C₁₄-BAK homologues

The separation of BAK homologues usually requires chromatographic column with low hydrophobicity and controlled silanol groups. According to previous work (Prieto-Blanco, M.C. et al., 2013a), mixtures of organic solvent and aqueous buffer with adjusted pH were also necessary in the mobile phase to achieve a good separation. In the present study, cyano propyl column was compared with a short reversed non end-capped C₁₈ column in terms of separation of homologues, analysis time and coupling robustness with IT-SPME. Longer C₁₈ columns were tested, but BAK homologues were not eluted from the columns in the assayed conditions. Different mixtures of acetonitrile:acetate buffer (50 mM, pH 5) (ranging from 65:35 to 95:5) in isocratic elution mode were tested by the short C₁₈ column. As can be seen in *Figure 60A*, a decrease of retention time with the increase of acetonitrile mainly affected to C₁₄-BAK homologue (25.8 min – 65% acetonitrile versus 19 min – 85%, at 10 $\mu\text{L min}^{-1}$). The peaks of the two homologues were overlapped when 95% of acetonitrile was used in the mobile phase. When the flow rate was increased to 20 $\mu\text{L min}^{-1}$, the BAK homologues were separated in less than 12 min by using 85% of acetonitrile (See *Figure 60B*).

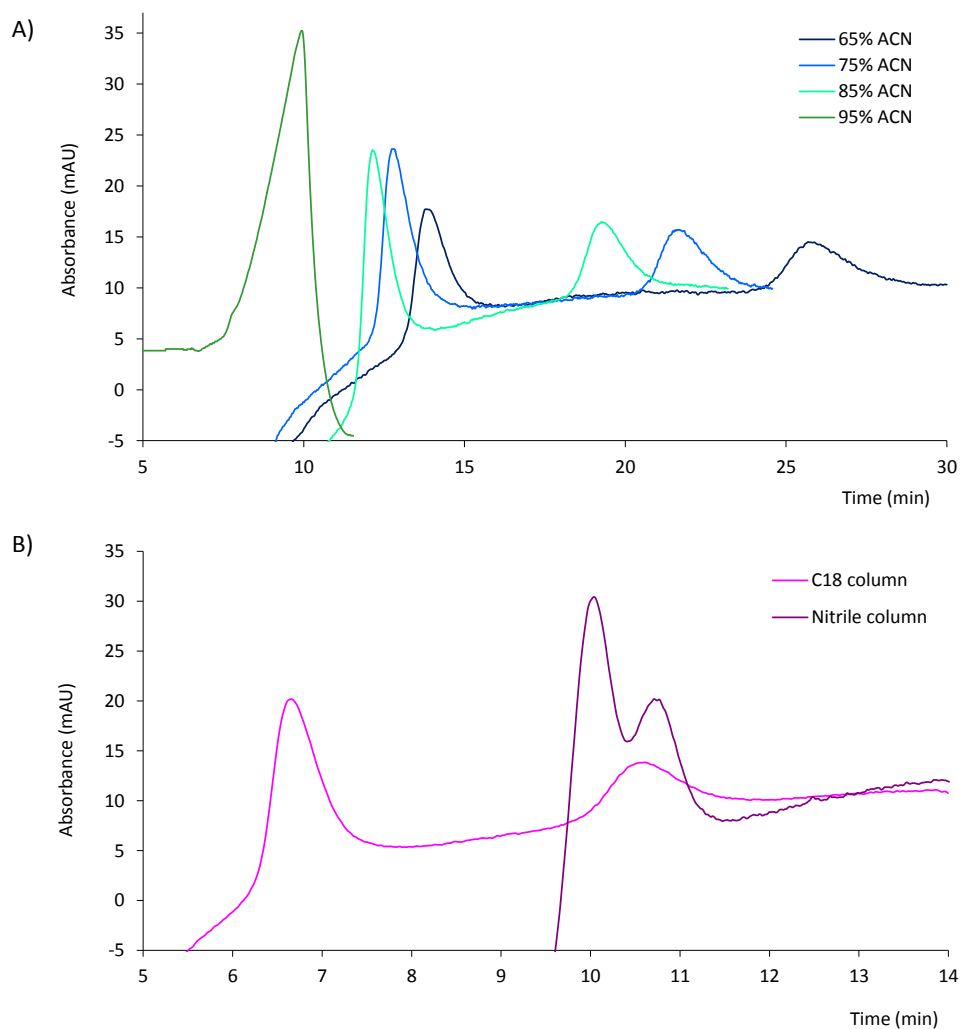


Figure 60. A) Effect of acetonitrile (ACN) percentage on the retention of C_{12} -BAK (first peak) and C_{14} -BAK (second peak) homologues at $0.5 \mu\text{g mL}^{-1}$ by using short C_{18} column. Flow rate = $10 \mu\text{L min}^{-1}$, B) Comparative separation of BAK homologues (at $0.5 \mu\text{g mL}^{-1}$) on C_{18} and nitrile capillary column. Conditions of mobile phase and flow rate: 85% ACN and $20 \mu\text{L min}^{-1}$ for C_{18} column; 65% ACN and $10 \mu\text{L min}^{-1}$ for nitrile column.

For the nitrile column, the analysis time was similar (13.5 min) to that provided by the non-encapped C_{18} , but the two homologues were not totally separated by using 65% of acetonitrile and $10 \mu\text{L min}^{-1}$ of flow rate. Precision achieved by the short C_{18} column was compared with that obtained by the established nitrile phase (See Table 24) and the results were similar. The short

non-encapped C₁₈ capillary analytical column improved the time of analysis and resolution of the BAK homologues.

Table 24. Precision and addition curves of BAK in presence of ADP from the raw material LONZABAC and from DECTOCIDE with the two chromatographic columns tested.

Column	Compound	RSD (%)		Standard addition curve y = a+bx			Working range ($\mu\text{g mL}^{-1}$)	
		Retention time (n=10)	Peak (n=5)	area	a \pm s _a	b \pm s _b ($\text{mL } \mu\text{g}^{-1}$)		R ²
ADP FROM LONZABAC 12.100								
C ₁₈	C ₁₂ -BAK	2	14 ^a	12 ^b	80 \pm 50	492 \pm 19	0.995	0.1-5
	C ₁₄ -BAK	2	11 ^a	5 ^b				0.1-5
CN	C ₁₂ -BAK	1	15	-	210 \pm 60	930 \pm 30	0.998	0.1-5
	C ₁₄ -BAK	1	17	-				0.1-5
ADP FROM DECTOCIDE								
C ₁₈	C ₁₂ -BAK	3 ^c	9 ^d	-	15 \pm 8	323 \pm 15	0.9985	0.1-1.5
	C ₁₄ -BAK	3 ^c	12 ^d	18	55 \pm 8	1681 \pm 14	0.9999	0.02-1

[Total BAK]= ^a 0.5 $\mu\text{g mL}^{-1}$, ^b 5 $\mu\text{g mL}^{-1}$; [C₁₂- BAK, C₁₄- BAK]= ^d 0.1 $\mu\text{g mL}^{-1}$

Optimization of the IT-SPME procedure

The extraction efficiency depends on parameters such as diphenyl percentage of the extractive phase and length of the capillary, replacing solvent in IT-SPME, sample solvent, processed sample volume and concentration of BAK in the sample. According to our previous study (Prieto-Blanco, M.C. et al., 2013a), a PDMS₆₅ GC capillary of 43 cm in length and a mixture of methanol:water (40:60) for replacing solvent were chosen. In order to optimize sample solvent and processed volume of sample, the raw material BAK at 80% was assayed by using the nitrile analytical column. The effect of the presence of acetonitrile in the processed sample was studied. Thus, two sample solvents were assayed: water and water:acetonitrile (50:50). Similar extraction efficiencies between the BAK homologues independently of concentration level were obtained using 50% of

acetonitrile in the sample solvent. Nevertheless, lower analytical signals were obtained if the acetonitrile was involved in the extraction. Due to the new assay required higher sensitivity because the BAK could be a minor component in the surfactant mixtures, the extraction was carried out using water as sample solvent. In this case, differences in the peak area for each homologue respect to the total area of the two homologues (% Homologue) with the concentration were observed. As can be seen in *Figure 61*, at concentrations of $5 \mu\text{g mL}^{-1}$ and lower, the analytical response for C_{12} -BAK was higher than that obtained for C_{14} -BAK.

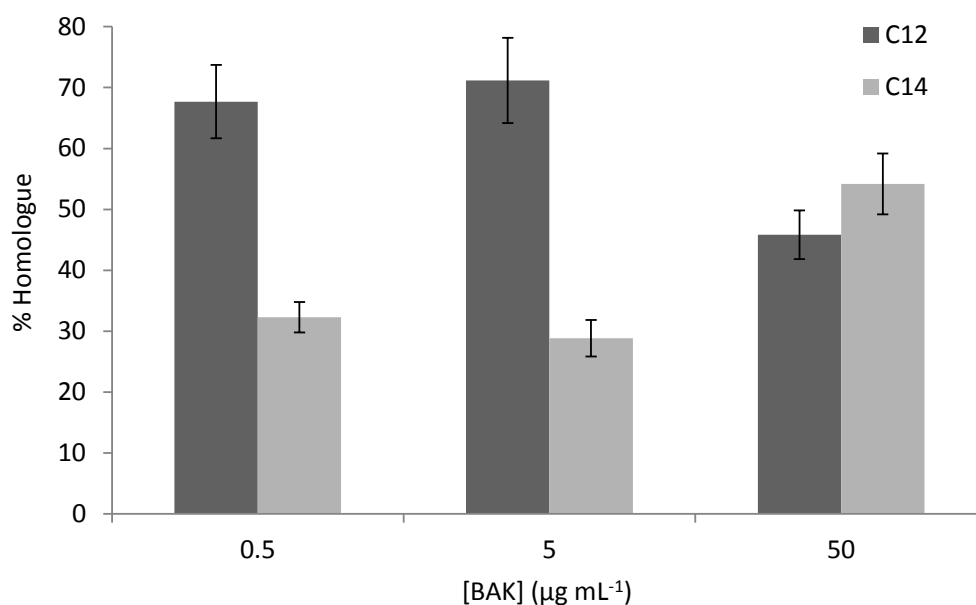


Figure 61. Effect of BAK concentration on extraction efficiency of each homologue when water is used as sample solvent. Conditions: nitrile column, acetonitrile:acetate buffer (65:35), flow rate = $10 \mu\text{L min}^{-1}$, $1000 \mu\text{L}$ for BAK 0.5 and $5 \mu\text{g mL}^{-1}$, and $100 \mu\text{L}$ for BAK $50 \mu\text{g mL}^{-1}$.

However, the behavior of homologues was opposite at $50 \mu\text{g mL}^{-1}$. Besides, the extraction efficiencies for the two homologues were more similar at the highest concentrations tested. The same mass of BAK ($0.5 \mu\text{g}$) was tested, but varying the concentration and the on line processed volume. The response obtained using $100 \mu\text{L}$ of $5 \mu\text{g mL}^{-1}$ of BAK was $89 \pm 3\%$ ($n = 3$) of that obtained using $1000 \mu\text{L}$ of $0.5 \mu\text{g mL}^{-1}$ of BAK. Comparable results in terms of efficiency

were obtained. Moreover, sample volumes of 100–1000 μL at 5 $\mu\text{g mL}^{-1}$ of BAK were passed through the IT-SPME capillary and their responses were measured.

Signals obtained by 1000 μL of sample were about 2–4 times higher than those obtained by 100 μL for C_{12} and C_{14} -BAK, respectively. As expected, higher analytical signals were obtained by increasing sample volume. According to this, 1 mL was the sample volume selected for concentrations lower than 35 $\mu\text{g mL}^{-1}$ of total surfactants.

Study of the influence of ADP-BAK mixtures in the BAK response

The effects of a potential competition between BAK and ADP on PDMS₆₅ capillary and/or chromatographic column were examined. For this purpose, assays were performed with two raw materials: BAK at 80% and LONZABAC with 90% of ADP, both are used to formulate commercial biocides. Different percentages of BAK in the mixtures with ADP were tested (See Table 25).

Table 25. Mixtures of BAK and ADP or TMTDAC.

BAK ($\mu\text{g mL}^{-1}$)	ADP ($\mu\text{g mL}^{-1}$)	[ADP]/[BAK]	TMTDAC ($\mu\text{g mL}^{-1}$)	[TMTDAC]/[BAK]
50	50	1	-	-
50	100	2	-	-
50	200	4	-	-
5	200	40	-	-
0.5	30	60	-	-
1.5	-	-	1.5	1
1.5	-	-	30	20

Under these conditions, the peak areas of homologues were similar to those obtained when the extraction was realized without ADP. Besides, for 50 $\mu\text{g mL}^{-1}$ of total BAK, the efficiency of extraction of C_{14} -BAK was slightly higher than C_{12} -

BAK in all cases (Figure 62a–c). Nevertheless, if the $[ADP]/[BAK]$ was high, a matrix effect was found (Figure 62d and e). For $0.5 \mu\text{g mL}^{-1}$ of total BAK representing 60 for $[ADP]/[BAK]$ concentrations ratio, the analytical response of C_{12} -BAK homologue was $19 \pm 3 \%$ of that obtained without presence of ADP. For C_{14} -BAK, the analytical response represented $61 \pm 9 \%$ ($n = 6$) (Figure 62e). This decreasing of response was observed with the two columns employed, thus the ADP effect is not related with the BAK retention on the analytical column (Figure 63).

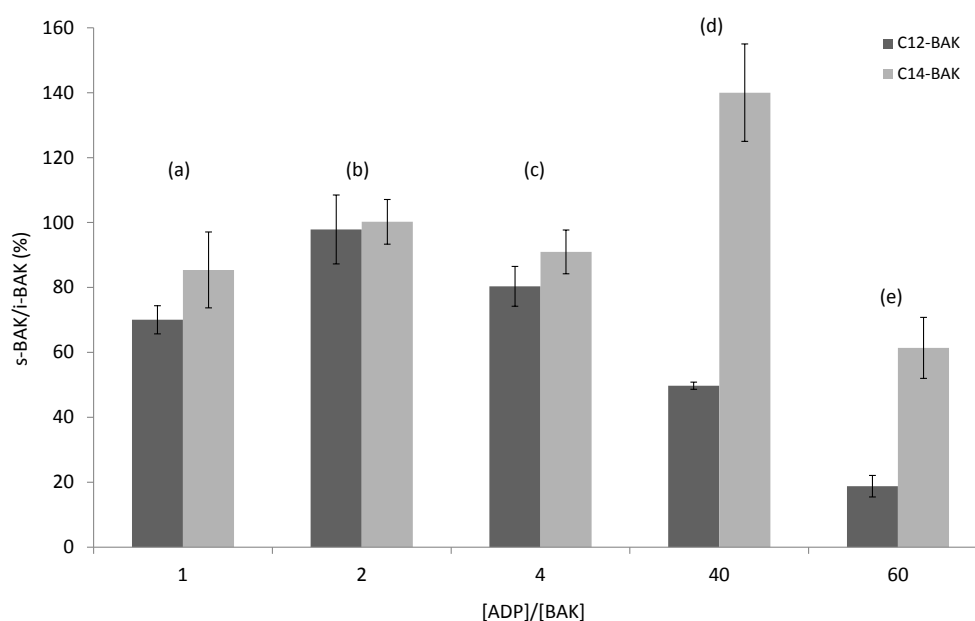


Figure 62. Percentage response of each homologue in simultaneous IT-SPME of BAK and ADP with respect of the response in individual BAK extraction (% $s\text{-BAK}/i\text{-BAK}$), at several relations of concentration of ADP and BAK (a) 1 (BAK $50 \mu\text{g mL}^{-1}$ and ADP $50 \mu\text{g mL}^{-1}$), (b) 2 (BAK $50 \mu\text{g mL}^{-1}$ and ADP $100 \mu\text{g mL}^{-1}$), (c) 3 (BAK $50 \mu\text{g mL}^{-1}$ and ADP $200 \mu\text{g mL}^{-1}$), (d) 40 (BAK $5 \mu\text{g mL}^{-1}$ and ADP $\mu\text{g mL}^{-1}$), (e) 60 (BAK $0.5 \mu\text{g mL}^{-1}$ and ADP $30 \mu\text{g mL}^{-1}$). Optimized conditions for nitrile column were employed.

Due to the low absorptivity of ADP, only BAK homologues are detected at working concentrations by the DAD detector. In order to determine low concentration of BAK in presence of ADP, a standard addition curve was performed with solutions which contained a fixed ADP concentration of $30 \mu\text{g mL}^{-1}$ and concentrations of BAK from 0.1 to $5 \mu\text{g mL}^{-1}$. The equations of the standard addition curves are showed in Table 24. The total area of

chromatographic peaks (sum of areas of C₁₂-BAK and C₁₄-BAK) versus total concentration of BAK added plot was used. The standard addition curves were performed using the two analytical columns tested obtaining a greater slope with nitrile column in the working range. This result is in accordance with the different lengths of the capillary analytical columns. One of the features of the matrix effect was the decrease of C₁₂-BAK response when the ADP/BAK concentration ratio was high, such as 40 and 60. The hydrophobic adsorption of BAK on PDMS₆₅ capillary could be performed by the alkyl chain (Chen, Y. *et al.*, 2012). In the case of ADP excess, which contains a C₁₂ chain, the C₁₂-BAK homologue could have less sites of adsorption on PDMS and then, the extraction efficiency could be lower.

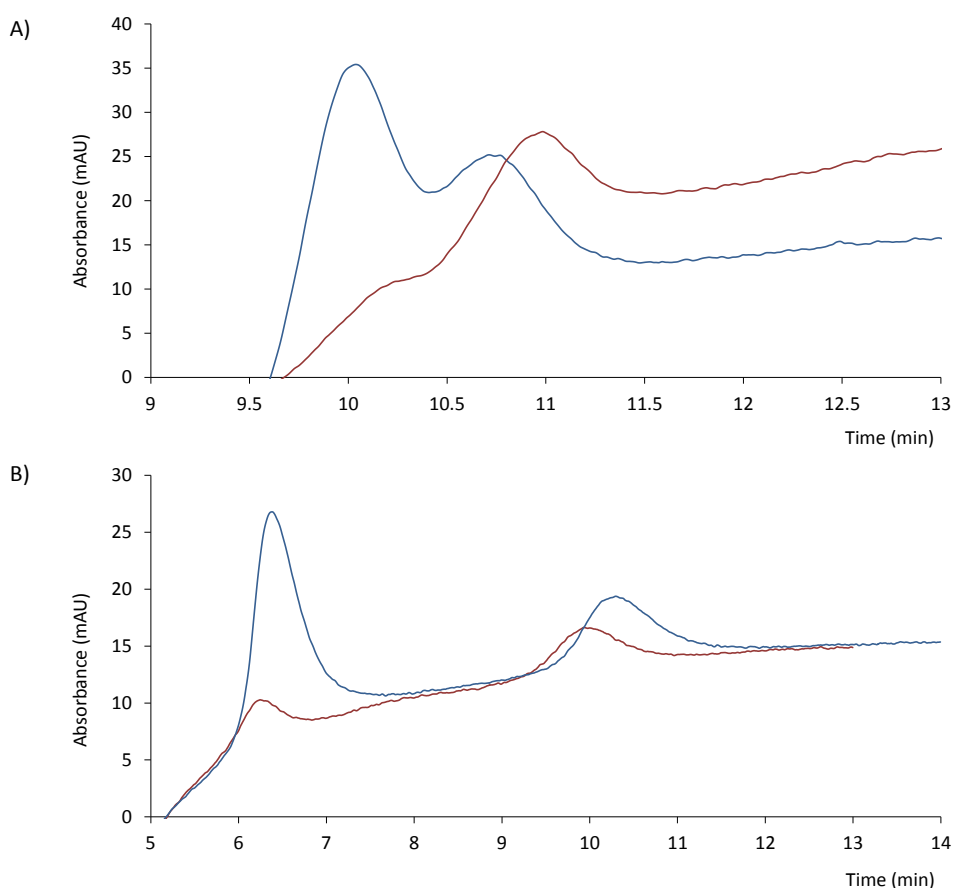


Figure 63. IT-SPME of $0.5 \mu\text{g mL}^{-1}$ of BAK in water (blue line) and simultaneous IT-SPME of $0.5 \mu\text{g mL}^{-1}$ of BAK in presence of $30 \mu\text{g mL}^{-1}$ of ADP (red line) by using (A) Nitrile column, acetone:nitrile:acetate buffer (65:35), Flow rate = $10 \mu\text{L min}^{-1}$ (B) Short C₁₈ column, acetone:nitrile:acetate buffer (85:25), Flow rate = $20 \mu\text{L min}^{-1}$.

Study of the influence of TMTDAC-BAK mixtures in the BAK response

Another QAC containing a C₁₄ alkyl chain such as TMTDAC (see Table 25) was assayed. Figure 64 shows the percentage response of each homologue in IT-SPME, at 1:1 and 1:20 [TMTDAC]/[BAK] concentrations ratios, with respect of the response in individual BAK extraction (% s-BAK/i-BAK). As it can be seen from the assayed mixtures, both BAK homologues have different extraction efficiencies. From this study it can be concluded that the competition between surfactants with same length of the alkyl chain is not the main contribution to the matrix effect. Previous works (Chen, Y. et al., 2012) have observed that the C₁₂-BAK sorption on polyacrylatefiber decreases with high concentration of electrolyte, especially in presence of divalent cations. Another phenomenon, that can be considered, is the formation of mixed micelles in systems with mixtures of cationic surfactants (Oelschlaeger, C. and Willenbacher, N., 2012). If from a specific relation of co-surfactant and BAK ([ADP]/[BAK] or [TMTDAC]/[BAK]) micelles with BAK homologues and co-surfactant are formed, a lower concentration of BAK monomers in solution is found and a lower area of the chromatographic peak is recorded.

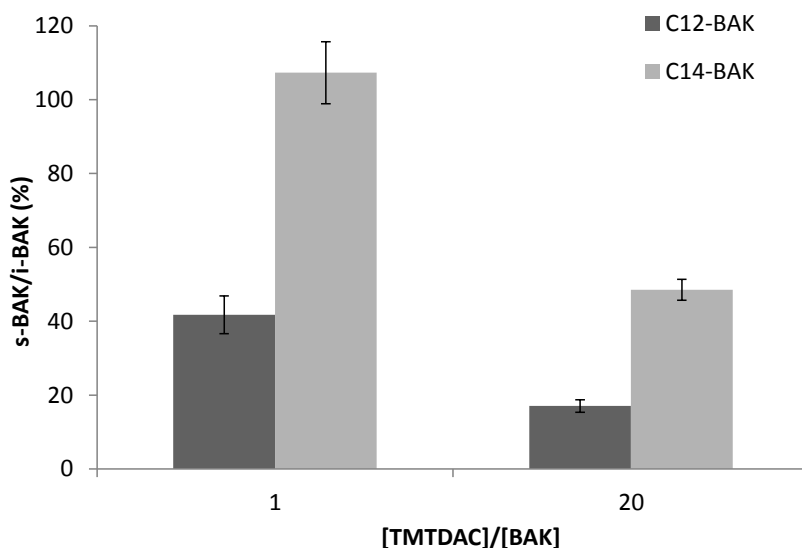


Figure 64. Effect of TMTDAC on extraction efficiency of C₁₂-BAK and C₁₄-BAK. Mixtures of 1.5 $\mu\text{g mL}^{-1}$ BAK with 1.5 and 30 $\mu\text{g mL}^{-1}$ TMTDAC. Conditions: Short C₁₈ column, acetonitrile:acetate buffer (85:25), Flow rate = 20 $\mu\text{L min}^{-1}$.

Determination of BAK in unknown biocide products

Three samples, called DECTOCIDE (DC1, DC2 and DC3), which include 4.2% of ADP, as well as water, a non-ionic surfactant, phosphoric acid and other minor components were tested. DC1 was a synthetic sample which contained ADP but not BAK. However, DC2 and DC3 were two unknown industrial samples suspicious of containing BAK. In order to check the matrix effects, BAK was added on the synthetic sample (DC1). Different [ADP]/[BAK] relations (1, 10 and 20) were tested using $1.5 \mu\text{g mL}^{-1}$ of BAK and the corresponding concentration of ADP ($1.5, 15, 30 \mu\text{g mL}^{-1}$) obtained from the biocide product. *Figure 65* shows the effect of ADP on extraction efficiency of BAK homologues. Similar behavior of the two homologues was observed when the relation [ADP]/[BAK] was 1. Nevertheless, C_{12} -BAK homologue presented the highest decrease of response at higher [ADP]/[BAK] relations, such as 10 and 20. For C_{14} -BAK, the matrix effect was produced at the highest [ADP]/[BAK] relation tested. In order to achieve suitable sensitivity and suitable conditions of IT-SPME, the biocide formulation was diluted to $720 \mu\text{g mL}^{-1}$. In this way, about $30 \mu\text{g mL}^{-1}$ of ADP were introduced in the IT-SPME-CapLC system. Under these conditions, standard C_{12} and C_{14} -BAK homologues at the same concentration ($30 \mu\text{g mL}^{-1}$) were added on the formulation without BAK (DC1). Addition standard lines, linear working ranges and correlation coefficients are shown in *Table 24*. As expected, the slope of C_{14} -BAK was 5 times greater than C_{12} -BAK. The LOQs were the lowest levels of the standard addition curves, $0.1 \mu\text{g mL}^{-1}$ for C_{12} -BAK and $0.02 \mu\text{g mL}^{-1}$ for C_{14} -BAK. LODs for C_{12} -BAK ($0.03 \mu\text{g mL}^{-1}$) and C_{14} -BAK ($0.006 \mu\text{g mL}^{-1}$) were also verified experimentally, calculated as 3/10 LOQ. The inter-day precision was evaluated by the RSD for the retention times and peak area (see *Table 24*). For studying the recovery of the described procedure, the sample (DC1) was spiked with $0.5 \mu\text{g mL}^{-1}$ of BAK at 80%. The recovery found for the sum of two homologues was $117 \pm 8\%$. The two samples suspicious of containing BAK (DC2 and DC3) were analyzed by the optimized method. The application of method showed the presence of the two BAK homologues at concentrations of $140 \pm 20 \mu\text{g mL}^{-1}$ and $43 \pm 8 \mu\text{g mL}^{-1}$ for C_{12} -BAK and C_{14} -BAK, respectively in the sample DC2 and below LODs for the sample DC3.

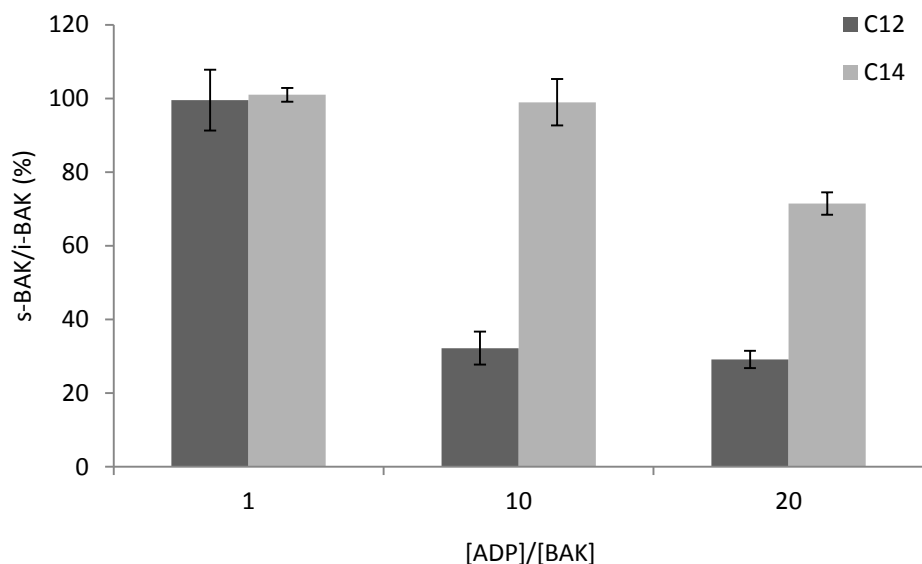


Figure 65. Effect of ADP on extraction efficiency of BAK. Mixtures of $1.5 \mu\text{g mL}^{-1}$ BAK with 1.5, 15 and $30 \mu\text{g mL}^{-1}$ of ADP from biocide product (sample DC1). Conditions: Short C_{18} column, acetonitrile:acetate buffer (85:25), Flow rate = $20 \mu\text{L min}^{-1}$.

Conclusions

New conditions of separation for rapid analysis of C_{12} and C_{14} -BAK homologues have been proposed by using a short capillary non end-capped C_{18} analytical column. Better resolution of homologues and a lower pressure of system have been achieved under these conditions than those optimized using nitrile based column. Water as sample solvent instead water-acetonitrile mixtures as in (Prieto-Blanco, M.C. et al., 2013a) was used, demonstrating the good versatility of IT-SPME for BAK estimation. Low LODs by an on-line technique without off-line treatment and using DAD detection have been achieved. The proposed method shows that for estimating BAK in mixtures of biocides is necessary to evaluate the matrix effect for obtaining reliable results. Different behaviors have been shown in function of the kind of co-biocide. If a tertiary amine like ADP is selected, the response of the BAK homologues compared to that provided by the BAK alone, depend on the ratio of concentrations ADP/BAK. While if the co-biocide is a QAC like TMTDAC, the responses of the homologues are always different. In all cases, C_{12} homologue response was more affected than C_{14} homologue response. These effects on BAK in the assayed mixtures could be

due to the formation of mixed micelles. The complex chemistry of the surfactants makes necessary an evaluation of matrix effects not only with changes of composition but also with different concentration relationships. Matrix effects depend on the kind of co-biocide in the mixture, ratio cobicide/BAK homologue and amount of total surfactant processed in the on-line system. Those influences have not been reported in the literature. This work demonstrates the need to develop new analytical methods for testing new biocides mixtures or to control industrial processes related with surfactants in a cost-effective way.

4.1.1.3 A new method for estimating DPA in GSRs as a new tool for identifying both, inorganic and organic ones, in the same sample

GSRs detection from firearms discharge may provide valuable forensic information. OGSR and IGSR components are deposited mainly onto hands after discharge a firearm. DPA is an important OGSR as indicator of firearm discharge for the identification of suspects. Due to DPA remains at low amounts on hands, its estimation requires highly sensitive analytical techniques. Thereby, IT-SPME-CapLC-DAD has been proposed. In order to achieve high sensitivity, factors such as the nature and length of the extractive phase and volume of sample processed have been optimized. In addition, several sampling tools such as samplers and extraction procedures have been studied. A complementary analysis of IGSRs by SEM-EDX has been carried out in order to confirm the presence of GSRs on shooter hands. Both analyses could be used as evidence in judicial proceedings of forensic field.

Optimization of the extraction procedure

a) DPA collecting

Several sampling tools were tested for DPA collection from shooter hands: adhesive tape lift, PDMS-based device of several PDMS:TEOS proportions (100:0, 70:30 and 50:50), dry cotton swab and wet cotton swab with non-skin-toxic solvents such as water, acetone and ethanol. According to European Chemical Agency (ECHA) base date, methanol and acetonitrile were not used due to their harmfulness and toxicity in contact with the skin, respectively. DPA working solution was dropped on a glass slide, 3 μL of 10 $\mu\text{g mL}^{-1}$. After it was air evaporated to dryness, the solid DPA was collected by the several sampling tools and extracted with 2 mL of water under vortex conditions. *Figure 66A* compares the mean peak areas of DPA extracted from slides and the RSDs to determine the suitability of the several sampling devices tested. The dry cotton swab achieved the highest analytical response with acceptable precision. The adhesive tape lift, which is used in the tape lift kit, showed an analytical response about 14 times lower than the dry cotton swab. Similar loss of peak area was observed with pure PDMS-based device. However, slow increase of analytical response was achieved when the TEOS proportion increased in the composition device. In the case of

PDMS:TEOS (30:70) device, the analytical response was improved in 4 times, compared with the response with pure PDMS device. This effect can be attributed to the increment on the hydrophilicity of the device as function of TEOS amount, suggesting the improvement of the analyte extraction. When the cotton swab was wet with water and ethanol, the analytical response decrease in an 80% and 97% respectively, compared with the response obtained by dry swab. It could be due to the wet swab spread the analyte by the slide surface and uncertainty RSD >30% can be explained based on the difficult-to-control this spread. When acetone was used as extractive solvent, DPA was not detected but a small peak at a retention time slightly lower than the analyte was observed (*Figure 66B*). As can be confirmed by the spectra depicted in the *Figure 65B inset*, this peak could be differentiated from the analyte peak by retention time and spectrum and it could be corresponds to some compound from cotton swab. From these results, dry cotton swab was chosen as the best sampling collector of DPA from shooter hands for the further work.

b) DPA extraction from the collector

Once the collector was selected, the second step was to optimize the extraction procedure from the collector. For this aim, non-assisted, UAE and VAE were studied. To test this, 3 μl of 10 $\mu\text{g mL}^{-1}$ DPA working solution (prepared in acetonitrile to favor evaporation) was spread on a glass slide. After the solvent evaporation, the tip of a dry cotton swab was used to extract DPA from the slide. The tip was introduced into a vial containing 2 mL of water under the three abovementioned conditions for 5 min (*See Section 3.3.1.2 for more details*). VAE offered the best results in term both analytical response (peak area) and RSD, as can be seen in *Figure 66C*. For evaluating the extraction efficiencies, the peak area ratios between non-assisted and assisted-extractions were calculated. Thus, a ratio of 2 and 5 were obtained by UAE and VAE, respectively. Satisfactory RSD of 9% for VAE was obtained and RSD of 32 % for UAE. From these results, we concluded that the best extraction procedure of DPA from cotton swab was VAE.

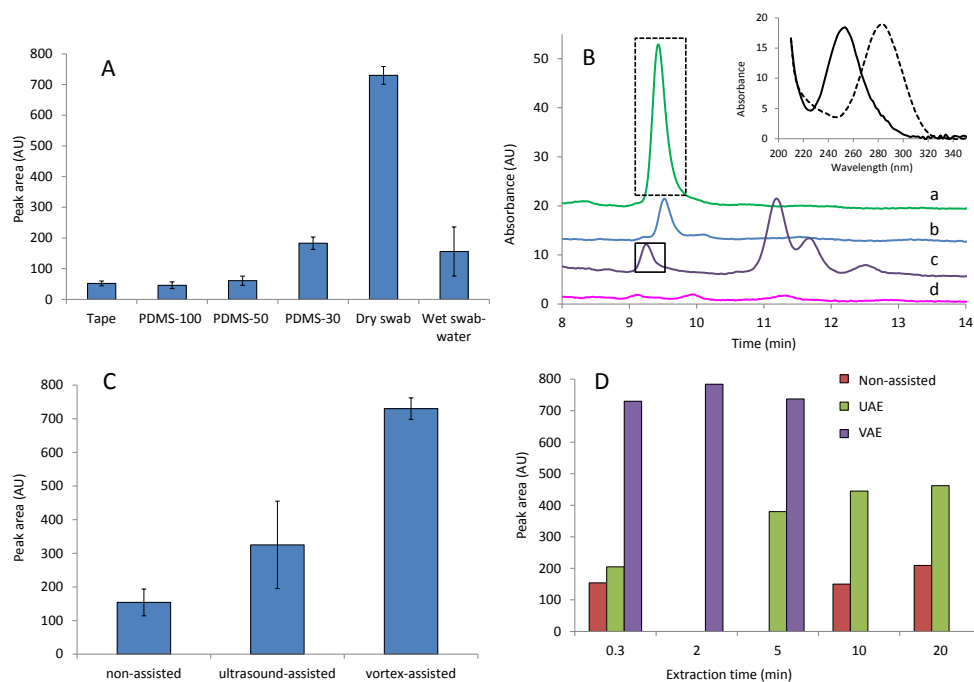


Figure 66. Comparison of peak areas obtained for standard solution ($3 \mu\text{L}$ of $10 \mu\text{g mL}^{-1}$ in 2 mL of water, 15 ng mL^{-1}) with different (A) sample collectors (B) solvents to wet cotton swab (at 10 ng mL^{-1}): dry (a), water (b), acetone (c) and ethanol (d), together with normalized spectra (inset) of DPA (black dashed line) and unknown compound (black solid line), (C) extraction modalities and (D) extraction time.

Effect of extraction time

Peak areas of DPA were compared as a function of different extraction times under optimum conditions: 20 s, 1, 2 and 5 min, as shown in *Figure 66D*. Longer times were not tested due to the discomfort with the manual vortex. No significant differences on peak areas were observed at several extraction times. Additionally, long times for non-assisted and UAE were also studied in order to investigate the improvement of analytical response but both procedure were not as efficient as VAE. Therefore, 20 s of VAE time was selected.

Effect of extraction solvent

The capacity of three solvents to remove the DPA from the cotton swab was investigated: acetonitrile, ethanol and water. Mixtures of 90:10 water:acetonitrile and water:ethanol and 100 % water were tested. 51% and 85% of decrease on peak area was observed when ethanol and acetonitrile, respectively, were included in the extraction solvent (See Figure 67). This result suggested that the analyte was not retained on the IT-SPME capillary column. Moreover, high peaks were observed at a retention time slightly lower than the analyte. These peaks were not detected when the analysis was carried out in solution, suggesting they were due to compounds extracted from cotton. Note that ethanol was the solvent which extracted more amount of interfering compounds. However, water offered the best results not only in terms of extraction and reduced interferences but also in terms of environmental performance, since water is a green solvent. Thus, water was chosen as optimum extraction solvent for this work. Aqueous extracts of DPA from hands were later processed by IT-SPME-Cap-LC as is described in the next point.

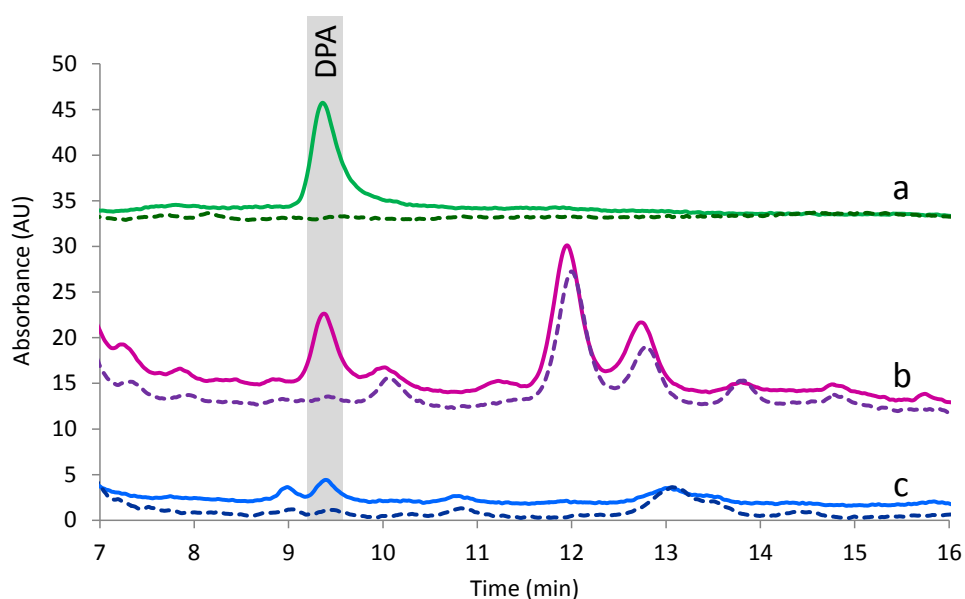


Figure 67. Chromatograms of blanks (dashed lines) and standard solution of 5 ng mL^{-1} DPA (solid lines) obtained with different extraction solvents: water (a), 90:10 water: ethanol (b) and 90:10 water: acetonitrile (c).

Optimization of the IT-SPME procedure and chromatographic conditions

Experiments were aimed to optimize the DPA extraction by IT-SPME, as well as the subsequent chromatographic analysis. Initially, two mobile-phase compositions in isocratic elution mode were tested, 60:40 and 70:30 acetonitrile:water (v/v). As can be seen in *Figure 68A*, both compositions were adequate to desorb DPA from the extractive capillary. However, a decrease of retention time and narrower peaks were achieved with the increase of acetonitrile and flow. It should be remarked that cross-contamination was observed when using isocratic elution mode with 70:30 acetonitrile:water. For this reason, gradient elution program (See *Section 3.5.1*) with 100% of acetonitrile during 4 min was employed as cleaning step.

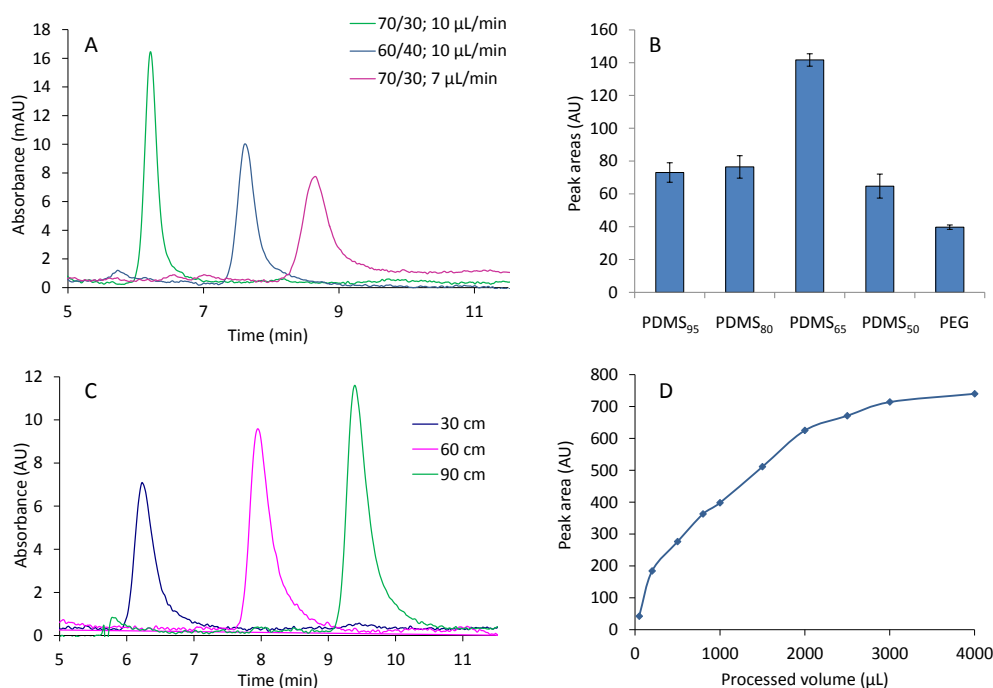


Figure 68. Effect of (A) acetonitrile percentage and mobile phase flow ($800 \mu\text{L}$ at 7 ng mL^{-1} , PDMS₆₅, 30 cm); (B) nature of the extractive phase ($800 \mu\text{L}$ at 5 ng mL^{-1} , capillary length 30 cm, optimum mobile phase); (C) capillary length ($800 \mu\text{L}$, 5 ng mL^{-1} , PDMS₆₅, optimum mobile phase) and (D) sample volume processed (5 ng mL^{-1} , PDMS₆₅, capillary length 90 cm, optimum mobile phase) on the DPA retention in IT-SPME.

As mentioned in the *Introduction Chapter*, IT-SPME is performed using a capillary column as the loop of the injection valve. The analytes are extracted during sample loading and transferred to the analytical column with the mobile phase by changing the valve position. This configuration is advantageous in order to achieve LODs required for detecting DPA deposited on shooter hands. Herein, several assays were carried out to optimize the extraction step. The nature of the extractive phase, the length of the capillary column and the volume of sample processed were evaluated. Five phases for IT-SPME were assayed: PDMS₉₅, PDMS₈₀, PDMS₆₅, PDMS₅₀ and 100% PEG (See Table 26).

Table 26. Characteristics of capillary columns employed in IT-SPME.

Extractive capillary	Coating	Coating thickness (μm)
PDMS ₉₅	5% diphenyl-95% PDMS	3
PDMS ₈₀	20% diphenyl-80% PDMS	3
PDMS ₆₅	35% diphenyl-65% PDMS	3
PDMS ₅₀	50% diphenyl-50% PDMS	3
Zebtron ZB-WAXplus	PEG	1

Figure 68B compares the analytical response (mean peak area) for DPA (5 ng mL⁻¹) with the different nature capillaries (30 cm length) when the volume of standard processed was 800 μL. As can be seen, PDMS₆₅ phase provided the highest analytical responses. This suggested that higher percentage of diphenyl groups in the extractive phase lead to increase on the analytical response. This result indicated that the extraction involves π–π interactions with the aromatic rings of DPA. However, PDMS₅₀ provided a decrease on the peak area. This effect could be attributed to the increment on the polarity of the extractive phase and so, the affinity towards the DPA decreased (log P=3.5). The same effect occurred with PEG capillary column due to its higher polarity. Thus, the PDMS₆₅ capillary column was selected for further experiments.

On the other hand, the effect of the capillary length on the analytical response (peak areas) was also studied by processing 800 μL of working solution of DPA (5 ng mL⁻¹) with PDMS₆₅ capillaries of 30, 60 and 90 cm. *Figure 68C* shows

the increment of the analytical response with the length of the capillary indicating that the amount of analyte extracted also increased. The peak area for DPA was improved in a 40% and 47% with the capillary columns of 60 and 90 cm, respectively, compared with the capillary of 30 cm. Capillaries longer than 90 cm did not improve the analytical response. As expected, a slight increment on the time retention of the analyte from 6.2 to 9.4 min was observed when increasing the capillary length from 30 to 90 cm. Due to the objective of this work requires high sensitivity, PDMS₆₅ of 90 cm was chosen as the optimal capillary column length.

Sample volumes processed up to 4 mL at 5 ng mL⁻¹ of DPA solution were studied. The results obtained are depicted in *Figure 68D*. As can be seen, a remarkable increase on the analytical response (peak area) with the increase of the sample volume was observed up to 2 mL. The signal increased very slightly from 2 to 4 mL more likely due to the breakthrough of DPA. Taking into account the required sensitivity, 2 mL was chosen as the optimum sample volume for further experiments. However, it was found that the swabs used in the present study absorbed about 125 µL of contact solution (*See Section 3.3.1.2*). According to this observation, further experiments were carried out by processing 1800 µL remaining in vial.

Although low extraction efficiencies (absolute recoveries) are achieved by IT-SMPE, the analytical responses can be improved significantly owing to the large volumes of sample that can be processed through the capillary column. The extraction efficiencies of the proposed methodology were estimated by comparing the amount of analyte extracted, which is the amount of the analyte transferred to the analytical column, with the total amount of analyte passed through the optimum extraction capillary. The amount of analyte extracted was established from the peak areas in the resulting chromatograms and from the calibration equations constructed through the direct injection of 72 µL of standard solutions of the analyte. This volume is the inner volume of the PDMS₆₅ capillary of 90 cm used for IT-SPME. The extraction efficiency obtained was 7% which is in accordance with those reported for this technique. In addition, a clean-up step was examined after sample loading by introducing 120 µL of nanopure water before changing the valve position. Significant loss of analyte was not observed, thus clean-up was applied in order to remove fibers or compounds from cotton which can be remain inside the capillary column. It was also tested to filter

solutions of DPA extracted from cotton swab through 0.45 μm nylon membranes to prevent the introduction of fibers from cotton swabs. Nevertheless, the analyte was not observed, may be owing to it was retained on nylon filter. Hence, samples were not filtered before injection.

Analytical performance

Relevant analytical parameters such as calibration equations, linear working range, LOD, LOQ and precision are shown in *Table 27*, both solution and swab-VAE procedure. Satisfactory linearity within the tested concentrations was achieved. The LODs and LOQs were calculated experimentally from solutions containing concentrations providing signal/noise of 3 and 10, respectively. LODs and LOQs by swab-VAE were 0.15 ng mL^{-1} and 0.5 ng mL^{-1} , respectively. Converted into the equivalent amount of DPA injected onto the system, the LOD and LOQ were 0.3 ng and 1 ng, respectively. These results showed that the sensitivity reached with the proposed procedure is adequate for estimating DPA on shooter hands. The precision for the analytical response was suitable at the working concentration range, with intra and inter-day RSDs of 9 % and 15 %, respectively ($n=4$). The precision of the retention times was also estimated obtaining acceptable RSD values of 1.5 % and 2.5 % for intra and inter-day, respectively ($n=3$, 15 ng mL^{-1}). Satisfactory results for the study in solution were obtained as *Table 27* shows. To test the extraction efficiency of DPA from samples (including sample collection by cotton swab and extraction from swab to water), the peak area of solution obtained after extraction ($2 \mu\text{L}$ of $10 \mu\text{g mL}^{-1}$ DPA spread on glass slide followed by the protocol described in *Section 3.3.1.2*) was compared with the peak area obtained for the equivalent concentration in solution directly injected (5 ng mL^{-1} of DPA). The extraction efficiency estimated was $37 \pm 5 \%$. Recovery study in samples at 10 ng mL^{-1} was performed and value obtained was $108 \pm 16 \%$.

Table 27. Analytical data for DPA determination by IT-SPME-CapLC-DAD; a : ordinate, b : slope, s_a and s_b : standard deviation of the ordinate and slope, respectively, R^2 : determination coefficient.

Procedure	Linear range (ng mL ⁻¹)	Linearity $y = a + bx$ (ng mL ⁻¹)			Precision (n=4, 15 ng mL ⁻¹)		LOD (ng mL ⁻¹)	LOQ (ng mL ⁻¹)
		$a \pm s_a$	$b \pm s_b$	R^2	RSD _{intra-day} (%)	RSD _{inter-day} (%)		
Solution	0.15 - 50	-7 ± 57	144 ± 2	0.9994	5	10	0.05	0.15
Swab	0.5 - 25	-13 ± 24	49.2 ± 1.7	0.9939	9	14	0.15	0.5

Analysis of samples

Several samples collected from hands of police officers after shooting test were analyzed by the optimized procedure. Additionally, the same procedure described for shooting hands (See 3.6.4.1 section) was carried out for the hands of each police before shooting to obtain blank samples. The samples were analyzed without identification of volunteers. Figure 69 shows the chromatograms for shooter (sample 2A) and non-shooter hand samples and UV-Vis spectra of standard and sample. Although unknown compounds were extracted from shooter hands, DPA was identified in samples by the concordance between retention time (9.4 min) and UV-Vis spectra of standard DPA and the suspect peak in the chromatogram of the sample. As can be seen in the figure, the chromatogram of a blank showed no peak interferences at the retention time of DPA.

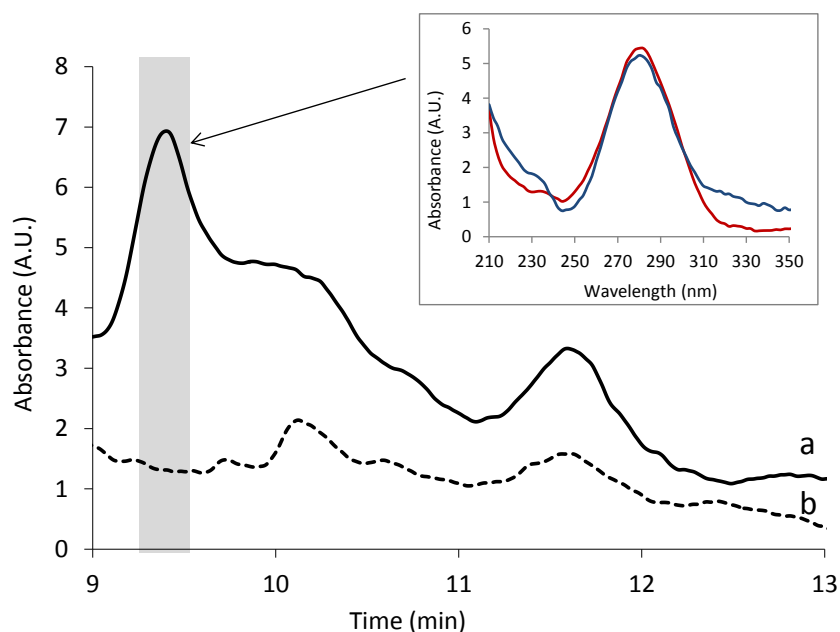


Figure 69. Chromatograms obtained for sample 2A (black solid line) and blank of non-shooter hand (black dashed line). The inserts correspond to the matching of the spectra of DPA found (blue line) in reference to the library of the standard (red line).

Quantification of the samples was carried out based on the regression equation previously obtained (See Table 27). Table 28 shows the samples screened and the quantification results. With a total of twenty one swab samples and six tape kit samples, DPA was found and quantified in seventeen swab samples (81 % of all swab samples analyzed) and, as can be expected due to tape lift was worth sampler, three tape samples produced a signal above LOQ but DPA was not detected in the other three. In the literature, few studies of DPA are focused in hands and LODs reported are higher to that provided by the proposed method (Bernal Morales, E. and Revilla Vázquez, A. L., 2004; Mei, H. et al., 2016; Tong, Y. et al., 2001). The paired t test was used to evaluate statistically differences between both hands, left and right. The p value obtained at 95% significant level was higher than 0.05 ($p=0.232$). From these results, we can conclude that the results from both hands were statistically equivalents.

Table 28. Samples and quantification by optimized extraction procedure followed by IT-SPME-CapLC-DAD. *tape lift kit samples quantified by regression equation 14 times lower than regression equation by cotton swab.

Police officer	Sample	Hand	Number of shots	Concentration (ng)
A	1 A	left	25	4.4
	2 A	right		3.8
B	3 B	left	12	2.7
	4 B	right		1.9
C	5 C	left	25	3.0
	6 C	right		3.8
D	7 D	left	25	2.8
	8 D	right		< LOD
E	9 E	left	25	2.5
	10 E	right		3.2
F	11 F	left	25	16.5
	12 F	right		3.4
G	13 G	left	25	< LOD
	14 G	right		< LOD
H	15 H	left	25	4.9
	16 H	right		< LOD
I	17 I	left	25	8.4
	18 I	right		9.5
J	19 J	left	25	8.0
	20 J	right		4.3
K*	21 K	left	25	< LOD
	22 K	right		< LOD
L	23 L	left and right	25	1.4
M*	24 M	left and right	25	3.6
N*	25 N	left and right	25	6.6
O*	26 O	left and right	25	6.9
P*	27 P	left and right	25	< LOD

IGSR particles identification

As can be seen in *Figure 70*, the presence of GSR particles from cotton swabs can be confirmed by naked eye and microscopically (*Burleson, G.L. et al., 2009*) before chromatographic analysis. Fibers of cotton swab remained clean after sampling a non-shooter hand (See *Figure 70A*). However, gunpowder particles with typical spherical shape and size up to 20 μm (*Bailey, M.J. et al., 2009*) were observed between cotton fibers (see red circles) after sampling a shooter hand (*Figure 70B*).

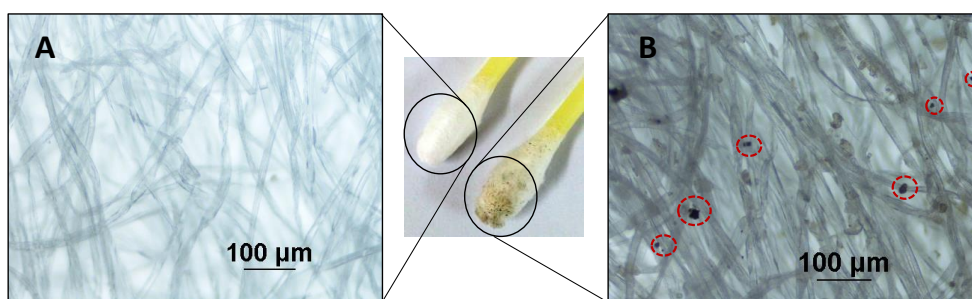


Figure 70. Visual and microscopically (10x magnification) inspection of cotton swab after sampling a non-shooter hand (A) and after sampling a shooter hand, sample 2A (B).

The same cotton sample (sample 2A) was also characterized by SEM/EDX after chromatographic analysis. It was possible due to some gunpowder particles remained on cotton swabs after DPA has been extracted. *Figure 71* shows a typical IGR particle with spherical shape and 38 μm of size (*Dalby, O. et al., 2010*). As can be observed in elemental analysis, predominant elements were Ba (46%) and Sb (44%) as reported in the literature (*Morelato, M. et al., 2012; Tarifa, A. and Almirall, J. R. et al., 2015*). Both inorganic and organic compounds have been identified in hand samples by SEM-EDX and chromatography, respectively. Hence, the presence of GSRs on sample hands is confirmed.

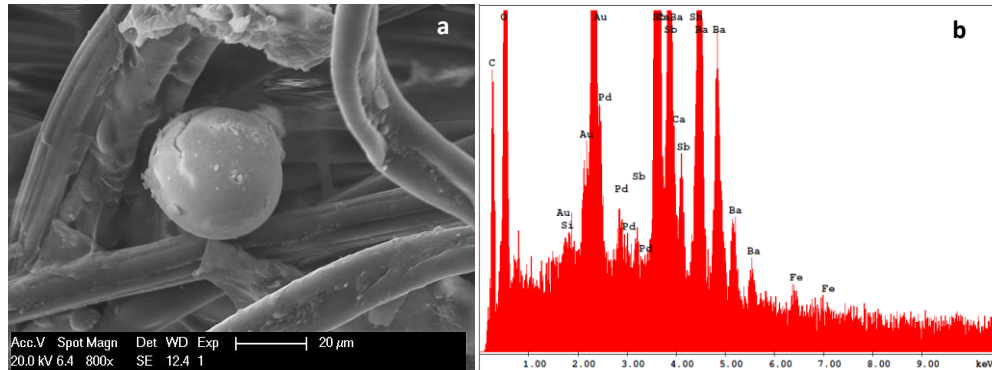


Figure 71. SEM image (a) and EDX spectra of IGSR found on swab sample (sample 2A) after shooting (b).

The other main of this work was to examine the morphology and elemental composition and distribution of GSR particles collected with the lift tape kit, the typical police collector. Only particles which can be identified as GSR by their composition and morphology were selected for SEM-EDX analysis. Roughly 6-7 particles per sample were studied. As reported in (Bailey, M.J. et al., 2009), this number of particles is approximately equivalent to the particles that can be recovered the shooter hand in a forensic scene. A portion between 3-40% of total surface of sample was explored to find this number of particles, depending on the sample. Figures 72 and 73 show the morphology and elemental data of particles found on adhesive tapes collected after shooting. Most of the particles observed were spherical. Less than 20 % of particles founded had irregular shape probably due to they are distorted after shooting. As shown, particles had several surfaces such as smooth, bumpy or covered with craters with or without metallic shine. Greater than 60% of the particles founded had smooth surface. Their morphology is an effect of conditions taking place during the firing. Particles can be perforated, capped, broken or stemmed (Wallace, J.S. et al., 2008). Results of SEM/EDX analysis of GRS particles founded on tapes from shooter hands are displayed in Table 29.

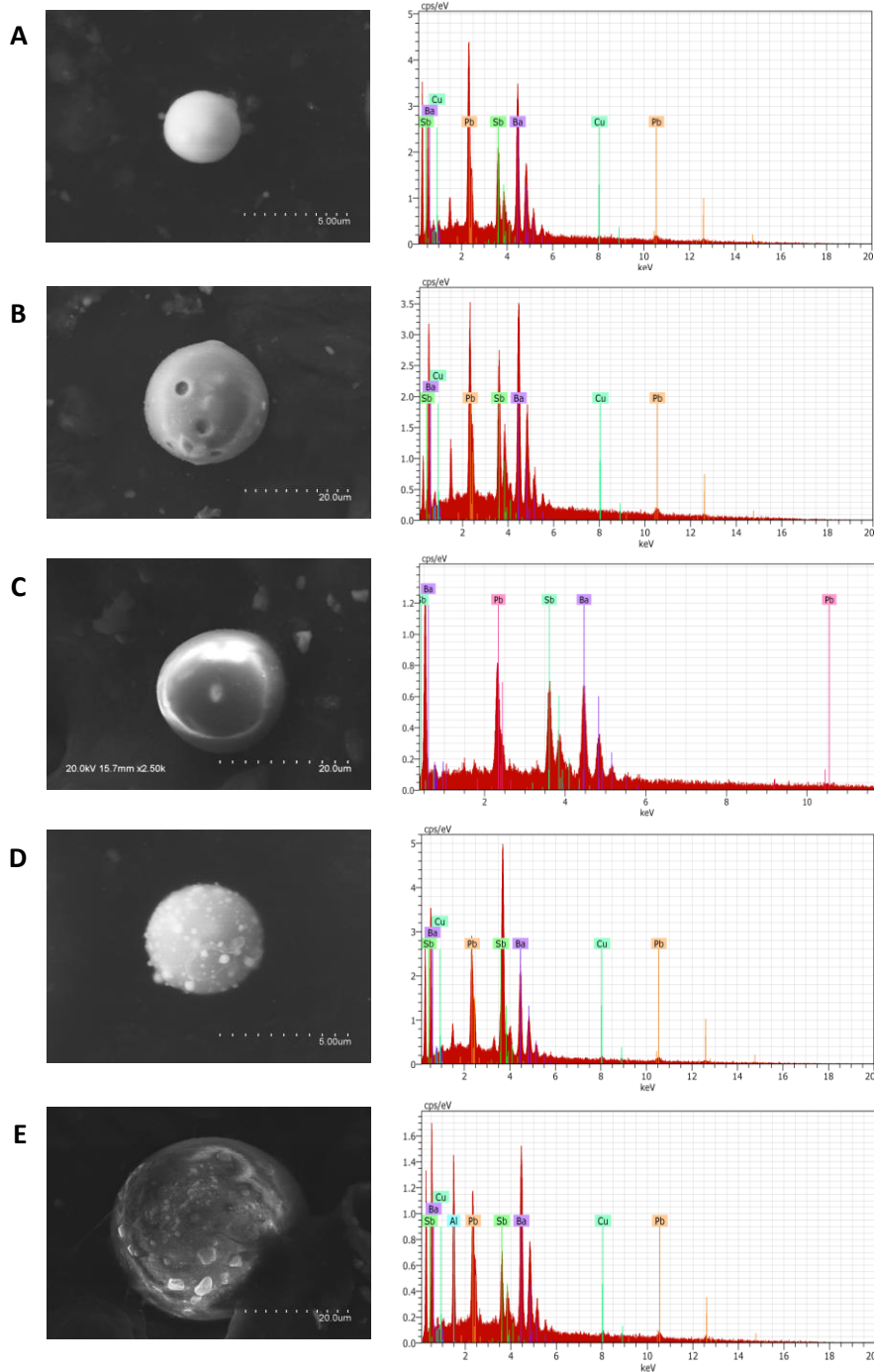


Figure 72. SEM images (left) and EDX spectra (right) of spherical particles found on tapes used to collect GSR after shooting a gun: sample 21K.2 (A), sample 22K.7(B), sample 25N.4(C), sample 21K.4 (D) and sample 24 M.6 (E).

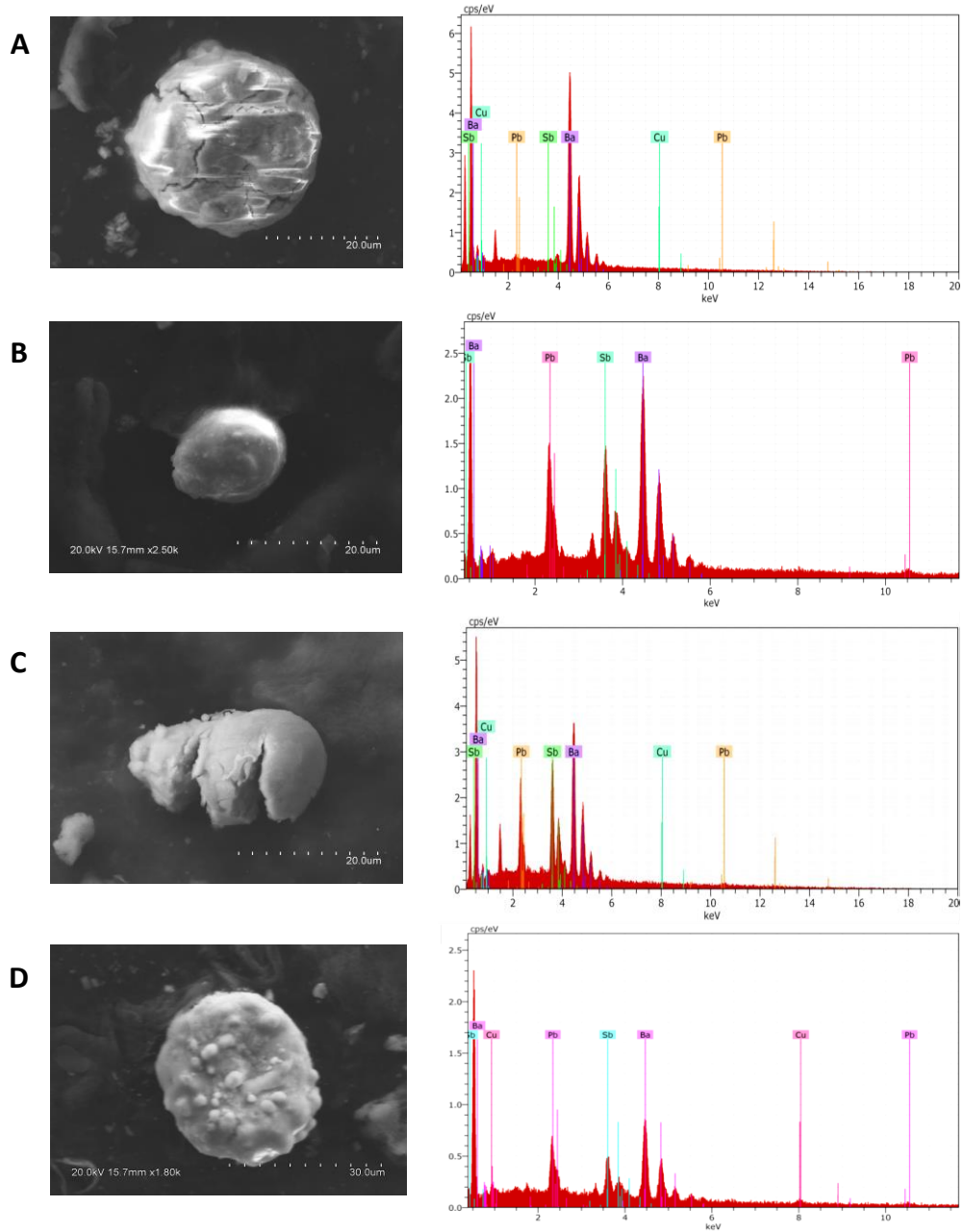


Figure 73. SEM images (left) and EDX spectra (right) of non-spherical particles found on tapes used to collect GSR after shooting a gun: sample 22K.2 (A), sample 25N.3 (B), sample 21K.1 (C), sample 25N.2 (D).

Table 29. Summary of shape, surface and elemental composition of GRS particles founded on tape lift kit from shooter hands.

Sample	GSR Particle	Shape	Surface	Elemental Composition (%)					
				Major			Minor/Trace		
				Ba	Sb	Pb	Cu	Al	Fe
21 K	21K.1	Irregular	Nonmetallic bumpy	62,5	33,2	4,3	X		
	21K.2	Spherical	Nonmetallic smooth	62,4	25,7	11,9	X		
	21K.3	Spherical	Nonmetallic bumpy	65,9	18,8	15,3	X		
	21K.4	Spherical	Nonmetallic bumpy	46,8	40,2	13,0	X		
	21K.5	Spheroidal	Nonmetallic smooth	65,7	14,8	19,5	X		
	21K.6	Spherical	Nonmetallic smooth	87,5	11,1	1,4	X		
	21K.7	Spherical	Nonmetallic bumpy	58,4	28,8	12,8	X		
22 K	22K.1	Spherical	Metallic smooth	61,5	33,5	5,0	X		
	22K.2	Irregular	Metallic bumpy	98,8	0,7	0,5			
	22K.3	Spherical	Nonmetallic smooth	48,0	37,3	14,7			
	22K.4	Spherical	Metallic smooth	57,0	37,1	5,9	X		
	22K.5	Spherical	Metallic smooth	61,8	32,7	5,5	X		
	22K.6	Spherical	Metallic smooth	79,0	16,8	4,2	X		
	22K.7	Spherical	Nonmetallic with hollows	50,6	33,4	16,0	X		
24 M	24M.1	Spherical	Metallic smooth	63,0	34,8	2,1			
	24M.2	Spherical	Metallic smooth	63,2	30,6	6,3			
	24M.3	Spherical	Nonmetallic bumpy	0,0	96,7	3,3		X	
	24M.4	Spherical	Metallic smooth	60,4	37,2	2,3		X	
	24M.5	Spherical	Nonmetallic smooth	51,1	34,5	14,3	X	X	
	24M.6	Spherical	Metallic smooth	69,2	20,3	10,5	X	X	
	24M.7	Spherical	Metallic smooth	54,8	37,3	7,9	X	X	
25 N	25N.1	Spherical	Metallic smooth	68,8	24,7	6,4			X
	25N.2	Irregular	Nonmetallic bumpy	72,0	17,8	10,2	X		
	25N.3	Spheroidal	Metallic bumpy	63,3	30,0	6,7			
	25N.4	Spherical	Metallic smooth	53,0	39,7	7,4	X		
26 O	26O.1	Spherical	Metallic smooth	63,6	34,2	2,2			
	26O.2	Spherical	Metallic smooth	61,7	35,2	3,0		X	
	26O.3	Irregular	Nonmetallic bumpy	40,0	33,8	26,2			
	26O.4	Spherical	Metallic smooth	0,3	4,9	94,9	X		
	26O.5	Spherical	Metallic smooth	62,7	31,2	6,3			
26O.6	Spherical	Metallic smooth	50,6	35,8	13,6				
27 P	27P.1	Spherical	Nonmetallic bumpy	53,5	38,3	8,2	X	X	
	27P.2	Spherical	Nonmetallic bumpy	57,4	30,9	11,7	X		
	27P.3	Spherical	Nonmetallic smooth	60,2	36,9	2,9	X		
	27P.4	Spherical	Nonmetallic smooth	57,6	30,9	11,5	X		
	27P.5	Spheroidal	Nonmetallic bumpy	48,9	30,7	20,5	X		
	27P.6	Spherical	Nonmetallic bumpy	61,3	31,7	7,0	X		

As observed, most of the particles had the characteristic elemental composition of GSRs which is mainly based on Pb, Sb, and Ba. All 37 GSR particles founded, 35 of which contained on average 61% of Ba, 30 % of Sb and 9% of Pb. The other two particles were excluded because contained 95 % of Pb and 97% of Sb probably from bullet, shell or cartridge. The mean values were calculated from results of *Table 29*. Moreover, some particles also contained other elements such as Al, Cu and Fe at trace levels. About 66% of samples contained traces of Cu, 20% Al and 3% Fe, while 12% of them contained both Al and Cu. Nevertheless, these minority elements cannot be considered an evidence of shooting. Even though these particles had similar elemental composition, their size varied over a range from 3 to 30 μm according to the literature (*Brozek-Mucha, Z. et al., 2007*).

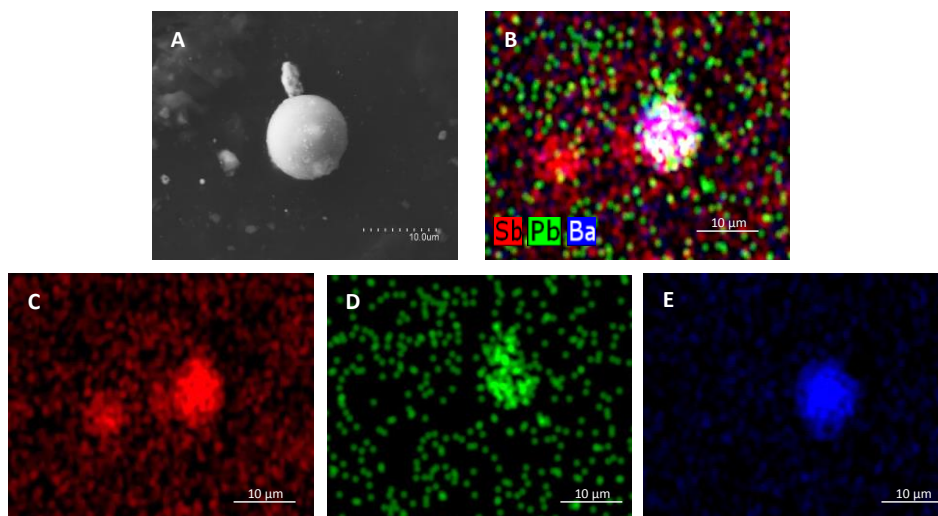


Figure 74. (A) SEM image, (B) overlay X-ray map of singles X-ray of Sb (C); Pb (D) and Ba (E) of particle found on a tape used to collect GSR on hands after shooting.

Spatial distribution of the majority chemical elements of a GSR particle was also observed by X-ray mapping. It consist in using colors for representing the elemental distribution (Cardinetti, B. et al., 2004). In this case, Sb appears red, Pb is green and Ba is blue. The X-ray mapped of sample 21K is shown together with its corresponding SEM image (Figure 74A). Both images of single elements (Figure 74B) and their overlay (Figure 74C-E) give us both the distribution and merging of the elements presents in the sample. As can be seen, dots representing Sb, Ba and Pb came together and mixed in a GSR although these elements are scattered throughout all sample. From the images, can be observed that predominant element was Ba, followed by Sb and Pb. Thus, these mapping results were according to the previous elemental composition studied. The results obtained by SEM/EDX can be considered as indicative of IGSRs particles on shooter hands.

Conclusion

This work presents a reduced sample treatment: sampling from shooter hands by using a cotton swab followed by VAE with water in short time. Aqueous samples were directly processed in the miniaturized IT-SPME-CapLC-DAD system for on-line clean-up and preconcentration of sample. It is worth notius that no toxic solvents and low cost material were employed. The efficiencies of the IT-

SPME have been tested for several natures and lengths of the extractive phase, as well as sample volume processed in order to improve the sensitivity. Highest analytical responses were obtained for the longest PDMS₆₅ capillaries (90 cm) more likely due to π - π interactions and 1.8 mL of sample. The proposed approach is a rapid, green and cost-effective option for detecting DPA on hand samples. Satisfactory LOD (0.3 ng) and precision ($RSD_{\text{intra-day}} = 9\%$, $RSD_{\text{inter-day}} = 14\%$) were achieved. In order to test the utility of the method for real cases, several shooter hands were collected by cotton swabs, then DPA extraction was carried out with water under vortex condition and finally, samples were processed by IT-SPME-CapLC. The results showed that DPA was found and quantified in 81 % of samples, so this method provides suitable selectivity and sensitivity at low concentration levels (ng mL^{-1}), which are concentrations typically found in hand samples. Additionally, IGSRs inspection of swab samples was carried out by microscopy in order to confirm the presence of GSRs on shooter hands. Furthermore, a few shooter hands were collected by tape lift kit obtaining insufficient sensitivity for DPA stimulation. If organic compounds are detected in combination with inorganic compounds, higher probative value can be achieved and false positives/negatives can also be reduced for discriminating shooter hands. In this work, a sensible chromatographic method to detect the organic compound DPA can be combined with IGSR analysis by microscopy in order to obtain a valuable evidence of GSR deposited on hands of a suspected shooter. Therefore, the proposed method is helpful to determine whether a person has fired a gun in a forensic investigation.

4.1.2 PDMS AS SUPPORTING MATERIAL FOR SENSOR DEVELOPING

The use of PDMS as encapsulant material of derivatizing reagents for the development of sensors has been studied in this Thesis. This Si-based material is a suitable support for developing solid sensors to use in aqueous media. The stabilization of the reagents as well as the diffusion of analytes from aqueous matrix into PDMS where the reagent is embedded has been studied. In order to improve the sensitivity, the polymeric matrix based on PDMS has been modified by adding the inorganic compound TEOS. Several amounts of TEOS have been tested for each application of these sensors. The derivatizing reagent is dispersed into TEOS and then this mixture is added into the polymeric matrix. This fabrication method presents advantages such as: (i) TEOS gives hydrophilicity to the polymeric matrix avoiding unwanted reactions, (ii) the hybrid matrix maintains the stability of the structure and (iii) the polymeric matrix protects the dyes preserving their optical properties. Thus, the derivatizing reaction is carried out in the sensor producing a color change. In addition, the presence of SiO₂NPs in the sensor has been studied in order to select the best composition which had good gelation properties, stability and accessibility of the analyte to the reagent. Semiquantitative analysis can be performed by visual inspection. Absorbance measurements by DR and/or color values by DI can be carried out for quantitative analysis. The developed sensors have been used for the in-situ detection of amines of interest in a wide range of fields, such as environmental, industrial and forensic. Increasing efforts have chiefly been focused on the search for these kind of colorimetric sensors that allow simple, rapid, low-cost, green and on-site analysis without the requirement of trained personnel.

This section has divided in the follow four subsections:

1. PDMS-based sensor containing NQS for the estimation of casein in effluents from dairy industries.
2. Sensor based on PDMS/TEOS/SiO₂NPs/NQS for controlling the dosage of the biocide ADP in industrial formulations.
3. A solid colorimetric sensor based on PDMS/TEOS/SiO₂NPs/NQS for the analysis of amphetamine-like street samples.
4. A passive solid sensor based on PDMS/Co(SCN)₂ for the in-situ colorimetric estimation of the presence of ketamine in illicit drug samples.

4.1.2.1 PDMS sensor containing NQS as dispositive for the estimation of casein in effluents from dairy industries

In this section, a colorimetric sensor based on the embedding of the derivatizing reagent NQS into a PDMS/TEOS/SiO₂NPs is proposed to estimate casein. As mention before, NQS is a reagent typically used to determine amines. This non-hazard reagent NQS forms colored derivatives with amines. Brown-grey and orange derivatives are obtained with primary and secondary amines in alkaline medium, respectively, making possible their colorimetric determination (*Quan-Min, L., Zhan-Jun, Y., 2007*). The fabrication of this sensor is based on the Patent ES248247B1. The evaluation of the main components in the effluents of dairy industries such as casein is important due to the environmental problems that can be caused. Therefore, this proposed sensor allows the in-situ monitoring of casein in dairy industries effluents. Casein is denatured applying heat and the amino acids formed are diffused from the solution to the sensor where the derivatization with NQS is produced. The sensing support changes its color from yellow to orange depending on the casein concentration. Thus, semiquantitative analysis of casein can be performed by visual observation. Quantitative analysis can be carried out by measuring the absorbance with a reflection probe or by an image-processing tool. The potential parameters which can affect the response of the sensor have been studied. The method validation has been done by applying the BCA (*Kralj, J.G. et al., 2014*).

Optimization of the PDMS–NQS sensor

Taking into account the nature of the analyte, the composition of sensing devices was optimized. For this aim, the amount of TEOS, SiO₂NPs and NQS were studied. Firstly, by keeping the amount of reagent and SiO₂NPs constant, different proportions of TEOS in the polymeric sensor were tested (50%, 60% and 80% TEOS). Large amounts of TEOS made more difficult the gelation process (e.g., 80%), probably owing to the fact that a lower PDMS content causes a slowdown in the co-condensation (gelification) process. As it was expected, the gelation process was depended on the ratio TEOS:PDMS. In addition, greater proportions of PDMS reduced the gelation while the viscosity increased (*Illescas, J.F. and Mosquera, M.J., 2011; Li, D et al., 2013*). As can be seen in *Figure 75A*, sensors with 50% TEOS–50% PDMS provided higher responses than those using 60% TEOS–40% PDMS. It should be noted that an increase of TEOS resulted in lower

responses. Although in these conditions, the viscosity of the gel was expected to be lower and the diffusion of the analyte higher, the sensor conditions were not the most adequate for the derivatization reaction. Based on these results, films with TEOS–PDMS ratio (1:1) were selected for further experiments.

The incorporation of SiO₂NPs to increase the porosity has been reported (*Li, D. et al., 2013*). The increase in the gel pore size prevents cracking. Therefore, different proportions of SiO₂NPs were studied (0.1% and 1%) and no cracking was observed in any case. *Figure 75B* shows, that the addition of higher amounts of SiO₂NPs decreased the analyte response. This effect can be explained by the fact that the addition of NPs increased surface roughness and it is one of the dominant factors determining the surface hydrophobicity (*Monoudis, P.N. et al., 2009*). Finally, different percentages of NQS reagent were tested (0.05%, 0.1% and 0.2%). *Figure 75C* shows the analytical signal (absorbance) versus the concentration of NQS, as it was expected the response increases as the amount of NQS increases. According to these results, the selected sensor composition was 50/50 weight ratio TEOS/PDMS, 0.1% (w/w) SiO₂NPs, 0.2% (w/w) NQS. In addition, the effect of the temperature in response of the NQS sensor was also evaluated. At room temperature the reaction kinetic was lower than that obtained by heating the standard solution or the samples at 100 °C during 10 min; that is to say that the sensor needed long times to respond to casein concentration (*Figure 75D*).

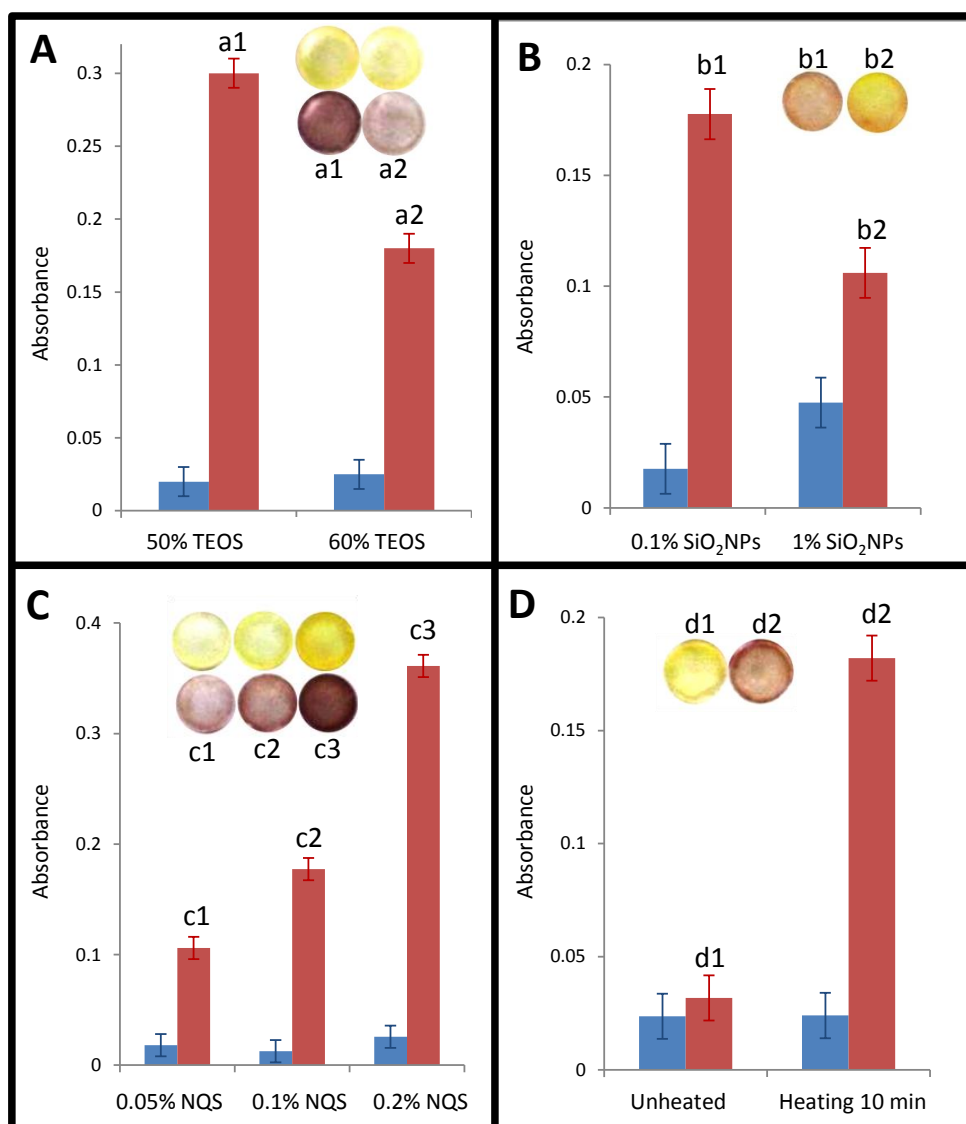


Figure 75. Optimization of sensor composition and temperature conditions. (A) TEOS percentage: 50% (a1) 60% (a2), (B) Proportion of SiO₂NPs: 0.1% (b1) and 1% (b2), (C) NQS percentage: 0.05% (c1), 0.1% (c2), 0.2% (c3). (D) Sensor at two different temperatures: (d1) room temperature, (d2) 100 °C for 10 min. Blue columns represent the signals of blanks and red columns show the signals of the sensor with casein stock solutions.

The denaturalization and the breakage of the peptide bonds of the casein takes place at high temperatures in basic or acid conditions. Thus, amino acids

from the casein react in the sensor with the NQS by heating the sample in basic medium. From these results, the procedure to follow was to introduce the sensor in a basic solution (pH 12) and to heat at 100 °C during 10 min. The casein molecule is formed from chains of amino acids. In order to test which amino acids reacts with the PDMS–NQS sensor, amino acids with different structure were selected as model compounds (leucine, proline, arginine and lysine). The analytical responses achieved were higher for lysine and arginine heating for 10 min at 100 °C than for proline and leucine (*Figure 76*). As it was expected, these differences in the reaction were determined by their structures. The typical structure of amino acids is composed of two functional groups: a carboxylic acid group ($-\text{COOH}$) and an amine group ($-\text{NH}_2$), along with a side-chain specific to each amino acid. Only lysine, arginine and histidine contain an additional amino group (*Devlin, T.M. et al., 1992*). Lysine and arginine are classified as basic-polar (*Timberlake, K.C., 1992*) because to the second amino group is protonated and often participates in hydrogen bonding and as a general base catalysis. The presence of a second amino group in the molecule enhances the reaction kinetic and the reaction product is observed quicker than when only one amino group is present in the molecule.

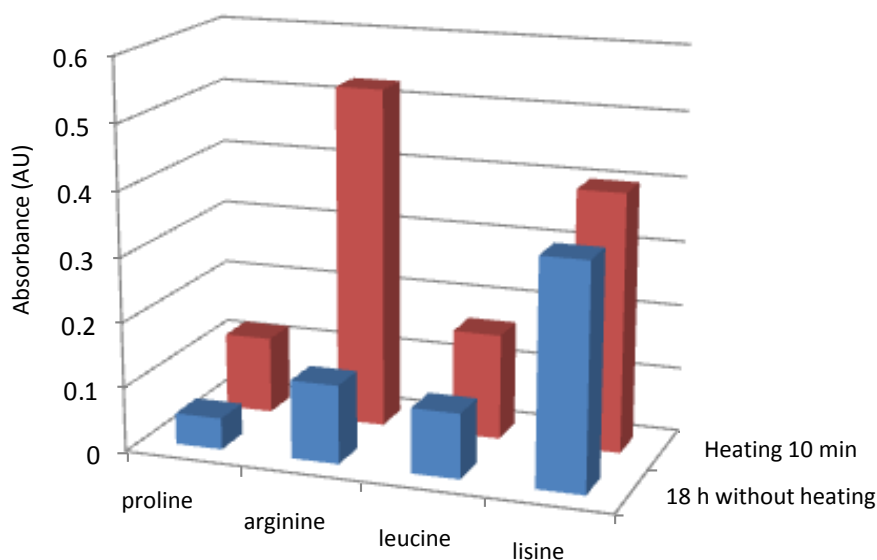


Figure 76. Sensor absorbance obtained for different amino acids at a concentration level of 0.01 M. Blue: signal from sensor at room temperature for 18 h. Red: sensor heated for 10 min in a water bath.

A kinetic study of the reaction between casein and PDMS–NQS sensor was further investigated. The kinetic data were obtained by registering the absorbance of colored sensors corresponding to a solution of 1 g L^{-1} of casein at five different times (0, 5, 10, 15 and 20 min). As shown in *Figure 77A* the signal increased as time progressed. By increasing the time, the analytical signal of the reaction product increased, however the blank signal also increased due to the degradation of the reagent in presence of the sample medium at high temperatures. Finally, an intermediate time (10 min) was chosen taking into account the maximum analytical response. The sample volume required for the analysis of casein was also studied. The sample volumes tested were 0.5 mL, 1 mL and 2.5 mL. *Figure 77B* shows the absorbance and images of the sensors for each sample size. The largest volume (2.5 mL) was chosen as the best option.

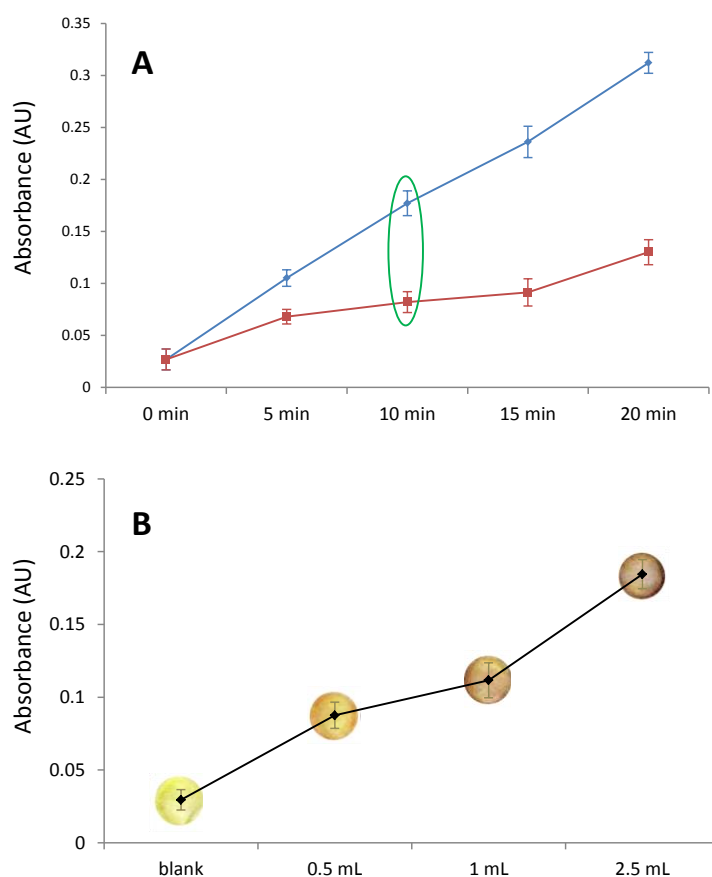


Figure 77. (A) Kinetic study. Red line: blank, Blue line: signal in presence of casein 1 g L^{-1} and (B) Optimization of the sample amount for the estimation of casein.

Therefore, the proposed sensor can be used for qualitative and quantitative determination of casein. The spectra at different concentration of casein are shown in *Figure 78*. It should be noted that the difference in the color of the sensor can be a powerful tool for monitoring the casein concentration by visual inspection since instrumentation is not required.

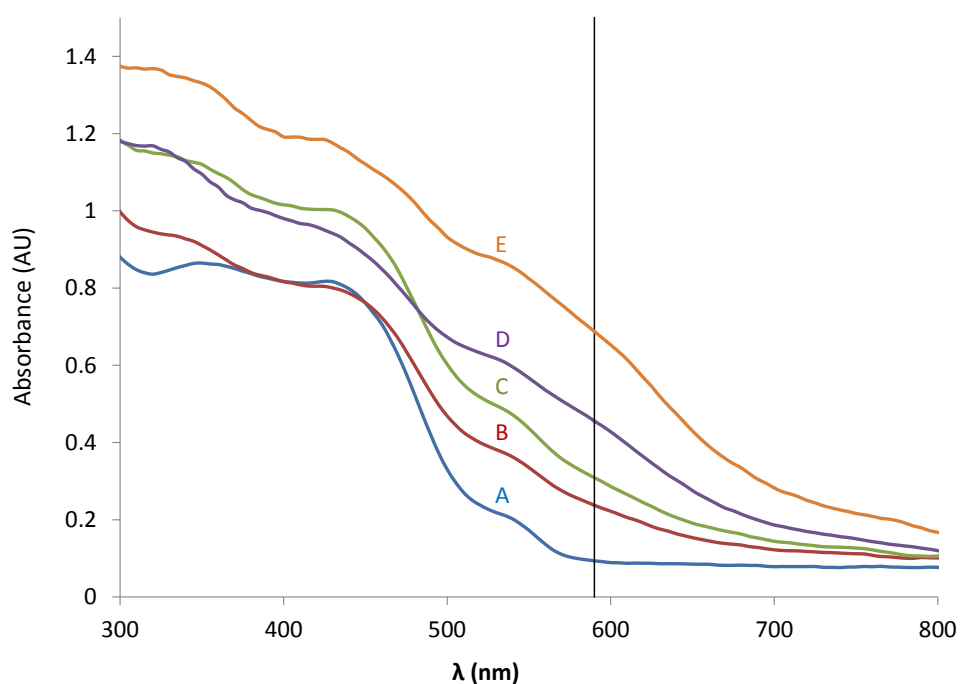


Figure 78. Spectra and images of the PDMS-NQS sensors at different concentration levels of casein. (A) Blank, (B) 15 mg L^{-1} (C) 50 mg L^{-1} , (D) 750 mg L^{-1} and (E) 2000 mg L^{-1} .

Interference study

The effect of interference by other compounds in the sample plays a key role in working out the selectivity of the sensor. The response of the sensor for the main compounds present in milk such as lactose and fat was studied. In both cases a negative response was obtained. The nitrogen composition of milk is mainly due to the protein content. Casein and albumin are the major proteins in milk and casein is found in mayor proportion. Casein/albumin (g L^{-1}) ratios are 4, 4.2 and 4.3 for milk goat, sheep and cow, respectively (*Park, Y.W. et al., 2007*). According to these data, the interference of albumin was evaluated. Different

concentrations ($1000 \text{ mg L}^{-1}/250 \text{ mg L}^{-1}$ and $500 \text{ mg L}^{-1}/125 \text{ mg L}^{-1}$ for casein/albumin) were assayed and the relative errors (%) obtained for the estimation of casein in presence of albumin were 4.5 and 18% for the two relations studied, respectively. The response of albumin was not significant compared with casein response at the above mentioned ratios. Thus, we can conclude that the method was appropriate for estimating casein in presence of albumin at the concentration level expected in this study.

Analytical parameters

Table 30 shows the calibration equations calculated for the response of the casein ($0\text{--}1500 \text{ mg L}^{-1}$) employing PDMS–NQS sensor, and using the DR probe and DI by measuring the colour of the sensor with a colour processing software. For casein concentrations higher than that of 2 g L^{-1} saturation of the sensor was observed and no significant differences in signals were observed. Linearity calibration equations were obtained by using the absorbance signal. The precision of the analysis was also evaluated. The intraday precision was evaluated at different concentrations (Figure 79). The RSD values were lower than 8%. These results indicated that the RSD values were independent of the concentration level.

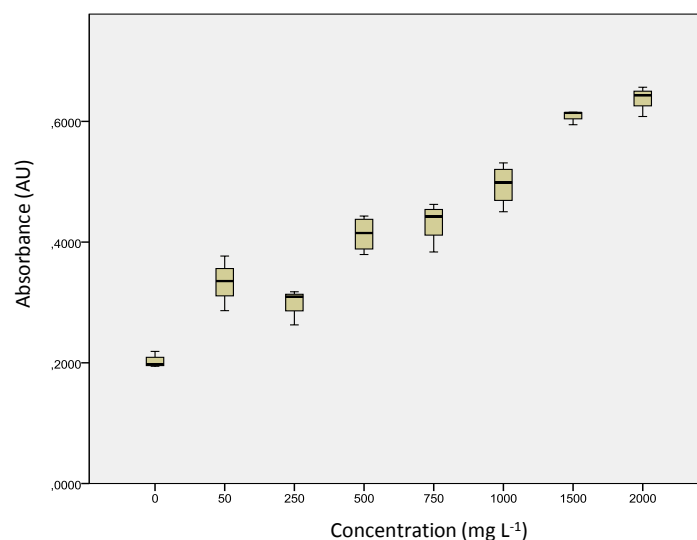


Figure 79. Intraday precision of DR method obtained from the values of the absorbance at 590 nm for different casein concentration.

For the interday precision, we compared the response of the sensor obtained with four sensors prepared in four different batches under identical conditions. The RSD values obtained for a concentration level of casein of 250 mg L^{-1} were lower than 12%. The low RSDs indicated that the proposed sensor is a reproducible device for practical applications. The LOD, calculated as the concentration that provided a signal-to-noise ratio of 3, and the LOQ were 15 mg L^{-1} and 45 mg L^{-1} , respectively. These values indicated that the proposed method is suitable for the estimation of casein in effluents.

The second procedure to perform quantitative analysis was DI analysis by GIMP software. The linear calibration equation was obtained with the logarithm of the concentration vs green RGB value. The analytical parameters are shown in *Table 30*. Similar results than those obtained with the DR were reached. Therefore, both procedures can be used if quantitative analysis is required. In order to validate the method, the BCA method was applied. In *Table 30* are also shown the analytical parameters obtained by using the BCA method. The BCA method provided higher slope than that obtained by using the PDMS–NQS sensor, nevertheless it is more tedious requiring the dairy reagent preparation and longer analysis time. In addition, the BCA method requires the dilution of the sample; consequently the concentrations that can be detected or quantified in the sample are higher than that reached by the sensor. Moreover, sensors were stable during at least 12 months at room temperature since their analytical response, this is their composition did not change within this period. The robustness of this sensor represents an advantage over the derivatizations in solutions due to the instability of most of the reagents employed.

Table 30. Analytical parameters obtained for casein determination in dairy sewages by the three methods assayed.

Method	Linearity $y=a+bx$ (mg L^{-1}) (n=6)			RSD (%) (n=4)	
	$a \pm s_a$	$b \pm s_b$	R^2	Intraday	Interday
DR	$(19 \pm 0.1) 10^{-2}$	$(30 \pm 2) 10^{-5}$	0.991	8	12
BCA	$(4 \pm 1) 10^{-2}$	$(110 \pm 5) 10^{-5}$	0.995	7	10
DI	86 ± 1	-10 ± 1	0.991	7	9

Analysis of samples

Different dairy wastewaters samples from a pilot plant were analyzed by using the proposed PDMS–NQS sensor. Samples from the different steps of the CIP process were analyzed. The sample S1 was collected at the end of the first rinse and the sample S2 was gathered 5 min after starting the acidic rinse. Sample S3 was collected during the alkaline rinse, when the basic solution had passed through the pipes for 5 min. Samples S4 and S5 were collected at the end of the first rinse in the neutral wash at 40 °C and 60 °C, respectively. The analysis of fat and lactose (Moliner-Martínez, Y. *et al.*, 2014b) content provided the following results: Sample S1 (0.4 g L⁻¹, 0.178 g L⁻¹), Sample S2 (0.15 g L⁻¹, 0.019 g L⁻¹), Sample S3 (0.25 g L⁻¹, 0.03 g L⁻¹), Sample S4 (0.25 g L⁻¹, 0.007 g L⁻¹), Sample S5 (0.6 g L⁻¹, 0.008 g L⁻¹), for fat and lactose, respectively. Casein values for each sample were obtained by applying BCA method acid assay and polymeric sensor probe. In Table 31 are shown the found concentrations of casein in the samples. For each sample, a F-test for homogenous variance (at 95 % significant level) was applied and no significant differences were obtained, so the methods were considered equally precise. The paired t test (at 95 % significant level) was used to evaluate the accuracy of the method. The BCA method was used as a reference method. The p-value obtained at 95 % significant level was higher than 0.05 in both cases (p-value = 0.259, by comparing reflectance mode and BCA, and p-value = 0.121, by comparing DI and BCA). From these results we can conclude that both methodologies provided statistically equal results, thus the proposed methods can be used to determine casein in dairy effluent samples. The response of albumin was negligible for both methods. For samples in which the concentration of both proteins will be similar, the method would result in the total protein just as the method of BCA would be.

Table 31. Found concentrations of casein mg L^{-1} obtained by the three quantification methods (bichinonic acid assay, and the two methods of measurement for the colorimetric sensor (DI and DR) in different samples.

Sample	Found concentration (mg L^{-1})		
	Colorimetric sensor		BCA
	DR	DI	
S1	1280 ± 160	1260 ± 150	1090 ± 60
S2	91 ± 11	80 ± 10	90 ± 20
S3	180 ± 20	99 ± 12	120 ± 30
S4	1090 ± 130	940 ± 112	1150 ± 40
S5	1320 ± 160	970 ± 110	1220 ± 50

Qualitative analysis

Recently, some efforts have been dedicated to manufacture of colorimetric sensors, since semiquantitative analysis by visual inspection avoiding the need of instrumentation is not only cost-effective, but also is highly required for application in real-time determination. The PDMS–NQS sensor proposed in this work, changes its color from yellow to orange-brownish as function of the casein concentration in the range $45\text{--}2000 \text{ mg L}^{-1}$. The sensor color variation was evident by visual observation, offering an appropriate approach to estimate casein in dairy wastewaters even at low concentrations. *Figure 80* shows the colorimetric images corresponding to different increasing concentrations of casein. These images allow a semiquantitative analysis to be deduced by visual inspection of a colorimetric reference card.

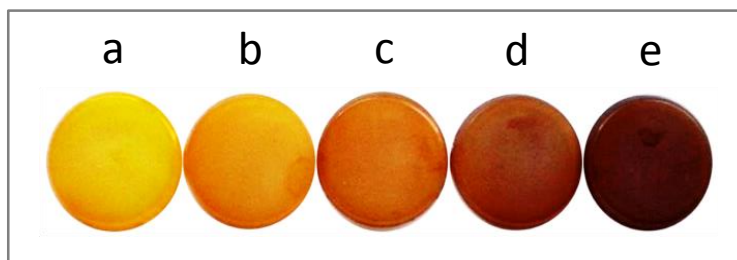


Figure 80. Images of PDMS–NQS sensors at different concentration levels of casein, (a) Blank, (b) 15, (c) 50, (d) 750 and (e) 2000 mg L^{-1} .

Conclusions

In this section, the applicability of PDMS as polymeric support of sensing devices doped with NQS for the estimation of casein in industrial samples has been demonstrated. The use of sensors sufficient flexible to handle an extensive range of substrate concentration is required because wastewaters from the dairy industry are usually produced intermitently, so the flow rates of these effluents change significantly. PDMS-NQS sensor allows an in-situ analysis, thus semiquantitative analysis of dairy effluents could be continuously performed. Reagent preparation and use of expensive equipments are not strictly necessary for casein determination through a reference color card. Also, quantitative analysis could be performed by using DR and DI analysis. The results obtained with both measurement methods were compared with BCA assay. All methods presented similar sensitivity and precision, but it was found that the BCA reagent was degraded while the polymeric sensor remained stable. Thus, the proposed sensor overcomes one of the main limitations of the conventionally used BCA assay, the degradation of the reagents. The main advantages of the NQS sensor are the rapidity, simplicity, portability and the minimization of reagent handling.

4.1.2.2 A solid sensor based on doped hybrid composites for controlling the dosage of ADP in industrial formulations

As demonstrated above, PDMS/NQS-based sensors change their colour in presence of primary and secondary amines in alkaline medium. In an attempt to extend the application of the PDMS-NQS sensor, it was evaluated for the in-situ estimation of ADP, a primary amine-based biocide, in industrial formulations. Although this biocide amine is essential component in detergents used in hygiene to prevent diseases, its potent biological activity can be a threat for human and environment. Different ratios of NQS, TEOS and SiO₂NPs embedded in PDMS have been optimized in order to improve the performance of the sensing device. Visual inspection has also been tested for semiquantitative analysis. Absorbance measurements by DR and/or color intensity measurements by DI of colored sensors have been evaluated for quantitative analysis. The validation of the method has been carried out by comparing these results with the results obtained with C₁₈ solid support derivatization. Detergent samples have been analyzed to demonstrate the performance of the proposed sensor.

Optimization of the sensor composition

The influence of different compounds in the sensor composition was studied in order to select the best hybrid composite which has good gelation properties, stability and good accessibility of the analyte to the reagent. First, different weight ratios of PDMS/TEOS (70/30, 50/50, 40/60, 20/80) were tested. TEOS modifies the matrix structure giving hydrophilicity, but maintaining the stability and inertness of PDMS. Additionally, TEOS promoted the better mixing of the organic and inorganic phase to provide a homogeneous dispersion and so, and homogeneous gel (Li, T. *et al.*, 2015). As a consequence, the hybrid matrix protects the embedded reagent and also preserves its optical properties. However, high percentages of TEOS (>80 %) resulted in an increase of the gelling time to almost 7 days at room temperature and broke easily. In contrast, sensors with lower percentages of TEOS were cured after 3h at 30 °C. Therefore, we tested sensors with TEOS percentages lower than 80 % to get favorable curing. Then, we studied the addition of SiO₂NPs (0.1 % and 1 %, w/w) in the PDMS/TEOS matrices, since SiO₂NPs can enhance the pore size of the polymeric matrix. As shown in *Figure 81A*, NPs prevented cracking of the polymeric film due to the reduction of the capillary pressure during the drying process (Li, D *et al.*, 2013).

The amount of TEOS and NPs was evaluated according to the analytical response of devices exposed to ADP (See Figure 81B).

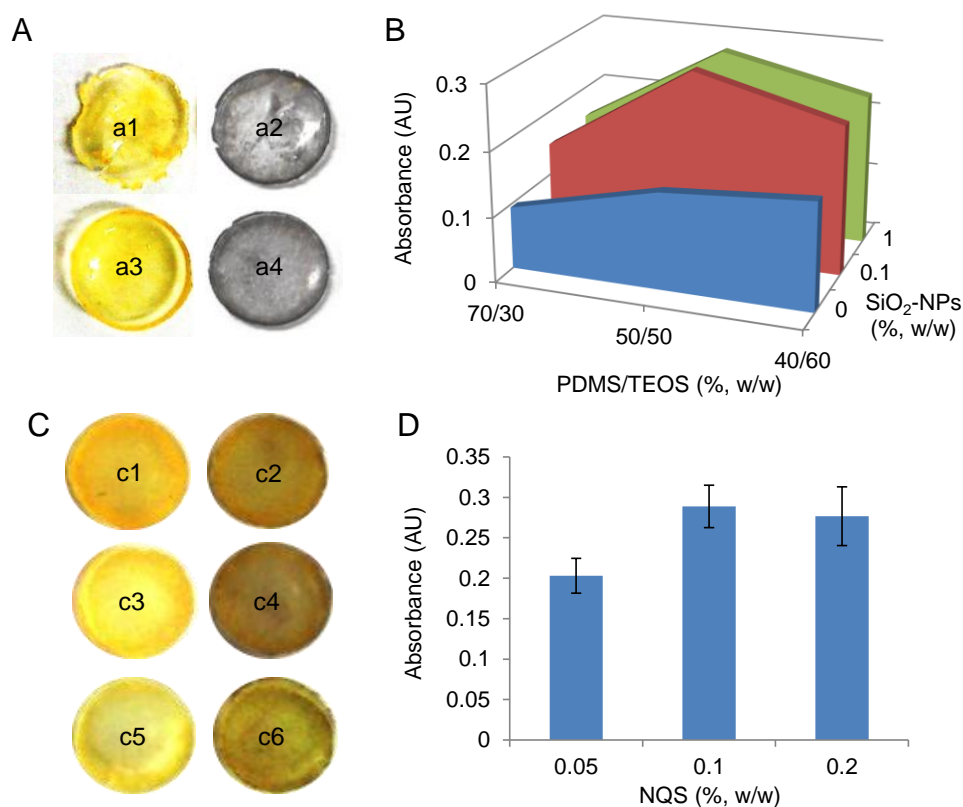


Figure 81. Optimization of sensor: (A) photographs of sensors without (a1, a2) and with 0.1 % (w/w) NPs (a3, a4), before (left) and after (right) exposition of 1 % (w/w) ADP during 20 min. Sensors prepared with PDMS/TEOS (50/50, w/w) and 0.1 % (w/w) of NQS. (B) Effect of different amounts of PDMS/TEOS and NPs (containing 0.1 % (w/w) of NQS). (C) Photographs of sensors with PDMS/TEOS (50/50, w/w), 0.1 % (w/w) of NPs and different NQS amounts (c1, c2) 0.2 (c3, c4) 0.1, (c5, c6) 0.05 % (w/w), blanks (left) and exposed to 0.5 % (w/w) ADP during 5 min. (D) Effect of the NQS amount on the analytical response.

As it was expected, an increase in the percentage of TEOS, resulted in an enhancement on the analytical response, since pore size is higher in presence of TEOS and so, permeability of the analytes into the polymeric matrix is also favored (Li, T. et al., 2015). However, when the percentage of TEOS was higher than 50 %,

the free volume decreased. Therefore, the mass transfer resistance increased, which resulted in a decrease in the permeation to the analyte and so, a decrease in the response. This effect is particularly appreciable in presence of SiO₂NPs, since the pore size is also influence by NPs. SiO₂NPs possess a dual function: to improve the response owing the enhancement on the permeability of the material and to provide a more homogenous color distribution, both attributable to the enhancement of the size of the network pores. It should be noted that higher amount of SiO₂NPs did not provide significant differences on the analytical response or in the mechanical stability. Herein, the reasonable addition of NPs was 0.1 % (w/w) in order to reduce the chemical consumption. According to these results, 50/50 weight ratio of TEOS/PDMS and 0.1 % (w/w) SiO₂NPs were chosen as the optimum composition. *Figure 82* shows the topography images obtained by Atomic Force Microcopy (AFM) for PDMS with embedded NPs and pristine PDMS. The corresponding height profiles along the marked lines are included at the bottom of each color map. From the different scales of these figures we can already conclude that the introduction of NPs in the PDMS matrix considerably modifies its surface morphology. *Figure 82A-B* allows the observation of the NPs distribution at the surface. More quantitatively, the surface of PDMS presents a roughness of 1 nm, while the same polymer with embedded NPs increases its roughness to 15 nm. Furthermore, *Figure 82C* shows SEM image of sensor finally chosen.

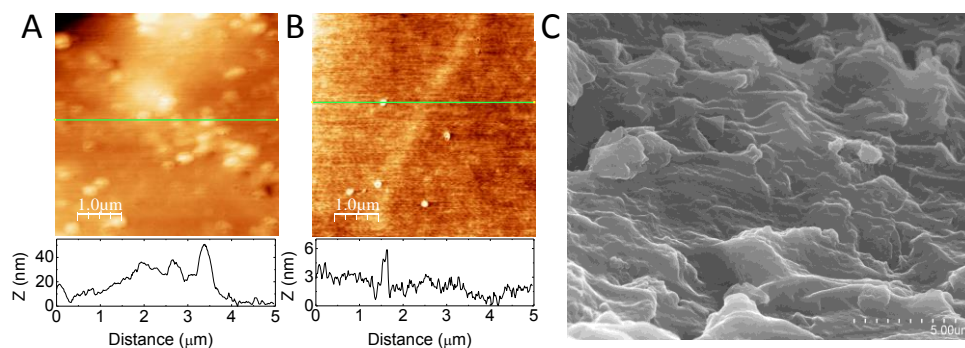


Figure 82. $5 \times 5 \mu\text{m}$ AFM topographic maps and corresponding height profiles along the marked lines: (A) Sensor of 50/50 TEOS/PDMS and 0.1 % (w/w) of NPs. Color scale from 0 to 120 nm. The embedded NPs are visible at the surface. (B) Sensor of 50/50 TEOS/PDMS without NPs. Color scale from 0 to 10 nm; (C) SEM image of sensor chosen which contains 50/50 TEOS/PDMS and 0.1 % (w/w) NPs.

Finally, different amounts of NQS (0.05 %, 0.1 % and 0.2 %, w/w) were also tested. The effect of the amount of the derivatizing reagent was optimized by choosing the maximum difference between blank and derivative response (Figure 81C and D). The results showed that the best response was obtained with 0.1 % (w/w) of NQS, so this amount was selected. From these results, we proposed a device with 50/50 weight ratio of TEOS/PDMS, 0.1 % (w/w) of NQS and 0.1 % (w/w) of SiO_2 NPs.

Reaction kinetic

Once the sensor was obtained, the analytical response as a function of time was studied between 30 s and 30 min by monitoring the color change (Figure 83). The color started to appear within the first 50 s and stabilized after about 6 min for 0.5 % (w/v) of ADP. According to these results 6 min were selected as the optimum time.

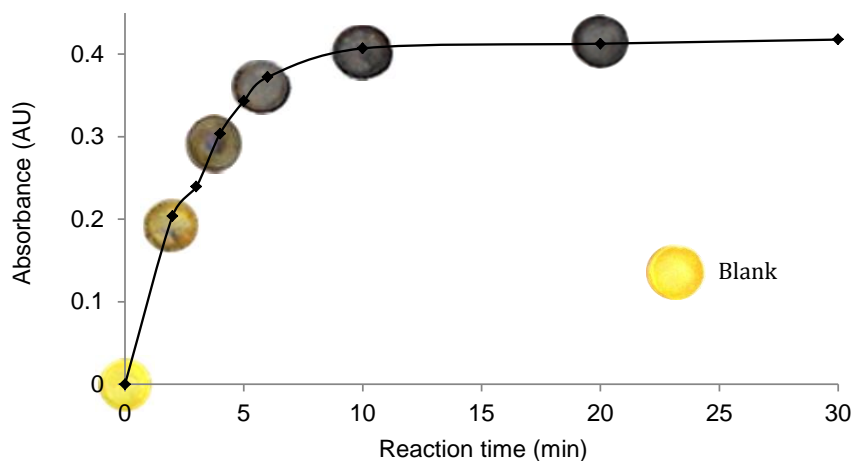


Figure 83. Variation of device response for 0.5 % (w/v) of ADP as function of the reaction time. The analytical signal was obtained by DR at 600 nm. Devices studied had optimum composition.

Sensor stability

The storage stability of the derivatizing reagent in aqueous solution was evaluated by measuring the absorption of a NQS solution ($2.4 \times 10^{-4} \text{ mol L}^{-1}$) stored in the dark and exposed to light during different times. Absorbance was measured at 380 nm against a blank of water. *Figure 84* shows the variation on the NQS solution spectra in response to the two storage conditions over a period of 9 days. The solution stored in the dark showed decrease in response after 1 day and this decrease was very significant at 9 days. The degradation of NQS exposed to light was more rapid than stored at the darkness (*Figure 84*). Thus, the use of NQS in solution procedure is limited by the NQS unstability.

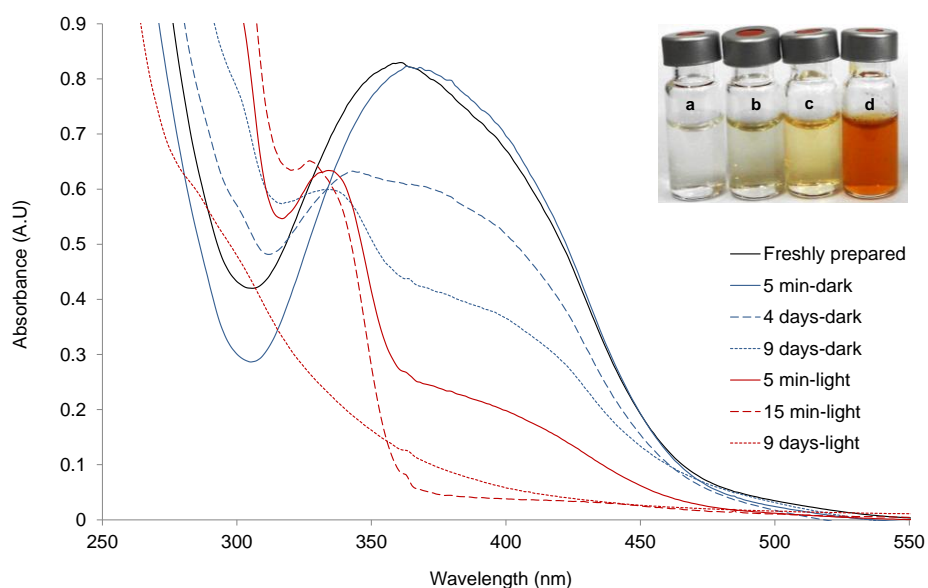


Figure 84. Spectra of the stability of NQS in aqueous solution over time under dark (blue lines) and light (red lines) storage. Responses are quantified as the absorbance at 380 nm of NQS $2.4 \times 10^{-4} \text{ mol L}^{-1}$. Inset: Photography of colorimetric responses of NQS solution against light at a) 5 min, b) 7 days, c) 0 min, d) 30 days.

The reagent NQS is unstable in solution but it remained stable inside the PDMS (Figure 85).

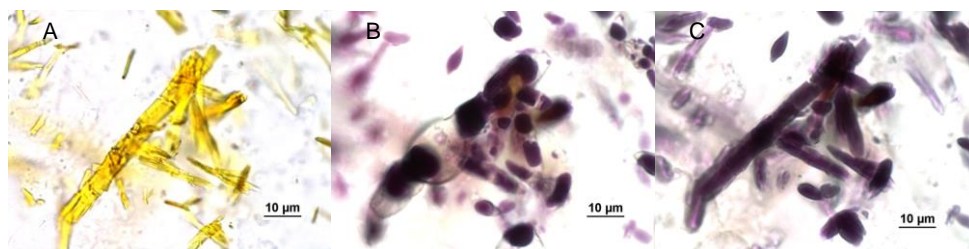


Figure 85. Microscopic photographs of (A) sensor of a blank, (B) sensor after 3 min and (C) after 6 min of 0.5 % (w/v) ADP contact at 100x magnification.

On the other hand, absorbance measurements by DR of sensors stored in the dark and exposed to light were measured during several times. Absorbance was measured at 600 nm against a blank. As can be seen in Figure 86, similar analytical

signals were registered for the different storage conditions over time. Therefore, NQS embedded into PDMS is more stable than NQS in solution. Sensors can be used for eight months after fabrication providing reproducible responses.

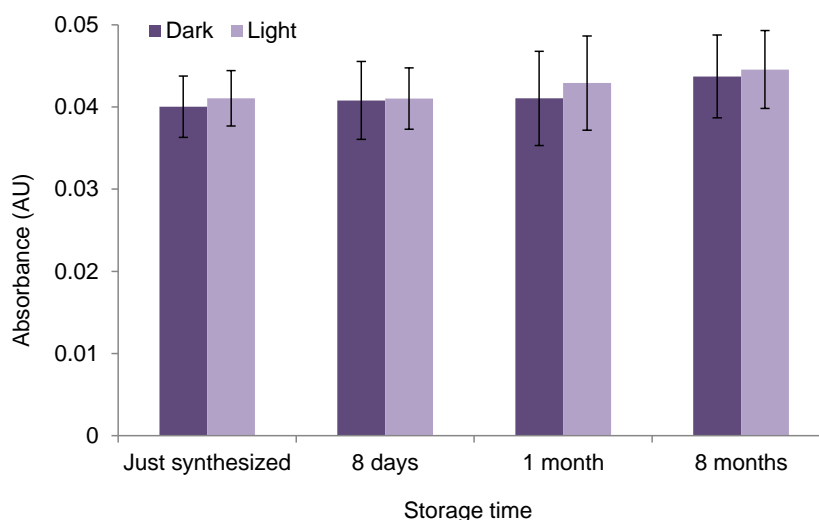


Figure 86. Stability of sensors under two storage conditions over time (in the dark and exposed to light) without ADP contact. Average responses and standard deviation for $n=3$.

The storage stability of the proposed sensors was evaluated by measuring the responses over a period of 8 months under two conditions: dark and light exposition. *Figure 87A* shows the variation of the analytical signal as function of the storage. As can be seen, there were not significant differences in the response, with RSD values of 4 %. Therefore, these results indicated that the analytical response obtained with the NQS based sensors did not depend on the storage conditions. Thus, composites can be directly used without daily reagent preparation. By another hand, taking into account that one of the main disadvantages of derivatization procedures is the reagent and reaction products instability, the NQS-ADP derivate stability in the sensor was studied from minutes to months after the reaction. The storage stability was evaluated by measuring the colorimetric response of sensors stored at room temperature in the dark. An average stability of $(98 \pm 3) \%$ ($n=8$) of the initial response was retained after 4 months of storage (*See Figure 87B*). These results indicated that derivatives inside sensors were also stable for long periods of time and so, the colorimetric response can be remeasured when required.

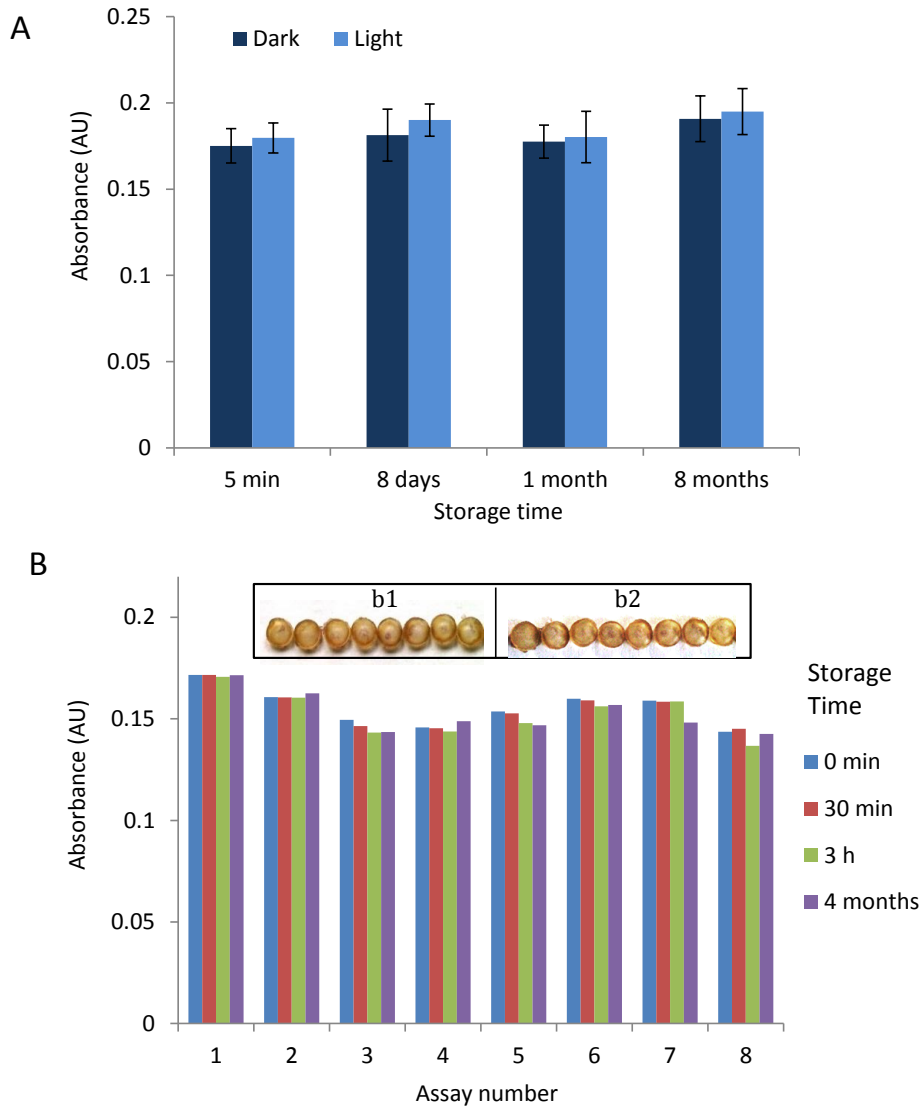


Figure 87. (A) Stability of sensor responses under two storage conditions over time (dark and sunlight exposition). Absorbance measurements of sensors just synthesized and after 8 days, 1 month and 8 months of being synthesized at 0.1 % (w/v) of ADP. Average responses and standard deviation for $n=3$. (B) Stability of colored sensor after reaction between NQS-ADP (0.1 % (w/v)). Absorbance measurements correspond to sensors just colored and colored after spending 30 min, 3 h and 4 months for $n=8$ assays. Inset: photographs of colored sensors after (b1) 30 min (b2) 4 months.

Colorimetric doped hybrid sensor responses

The optimized sensors were tested for semiquantitative and quantitative determination of ADP. The primary amine groups of ADP formed a gray-brown derivative with NQS under basic pH conditions. Thus, the color of the device changed from yellow-orange to gray-brownish after 6 min of immersion in the ADP solution (Figure 88A). Figure 88B shows the colorimetric response as function of the concentration. The absorbance at 600 nm increased when concentration increased up to 1 %. At higher concentrations the response kept constant due to the saturation of the sensing device. Visual inspection of the colored sensors allows a semiquantitative estimation of ADP concentration (See photograph inset Figure 88B).

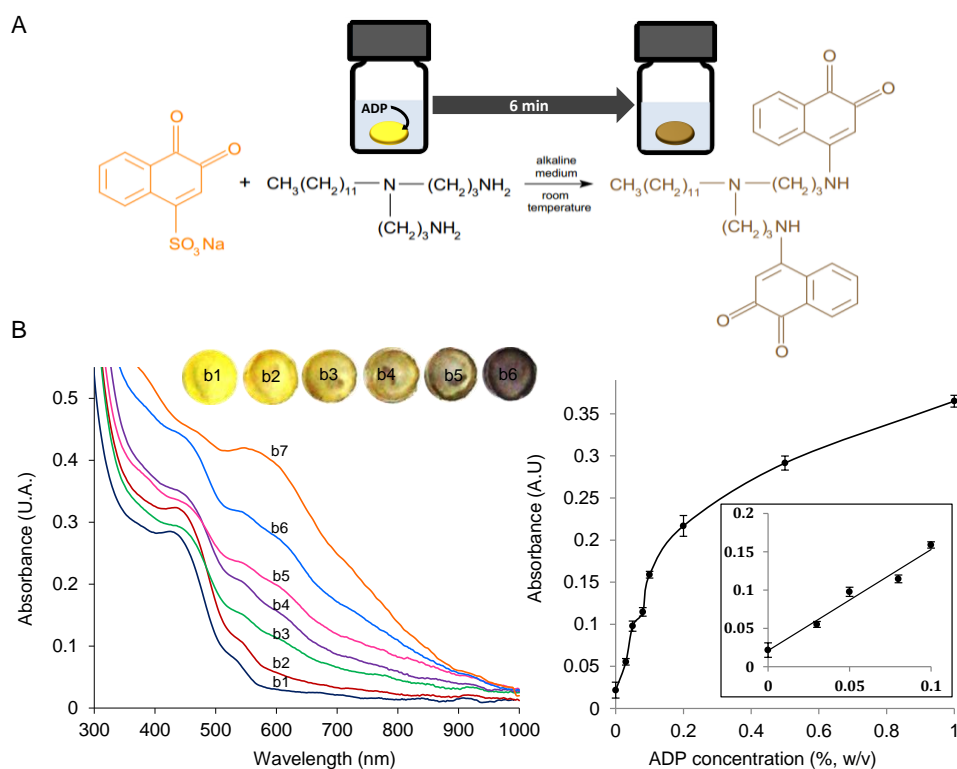


Figure 88. (A) Reaction scheme of ADP with NQS, together with a picture of the derivatization procedure. (B) Left: spectra of ADP response at different concentrations together with the photographs of devices (b1) Blank, (b2) 0.015 %, (b3) 0.05 %, (b4) 0.1 %, (b5) 0.2 %, (b6) 0.5 % and (b7) 1 % (w/v) of ADP. Right: calibration curve and linear plot (inset) of colored sensors at 600 nm of absorbance. Stoichiometry 2:1 (NQS:ADP).

Analytical performance

Table 32 shows the calibration equations by using two different measurement modalities (absorbance and color intensity measurements). RGB color mode was selected according to previous works (*Ornatska, M. et al., 2011*). A linear behavior of analytical signal versus ADP concentration was observed at concentrations up to 0.1 % (w/v) with both modalities. These results were compared with those obtained with a previously described method based on C₁₈ solid support NQS-derivatization (*Moliner-Martínez, Y. et al., 2004*). Better linearity was obtained employing absorbance measurements instead of color intensity measurements. These results were comparable with those obtained by using C₁₈ cartridges. Satisfactory intra and inter-day RSDs have been achieved (5-12 %) by the sensors in both modalities at a concentration level of 0.05 % (w/v) of ADP. Adequate batch-to-batch precision was obtained for four sensors fabricated in four different syntheses following the same procedure. *Table 32* also shows LOD and LOQ calculated as $3 s_{\text{blank}}/b$ and $10 s_{\text{blank}}/b$, respectively, where b is the slope of linear calibration curve and s_{blank} is the standard deviation of the absorbance or color intensity of ten blanks. Similar LODs were obtained by C₁₈ solid support and polymeric sensors derivatization with posterior absorbance measurements. The LOD for ADP reported in previously published works (*Mondin, A. et al., 2014*) is lower than that achieved with the proposed PDMS-based sensor. However, the LOD reached with the proposed method is adequate taking into account the percentage of ADP in industrial formulations. In order to test the selectivity of the method, an interference study was carried out. The absorbance and color intensity of a synthetic matrix containing some common compounds present in detergents such as lactic acid, ethylenediamine-tetraacetic acid, isopropyl alcohol, phosphoric acid and nitrilotriacetic acid at percentages of 4 %, 16 %, 2 %, 1.4 % and 7 %, respectively were measured. The analytical response was compared with the sensor response in synthetic samples that contained ADP. There was not colorimetric response for the interferents assayed. Moreover, compounds such as N-dodecyl-1,3-propanediamine and N-dodecylamine can be present in LONZABAC raw material as impurities at percentages around 9 % and 1%, respectively. No colorimetric response was observed for these compounds at the concentration levels present in standards and or samples (below 0.01 % and 0.001 % for N-dodecyl-1,3-propanediamine and N-dodecylamine, respectively). Those percentages were well below the LODs calculated for these compounds, 0.02 % for N-dodecyl-1,3-propanediamine and 0.04 % for N-dodecylamine. Thus,

it can be concluded that the proposed sensor provides a selective determination method for ADP in industrial samples.

Table 32. Figures of merits obtained with the different measure approaches for the ADP determination with the proposed NQS-sensor, and comparison with the figures of merit obtained with C₁₈-solid-support derivatization.

Procedure	Linear range (% w/v)	Linearity $y = a + bx$ ^{a,b,c}			RSD _{intra-day} (%); (n)	RSD _{inter-day} (%); (n)	LOD (% w/v)	LOQ (% w/v)
		$a \pm s_a$	$b \pm s_b$ (% v/w)	R^2				
Sensor/DR ^a	0.016 - 0.1	0.02 ± 0.01	1.32 ± 0.13	0.989	7; (6)	12;(4)	0.018	0.06
Sensor/DI ^b	0.04 - 0.1	0.011 ± 0.001	0.043 ± 0.003	0.982	5; (6)	11;(4)	0.013	0.04
C ₁₈ -SPE ^c	0.04 - 0.1	0.06 ± 0.02	4.9 ± 0.2	0.993	4; (3)	8; (3)	0.012	0.04

^a Absorbance at 600 nm in DR mode vs concentration (% w/v);

^b (1/green color intensity) vs concentration (% w/v);

^c Absorbance at 480nm vs concentration (% w/v).

Application to detergent industrial formulations

The applicability of the sensor to estimate ADP was evaluated by analyzing different formulations of detergent samples (S1-S3). As it was expected in all the analyzed samples, a semiquantitative analysis could be performed by the color change observed in the sensor after the addition of ADP. Table 33 shows the found ADP concentrations in samples. Firstly, a statistical study of the precision achieved with each procedure, DR and DI, compared with the C₁₈-SPE solid support NQS-derivatization was carried out. The F-test for homogeneous variance (at 95 % significance level) was tested for each sample, and no significant differences were obtained (the values of F_{cal} for each sample with each procedure were in the range 0.2067–5.4774, which were lower than F_{stat} 0.39 at 95 %), so both methods can be considered equally precise. In order to validate the results obtained with the sensor, the same samples were analyzed with the C₁₈-SPE solid support NQS-derivatization. A linear regression with C₁₈ support derivatization versus the values obtained with sensors was tested to check if the joint confidence region for slope and intercept included the point (intercept=0, slope=1). Using as x the values obtained with C₁₈ solid support derivatization and y the values obtained by using the composites, the point (0,1) was included in the

joint confidence region, and thus, there were not statistical differences between the results provided by both methods, so it can be concluded that both methodologies provided comparable results (at 95 %). In addition, a statistical comparison of the results obtained with the proposed PDMS sensor and the percentages of ADP labeled by the manufacturer were carried out by using a t-test. The t experimental values calculated when the DR measurements were used, were 0.3464, 1.7321 and 2.7713 for S1, S2 and S3, respectively. The t experimental values obtained when the color intensity measurements were carried out were 0.3464, 3.0311 and 1.0825 for S1, S2 and S3, respectively. In all cases, these values were in accordance with the labeled values at a significance level of 95% ($t_{\text{tabulated}}=4.3027$). Matrix effects were evaluated by spiking the detergent samples with a known concentration of ADP. For C_{18} solid support derivatization, the recovery values were between 78 % and 109 % while using derivatization into sensors, the recovery ranged between 80 % and 112 %. Hence, in both cases, the recovery values showed that matrix effect was not present under the optimized experimental conditions. These results demonstrated that the use of sensors is a good alternative to develop suitable, reliable and precise device for ADP estimation.

Table 33. Concentration of ADP found in the analysed samples obtained with the PDMS-based sensor by DR and DI. Comparison with the results obtained with C_{18} Solid-Support derivatization.

Procedure	S1 (% w/v)	S2 (% w/v)	S3 (% w/v)
Sensor/DR	4.1 ± 0.5	2.7 ± 0.3	1.52 ± 0.05
Sensor/DI	3.8 ± 0.7	2.3 ± 0.4	1.50 ± 0.16
C_{18} -SPE	4.4 ± 0.3	3.1 ± 0.2	1.67 ± 0.04

Comparative study of different strategies

Table 34 compares the main analytical properties of the different tested procedures. The commended strategy is the derivatization into sensors owing to the simplification of the entire analytical process. The higher stability of the NQS embedded into the polymeric matrix allows the use of sensors after long time of their fabrication. Once the sensor is synthesized, it can be directly used for controlling the ADP dosage in industrial formulations since it does not need

reagent preparation. The sensors and a vial containing the sample are the unique material required to perform the analysis. Moreover, the small size of the sensors reduces costs in reagents and it allows a cost effective analysis. By contrary, C₁₈ solid support derivatization, as well as procedures with NQS in solution require more steps: NQS solution just prepared before use, derivatization and extraction of derivatives.

Table 34. Comparison of different properties of the procedures assayed. More +: better option.

Steps	C ₁₈ -SPE	Sensor/DR	Sensor/DI
	Cartridge and NQS solution preparation, sampling, derivatization, extraction	Derivatization	Derivatization
Portability	+	++	+++
LOD (% w/v)	0.012	0.018	0.013
Rapidity	+	+++	+++
Cost	+	++	+++

Conclusions

This study presents a colorimetric sensor based on NQS immobilized in PDMS/TEOS/SiO₂NPs to control the dosage of ADP in detergent samples from industrial formulations. The simplicity and the low amounts of reagents required results in a low cost fabrication process. The sensor is synthesized in approximately 3 h, and no leaching of the reagent to the solution is observed. However, it allows the fast diffusion of the analyte from the matrix to the sensor and the reaction with the entrapped NQS. The main advantage of the proposed sensor is its long-term stability (more than 8 months after fabrication). Moreover, the assay does not require addition of external reagents, because all the reagents needed are immobilized in the sensor allowing a rapid estimation. The color change is observed when the sensor is immersed in the ADP solution without sample pretreatment or conditioning. The color change depends on the concentration level. Thus, semiquantitative analysis can be made by naked eye and/or quantitative analysis can be carried out by DR and/or DI. In order to avoid additional instrumentation, a smartphone with a free software could be used to improve the portability. The sensor provides good LODs and precision and it can

be considered viable device owing to its portability, stability, reliability and low cost. Thus, the developed procedure is a green, rapid, and simple alternative for ADP estimation without trained personnel or complicated sample treatment.

4.1.2.3 A solid colorimetric sensor for the analysis of amphetamine-like street samples

A rapid and low-cost kit for the in-situ screening of illicit drugs such as AMP, MAMP, MDMA and MDA is developed. The proposed kit is based on the same sensor used for the casein and ADP detection previously explained, that is, a sensor constituted of PDMS/TEOS/SiO₂NPs doped with NQS reagent. In-situ screening is possible through the observation of color of the sensor after its introduction into a basic solution with the sample. After reaction, quantitative analysis has been carried out in the lab by direct measurement of the absorbance by DR and also by measurement of color intensity after processing its DI. The kit has been applied to ecstasy street samples and the accuracy has been validated by comparing the results with those obtained by LC. The tested samples have been also characterized by FTIR-ATR spectroscopy.

Effect of sensor shape and composition on the optical response

The sensor composition is a key parameter in order to reach quality analytical responses. Moreover, in this work, the shape of the sensing devices was also evaluated using AMP as model compound. Square sensors of 2 x 2 mm side and 1 mm thickness were tested by introducing them in vials containing 0.01 g of AMP in 1 mL of buffer (final concentration, 0.01 g mL⁻¹). It was observed that the formation of the color at the edges of the sensor started a few minutes after its introduction into the AMP solution, but the complete coloration of the sensor required approximately 20 min. Circular sensors (8 mm diameter, 1 mm thickness) were also tested for solutions with the same concentration of AMP. Faster responses were observed for the circular sensors, and complete color development was reached in 10-15 min. In order to reduce the amount of reagent and materials, small circular sensors of 3 mm of diameter and 1 mm of thickness were selected for further assays. The effect of the proportion of PDMS to TEOS on the sensor response was evaluated for sensors exposed to AMP and MAMP. The PDMS/TEOS ratios tested were 100/0, 50/50 and 40/60 (w/w). SiO₂NPs at a percentage of 0.1 % (w/w) were added to increase the matrix porosity and to reduce the cracking of the sensor (*Li, D. et al., 2013*). The results of this study are depicted in *Figure 89*. As it can be seen from *Figure 89A*, sensors with a 50/50 PDMS/TEOS weight ratio provided the highest analytical signals. In addition, this composition also lead to the most homogeneous color distribution, as derived

from *Figure 89B*, which shows pictures of the sensors obtained after their exposure to solutions of the tested compounds. This was confirmed with microscopic photographs (*Figure 89C*).

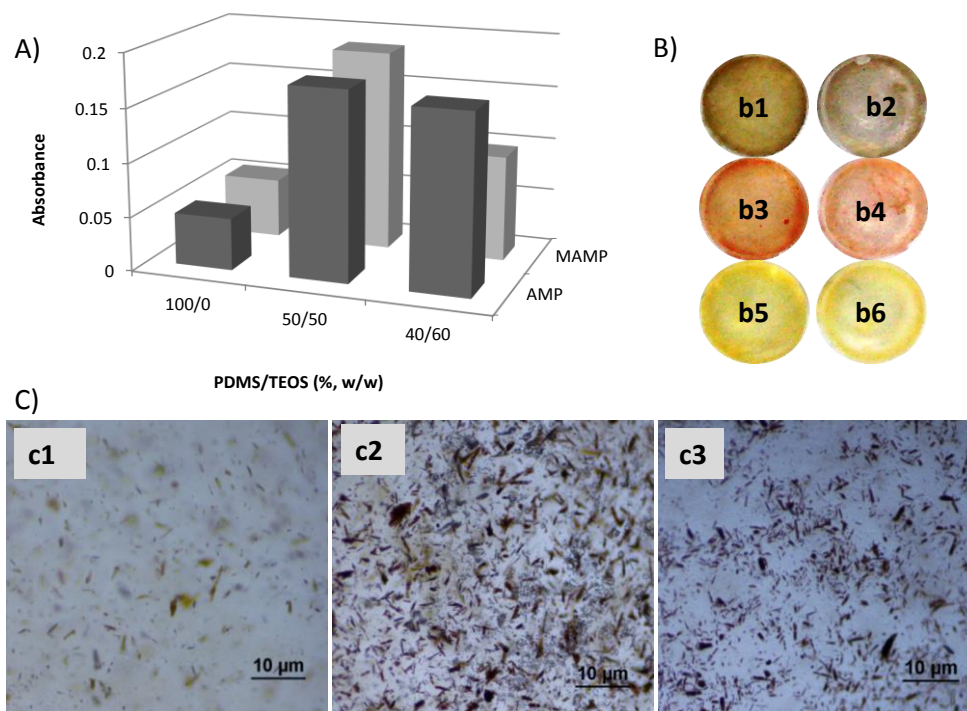


Figure 89. Optimization of sensor composition. (A) Effect of different weight ratios of PDMS/TEOS on the analytical response, (B) Photographic images of sensors containing 50/50 (left) and 40/60 (right) of PDMS/TEOS (w/w) exposed to AMP (b1, b2) and MAMP (b3, b4) and blanks (b5, b6) and (C) Microscopic photographs at 10x magnification obtained for PDMS sensors (c1), PDMS/TEOS 50/50 (w/w) sensors (c2), and PDMS/TEOS 40/60 (w/w) sensors (c3). Conditions: 0.01 g mL^{-1} of AMP and MAMP, 10 min, 0.1 % NQS and 0.1 % NPs.

Analytical characteristics of the sensors

The responses of the developed sensors to solutions of AMP, MAMP, MDMA and MDA (0.01 g mL^{-1}) as a function of the exposure time were evaluated. For this purpose, the absorbances were registered at different times up to 20 min. The results are shown in *Figure 90*. According to the results of this figure, 10 min were

selected as a compromise between the analytical signal and the total analysis time.

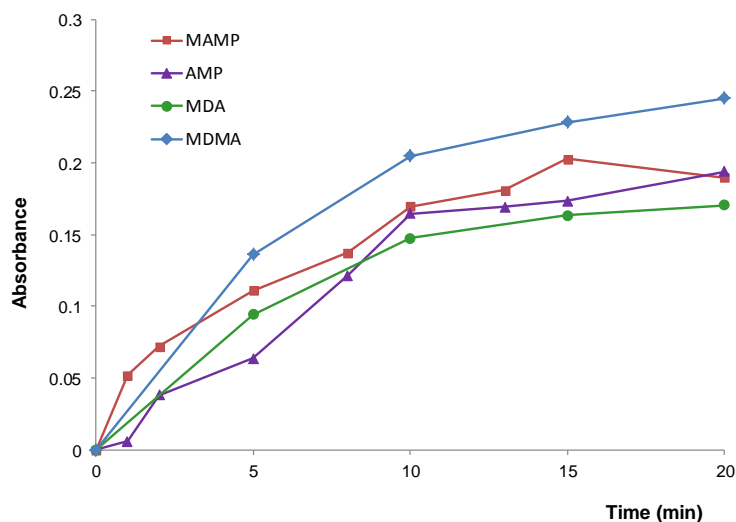


Figure 90. Absorbance at 525 for AMP and MDA (primary amines) and 600 nm for MAMP and MDMA (secondary amines) recorded against a reagent blank at different reaction times. Conditions: sensor composition of 0.1 % NQS, 0.1 % NPs, 50/50 PDMS/TEOS; analyte concentration of 0.01 g mL^{-1} .

As expected, different colors were observed depending on the type of amino group present in the analyte, orange for amphetamines with secondary amine groups (MAMP and MDMA) and grey-brown for compounds with primary amine groups (AMP and MDA). This can be observed in *Figure 91*, which shows the absorbance responses as a function of the analyte concentration. It has to be noted that slight deviation on the spectral shape observed in some of the registers did not affect the absorbances measured at the working wavelengths. *Figure 91* also shows photographic images obtained for sensors exposed to different concentrations of AMP and MAMP.

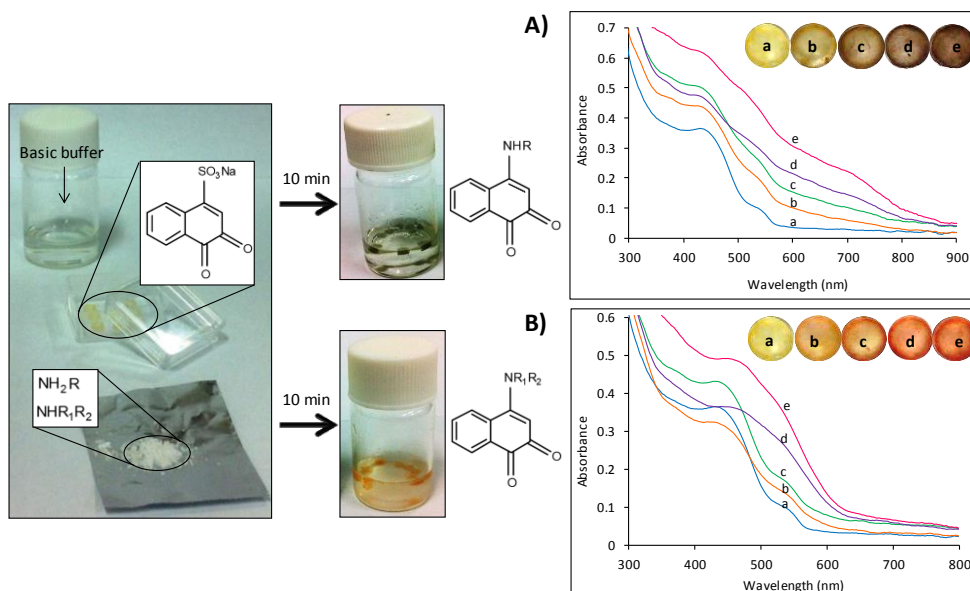


Figure 91. Photographic image of the analysis by the colorimetric kit (composed by a vial with basic buffer, NQS-PDMS sensors and powder/pill drug) for AMP (above) and MAMP (down), together with absorbance spectra at different concentrations a) blank, b) 0.005, c) 0.01, d) 0.03 and f) 0.05 g mL⁻¹ of AMP (A) and MAMP (B). Inset: photographic image of sensors containing previous concentration levels. Optimal conditions.

The reliability of the proposed procedure was tested by analyzing aqueous solutions containing AMP, MAMP, MDA and MDMA. The concentrations studied were 0.0025-0.05 g mL⁻¹ for AMP and MAMP, and 0.0025-0.025 g mL⁻¹ for the ecstasy-type analytes (MDMA and MDA). The calibration equations, precision data and LODs obtained by using DR and DI are shown in *Table 35* and *Table 36*, respectively. Satisfactory linearity was obtained with the two approaches tested. The precision was evaluated by obtaining the intra and inter-day precision at a concentration of 0.015 g mL⁻¹ of the tested drugs. The batch-to-batch RSD values were lower than 15 % in all instances. These results indicated that the proposed procedures have adequate precision. The LODs (calculated as $3s_a/b$, where s_a is the standard deviation of the intercept and b is the slope of linear calibration graph) were in the 0.002-0.005 g mL⁻¹ range. According to the above results, the analytical performance of the two proposed approaches is similar, although the inter-day precision was slightly better with the DI-based approach.

Table 35. Analytical data for the estimation of AMP, MAMP, MDA and MDMA by using DR. Absorbances measured at 525 nm and 600 nm for secondary and primary amines, respectively. Concentrations expresses in g mL^{-1} ; s_a and s_b : standard deviation of the ordinate and slope, respectively.

Compound	Linearity, $y = a + bx \text{ (mL g}^{-1}\text{)}$	RSD _{Intra-day} , n=3 (%)	RSD _{Inter-day} , n=3 (%)	LOD (g mL^{-1})
AMP	$a; s_a: 0.05; 0.01$ $b; s_b: 5.9; 0.9$ $R^2 = 0.985$	11	14	0.004
MAMP	$a; s_a: 0.119; 0.005$ $b; s_b: 5.2; 0.2$ $R^2 = 0.992$	4	12	0.003
MDA	$a; s_a: 0.03; 0.003$ $b; s_b: 3.7; 0.5$ $R^2 = 0.990$	10	13	0.002
MDMA	$a; s_a: 0.05; 0.01$ $b; s_b: 7.9; 0.5$ $R^2 = 0.996$	7	11	0.002

Table 36. Analytical data for the estimation of AMP, MAMP, MDA and MDMA by using color intensity of the DI. Concentrations expresses in g mL^{-1} ; s_a and s_b , standard deviations of the ordinate and the slope, respectively.

Compound	Linearity, $y = a + bx \text{ (mL g}^{-1}\text{)}$	RSD _{Intra-day} , n=3 (%)	RSD _{Inter-day} , n=3 (%)	LOD (g mL^{-1})
AMP	$a; s_a: 0.014; 0.001$ $b; s_b: 0.42; 0.03$ $R^2 = 0.968$	2	7	0.005
MAMP	$a; s_a: 0.012; 0.001$ $b; s_b: 0.212; 0.013$ $R^2 = 0.981$	3	7	0.004
MDA	$a; s_a: 0.013; 0.001$ $b; s_b: 0.20; 0.07$ $R^2 = 0.983$	7	11	0.005
MDMA	$a; s_a: 0.014; 0.001$ $b; s_b: 0.28; 0.02$ $R^2 = 0.994$	5	9	0.003

The proposed conditions were applied to other substances used as adulterants and diluents in clandestine samples. The compounds examined were diluents such as caffeine, EP, procaine, paracetamol, ibuprofen, acetylsalicylic

acid, levamisole, starch, mannitol, sucrose, glucose, lactose and magnesium sulfate. The sensors were also tested for other drugs such as cocaine, cannabinol, cannabidiol, tetrahydrocannabinol and scopolamine. All the tested compounds were assayed individually at a concentration of 0.005 g mL^{-1} . The visual inspection of the sensors revealed that their color was not changed by any of the tested compounds, except EP and procaine. These two compounds rendered the sensors indistinguishable to those obtained for primary amphetamines.

Although the two compounds are rarely found in ecstasy pills (*Nguyen, T.A.H. et al., 2015*) they possess amino groups which can react with NQS. Thus, if a sample is positive for primary amphetamines, a confirmatory test would be required to check the presence of EP and/or procaine. The requirement of a confirmatory test (typically a chromatographic assay) is a limitation found in most of the proposed on-site colorimetric tests (*Camilleri, A.M. et al., 2005*). The stability of the sensor over the time was also examined. Since the application of NQS as a colorimetric reagent requires freshly preparation, derivatization with NQS in solution would not be useful for on-site analysis. Unlike in aqueous solutions, NQS remains stable inside the PDMS/TEOS matrix (*See Section 4.1.2.2*). In the present study, the response of the sensors over the time was evaluated using MAMP as model compound. The sensors were put into contact with the solutions of MAMP (0.01 g mL^{-1}). After the reaction time, the sensors were removed from the sample vials, and stored dry in polyethylene bags at ambient temperature until measurement. The absorbance of sensors was measured after different storage times; the responses for blanks were also registered. The results can be seen in *Figure 92*. This figure shows excellent storage stability of the sensors over a period up to three years, with RSD of the signals $\leq 10 \%$. On the other hand, once the sensor is removed from the sample solution the response remained stable within experimental variations for several weeks, which would allow further processing of the sensor, if required. As an example, RSDs $\leq 7 \%$ were found for signal values registered 4 months after the first measurement carried out immediately after exposure of the sensor to MAMP ($n=5$).

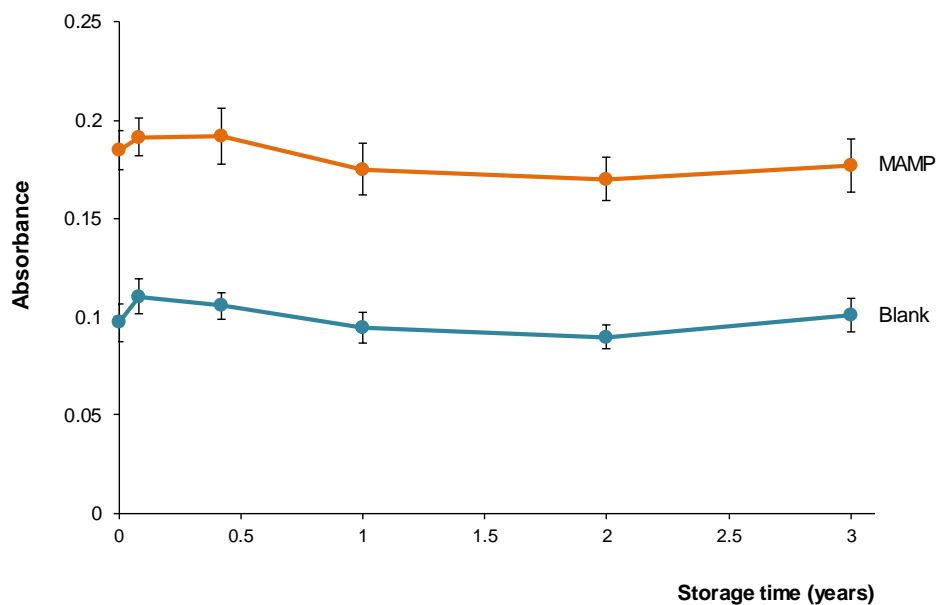


Figure 92. Stability of the sensors. Responses are expressed as the absorbance of sensors after their immersion into a buffer solution containing 0.01 g mL^{-1} of MAMP or into the buffer (blanks). Average responses and standard deviation for $n=3$.

Application to ecstasy samples

Different street samples with active drugs and additives were analyzed using the proposed colorimetric kit by using both DR and DI. The results were compared with those obtained by LC-FLD and precolumn derivatization using conditions described in a previous work (Herráez-Hernández, R. et al., 2001). The samples were also characterized by FTIR-ATR. In Figure 93A are depicted the chromatograms obtained for some of the samples assayed as well as for a blank and for a standard solution of AMP, MDMA and MAMP.

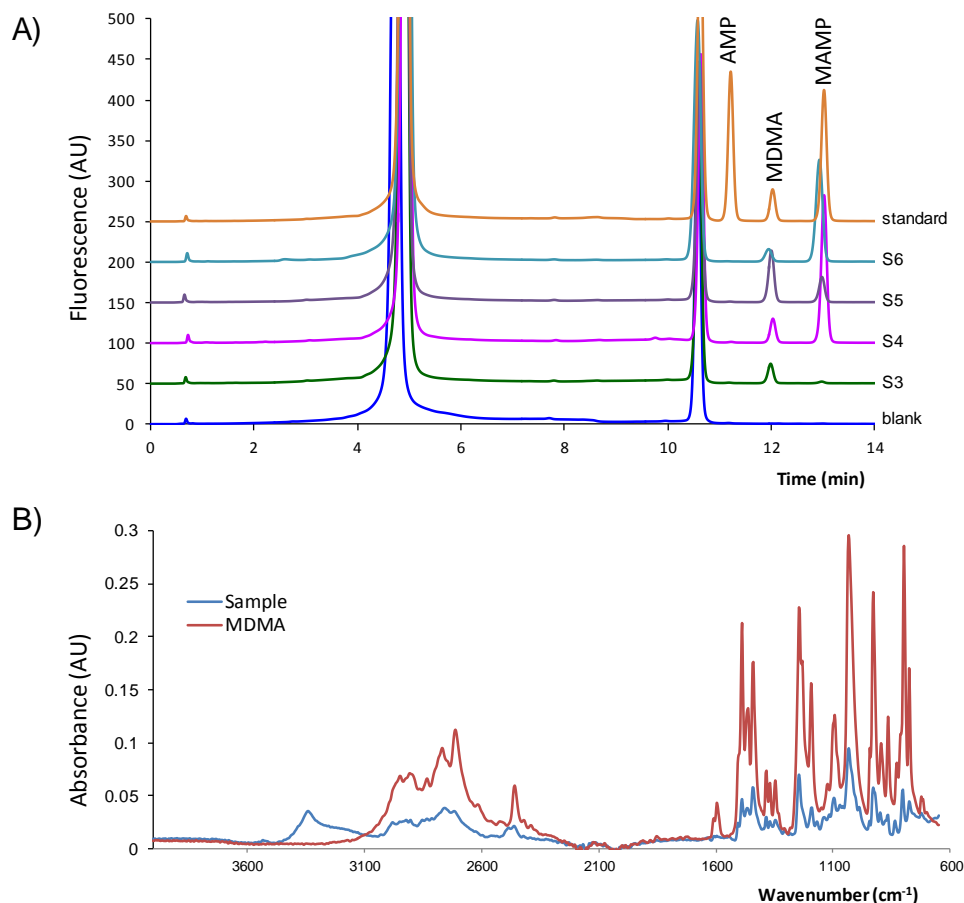


Figure 93. A) Chromatograms obtained for a blank (water), a standard solution of MDMA (16.5 mg mL^{-1}), a street samples containing MDMA (S3), and samples containing mixtures of MDMA and MAMP (S4: (27.4 ± 0.6) % of MDMA and (46 ± 4) % of MAMP; S5: (65 ± 5) % of MDMA and (5.1 ± 0.2) % of MAMP; S6: (17 ± 1) % of MDMA and (34 ± 1) % of MAMP). B) FTIR-ATR spectra obtained for a street sample (S1) and for pure MDMA.

The results obtained by LC showed that MDMA was the only amphetamine-type compound found in three of the tested samples (S1-S3), whereas the other samples assayed (S4-S6) contained mixtures of MDMA and MAMP (the percentages of both drugs composition S4-S6 is indicated in this figure). It should be noted that the RSDs of the results obtained by the LC approach ranged from 2 to 9 %; which are consistent with those previously reported (Herráez-Hernández, R. *et al.*, 2001). No other peaks corresponding to compounds reactive towards

FMOc such as EP were observed in the samples (retention time of the EP-FMOc derivative under the chromatographic conditions used, 8.7 min). In *Figure 93B* is shown the FTIR-ATR spectra obtained for one of the samples (S1) and also the spectra obtained for pure MDMA. Characteristic bands of MDMA were observed in the spectrum of illicit sample at 2710 cm^{-1} (N-H stretching of amine), 2454 cm^{-1} (C-H stretching of CH_3 group), 1488 cm^{-1} (C-H bend), 1244 and 1030 cm^{-1} (C-O-C stretching of methoxy group) and 930 cm^{-1} (C-O stretching). The absorbances of sample were lower than those of the pure MDMA. Moreover, the infrared spectrum of the sample showed an additional band at 3300 cm^{-1} (O-H stretching). Thus, it was hypothesized that the illicit sample could contain MDMA together with other substances such as lactose, starch, mannitol, or paracetamol owing to their O-H stretching band. Although EP could also be another possible adulterant in the street samples, the LC registers showed that this compound was not present in any of the tested samples.

Finally, in order to evaluate the accuracy of the developed sensors, the percentages of MDMA and MAMP in the street samples were calculated measuring the absorbance by DR and color intensity of DI and the calibration equations of *Tables 35* and *36*. The results were compared with those achieved by the LC reference method using the external calibration equations obtained from standard solutions of the analytes at concentrations within the $1\text{-}20.0\text{ mg L}^{-1}$ range. The results obtained are summarized in *Table 37*. For samples S3-S6 the sensor responses were proportional to the sum of the percentages of MDMA and MAMP. It has to be remarked that the same can be expected for other sensors that have been proposed for MAMP detection (*Choodum, A. et al., 2015; Yarbakht, M. and Nikkhah, M., 2015*). The composition of those samples listed in *Table 37* is given as the sum of the percentages of MDMA and MAMP expressed as MDMA. As observed in this table no significant differences were found between the results obtained by the proposed sensor-based approaches and by the reference method. It was therefore concluded that the developed colorimetric sensor provide accurate results.

Table 37. Composition of the ecstasy street samples obtained by the sensor-based approaches and by the LC reference method. (*) Sum of the percentages of MDMA and MAMP expressed as MDMA.

Sample	MDMA percentage (%)		
	Sensor/DR	Sensor/DI	LC
S1	36 ± 6	-	36.1 ± 1.4
S2	21.2±1.2	24 ± 3	19.4 ± 0.7
S3	25 ± 8	19 ± 2	21.8 ± 0.9
S4	64 ± 12	52 ± 4	63 ± 2*
S5	76 ± 3	74 ± 5	69 ± 4*
S6	49.6 ± 1.1	41 ± 3	43.5 ± 0.9*

Conclusions

The purpose of this work has been the development of a colorimetric kit for in-situ screening of amphetamine-like drugs in street samples. This kit is based on a sensor obtained by embedding NQS into a PDMS/TEOS/SiO₂NPs matrix. The sensor allows the visual differentiation of the analytes according to their amine groups: brown-grey color for primary amines (e.g. AMP, MDA) and orange for secondary amines (e.g. MAMP, MDMA). After a positive finding, the sensor can be transported to the lab for further quantitative analysis by any of the proposed methodologies: (i) by measuring the absorbance by DR, or (ii) by taking a photograph of the sensor and processing the color values of DI; in such case, a portion of the sample has to be weighed in the field (a portable balance would be required). If image processing is the option selected, the photographs of the sensors could be taken in the field. After a positive finding another portion of the street sample can be moved to the lab, and then analyzed with the sensors by any of the two proposed methodologies. This would be the option of choice if quantitative results with a high level of accuracy are required. The main advantages of the proposed kit for in-situ tests are that it neither needs expensive instrumentation nor trained personnel, and that is portable easy to use, rapid, and economic (the estimated cost per sensor is < 0.02 €). The sensors have excellent long term stability, and do not require special package and/or storage conditions. Therefore, the proposed colorimetric kit is a very useful tool for on-site screening of amphetamine-like street samples. Furthermore, the procedure

provided suitable linearity, precision and accuracy for the quantification of the tested drugs. In principle, many other reagents can be embedded into PDMS, which suggests that multi-analyte detection kits could be developed through the combination of different sensors.

4.1.2.4 A passive solid sensor for in-situ colorimetric estimation of the presence of ketamine in illicit drug samples

In an attempt to extend the applicability of PDMS as encapsulant material of derivatizing reagents, a sensor based on Co(SCN)_2 immobilization in PDMS has been developed for the estimation of ketamine in illicit drug samples. The sensor is exposed to solutions of ketamine at a basic pH and its color changes from brown to blue-purple due to the interaction between ketamine and Co(SCN)_2 . The sensor enables the visual identification of ketamine in a few minutes. Quantification is also possible through the measurement of the absorbance by DR. The reliability of the developed sensors has been tested by analyzing illicit drug samples. The tested samples were also processed by FTIR-ATR and LC for comparison purposes.

Preparation of the sensors

Different sensor compositions were assayed (*See Table 16 in 3.4.2 Section*). Successful polymerization for the PDMS sensors was observed at a 35 °C in relatively short times (< 8 h) even for the highest percentage of reagent assayed. However, PDMS/TEOS-based sensors required up to three-five days for gelification. In all instances, a visual inspection of the sensors revealed that the distribution of the reagent particles into the polymeric matrix was suitable. This was confirmed by obtaining the microscopic images (*See Figure 94A*).

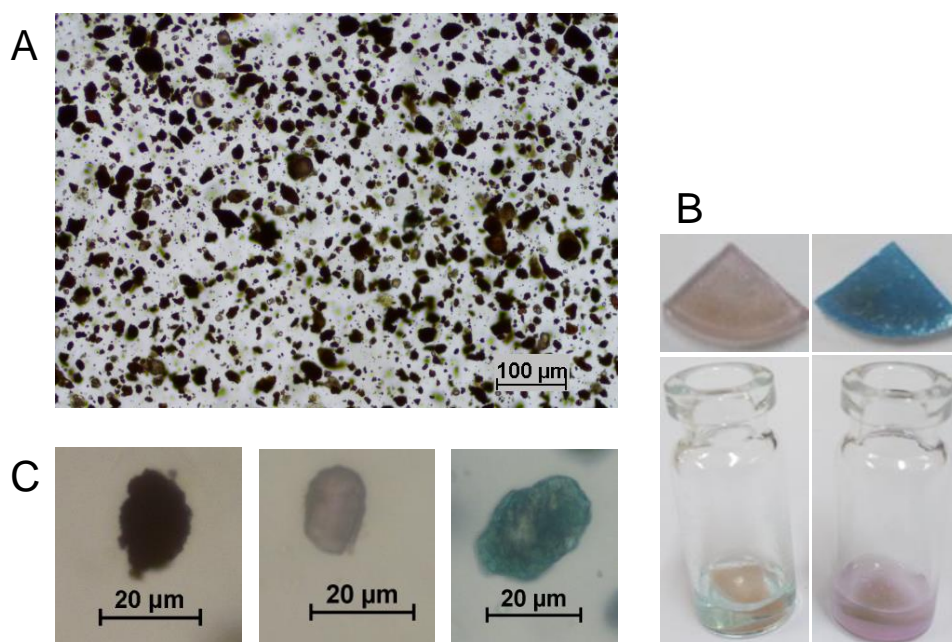


Figure 94. Microscopic photographs of: (A) Sensor containing 0.6 % of reagent in PDMS (w/w). (B) Sensors containing 0.3 % of reagent in PDMS (w/w) during (down) reaction and 30 min after reaction (up) exposure to a blank (left) and to a solution of ketamine $25000 \mu\text{g mL}^{-1}$ (right); (C) detail of reagent particle in a sensor containing 0.3 % of reagent in PDMS (w/w) (left), a sensor exposed to a blank (center) and a sensor exposed to a solution of ketamine $25000 \mu\text{g mL}^{-1}$ for 15 min (right).

On the other hand, freshly prepared sensors showed a brown color which is characteristic of the $\text{Co}(\text{SCN})_2$ reagent. However, slow changes to pink-blue pale tonalities were sometimes observed when the sensors were exposed to different ambient conditions. Changes were more intense in the presence of TEOS. According to the literature, color changes can be attributed to the variation of coordinate water molecules as a function of the humidity (Haddoub, R. et al., 2011). This is consistent with the fact that blue tonality was also more remarked for the sensors containing TEOS as they exhibit higher affinity for water molecules. In the present study, slight changes in the color of unused sensors had not effect on the test results. This is because the proposed methodology involves the immersion of the sensors into an aqueous media.

The effect of the percentage of reagent on the absorbances was evaluated within the 0.1 - 0.9 % (w/w) range. The responses of the sensors were evaluated using standard solutions of ketamine at different concentrations of drug. Aliquots of the samples were mixed with the same volume of 0.1 M NaOH and the sensors were immersed into them. For the sensors containing the highest reagent percentage (0.9 %, w/w) a small portion of reagent diffused through the solution. As a result, the purple precipitate characteristic of the Morris reaction was observed around the sensors a few min after their exposure to solutions containing a high concentration of ketamine ($25000 \mu\text{g mL}^{-1}$) (See *Figure 94B*). After a few min, the precipitate disappeared while the sensor color changed from brown to blue-purple. These observations demonstrated that ketamine diffused from the solution to the sensor, so that the complex is formed inside the polymeric matrix. The formation of the ketamine derivative around the reagent particles immobilized in the PDMS was confirmed by obtaining the microscopic images of the sensors (See *Figure 94C*).

For a given concentration of ketamine and reaction time the blue-purple color of the sensor was more intense as the percentage of reagent increased (w/w). However, the highest differences on the measured absorbances between solutions of ketamine and blanks were observed for the sensors containing 0.3 % of reagent. This is illustrated in *Figure 95*, which shows the variation of the absorbances at the working wavelength (625 nm) for both, a blank and a solution of ketamine ($700 \mu\text{g mL}^{-1}$). In other words, the contribution of the sensor itself to the analytical signal increased as the percentage of reagent increased. These results can be explained by the fact that, as stated earlier, when introduced in an aqueous media the sensors also developed a blue-pale color due to the hydration of the reagent. In addition, the reagent exhibits a characteristic band at 672 nm (brown). For the sensors with the highest reagent content, the brown tonality still was visible after reaction. Therefore, the employment of PDMS sensors containing 0.3 % of reagent (w/w) was considered the best option for quantitative purposes. The addition of TEOS was discarded because, as stated earlier, the preparation of the sensors involved longer times and they exhibited high background absorbances.

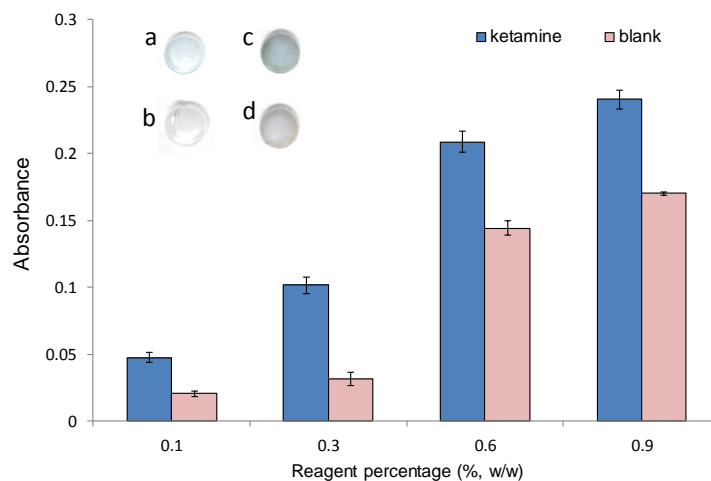


Figure 95. Effect of the percentage of reagent in PDMS sensors on the absorbances (625 nm) for a blank and for a solution of ketamine ($700 \mu\text{g mL}^{-1}$); time of exposure, 10 min. Inset: Photographic images of sensors containing 0.3% of reagent exposed to (a) a solution of ketamine, (b) a blank; sensors containing 0.9% of reagent exposed to (c) a solution of ketamine and (d) a blank. Concentration of ketamine, $1000 \mu\text{g mL}^{-1}$; time of exposure, 10 min; time until measurement, 5 min.

In order to evaluate the effect of the sensor size sensors with the same composition and two different sizes were compared; according to the above results, PSMD-based sensors containing 0.3 % (w/w) were selected. Portions of 0.030 g or 0.20 g of the same reagent/PDMS-curing agent dispersion were placed in 6 mm or in the 15 mm diameter wells, respectively. After curing, the obtained sensors were tested for working solutions of ketamine at a concentration of $1000 \mu\text{g mL}^{-1}$. For the largest sensors, 1 mL of the working and the NaOH solutions were used. The results showed that complete and homogeneous color development required longer times when using the largest sensors. Consequently, 6 mm diameter sensors containing 0.3 % of reagent into PDMS were selected for further work.

On the other hand, the absorbances at 625 nm of sensors kept at ambient conditions in polyethylene bags were measured after different storage times over a period of two months. The results showed signal variations ranging from + 5 % to - 11 % with respect to those measured for freshly prepared sensors. These variations were comparable to those observed for the repeated measurements of

freshly prepared sensors. It was therefore concluded that the sensors were stable for at least two months without using special storage conditions.

Optimization of the reaction conditions

In preliminary experiments it was confirmed that a basic media was necessary for the reaction to take place (no response was observed for ketamine in water); however, no significant differences in the absorbances were obtained within the 10-14 pH range.

In order to study the effect of the reaction time on the absorbance, the selected sensors were exposed to solutions of ketamine ($500 \mu\text{g mL}^{-1}$) for different times. Next, the sensors were removed from the vials, and their colours were visually monitored; their absorbances at 625 nm were also measured by DR. As observed in *Figure 96A*, the color intensity of the derivative formed by ketamine increased with the reaction time up to 10 min, and then remained approximately constant. Once removed from the reaction media, the intensity of the color slightly increased with time, as depicted in *Figure 96B*. However, according to this figure the difference between the absorbances measured at different times for a blank and a solution of ketamine remained approximately constant, at least within the 0-30 min interval. Based on the above results, a reaction time of 10 min was selected, and the differences of absorbances registered for a sample and for a blank, both measured 5 min after the removal of the sensors from the vials, were used as analytical signal.

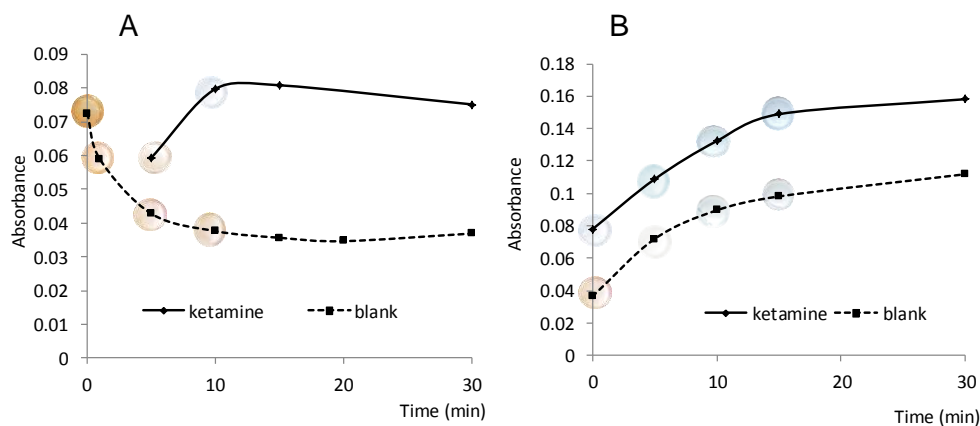


Figure 96. Effect on the absorbances measured for a blank and a solution of ketamine ($500 \mu\text{g mL}^{-1}$) of: (A) the time of reaction, and (B) the time elapsed between reaction and measurement. In (A) the absorbance was measured immediately after the removal of the sensor from the sample; in (B) the reaction time was of 10 min. The conditions selected as optima were: reaction time, 10 min; time until absorbance measurement, 5 min.

Analytical parameters

Analytical data for ketamine were established under the experimental conditions described above. The results obtained are summarized in *Table 38*. The proposed assay provided suitable linearity up to concentrations of ketamine of $1000 \mu\text{g mL}^{-1}$ (4.21 mM). The LOD was calculated as $3 s_{\text{blank}}/b$ where b is the slope of the calibration curve and s_{blank} is standard deviation of the ordinate intercept. The calculated LOD was $100 \mu\text{g mL}^{-1}$. It should be noted that visual detection of ketamine was possible for concentrations of ketamine $\geq 300 \mu\text{g mL}^{-1}$ (equivalent to 30 μg of drug). Thus, the minimum detectable amount of ketamine is three times higher than the amount detectable by UV spectrophotometry; similar results have been reported for this reaction using RGB image analysis (*Musile, G. et al., 2015*).

The precision was evaluated through the processing of ketamine solutions of an intermediate concentration ($500 \mu\text{g mL}^{-1}$). The intra and inter-day RSD values were 7 % and 10 %, respectively ($n=3$). The batch-to-batch RSD for three different syntheses of sensors and the same concentration of ketamine was 13 %. These results indicated that the proposed sensors provide adequate precision.

The sensor response was examined for other drugs and possible adulterants or diluents that are often used in combination with ketamine. The compounds tested were AMP, MAMP, MDMA, cocaine, EP, scopolamine, caffeine, acetaminophen, ibuprofen, acetylsalicylic acid, starch, saccharose, glucose, lactose and magnesium sulfate. Individual solutions of the tested compounds at concentration of 400-1000 $\mu\text{g mL}^{-1}$ were prepared by dissolving the pure compounds in nanopure water. Aliquots of 100 μL of these solutions were mixed with 100 μL of 0.1 M NaOH and analysed with the sensors. Under the proposed conditions no interference was found.

Table 38. Analytical data obtained by using the developed sensors.

Linearity* ($y=a + bx$), n= 6			RSD _{Intraday} (n=3)	RSD _{interday} (n=3)	LOD ($\mu\text{g mL}^{-1}$)
$a \pm s_a$	$b \pm s_b$ ($\text{mL } \mu\text{g}^{-1}$)	R^2			
0.003 ± 0.003	$(8.7 \pm 0.6) 10^{-5}$	0.99	7	10	100

*tested concentration range: 200-1000 $\mu\text{g mL}^{-1}$; b expressed as $\text{mL } \mu\text{g}^{-1}$.

Application to real samples

The developed sensors were applied to the analysis of three illicit street samples (S1-S3) suspected to contain ketamine. For this purpose accurately weighted portions of the samples were diluted in water to adjust the concentration of ketamine within the linear working interval (Table 38). Then aliquots of 100 μL were processed under the proposed conditions. The samples were also characterized by FTIR-ATR. In order to establish the identity of possible sample constituents, the FTIR-ATR spectra of the drugs and adulterants included in the selectivity study were also registered and compared with those of the samples. Additionally, a procedure was developed for the identification and quantification of ketamine in the samples by LC-UV-DAD. The elution and detection conditions were selected in order to achieve a satisfactory separation of ketamine from other sample constituents. For quantification purposes, a calibration graph was obtained for ketamine within the 5-100 $\mu\text{g mL}^{-1}$ concentration range. When using the developed sensors positive responses to ketamine were found in two of the samples assayed (S1 and S2). The presence of ketamine in both samples was confirmed by LC. The later technique also gave a

negative result for ketamine in sample S3. However, by FTIR-ATR ketamine could be only identified in one of the samples that gave positive response with the sensors (S1).

As an illustrative example, the UV, FTIR-ATR and chromatographic registers obtained for one of the samples assayed (S1) are shown in *Figure 97*. As observed in this figure, the color of the sensor indicated a positive response to ketamine; the characteristic band of the ketamine complex (maximum of absorption at 625 nm) was observed in the spectra recorded for the sensor, as depicted in *Figure 97A*. The FTIR-ATR spectra (*Figure 97B*) showed characteristic bands of ketamine at 2670 cm^{-1} (N-H stretch amine salt and CH_3 stretch), 1719 cm^{-1} (RC=O stretch cyclic ketone), 1577 cm^{-1} (N-H bend amine and C=C aromatic stretch), 1118 cm^{-1} (in plane C-H bend, C-N stretch), 771 cm^{-1} (out of plane aromatic C-H bend and Cphenyl-Cl monosubstituted) and 704 cm^{-1} (out of plane ring C=C bend and Cphenyl-Cl monosubstituted). The comparison of the spectrum registered for the sample with those of the possible adulterants suggested the presence of caffeine (*see also Figure 97B*). Characteristic bands of caffeine were observed at $3095\text{-}2935\text{ cm}^{-1}$ (CH_3 stretch), 1690 and 1640 cm^{-1} (C=O and phenyl stretch), $1596\text{-}1543\text{ cm}^{-1}$ (C=N and N-C=O stretch), $1477\text{-}1428$ (Phenyl stretch, CH bend, C=N stretch), $1398\text{-}1353\text{ cm}^{-1}$ (CN stretch), $1282\text{-}1182\text{ cm}^{-1}$ (C=O stretch, CN stretch), $1062\text{-}1021\text{ cm}^{-1}$ (C=O, CN and C-C stretch) and 853 cm^{-1} (C-C stretch). The high intensities of bands from caffeine suggested that the sample contained a high percentage of this compound. Finally, the chromatograms obtained for the sample showed a peak of suspected ketamine at 8.3 min; the identity of this peak was checked by comparing the UV spectra of such peak with that registered from a standard solution of ketamine. As depicted in *Figure 97C*, good concordance was also observed between the two spectra. It should be noted that the intense peak at a retention time of 3.8 min found in the sample was identified as caffeine. This adulterant was also found in sample S2. As regards sample S3, the FTIR-ATR and chromatographic registers obtained suggested the presence of a significant amount of acetaminophen.

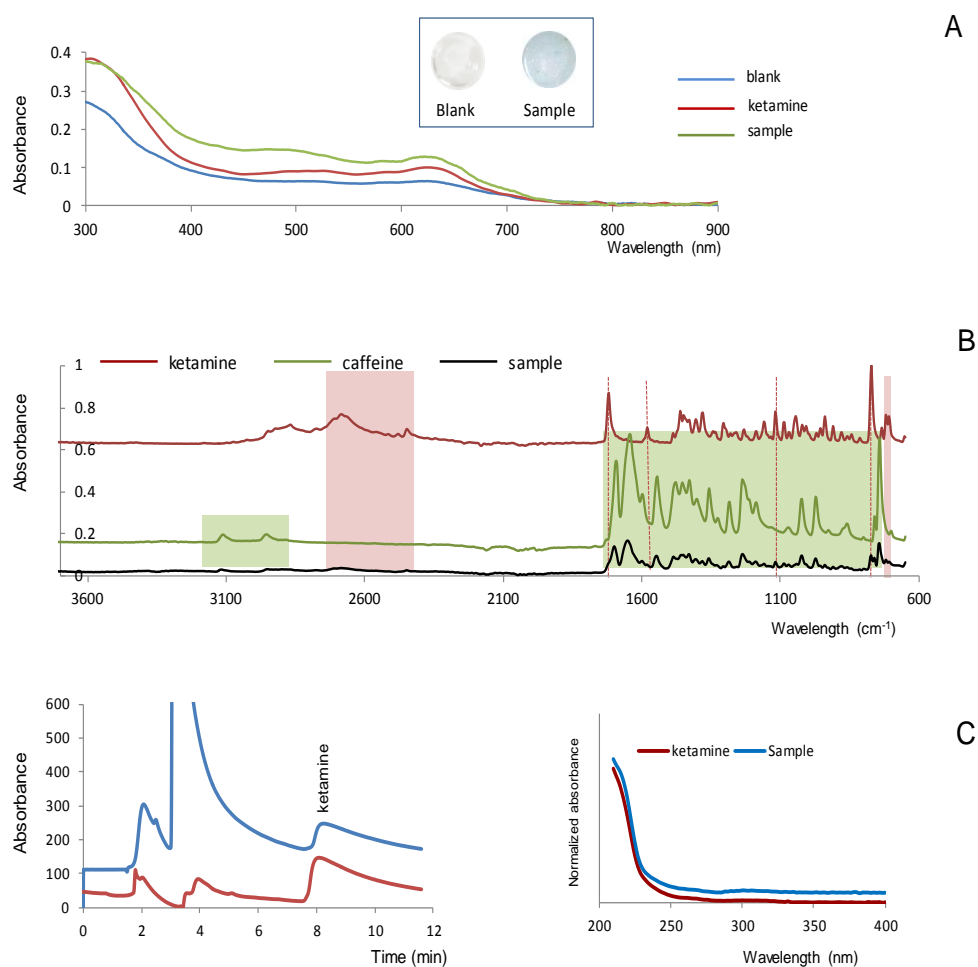


Figure 97. Results obtained for sample S1: (A) sensor absorbance spectra registered for a blank, for a standard solution of ketamine ($500 \mu\text{g mL}^{-1}$) and for the sample solution; inset: sensor images obtained for a blank and for the sample solution; (B) FTIR-ATR spectra obtained for the sample, pure ketamine and pure caffeine; (C) left: chromatograms obtained for a standard solution of ketamine ($50 \mu\text{g mL}^{-1}$) and for the sample solution; right: normalized spectra of ketamine and suspected ketamine in the sample. The sample solution in (C) was a dilution 1:10 of the sample in (A).

Finally, in order to check the performance of the proposed assays for quantitative analysis the percentage of ketamine in samples positive to ketamine (S1 and S2) was established with the developed sensors, and the results were compared to those obtained by the LC method. The values obtained are listed in

Table 39. This table shows that the proposed method provided results comparable to those obtained by the reference method (sample S1, $t_{\text{calculated}} = 1.69$, $t_{\text{tabulated}} = 2.776$; sample S2, $t_{\text{calculated}} = 2.92$, $t_{\text{tabulated}} = 4.30$; values of $t_{\text{tabulated}}$ at a 95 % confidence level).

Table 39. Comparison of the results obtained for the drug street samples with the developed sensors and the LC reference method ($n = 3$).

Sample	Ketamine percentage (%)	
	Sensor	LC
S1	13.7 ± 1.6	12.0 ± 0.6
S2	1.1 ± 0.2	1.24 ± 0.01
S3	negative	negative

Utility

In the last years, different modifications of classic colorimetric assays have been proposed aimed at reducing the manipulation of solutions, thus facilitating on-site analysis. This is the case of the test for ketamine based on its reaction with cobalt thiocyanate (Morris test), which was originally proposed under a conventional solution derivatization scheme (Morris, J.A., 2007). For example, a solid reagent by immobilizing $\text{Co}(\text{SCN})_4^{2-}$ onto a silica nanostructured support has been reported (Madda B. et al., 2015). The preparation of the reagent entailed several operations: synthesis of the tetrathiocyanate complex and its immobilization onto silica NPs (previously activated with concentrated HCl at 120 °C for 24 hours), isolation, purification with diethyl ether and drying of the intermediate product, and then, treatment with a solution of NaOH to produce basic cobalt tetrathiocyanate@NS. The assay involved the treatment of a portion of the basic cobalt tetrathiocyanate @NS reagent with a drop of the sample. Musile et al. described a microfluidic device prepared by creating channels onto a chromatographic paper using wax printing and thermal lamination (Musile, G. et al., 2015). The device was designed to detect different drugs by placing in the channels the appropriate reagents. For the detection of ketamine, aliquots of $\text{Co}(\text{SCN})_2$ and a NaOH solutions were placed in different areas of a channel; an

aliquot of the sample were put into contact with the basic area, and then carried over the cobalt thiocyanate reagent with a water/acetone mixture. The method proposed in the present study uses the same reaction but a different detection mechanism: entrapment of the reagent into PDMS and reaction within the polymeric matrix (ketamine molecules diffuse from the sample solution to the PDMS matrix). The above approaches are suitable for the detection of ketamine in aqueous samples, but they are different in terms preparation and stability of the reagent/detection device, as well as in their analytical performance.

The main advantage of the method proposed in this work is that the sensors can be prepared easily and no additional reagents or instrumentation is involved (only a oven operating at 35 °C is required); the sensors are chip and show suitable long-term stability (no special storage conditions are required). An advantage of the microfluidic approach is that different drugs can be tested simultaneously, although the low stability of this device is a limitation (it can be used for ten days when stored at ambient temperature, and for 30 days if it is plasticized and kept away from light sources and at 4 °C). Thus, the PDMS sensors are better suited for on-site applications (no information on the stability of the basic cobalt tetrathiocyanate @NS reagent was reported in *Madda B. et al., 2015*).

On the other hand, the three approaches allow the rapid detection of ketamine in aqueous samples, but in the assay proposed by Maddah et al. (*Madda B. et al., 2015*) the color change can be observed in shorter times, probably because the analyte molecules come directly into contact with the active groups of the solid reagent, whereas in the methods using paper microfluidic devices and PDMS sensors the diffusion of the analyte molecules from the sample bulk to the reagent is required for the reaction to take place.

The three methods have been tested for similar concentrations of ketamine, and the minimum amount of drug detectable by naked eye reported is also similar. The sensors-based assay provides better linearity and precision than those attained by the microfluidic-based approach (no information on the linearity, precision and accuracy achieved with the basic cobalt tetrathiocyanate @NS reagent was reported in *Madda B. et al., 2015*). It has to be remarked that only the PDMS-based sensors procedure has been validated for illicit dug samples. The sensitivity attained by the proposed procedure is satisfactory for the detection and quantification of ketamine in illicit samples even if the ketamine is low (*Table*

38). However, the sensors cannot be applied to detect ketamine in biological fluids as the concentration found, even for chronic abusers, are typically in the low to sub $\mu\text{g mL}^{-1}$ range (Cheng, W.-C. *et al.*, 2007). To the best of our knowledge, none of the colorimetric assays proposed as presumptive tests for ketamine allow the detection of these compounds in biological fluids.

Conclusions

In spite of the increasing consumption of ketamine, the number of colorimetric assays proposed for the identification of ketamine is still very limited, and only a few of them have been validated for drug street samples (Musile, G. *et al.*, 2015; Maddah, B. *et al.*, 2015). In addition, the identification of ketamine by existing spot colorimetric tests often fails in samples containing other drugs or adulterants (Camilleri, A.M. and Caldicott, D., 2005). In the present work, a solid colorimetric sensor has been developed for the presumptive detection of ketamine based on its reaction with $\text{Co}(\text{SCN})_2$ in basic media (Morris reaction). Sensors were prepared by embedding the solid reagent into a PDMS matrix. When the sensors are exposed to ketamine solutions, the drug diffuses to the PDMS matrix and reacts in the surface of the reagent particles, causing a change in the color from brown to blue-purple. Sensor responses can be obtained in a few minutes, being 30 μg the minimum detectable amount by naked eye.

Under optimized conditions, the sensor can also be used for the quantification of ketamine through the measurement of the absorbance by DR. The results obtained by the proposed assay for illicit street sample show good concordance with those obtained by LC, even for percentages of ketamine in the samples as low as 1-2 %.

The sensors are very cost-effective and easy to prepare, and no special conditions for their storage or employment are required. The proposed assay minimizes risks associated with the manipulation of harmful liquids, so it is well suited for on-site presumptive tests.

4.1.3 C₁₈ AS PHASE FOR MSPD

During the past years many innovative extraction techniques have been developed as alternative to classical multi-step methods for sample treatment. Among them, MSPD is a sample preparation technique with increasing acceptance in solid, semi-solid and viscous samples (García-López, M. *et al.*, 2008; Ramos, L., 2012) due to the reduction of sample and solvents consumption and does not need special instrumentation. The selectivity and efficiency of MSPD is mainly dependent on the sorbent material used. Most reported methods used reversed phase SPE materials, such as C₁₈ phase for the dispersion and retention of lipophilic analytes. Based on a previous method developed for the quantification of DEHP in sediment samples, bondesil C₁₈ phase has been used as MSPD sorbent, integrating disruption, clean-up and solid phase derivatization for the determination of amphetamines in air.

4.1.3.1 Determination of amphetamines in hair by integrating sample disruption, clean-up and solid phase derivatization

The utility of C₁₈ as sorbent phase for MSPD to analyze amphetamines in hair samples has been evaluated. The proposed approach is based on the employment of MSPD for matrix disruption and clean-up, followed by the derivatization of the analytes onto the sample blend. The fluorogenic reagent FMOC has been used for precolumn derivatization. Different conditions for MSPD, analyte purification and solid phase derivatization have been tested, using AMP, MAMP, EP and MDMA as model compounds. The results have been compared with those achieved by using UAE and by MSPD combined with conventional liquid-phase derivatization. Thus, a rapid approach is proposed for the analysis of amphetamines-type drugs in hair.

UAE

In *Figure 98* are shown the chromatograms obtained for water (*Figure 98a*) and for a standard solution of the analytes (*Figure 98c*), as well as those obtained for blank hair (*Figure 98b*) and for hair spiked with the analytes (*Figure 98d*). As it can be seen from this figure, the chromatograms obtained for the hair samples showed chromatographic profiles similar to those of the aqueous solutions, although higher backgrounds were observed for the hair samples, especially at

lower retention times. Two intense peaks corresponding to the unreacted FMOC and a degradation product were observed at 4.7, and 10.4 min, and a minor peak was also observed at 12.6 min. Such peaks are typically found when using FMOC as derivatization reagent (Campíns-Falcó, P. et al., 2009; Cháfer-Pericas, C. et al., 2004; Herráez-Hernández, R., 2001).

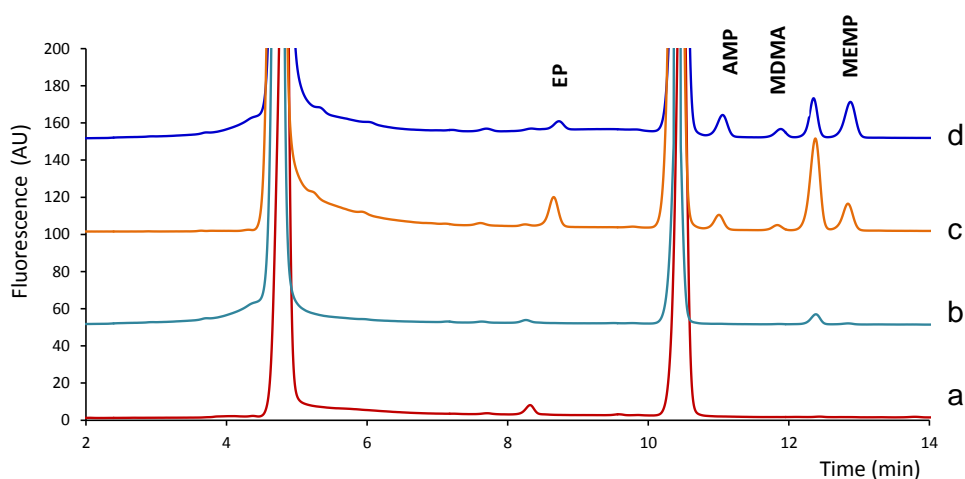


Figure 98. Chromatograms obtained for aqueous solutions and for hair samples treated by the UAE alkaline digestion method: (a) blank (water), (b) blank hair, (c) an standard solution of the amphetamines ($0.5 \mu\text{g mL}^{-1}$, each compound), and (d) a spiked hair sample (25 ng mg^{-1} , each compound).

Quantitative studies were performed using hair samples spiked with the analytes at concentrations within the $25\text{--}200 \text{ ng mg}^{-1}$. The results are summarized in *Table 40*. As it can be observed, linear responses were obtained for the tested analytes. The recoveries, established from the slopes of calibration, as well as the LODs and LOQs are also listed in *Table 40*.

Table 40. Analytical parameters of the methods tested.

Method	Concentration interval (ng mg ⁻¹)	Analyte	Linearity*		Recovery (%)**	LOD (ng mg ⁻¹)
			y=ax+b (mg ng ⁻¹)	R ²		
UAE/ solution	25-200	EP	y = (1.06 ± 0.10)x + (17 ± 11)	0.980	67	7.5
		AMP	y = (2.08 ± 0.11)x + (22 ± 14)	0.993	97	5.0
		MDMA	y = (0.91 ± 0.04)x + (4 ± 5)	0.993	99	7.5
		MAMP	y = (3.8 ± 0.16)x + (10 ± 20)	0.996	122	2.5
MSPD/ solution	10-50	EP	y = (1.84 ± 0.16)x + (-5 ± 5)	0.990	94	5.0
		AMP	y = (7.4 ± 0.4)x + (-10 ± 12)	0.980	109	2.5
		MDMA	y = (2.30 ± 0.08)x + (4 ± 3)	0.990	88	2.5
		MAMP	y = (18.4 ± 0.8)x + (-9 ± 20)	0.990	110	1.0
MSPD/ solid phase	2-20	EP	y = (6.0 ± 0.3)x + (12 ± 4)	0.993	84	0.75
		AMP	y = (16.9 ± 1.1)x + (-12 ± 9)	0.995	118	0.5
		MDMA	y = (3.9 ± 0.2)x + (15 ± 4)	0.980	98	0.75
		MAMP	y = (20.5 ± 1.6)x + (7 ± 20)	0.990	109	0.25

*Established from four concentrations assayed in triplicate.

**Established from the ratios of the slope of calibrations (concentration expressed as $\mu\text{g mL}^{-1}$ of the analytes in the processed extracts as $\mu\text{g mL}^{-1}$) and the slopes of calibrations obtained from standard solutions of the analytes.

MSPD procedure

A) Type and amount of sorbent material

Initially, the effect of the type of dispersant on sample disruption was evaluated as an effective sample disaggregation is essential to achieve accurate results. Silica, alumina and bondesil C₁₈ were the phases tested. In this study, 50 mg of the samples was mixed with 400 mg of the dispersant, and blended gently with a pestle for 5 min. A visual inspection of the blends obtained after the grinding step revealed that in all instances the samples were well dispersed, although when using silica several small pieces of hair were still visible after grinding. Apparently, the employment C₁₈ phase resulted in suitable sample disruption. A C₁₈ phase was used in further studies because it is a retentive

material for amphetamines, and thus, it could be used not only to disrupt the sample, but also for subsequent clean-up (*Herrález-Hernández, R. Et al., 1996a*). It was also tested if the addition of an aliquot of NaOH to the hair samples before grinding could facilitate sample disruption making possible the use of shorter grinding times. In this study, 50 mg of the samples was placed in glass mortars and then, 1 mL of 6 M NaOH was added. After 5 min, 400 mg of C₁₈ phase was added and the mixture was ground for 5 min. However, for the amounts of sample and dispersant used, the semi-solid consistence of the sample dispersant mixture made more difficult to obtain the required homogeneity after the grinding step. Therefore, this option was discarded. Next, the sample to sorbent ratio was optimized. MSPD is well suited for miniaturization and thus, it is adequate for the analysis of hair samples as the amount of sample used for the analysis of drugs in hair is typically <100 mg (*Baciu, T. et al., and Vogliardi, S. et al., 2015*). According to previous experiences with environmental samples, the minimum amount of sample and sorbent that can be handled in the glass mortars with suitable reproducibility is about 0.4–0.5 g (*Campins-Falcó, P. et al., 2008; Moliner-Martínez, Y. et al., 2012*). For this reason, in the present study the amount of sorbent was fixed at 400 mg and the amount of sample was varied. Hair portions of 25, 50 and 100 mg were assayed (equivalent to sample to sorbent ratios of 1:16, 1:8 and 1:4, respectively).

Although sample to sorbent ratios of 1:1-1:4 are used in a large majority of the reported MSPD assays (*Ramos, L., 2012*), in the present study the blend obtained for a 1:4 ratio was unsuitable because several hair segments were still visible after the grinding step. Apparently, the blends obtained when using 1:8 and 1:16 ratios were homogeneous, but in order to ensure a sample disruption as much effective as possible the amount of sample chosen was 25 mg (sample to sorbent ratio of 1:16). In *Figure 99* are shown the photographs corresponding to a portion of the 25 mg of hair (*Figure 99a*), the blend resulting after grinding it with 400 mg of C₁₈ phase (*Figure 99b*), as well as the blend once transferred to a SPE tube (*Figure 99c*). As observed in this figure the dispersion of the sample in the blend was satisfactory. This was confirmed by using light microscopy. In *Figure 100* are shown the microscopic images obtained for a C₁₈ phase ground for 5 min (*Figure 100a*), a hair sample (*Figure 100b*), and the blend obtained by grinding 400 mg of C₁₈ phase and 25 mg of hair for 5 min (*Figure 100c*). The dark zones in the blend (*Figure 100c*) correspond to the hair fragments obtained after sample grinding. As it can be deduced from this figure, the grinding step resulted in much

smaller hair fragments, which confirmed that under the proposed conditions sample disruption was effective and lead to a homogeneous dispersion of hair in the blend.

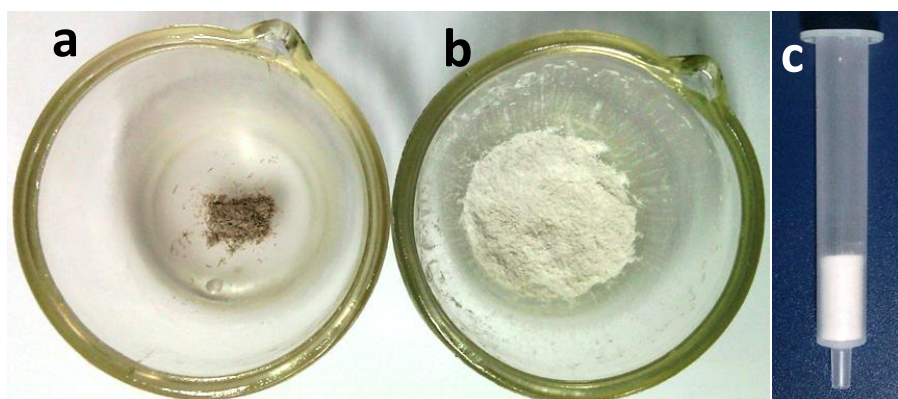


Figure 99. Photographs of: (a) a hair sample (25 mg), (b) the blend obtained after grinding the sample with 400 mg of the C_{18} phase, and (c) the blend transferred to an extraction tube.

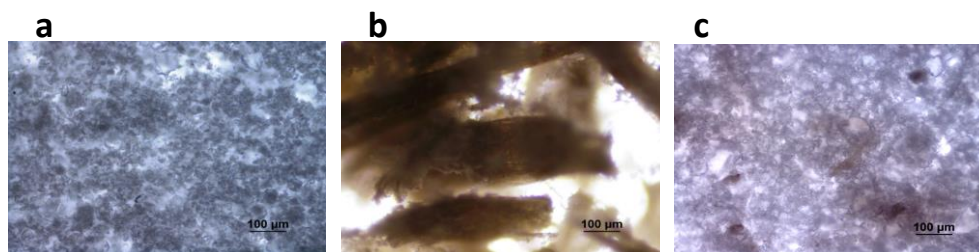


Figure 100. Photographs obtained by light microscope of: (a) C_{18} sorbent ground for 5 min, (b) a hair sample, and (c) the blend obtained after grinding the sample and the C_{18} dispersant for 5 min. Ratio sample to dispersant, 1:16.

B) Washing solvent

Next, different conditions were evaluated for washing the cartridges in order to eliminate matrix components. Spiked hair samples were ground under the optimized MSPD conditions, and after transferring the obtained blends to the extraction tubes, clean-up was effected by flushing through them a portion of a washing solvent. Water and 0.05 M carbonate buffer of pH 10.5 were tested as

washing solvents; acidic solvents were not used in order to prevent losses of the amphetamines during the washing step due to their protonation (Herráez-Hernández, R. et al., 1997). After washing, the blends were dried with air, and acetonitrile was passed through the SPE tubes in order to desorb the analytes. In this study the volume of acetonitrile used for desorption of the analytes was 2 mL (the desorption volume optimization is described below). The extracts were collected into glass vials and then, 250 μL aliquots were derivatized in solution as described in Section 3.5.3. In Figure 101 are shown the chromatograms obtained for a spiked hair sample when flushing the sample disperser blend with 2 mL of water (Figure 101a) and 2 mL of carbonate buffer (Figure 101b). The background peaks observed in the chromatograms were quite similar but higher analytical responses were achieved for the analytes when using carbonate buffer as washing solvent. This indicates that with water the retention of the analytes was lower because they were partially protonated (pK_a values of 9.8–10.3), which is consistent with previous results (Herráez-Hernández, R. et al., 1996b). It should be noted that the background chromatograms observed for hair samples after MSPD were similar to those obtained for hair treated by UAE (Figure 98d). On the other hand, when increasing the volume of buffer up to 4 mL the peak areas of the analytes remained constant within experimental variations (Figure 101c). Therefore, flushing the tubes with 2 mL of carbonate buffer was selected as the best option for clean-up.

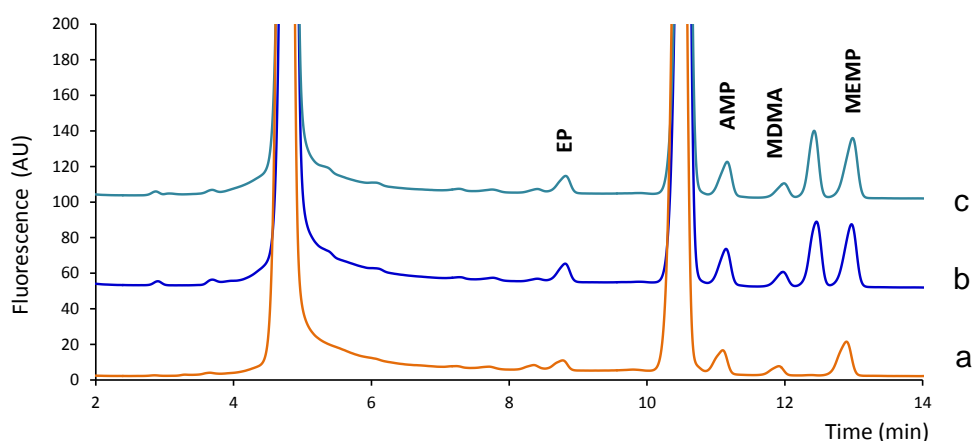


Figure 101. Chromatograms for hair samples spiked with the analytes (25 ng mg^{-1}) treated by MSPD/solution derivatization method using in the washing step: (a) 2 mL of water, (b) 2 mL of carbonate buffer, and (c) 4.0 mL of carbonate buffer as washing solvents.

C) Desorption

Indeed, the volume of solvent used for desorption of the analyte should be as low as possible in order to avoid an excessive dilution of the analytes in the final extracts. In order to optimize the volume of acetonitrile for desorption, aliquots of 1 mL of this solvent were passed through the extraction tubes after the washing and drying steps, and collected separately into 2 mL glass vials. Then, 250 μ L of the extracts was subjected to the solution derivatization method. All the tested amphetamines were mostly found in the first 1 mL fraction of acetonitrile, but significant portions of the drugs were also found in the second 1 mL fraction. In further experiments it was observed that highest responses for the analytes were obtained when flushing through the tubes 1.5 mL of acetonitrile. Consequently, this was the volume selected in the optimized procedure. Samples spiked with different amounts of the analytes were processed under the optimized MSPD/solution derivatization method. The concentrations assayed and analytical parameters obtained are listed in *Table 40*.

Integrated MSPD/solid phase derivatization

The possibility of effecting the derivatization of the analytes inside the cartridge was evaluated. According to the basis of solid support reactions, the pH conditions necessary for the reactions to take place can be achieved by flushing through the tubes an aliquot of buffer before adding the reagent solution. When the same buffer solution can be used for clean-up and derivatization (as in the present case), the entire procedure can be simplified because after the washing step, the derivatization and desorption of the analytes can be carried out simply by flushing an aliquot of the reagent through the SPE tubes, provided that the reagent solution is prepared in a high elution strength solvent (acetonitrile in the present instance). The experimental parameters affecting the solid support assisted derivatization were optimized. In this study spiked hair samples were subjected to optimized MSPD procedure, and the resulting blends were transferred to the extraction tubes and then derivatized. The parameters tested were the reaction time, the pH of the carbonate buffer and the concentration of FMOC in the derivatization solution. The results are depicted in *Figure 102*. According to this figure, the optimum reaction time and pH were 5 min and 10.5 (*Figure 102A and B*), respectively, which were also the optimum values found for

the analysis of amphetamines in other matrices (Herráez-Hernández, R. et al., 2001). It has to be remarked that, unlike the derivatizations in solution, the employment of 1 mM FMOC was unsuitable because the presence of intense peaks corresponding to the excess of reagent disturbed the measurement of the AMP-FMOC peak areas. Therefore, lower concentrations of FMOC (0.1 mM and 0.01 mM) were assayed. Best results were obtained by flushing the tubes with 1.5 mL of 0.1 mM FMOC (Figure 102C). On the basis of the results of the above sections and also the results of Figure 101, the conditions finally selected for the estimation of amphetamines in hair samples were: 25 mg of conditioned hair was mixed with 400 mg of C₁₈ sorbent and ground for 5 min; the mixture was then transferred to an extraction tube, 2 mL of carbonate buffer (pH = 10.5) was flushed through the tube and, after drying with air, the tube were flushed with 1.5 mL of 0.1 mM FMOC solution (in acetonitrile). After 5 min, the collected extracts were injected into the chromatograph.

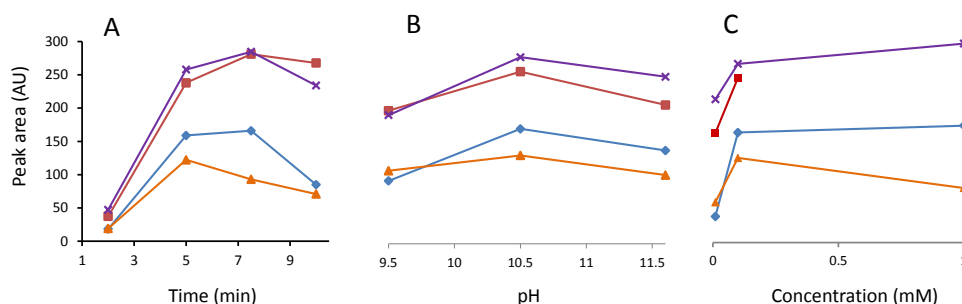


Figure 102. Effect of the derivatization conditions on the analyte responses obtained with the integrated MSPD/solid support derivatization method: (a) reaction time, (b) pH of the buffer, and (c) concentration of the FMOC solution. Tested for a sample containing 20 ng mg⁻¹ of each analyte.

Under these conditions, the chromatographic profiles were similar to those observed for the alkaline digestion and MSPD/solution derivatization methods, but significantly higher signals were registered for amphetamine-FMOC peak. Therefore, the proposed method could be applied to measure lower concentrations of the analytes. This is illustrated in Figure 103, which shows the chromatograms obtained for spiked hair samples treated by the three methodologies tested. The proposed integrated MSPD/solid phase derivatization

method was applied to samples spiked with 2–20 ng mg⁻¹ of the analytes. As illustrative examples, in *Figure 104* are shown the chromatograms obtained for blank hair (*Figure 104a*), and hair spiked with the analytes at different concentration levels within the tested range (*Figure 104b-d*). Although different peaks corresponding to matrix compounds were observed in the elution zone of the AMP-FMOC derivative, peak areas could be satisfactorily measured. The linearity, recovery and LODs parameters are listed in *Table 40*. Accuracy and precision studies were carried out at three different concentration levels. The results obtained are summarized in *Table 41*.

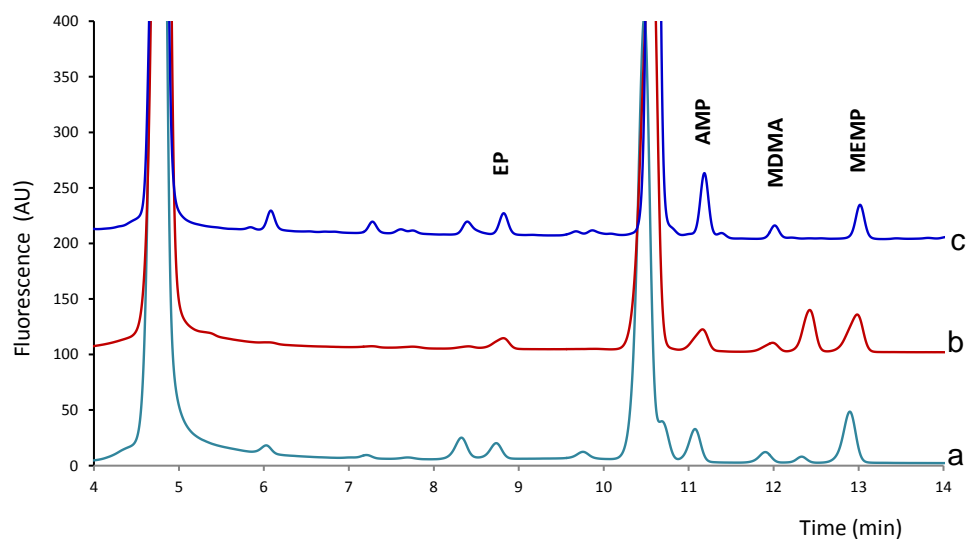


Figure 103. Chromatograms obtained by the three approaches tested: (a) hair sample spiked with 100 ng mg⁻¹ of each analyte treated by the UAE alkaline digestion/solution derivatization method, (b) hair sample spiked with 25 ng mg⁻¹ of each analyte treated by the MSPD/solution derivatization method, and (c) hair sample spiked with 10 ng mg⁻¹ of each analyte treated by the integrated MSPD/solid phase derivatization method.

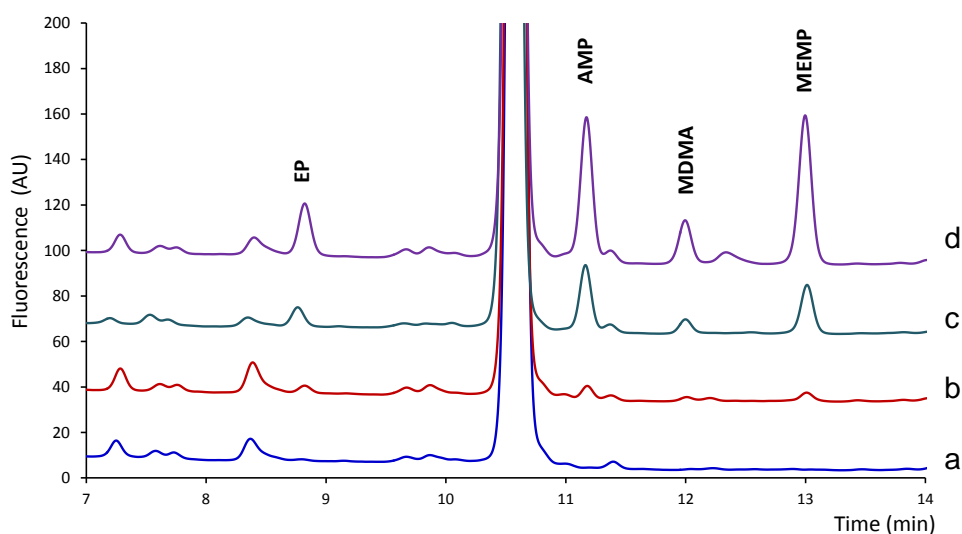


Figure 104. Chromatograms obtained with the integrated MSPD/solid support derivatization method for: drug-free hair sample (a), and for hair samples spiked to contain the analytes at concentrations of (b) 2 ng mg^{-1} , (c) 10 ng mg^{-1} and (d) 20 ng mg^{-1} .

Reliability of the proposed method

The results of *Table 40* indicate that MSPD is a reliable alternative to alkaline digestion by UAE for sample treatment in the determination of amphetamines in hair. Even when combined with a classical solution derivatization approach, the sensitivity obtained by MSPD is improved with respect to that attainable by the alkaline digestion method. The sensitivity is further improved if MSPD is combined with solid phase derivatization. The concentrations that can be detected and measured are about one order of magnitude lower than those that can be measured with the alkaline digestion-based procedure. This can be explained by the fact that solid phase derivatization avoids the dilution of the analyte as desorption and derivatization are simultaneously effected; the addition of a buffer to set the pH for the derivatization is also avoided. On the other hand, the LODs and LOQs achieved with the MSPD/solid phase derivatization method are comparable to that reported by many of the procedures found in the literature (*Baciu, T. et al., 2015; Vogliardi, M. et al., 2015*) but the proposed approach is generally simpler and more rapid. The LODs reported in a majority of the methods range from 0.05 to 0.5 ng mg^{-1} , although values lower than 1 pg mg^{-1} were reported using a microfluidic device (*Zhu, K.Y. et al., 2012*); it has to be remarked

that most of those methods involve solvent evaporation operations to reconcentrate the analytes after their extraction from the hair matrix. The employment of a C₁₈ phase allows the simplification of the sample treatment because this phase can be used not only to disrupt effectively the sample but also to purify the target analytes as SPE-based procedures. In the present instance, the selectivity was adequate for LC analysis after derivatization with FMOC, and no additional clean-up was necessary, not even the employment of an extra sorbent layer in the SPE tubes. On the other hand, the recovery values indicate that the analytical responses were similar to those obtained for standard solutions of the amphetamines; the same behavior was previously observed for urine and plasma samples (*Campíns-Falcó, P. et al., 2009; Herráez-Hernández, R. et al., 1996*). The proposed method also provides suitable accuracy and precision (*See Table 41*).

Table 41. Accuracy and precision of the proposed integrated MSPD/solid phase derivatization method.

Analyte	Added concentration (ng mg ⁻¹)	Intraday (n=3)		Interday (n=4)	
		Found concentration (ng mg ⁻¹)	RSD (%)	Found concentration (ng mg ⁻¹)	RSD (%)
EP	2.0	2.3 ± 0.4	17	2.4 ± 0.4	17
	10.0	9.6 ± 0.5	5	9.2 ± 0.9	10
	20.0	20.7 ± 0.8	4	21 ± 2	9
AMP	2.0	1.9 ± 0.2	11	2.2 ± 0.2	9
	10.0	10.20 ± 0.16	2	10.5 ± 0.7	7
	20.0	20.1 ± 0.8	4	22 ± 2	9
MDMA	2.0	2.4 ± 0.5	20	1.9 ± 0.3	17
	10.0	10.7 ± 0.9	8	10.9 ± 0.8	7
	20.0	21 ± 1	5	21.0 ± 1.2	6
MAMP	2.0	2.3 ± 0.3	13	2.4 ± 0.3	13
	10.0	9.4 ± 0.5	5	9.8 ± 0.7	7
	20.0	20.1 ± 0.5	3	20.8 ± 1.1	5

The concentration of the analytes in hair of drug abusers reported in the literature are typically in the 0.5–10.0 ng mg⁻¹ range (*Chang, Y.J. et al., 2014; Taberner, M.J. et al., 2009; Zhu, K.Y. et al., 2012*) although concentrations < 0.1 ng mg⁻¹ were reported by Wada et al. using alkaline digestion followed by the extraction of the analytes into n-heptane, evaporation to dryness and

derivatization of the analytes for their separation by LC with chemiluminescence detection (Wada, M *et al.*, 2013). Concentrations up to 68.9 ng mg⁻¹ have been reported for MAMP (Miyaguchi, H. and Inoue, H., 2011). Therefore, the sensitivity attainable with the proposed method can be considered suitable for the analysis of abusers' hair. The proposed method was tested for hair of different volunteers which had not consumed amphetamine (including dyed hair), as well as for a sample obtained from an abuser, and no interfering peaks in the elution zone of the analyte-FMOC derivative were observed in the chromatograms. On the other hand, for some of the samples assayed (including the abuser's hair) the solvents collected during the sample preconditioning were analyzed. The resulting chromatograms confirmed the absence of the analytes in the washing solvents. In *Figure 105* is shown the chromatogram of a real hair sample obtained from an abuser. The concordance between the retention times of the sample peaks and those of spiked hair samples (*Figure 105A*) indicates the presence of MAMP (at a concentration < LOQ). This is consistent with the chromatogram obtained after fortifying the real sample with the analytes (*Figure 105B*). Nevertheless, for confirmative tests LC-MS/MS would be required. The sample sorbent blend resulting after the extraction/derivatization of this sample was transferred to clean a glass mortar and the analytical procedure was repeated, but none of the analytes were detected, which is in agreement with the recovery values of *Table 40*.

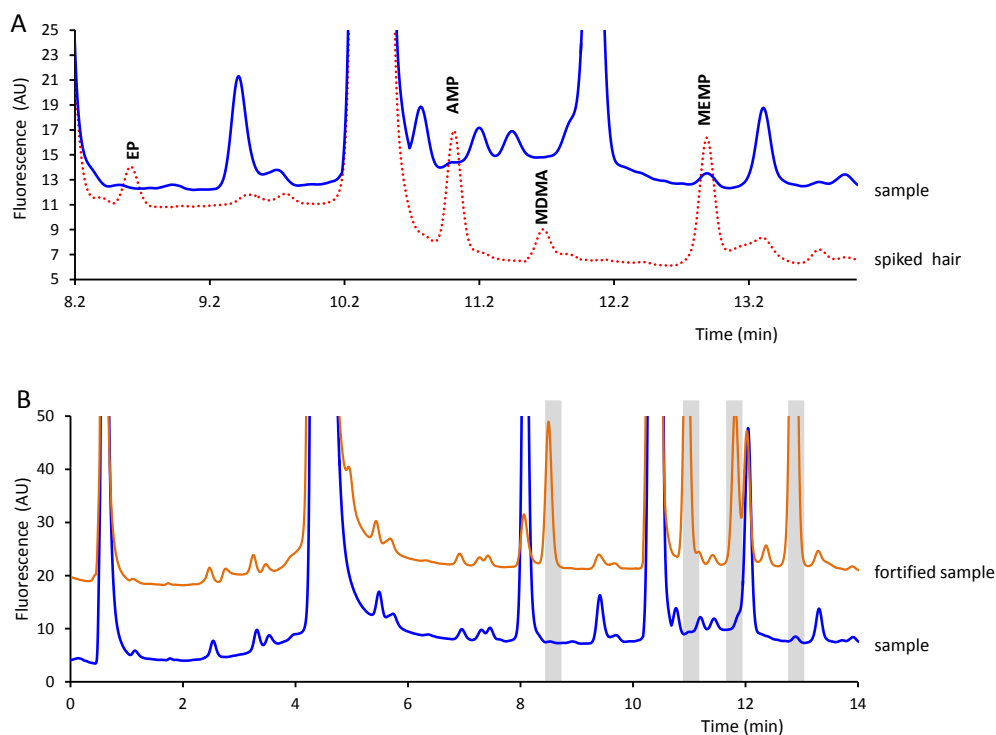


Figure 105. Chromatograms obtained for: (A) a real hair sample positive for MAMP and for a blank hair sample spiked with 2 ng mg^{-1} of each analyte, and (B) the real hair sample and the same sample fortified with 20 ng mg^{-1} of each analyte; the dark zones in (b) indicate the elution windows for the target compounds.

Conclusions

In this work, it has been illustrated the potential of combining MSPD and solid phase derivatization for the analysis of amphetamine and related compounds in hair samples. A C_{18} sorbent can be used for the effective disruption of the sample and retention of the analytes. In such a way, clean-up can be effected using a conventional SPE scheme once the MSPD blend has been transferred to the extraction tube. Clean-up conditions have been selected to facilitate the subsequent solid phase derivatization of the target compound. Therefore, the method integrates sample disruption, clean-up and derivatization, resulting in a very simple and rapid procedure. Under the proposed conditions, the entire procedure (grinding, transfer of the blend to the extraction tubes, clean-up and derivatization) can be completed in less than 15 min. This is a clear

advantage as many of the procedures reported in the literature involve much longer times for sample preparation (*Baciu, T. et al., 2015 and Vogliardi, S. et al., 2015*). In addition, no solvent evaporation or additional clean-up is required, and the consumption of materials and reagents is lead to a minimum. Therefore, the proposed methodology is in accordance with the principles of green chemistry. To our knowledge, this is the first method that combines MSPD and solid phase derivatization.

4.1.4 Mesoporous silica as sensing layer for MEMS

4.1.4.1 Screen-printed piezoelectric resonant transducers coated with MCF silica for gas detection

Optimization of screen-printing fabrication

A) Study of LBCu composition

Two formulas of piezoelectric inks with different LBCu composition were tested (*Table 42*) in order to study their effect on the sintering and electromechanical properties for gas testing.

Table 42. Weight percentages and mass of each component in 40 g of piezoelectric powder.

Materials	Suppliers	Particle size (μm)	Mass (g) (40 g of total mass)		Weight %	
			Formula ^A	Formula ^B	Formula ^A	Formula ^B
PZT	Ferroperm	11.473	38.8000	38.800	97.0000	97.0000
Li ₂ O ₃	Alfar Aesar	19.541	0.3000	0.1063	0.7500	0.2657
Bi ₂ O ₃	Alfar Aesar	3.176	0.4800	0.6703	1.2000	1.6785
CuO	Sigma Aldrich	3.662	0.4200	0.4234	1.0500	1.0585

^A *Debéda, H. et al., 2013.*

^B *Medesi, A. et al., 2014.*

B) Study of size and shape of sensor

Two types of sensors were fabricated, disks and cantilevers. For both sensors, the sacrificial layer paste used in previous works (*Debéda, H. et al., 2013; Debéda, H. and Lucat, C., 2014*) was a mixture of 60 w% epoxy CV59 and 40w% SrCO₃, which required a dissolution step by ultrasonic bath with H₃PO₄ 1 M. To avoid this tedious step, the conventional sacrificial layer has been replaced by a commercial sacrificial paste, which is satisfactory removed during the firing process.

For disks, smaller sizes than previous disks developed by PRIMS group (IMS Laboratoire, Bordeaux University) (Debéda, H. and Lucat, C., 2014) were fabricated to solve cracking problems of PZT layer due to the bottom electrode. Figure 106 shows the new size and shape of disk sensors. Moreover, the number of gold bottom layers was increased from 1 to 2.

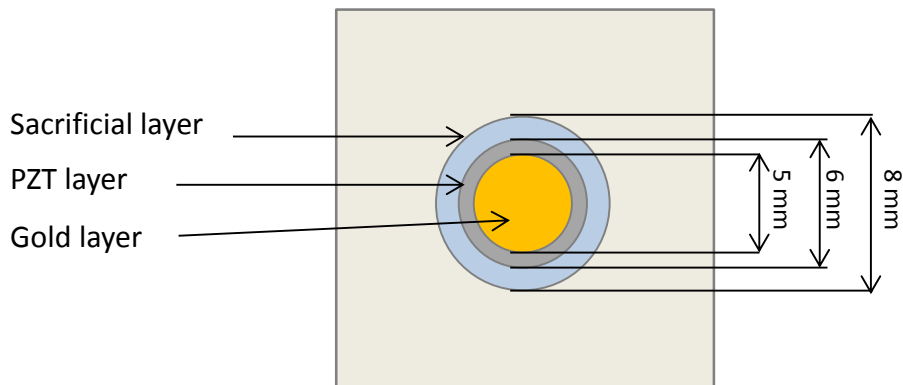


Figure 106. Design of disk fabricated in this work.

The different fabrication steps for disks are given in Figure 107. Two sacrificial layers (circular shape of 8 mm of diameter) were first screen-printed on an aluminum nitride substrate and polymerized 20 and 30 min, for the first and second layer respectively, at 120 °C. Secondly, two bottom gold electrode layers (5 mm diameter) were deposited on the sacrificial layer and dried 15 min each layer at 120 °C. Then, PZT layer (6 mm diameter) was printed and dried at 1 °C min⁻¹ to 120 °C before its maintaining 30 min. Finally, top gold electrode layer was deposited on (5 mm diameter) and dried 15 min at 120 °C. Once all the layers were deposited and dried, the samples were isostatically pressed to improve densification, then co-fired to remove sacrificial layer and sintering and finally, poled (50 KV cm⁻¹, 280 °C) as before described.

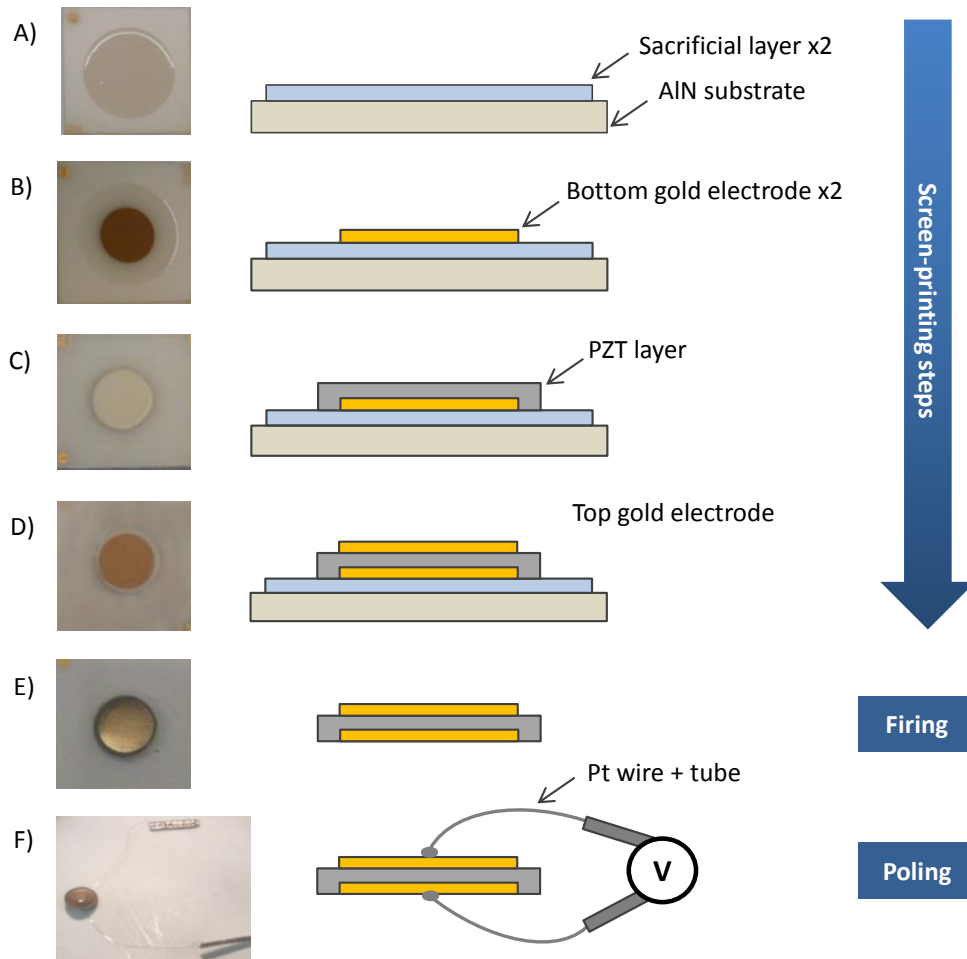


Figure 107. Fabrication steps of disk A) screen-printing of sacrificial layer, B) screen-printing of bottom gold electrode, C) Screen-printing of PZT layer, D) Screen-printing of top gold electrode E) Sacrificial layer elimination after firing, F) Poling of PZT wired disk (cross view), together with photographies of the top view of the disk step by step.

As microscopic images shown, satisfactory samples without bubbles were obtained before firing (Figure 108A). After firing, no significant defects were observed (Figure 108B) although the alignment was then improved to get symmetric geometry (Figure 108C and D). The cracking of the PZT was avoided and also the disks were not stuck on the substrate. Similar disks were observed by light microscope for two LBCu formulas.

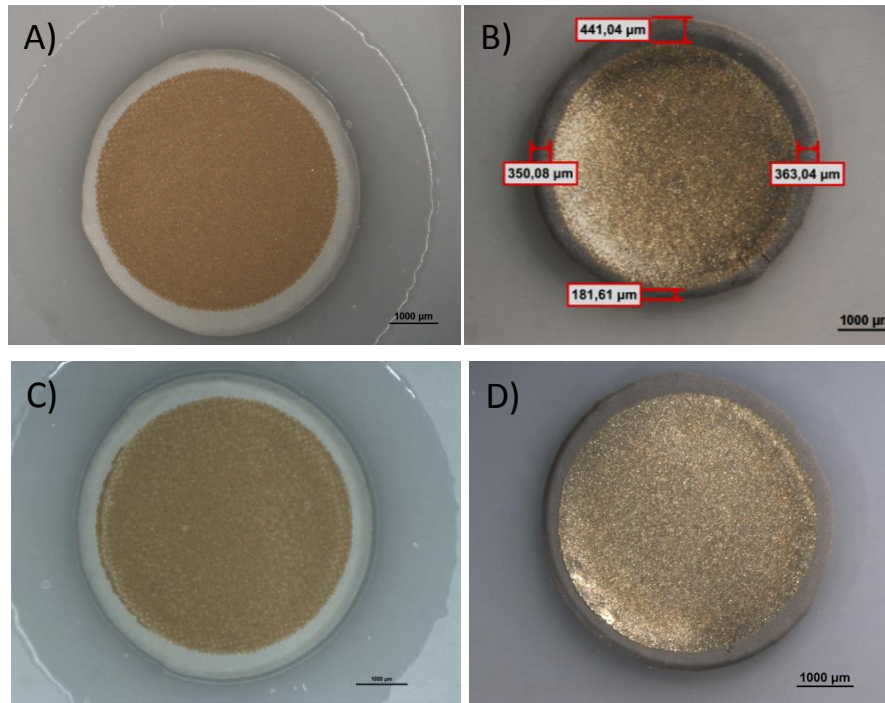


Figure 108. Microscopic images at $\times 6$ of top view of disk before (A) and after firing (B), aligned disk before (C) and after firing (D). Disks fabricated with formula reported in (Debéda, H. et al., 2013).

The same process was carried out for fabricating cantilevers. Firstly, anchor pad based on PZT or glass-ceramic ink was deposited on the substrate (alumina or AlN) and dried at $1\text{ }^{\circ}\text{C min}^{-1}$ to $120\text{ }^{\circ}\text{C}$ maintaining 30 min for PZT or 20 min at $120\text{ }^{\circ}\text{C}$ for glass-ceramic. Secondly, sacrificial layers (two or three) were deposited on the substrate and polymerized 20 and 30 min, for the first and second-third layer respectively, at $120\text{ }^{\circ}\text{C}$. Next, two bottom gold electrode were printed on the sacrificial layer and dried 15 min each layer at $120\text{ }^{\circ}\text{C}$. Then, PZT cantilever was printed and dried at $1\text{ }^{\circ}\text{C min}^{-1}$ to $120\text{ }^{\circ}\text{C}$ before its maintaining 30 min. Finally, top gold electrode was printed and dried 15 min at $120\text{ }^{\circ}\text{C}$. *Figure 109* shows the steps of the fabrication of cantilevers by screen-printing technique with the sacrificial layer method. Once all the layers were deposited and dried, the samples were isostatically pressed, then co-fired and finally, poled as described in *Methodology Chapter*.

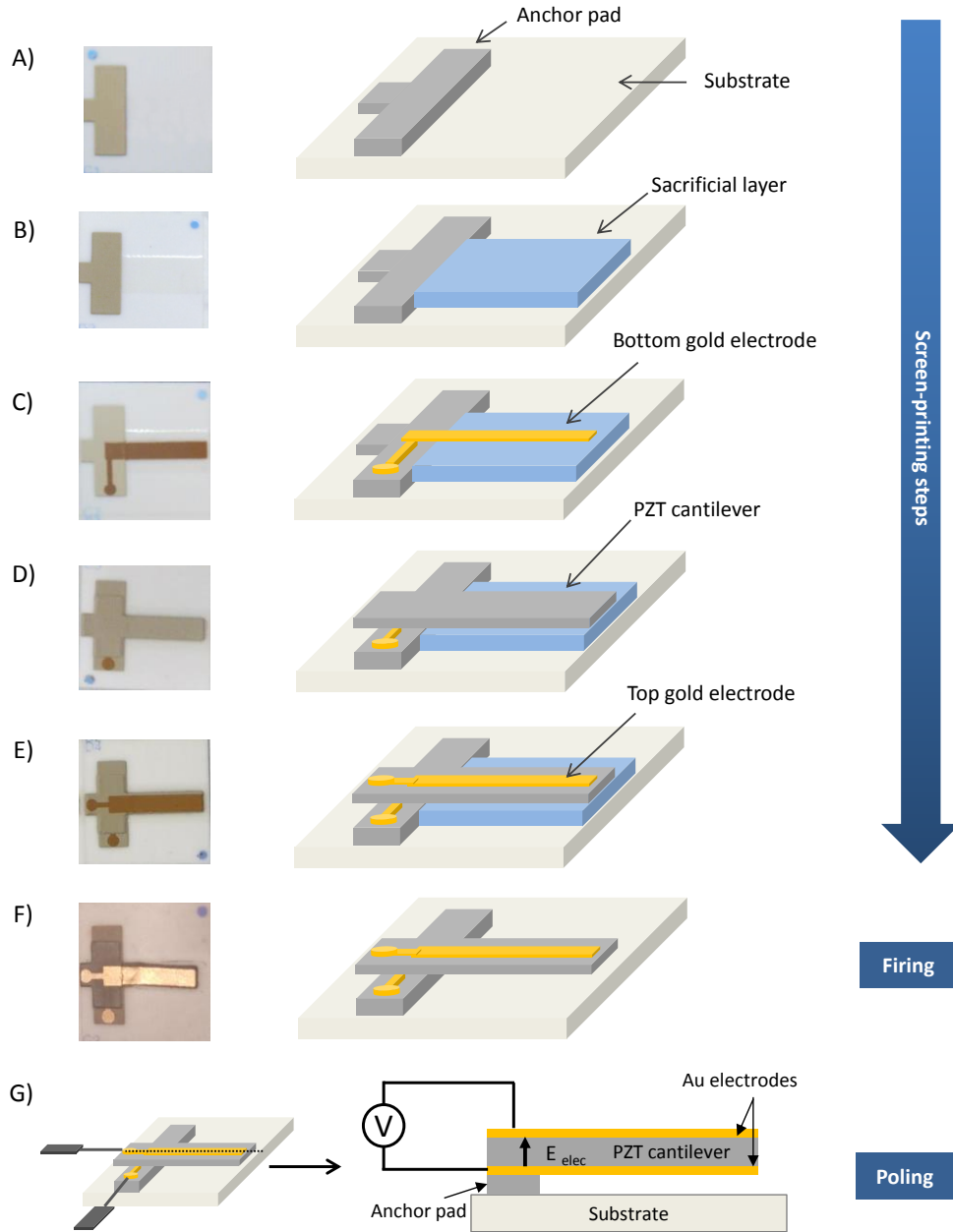


Figure 109. Real photographs and scheme of the top view of fabrication steps of the cantilevers A) Screen-printing of anchor pad B) Screen-printing of the sacrificial layer C) Screen-printing of the bottom gold electrode D) Screen-printing of the cantilever E) Screen printing of the top gold electrode, F) Sacrificial layer elimination after firing G) Poling of wired cantilever with the cross view.

For the cantilevers, a new design was printed in order to avoid the cracking problems of the design of previous works (Clément, P. et al., 2016; Debéda, H. and Lucat, C., 2014). In this new design, the anchor was extended and the width and length of gold layers were increased in order to achieve the location of top gold layer on anchor avoiding its cracking at junction between anchor and substrate (Figure 110A). These cantilevers were printed on Al_2O_3 due to the good adhesion of inks on it. Before firing, cracks were not observed (Figure 110B). After firing, the cracking problem of the top gold layer between anchor and substrate of previous designs was solved thank to the new design. Nevertheless, sensors (two LBCu formulas studied) cracked at junction of cantilever and anchor after firing as can be seen in the microscope picture in Figure 110C.

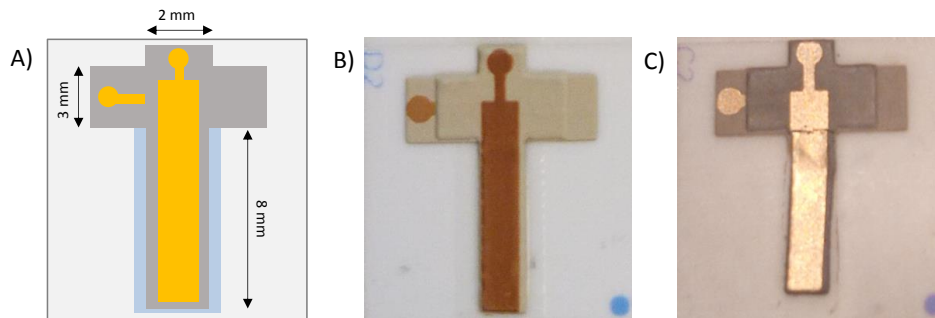


Figure 110. A) Design of the cantilever, B) Photography of cantilever before firing and C) Photography of cantilever after firing, fabricated on Al_2O_3 substrate.

In order to avoid the crack at junction, different substrate types (Al_2O_3 and AlN), anchor material (glass-ceramic and PZT) and printing parameters (print gap and print pressure) were tested. Firstly, cantilevers printed on Al_2O_3 and AlN were tested in order to check the sticking of the free-standing PZT on the substrate. For this purpose, different materials for printing anchor pad were required depending on the substrate to get good adhesion. Thus, PZT and glass-ceramic material were required to print anchor on Al_2O_3 and AlN substrate, respectively. Furthermore, the anchor layer should be at the same level than sacrificial layer without gap between them to avoid the cracking at junction. Table 43 summaries the thickness of layers measured by the profilometer.

Table 43. Thickness measurements of anchor and sacrificial layers for cantilever fabrication. On average of 200 μm was employed for each measurement by the profilometer.

Substrate	Layer	Print gap (mm)	Print pressure (kg)	Thickness (μm)
Al_2O_3	Sacrificial (x2)	0.7	4	45.2 ± 1.4
Al_2O_3	PZT	0.7	4	44.0 ± 1.7
Al_2O_3	PZT	0.3	4	47.8 ± 1.2
AlN	Sacrificial (x2)	0.7	4	43.7 ± 1.2
AlN	Green (x1)	0.7	4	38.2 ± 0.2
AlN	Green (x2)	0.7	4	61.1 ± 0.7
AlN	Green (x2)	0.7	5	49.2 ± 0.9
AlN	Green (x1)	0.7	6	25.3 ± 0.4
AlN	Green (x2)	0.7	6	47.5 ± 1.5

For PZT anchor on Al_2O_3 , 0.3-0.7 mm of print gap (distance between mesh and substrate) were tested. However, no significant differences of thickness were obtained varying this parameter. Print gap of 0.3 mm was selected due to smoother surface of anchor (*Figure 111A*). In addition, the gap between anchor and sacrificial layer was also an important effect to check. As can be seen in *Figure 111B*, a gap around 130 μm was obtained when sacrificial layer is firstly printed. Thus, the anchor should be printed before in order to obtain an overlap. For the glass-ceramic anchor, different print pressures were tested. The thickness of one layer of glass-ceramic anchor was lower than two sacrificial layers, thus two layers of anchor were required. However, the thickness of two layers was excessive and so, an increase of pressure printing of 6 kg was required to decrease the thickness in order to obtain a satisfactory alignment between anchor and sacrificial layers.

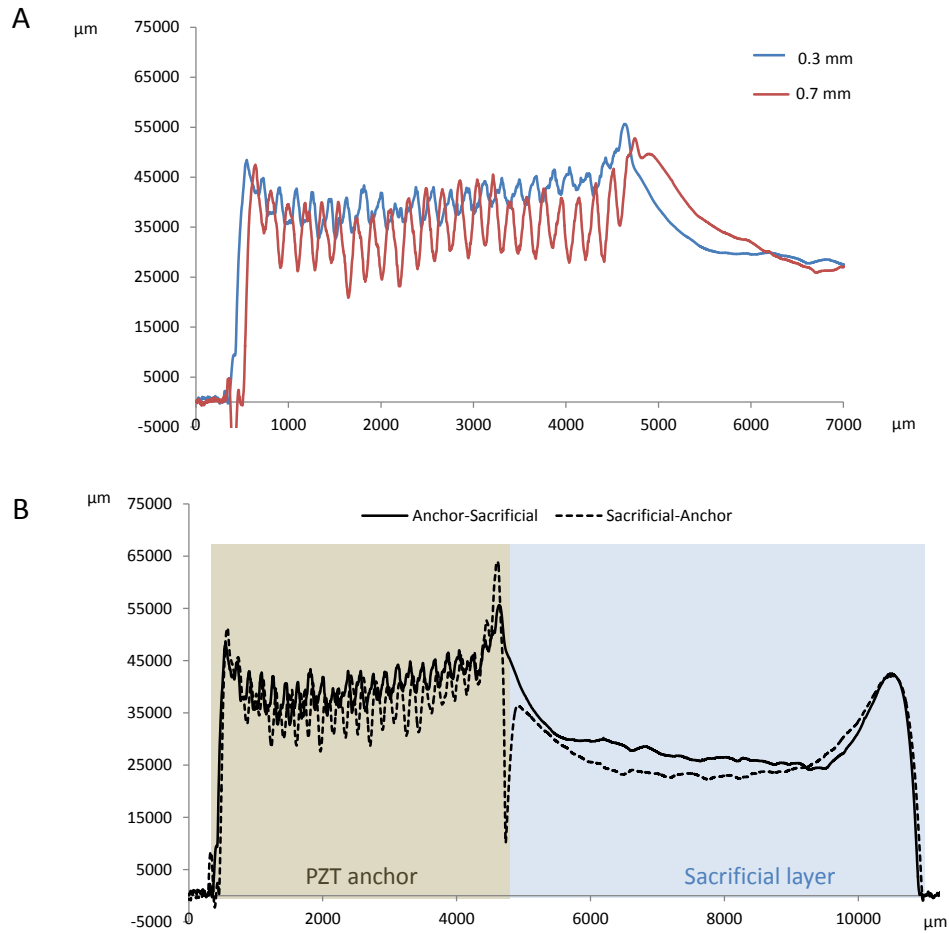


Figure 111. Pictures of thickness profile before firing of A) PZT anchor-Sacrificial layers on Al₂O₃ with different print gap of anchor, B) Different print order of anchor and sacrificial layer.

Once the printing parameters were optimized, cantilevers were printed under selected conditions and were observed by microscope. Before firing, the first layer of bottom gold electrode was broken (Figure 112A and B) but the second was not broken (Figure 112C and D), and so, the sensors were fired.

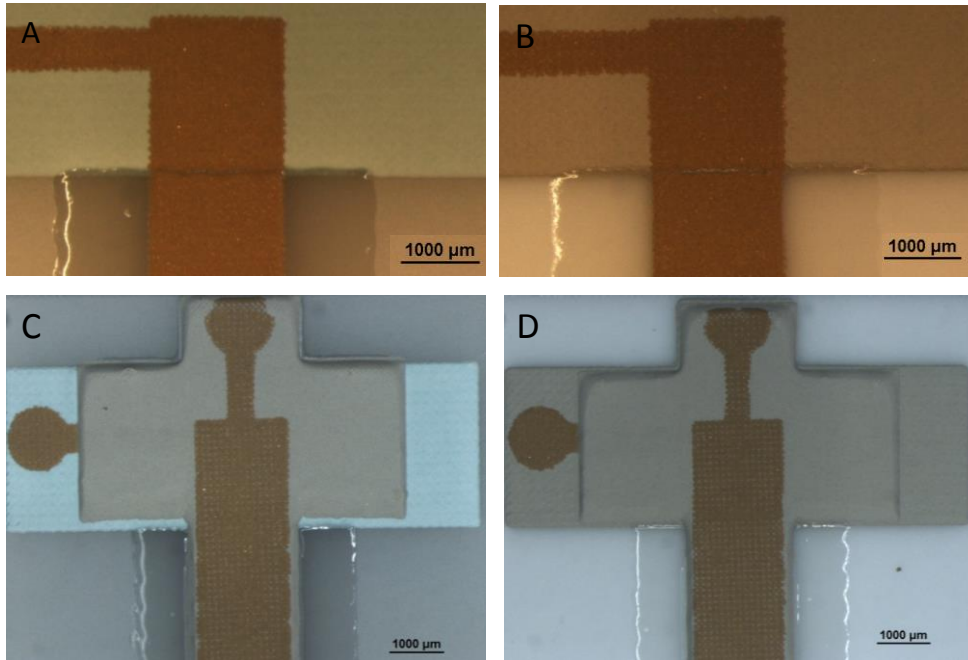


Figure 112. Microscopic images of A,B) first layer of bottom gold electrode, C,D) cantilevers before firing. Left: glass-ceramic anchor on AlN, Right: PZT anchor on Al₂O₃.

The crack at junction between anchor and sacrificial was observed after firing in both cases. For the Al₂O₃ substrate (*Figure 113A*), the breakage of the cantilevers is maybe due to two effects: (i) the PZT anchor pad has a good adhesion on Al₂O₃, thus it sinters but slight shrinks after firing and (ii) the free-standing PZT layer has good adhesion on Al₂O₃ especially if the sacrificial layer is thin. From *Figure 113B*, lower breakage of cantilever was observed maybe due to the bad adhesion of free-standing PZT on AlN. From these limitations, a possible solution could be proposed such as the use of milled PZT to change the particle size, which affects the sintering and, therefore the addition.

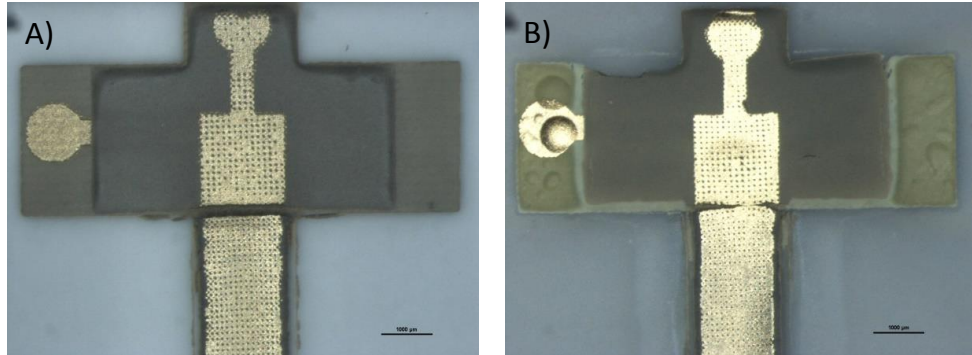


Figure 113. Microscopic pictures of cantilevers after firing on Al_2O_3 (A) and AlN (B).

Physico-chemical characterization

A 3D profile analysis was carried out with the profilometer Alpha-Step IQ Surface Profiler before densification step. *Figure 114A* shows a homogeneous deposition of each consecutive screen printed layer for two formulas of disks. The topographic measurements demonstrate that the thicknesses of the disks were approximately 100 ± 2 and 118 ± 6 μm, for formula A and B respectively. For cantilevers, the thickness of 114 ± 4 μm remains constant along its length and width as *Figure 114B* shown as example. Each sensor was measured at three different points.

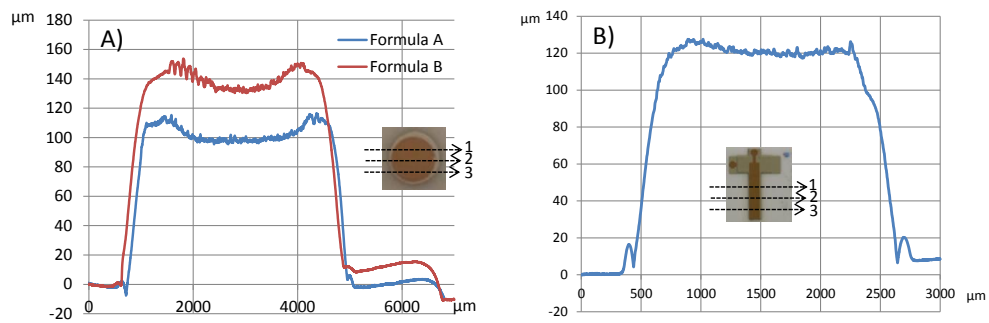


Figure 114. 3D profile analysis of the cross-section axis of A) Disks (two formulas) and B) Cantilever (first batch) with formula A (Debéda, H. et al., 2013), before firing.

Electro-mechanical characterization

Fired and poled sensors were afterwards characterized by using an impedance analyser. The analyzer was adjusted in one of the resonant frequencies of the material to extract different data allowing the evaluation of the inductive behavior of samples. Two formulas of disks were compared to commercial disks by the impedance analyser. *Figure 115* shows the curves of conductance (G), susceptance (B), impedance (Z) phase and $|Z|$ for the disks. As can be seen, the profile of disks with formula A (Debéda, H. et al., 2013) was similar to commercial disks.

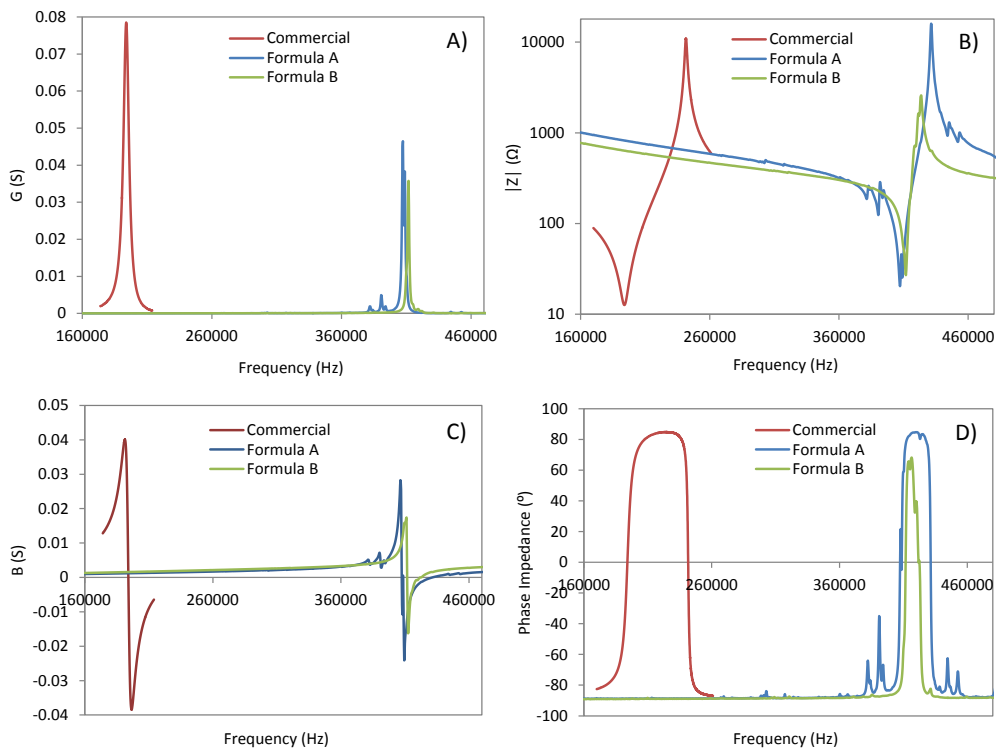


Figure 115. Graphic of A) Conductance, B) $|Z|$, C) Susceptance and D) Impedance phase measurements of disks fabricated with two formulas A (Debéda, H. et al., 2013) and B (Medesi, A. et al., 2014) and commercial disk.

From these measurements, figures of merit such as the mechanic quality factor (Q_m) and effective translation of electric to mechanical energy coefficient (K_{eff}) were calculated by the equations shown in *Figure 116*.

$$K_{eff} = \sqrt{\frac{f_M^2 - f_m^2}{f_M^2}}$$

$$Q_m = \frac{f_r}{\Delta f}$$

Figure 116. Equations used for the calculation of K_{eff} and Q_m , where f_m is the frequency at the minimum impedance (Z), f_M is the frequency at the maximum impedance, f_r is the resonance frequency at G maximum, $\Delta f = f_2 - f_1$ is the width of peak, where f_1 is the frequency at the maximum B and f_2 is the frequency at the minimum B .

Table 44 compares K_{eff} of disks fabricated and commercial disk. The disk with formula A (*Debéda, H. et al., 2013*) showed the best piezoelectric properties with a first resonance peak of in-plane radial mode $f_r \approx 407$ kHz, $K_{eff} \approx 33.5\%$ and $Q_m \approx 280$. The piezoelectric performance of the fabricated disks was lower than those of commercial disk due to poor sintering. Note that the shift to higher resonance frequencies of fabricated sensors is due to smaller size than the commercial disk.

Table 44. Comparison of K_{eff} .

Coefficient	Formula A disk	Formula B disk	Commercial disk
% K_{eff}	33.5	23.52	59.6

Gas test

A cantilever with different design was functionalized by MCF silica (*See 3.4.4 Section*). Uniform functionalization of the MCF silica was carried out to improve the surface reactivity. *Figure 117* shows a photography of the functionalized cantilever used for gas sensor application. The mesoporous silica deposited mass is estimated to be around 200 μg .

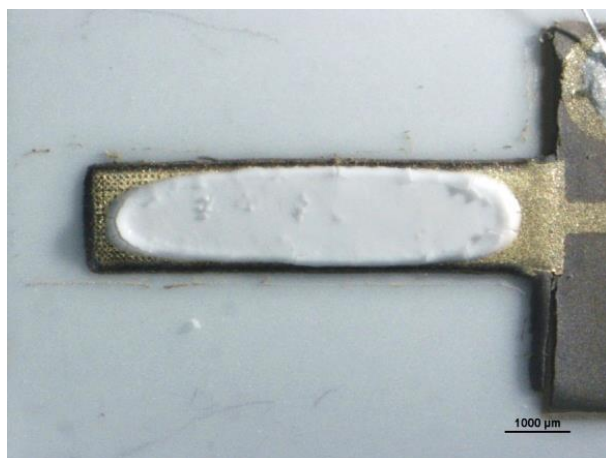


Figure 117. Microscopic photography of the functionalized cantilever by MCF mesoporous silica.

Furthermore, to estimate the sensing material loading, the conductance of the first 31-longitudinal mode of the cantilever is measured before and after sensing material deposition (*Figure 118A*). Due to mass change of the coating, a negative frequency shift (1638 Hz) was measured. This leads to a mass sensitivity for the cantilever of $8 \text{ Hz } \mu\text{g}^{-1}$. Q_m for cantilever before deposition of mesoporous silica was 222, while Q_m for cantilever after functionalization was 102 due to the mass increment of the coating.

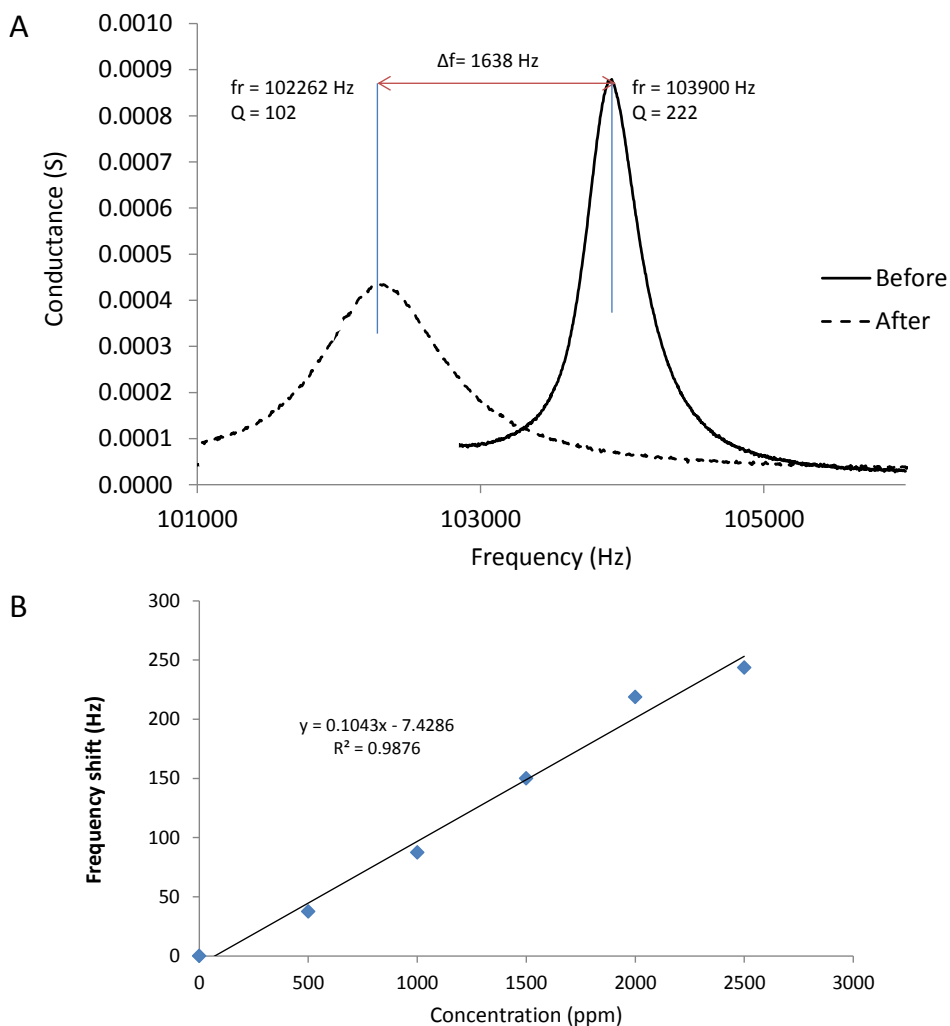


Figure 118. A) Spectrum of the conductance for the first longitudinal mode before and after deposition of MCF silica layer and B) Relative resonant frequency shifts as a function of humidity.

The functionalized cantilever was tested under humidity. Due to the porosity of the materials used, the humidity is a key factor to check. The cantilever was placed in a gas chamber where different concentrations of water were introduced (See Section 3.5.5). The performance of functionalized cantilever was evaluated under humidity using the 31-longitudinal vibration mode. Figure 118B shows the resonant frequency shifts due to mass change as function of the concentration of humidity. A low sensitivity of 0.1 Hz ppm^{-1} was measured for the humidity test,

indicating its potential application as gas sensor. Based on these preliminary studies, functionalized screen-printed piezoelectric cantilever with MCF silica is a promising sensor for the VOCs detection for environmental purposes.

Conclusions

A new design of miniaturized disk has been successfully fabricated by using an alternative material for sacrificial layer which is removed during the firing step. The effect of LBCu composition on the electromechanical behaviour has been studied. The disks with a composition of 0.75% Li_2O_3 , 1.2% Bi_2O_3 and 1.05% CuO have achieved similar electro-mechanical properties to commercial disks ($K_{\text{eff}} \approx 33.5\%$). The new design of the cantilevers has given rise to fabrication problems and printing parameters modification has not been solved them. Due to the specific area of MCF mesoporous silica to detect VOCs, this material has been drop-coated on the top gold electrode of screen-printed PZT cantilever as sensitive layer. The functionalized cantilever has been tested under humidity and the low sensitivity (0.1 Hz ppm^{-1}) obtained suggests the potential applicability of this MCF functionalized cantilever as portable VOCs sensor for environmental purposes.

4.2 C-BASED MATERIAL

4.2.1 Application of CNTs modified coatings for the determination of amphetamines by IT-SPME-CapLC

The potential utility of CNTs as an extractive phase has been evaluated in order to extend the IT-SPME methodology to drug analysis in oral fluid. Different PDMS-based extractive capillaries both unmodified and modified with CNTs (MWCNTs and SWCNTs) have been compared. AMP, MAMP and EP have been selected as model compounds because they are among the most frequently detected drugs in oral fluid from drivers. According to the results obtained in previous studies, in the present section the fluorogenic reagent FMOC has been selected for derivatization of amphetamines in order to make them more amenable for chromatography and/or to enhance the sensitivity. The amphetamine derivatives formed have been processed by in-valve IT-SPME coupled on-line to CapLC-FLD.

Optimization of the IT-SPME and chromatographic conditions

Experiments were carried out in order to optimize conditions for transferring FMOC derivatives from the extractive capillary of the IT-SPME device to the analytical column, as well as for the subsequent chromatographic separation. In these studies, unmodified capillaries were used for IT-SPME. The mobile-phase was a mixture acetonitrile-water and flow-rate was $20 \mu\text{L min}^{-1}$. When in-valve IT-SPME is coupled on-line to CapLC, a compromise has to be reached between optimal conditions for the IT-SPME and for the chromatographic separation. In the present study, conditions were selected to achieve suitable separation of the three analytes of interest in the minimum time of analysis. Indeed, extending the proposed methodology to other amphetamine-like compounds would require different separation conditions (for example, a longer column).

Two mobile-phase compositions were tested, 50:50 and 70:30 acetonitrile:water (v/v). The results obtained demonstrated that both compositions were adequate to desorb the FMOC derivatives from the extractive capillary. However, best chromatographic separation was achieved by using a mixture acetonitrile:water 70:30 (v/v) (See *Figure 119*), which was the eluent composition selected for further work. The dead times observed in the

chromatograms were higher than those expected for a conventional capillary chromatographic separation due to the inclusion of the extractive device. It has to be noted that the EP derivative eluted on the tail of the FMOC peak; for this reason, peak areas for this analyte were calculated throughout the study by the tangent skimming integration method.

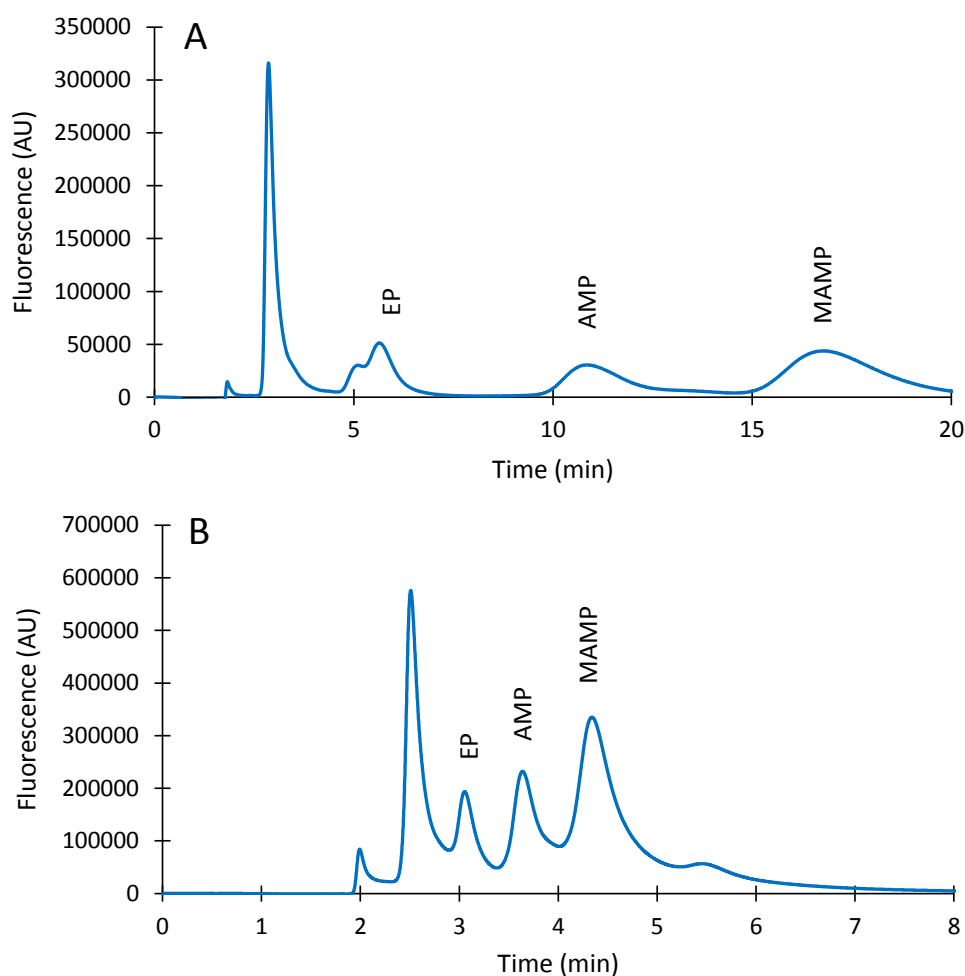


Figure 119. Chromatograms obtained for a standard solution containing AMP, MAMP and EP ($8 \mu\text{g mL}^{-1}$, each) using a percentage of acetonitrile in the mobile phase of: (A) 50 % and (B) 70 %, using an unmodified PDMS₆₅ extractive capillary (30 cm length) for IT-SPME.

On the other hand, the effect of the capillary length on the analytical responses (peak areas) was evaluated by processing solutions of the same

concentration of amphetamines with PDMS₆₅ capillaries of 30, 40 and 50 cm. In principle, an increment in the capillary length increases the surface area available for extraction, and thus, the amount of analyte extracted also increased. A slight increment on the analyte peak areas was observed when extending the capillary length from 30 cm to 40 cm. Unfortunately, the amount of unwanted products extracted also increases. In the present case, the chromatographic profile observed for an extractive capillary of 50-cm length was unsuitable due to the large amount of unreacted FMOc extracted and transferred to the analytical column (See Figure 120). Consequently, capillaries longer than 40 cm were considered for further assays.

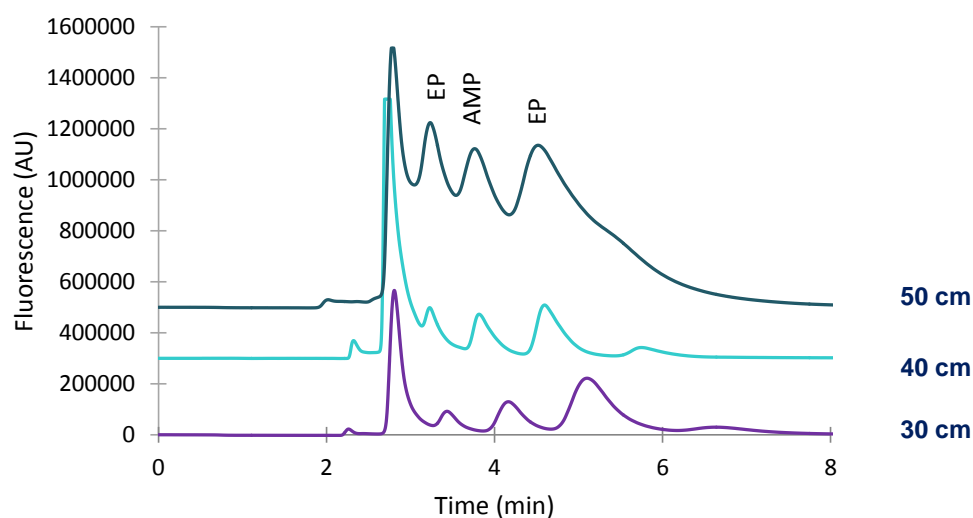


Figure 120. Chromatograms obtained for a standard solution containing AMP, MAMP and EP ($8 \mu\text{g mL}^{-1}$, each) with PDMS₆₅ extractive capillaries of different length.

Evaluation of the extraction efficiencies

The extraction efficiency was evaluated for unmodified PDMS₉₅ and PDMS₆₅ capillaries, as well as for PDMS₉₅ capillaries after their functionalization with c-SWCNTs, and PDMS₆₅ capillaries functionalized with c-SWCNTs or with c-MWCNTs. The length of PDMS₉₅ capillaries was 36 cm, whereas all PDMS₆₅ capillaries were 40 cm length. The mean peak areas obtained for the tested capillaries are depicted in Figure 121; it has to be mentioned that AMP and MAMP peak areas were calculated by a valey-to-valey integration approach.

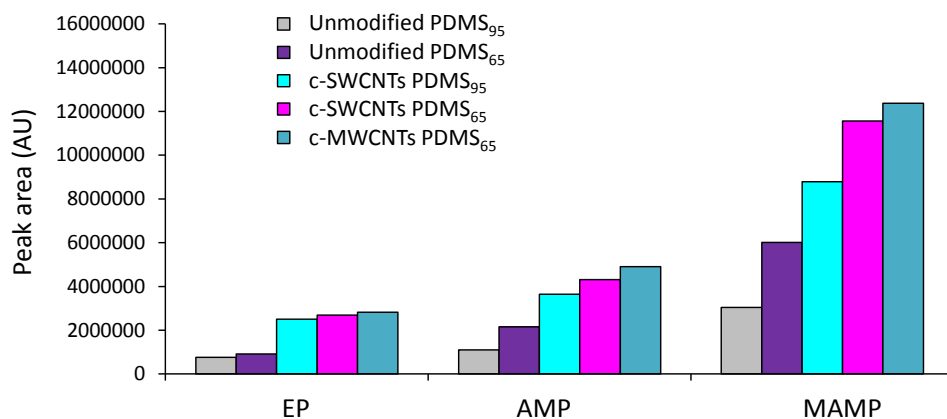


Figure 121. Peak areas obtained for a standard solution of the amphetamines tested ($8.0 \mu\text{g mL}^{-1}$, each) with different extractive capillaries: unmodified PDMS₉₅ (36 cm), unmodified PDMS₆₅ (40 cm), c-SWCNTs functionalized PDMS₉₅ (36 cm), c-SWCNTs functionalized PDMS₆₅ (40 cm) and c-MWCNTs functionalized PDMS₆₅ (40 cm).

In order to compare the extraction efficiencies, the preconcentration rates (established as the peak area ratios between two given capillaries) were also calculated (Jornet-Martínez, N. *et al.*, 2015b). The results are summarized in Table 45.

Table 45. Preconcentration rates (PRs) values found for the extractive capillaries tested.

Capillaries compared	PR		
	EP	AMP	MAMP
Unmodified PDMS ₆₅ /Unmodified PDMS ₉₅	1.2	2.0	2.0
c-SWCNT PDMS ₉₅ /Unmodified PDMS ₉₅	3.3	3.3	2.9
c-SWCNT PDMS ₆₅ /Unmodified PDMS ₆₅	2.9	2.2	1.9
c-SWCNT PDMS ₆₅ /c-SWCNTs PDMS ₉₅	1.1	1.2	1.3
c-MWCNT PDMS ₆₅ /c-SWCNTs PDMS ₆₅	1.0	1.1	1.1

First, the solutions containing the three amphetamines were assayed onto the two unmodified capillaries tested. Higher analytical responses for the three analytes were obtained with the PDMS₆₅ phase, as it can be seen in *Table 45*. It can be deduced that a higher percentage of diphenyl groups in the extractive phase lead to higher extraction rates. This suggests that the extraction involves π - π interactions with the FMOc derivatives, which is consistent with the fact that the extracted compounds possess three aromatic rings.

The effect of the presence of CNTs in the extractive coating was investigated for the PDMS₉₅ and PDMS₆₅ capillaries. In *Figure 122* are depicted the chromatograms obtained for an unmodified PDMS₉₅ capillary and the same capillary functionalized with c-SWCNTs. As observed, the presence of c-SWCNTs in the extractive phase affected not only the peak areas of the FMOc derivatives, but also their retention times. Higher retention times were observed with the c-SWCNTs coated phase, which indicates that the interaction between the extractive phase and the FMOc derivatives is stronger in the presence of CNTs, most probably by a π - π mechanism (*Jornet-Martínez, N. et al., 2015b*). This can also explain the higher peak areas observed with the c-SWCNTs functionalized coating; the analyte responses were about three times higher with the modified coating (See *Table 45*).

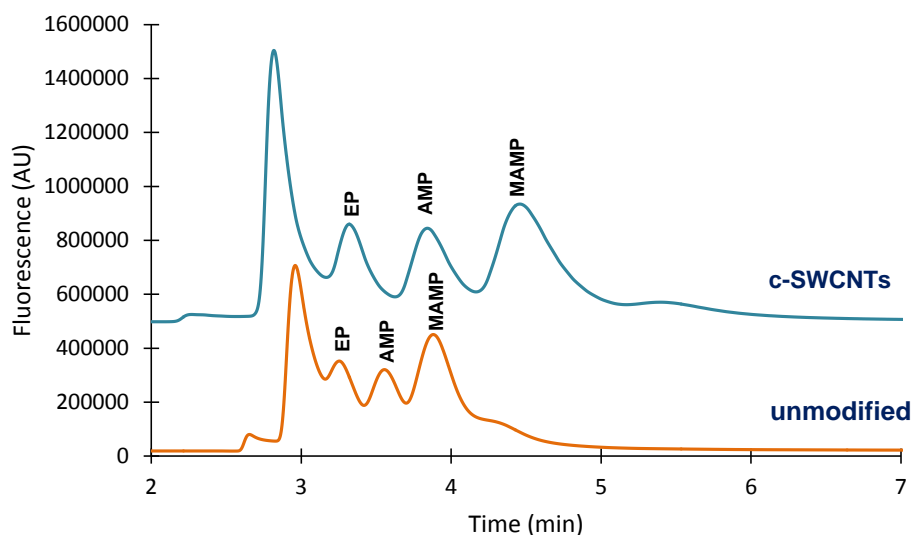


Figure 122. Chromatograms obtained for a standard solution of the amphetamines tested ($8 \mu\text{g mL}^{-1}$ each) with the unmodified PDMS₉₅ and the c-SWCNTs functionalized PDMS₉₅ capillaries.

Similar results were observed for the PDMS₆₅ capillaries. This is illustrated in *Figure 123*, which shows the chromatograms obtained for unmodified PDMS₆₅ capillary and the same capillary after the introduction of c-MWCNTs. However, the increment in the analytical signals was more moderate than with the PDMS₉₅ capillaries, especially increased in the presence of c-MWCNTs, chromatographic peaks are narrower. As a result, not only the sensitivity but also the resolution improved with the introduction of CNTs.

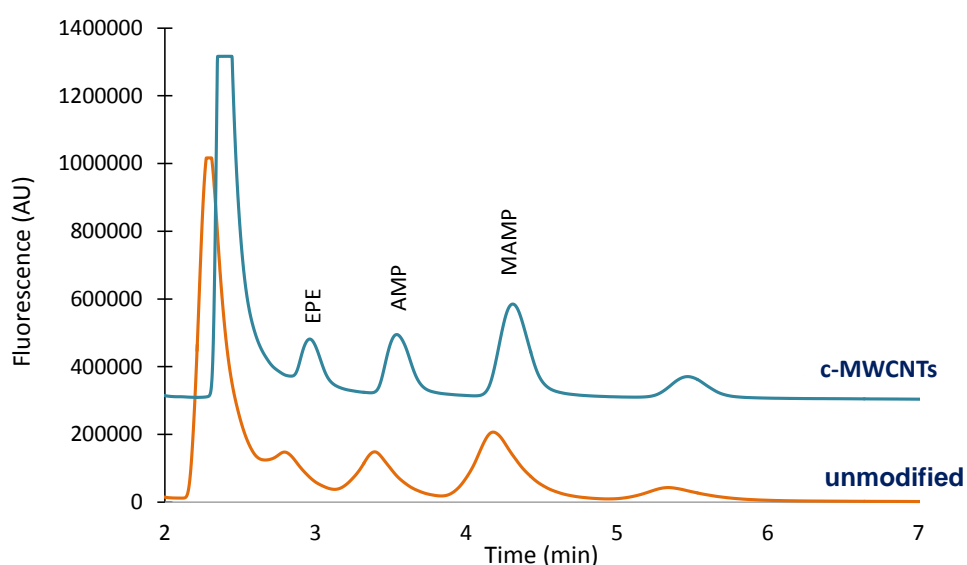


Figure 123. Chromatograms obtained for a standard solution of the amphetamines tested ($8 \mu\text{g mL}^{-1}$ each) with the unmodified PDMS₆₅ and the c-MWCNTs functionalized PDMS₆₅ capillaries.

On the other hand, the effect of the type of CNTs on the extractive phase was evaluated for a PDMS₆₅ capillary. *Figure 124* shows that both c-SWCNTs and c-MWCNTs modified coatings provided similar chromatographic profiles, although the peak areas were slightly higher for the c-MWCNTs functionalized capillary. The chromatographic profiles obtained when using the PDMS₆₅ capillaries were better than those observed with the PDMS₉₅ capillaries (*Figures 122–124*).

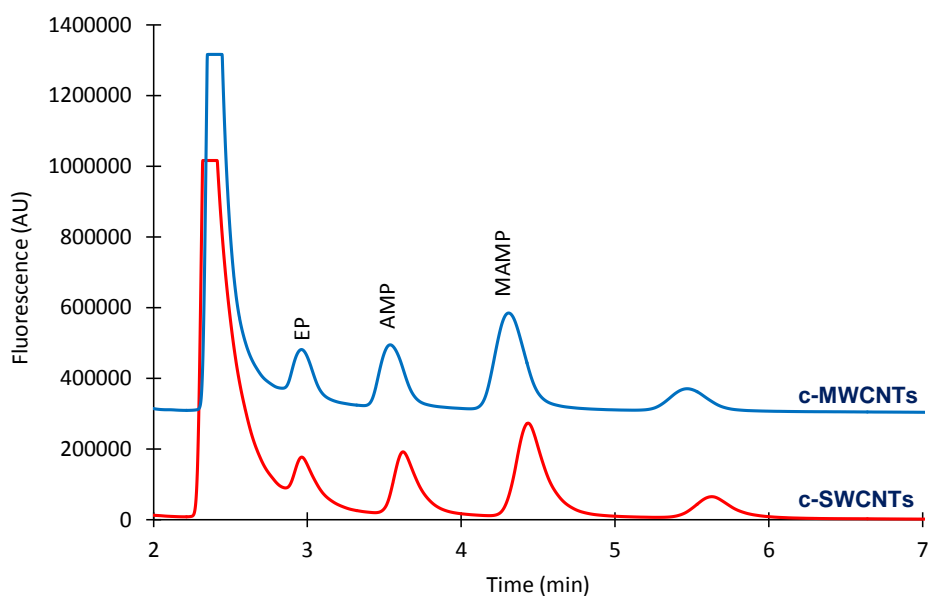


Figure 124. Chromatograms obtained for a standard solution of the amphetamines tested ($8 \mu\text{g mL}^{-1}$, each) with the c-SWCNTs and the c-MWCNTs functionalized PDMS₆₅ capillaries.

Finally, the loading capacity was examined by processing solutions of the tested analytes at concentrations ranging from 2 to $10 \mu\text{g mL}^{-1}$ with different capillaries. The results are depicted in Figure 125. As it can be deduced from this figure, a linear relation between concentration and peaks areas was observed within the tested concentration interval with the PDMS₆₅ columns. However, poor linearity was observed for the PDMS₉₅ columns regardless the presence of CNTs in the extractive coating. For the PDMS₉₅ capillaries, better correlation was observed between peak areas and concentration within the $2\text{--}8 \mu\text{g mL}^{-1}$ range (See Table 46), which indicates that their loading capacity was lower than that of the PDMS₆₅ capillaries.

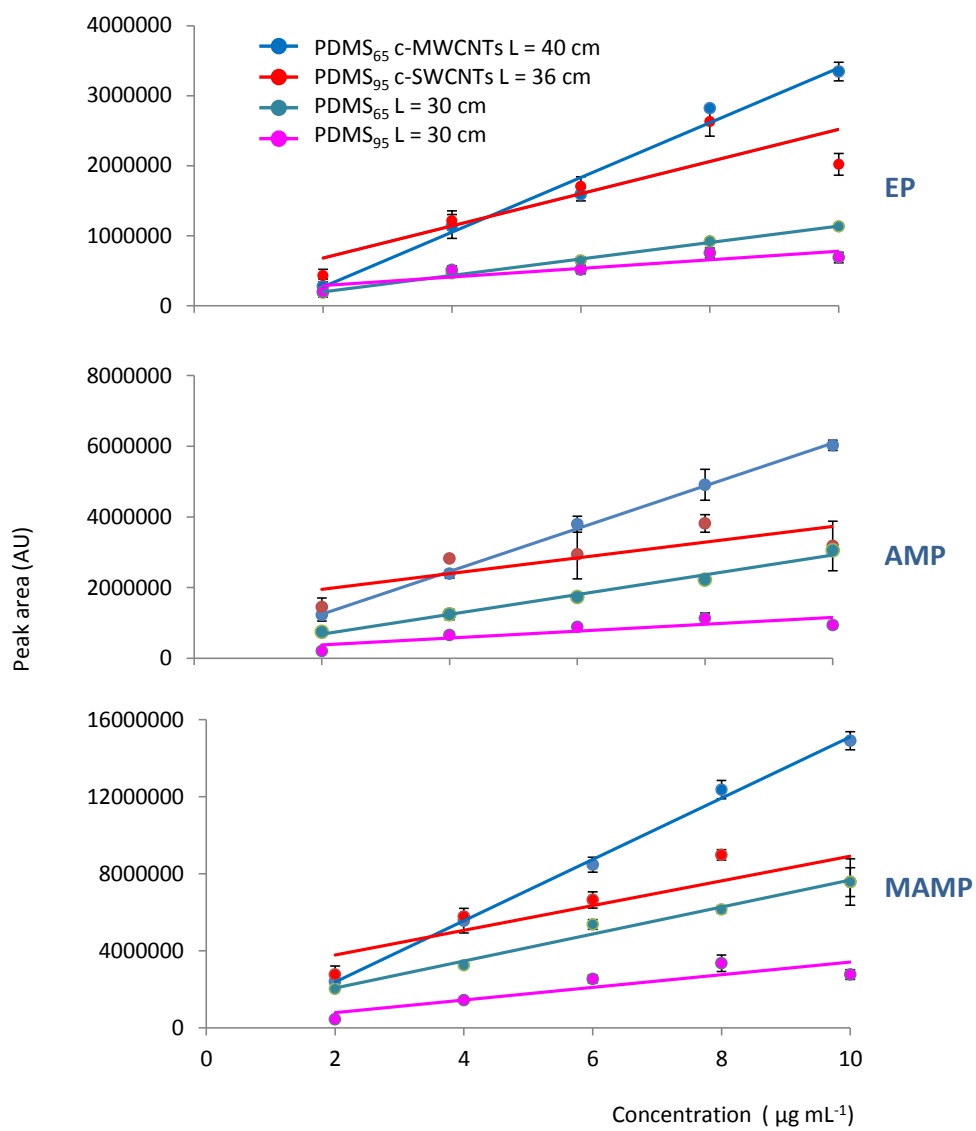


Figure 125. Peak areas obtained for different concentrations of the amphetamines tested within the 2–10 $\mu\text{g mL}^{-1}$ concentration range with different extractive capillaries.

Table 46. Response vs concentration linearity data.

Capillary	Concentration Interval ($\mu\text{g mL}^{-1}$)	Linearity ($y = ax + b$)		
		EP	AMP	MAMP
PDMS ₆₅ c-MWCNTs L= 40 cm	2.0–10.0	$a = (39 \pm 3) \times 10^4$ $b = (-5 \pm 2) \times 10^6$ $R^2 = 0.980$	$a = (606 \pm 14) \times 10^3$ $b = (3 \pm 9) \times 10^5$ $R^2 = 0.998$	$a = (159 \pm 5) \times 10^4$ $b = (-8 \pm 3) \times 10^6$ $R^2 = 0.997$
PDMS ₉₅ c-SWCNTs L= 36 cm	2.0–10.0	$a = (23 \pm 7) \times 10^4$ $b = (2 \pm 5) \times 10^6$ $R^2 = 0.764$	$a = (22 \pm 9) \times 10^4$ $b = (2 \pm 6) \times 10^6$ $R^2 = 0.658$	$a = (64 \pm 8) \times 10^4$ $b = (21 \pm 14) \times 10^5$ $R^2 = 0.962$
	2.0–8.0	$a = (35 \pm 4) \times 10^4$ $b = (-27 \pm 15) \times 10^4$ $R^2 = 0.987$	$a = (36 \pm 8) \times 10^4$ $b = (9 \pm 4) \times 10^5$ $R^2 = 0.910$	$a = (97 \pm 14) \times 10^4$ $b = (11 \pm 8) \times 10^5$ $R^2 = 0.96$
PDMS ₆₅ L= 30 cm	2.0–10.0	$a = (117 \pm 4) \times 10^3$ $b = (-3 \pm 3) \times 10^5$ $R^2 = 0.997$	$a = (28 \pm 2) \times 10^4$ $b = (11 \pm 13) \times 10^4$ $R^2 = 0.990$	$a = (70 \pm 5) \times 10^4$ $b = (6 \pm 3) \times 10^6$ $R^2 = 0.983$
PDMS ₉₅ L= 30 cm	2.0–10.0	$a = (61 \pm 17) \times 10^3$ $b = (17 \pm 11) \times 10^5$ $R^2 = 0.810$	$a = (10 \pm 3) \times 10^4$ $b = (2 \pm 2) \times 10^6$ $R^2 = 0.750$	$a = (33 \pm 9) \times 10^4$ $b = (1 \pm 6) \times 10^5$ $R^2 = 0.800$
	2.0–8.0	$a = (8 \pm 2) \times 10^4$ $b = (8 \pm 1) \times 10^5$ $R^2 = 0.910$	$a = (15 \pm 2) \times 10^4$ $b = (3 \pm 10) \times 10^4$ $R^2 = 0.972$	$a = (49 \pm 2) \times 10^4$ $b = (-52 \pm 10) \times 10^4$ $R^2 = 0.997$

Taking into account the absolute peak areas and chromatographic profiles, as well as the linear working interval, a c-MWCNTs coated PDMS₆₅ capillary of 40 cm length was selected as the best option for further experiments.

Application to the quantification of amphetamines in oral fluid samples

In the analysis of drugs in oral fluid, samples are usually collected by spitting or by using sweat wipes, sponges or swabs (Lledo-Fernandez, C. and Banks, C.E., 2011; Samyn, L. et al., 2007). Owing to its high viscosity, the direct loading of oral fluid into the IT-SPME capillary was unsuitable, even after dilution with the buffer and FMOc solutions. For this reason, in the present study cotton swabs were used to collect oral fluid. In order to simplify the analytical procedure and to avoid excessive dilution of the analytes, the swabs were directly immersed into vials containing the derivatization solution. In such a way, the analytes were simultaneously extracted from the swabs and derivatized. Finally, aliquots of the resulting solutions were removed from the vials and processed by IT-SPME with a

c-MWCNTs coated PDMS₆₅ capillary. The reliability of the proposed approach was first tested with standard solutions of the analytes.

Preliminary experiments were carried out to estimate the volume of the sample that could be absorbed with the swabs. Volumes of the working solutions ranging from 50 to 200 μL were introduced into 2 mL glass vials, and then swabs were put into contact with these solutions. It was found that the swabs used in the present study absorbed about 125 μL of the standard solutions containing the amphetamines in glass vials; then the tips of the swabs were put into contact with the working solutions until the liquid was totally absorbed. Next, the swabs were immersed into another vial which contained the derivatization solution (250 μL of the 0.1 mM FMOc solutions). Finally, aliquots of the resulting solutions were processed by IT-SPME and chromatographed. The effect of volume of the extracts loaded into the IT-SPME capillary was tested within the 10–50 μL interval. A volume of 20 μL was found to be the best option, as higher volumes did not significantly increase the signal, probably due to the high percentage of acetonitrile in the extracts, whereas the peak corresponding to the excess of FMOc interfered with the measurement of the FMOc-EP peak. Under such conditions, good linearity and reproducibility was found within the tested concentration intervals (1–10 $\mu\text{g mL}^{-1}$ for AMP and MAMP and 2–10 $\mu\text{g mL}^{-1}$ for EP (See Table 47).

Table 47. Linearity and precision achieved with the proposed extraction-derivatization-IT-SPME-CapLC method for AMP, MAMP and EP within the 1–10 $\mu\text{g mL}^{-1}$ (2–10 $\mu\text{g mL}^{-1}$ for EP) concentration interval (values obtained with the c-MWCNTs coated PDMS₆₅ capillary of 40 cm length).

Compound	Linearity, $y = ax + b$ (n=8)*			Precision**, RSD%(n=3)
	$a \pm s_a$	$b \pm s_b$	R^2	
EP	$(229 \pm 8) \times 10^3$	$(-18 \pm 4) \times 10^4$	0.991	5
AMP	$(402 \pm 15) \times 10^3$	$(-39 \pm 8) \times 10^4$	0.991	3
MAMP	$(606 \pm 22) \times 10^3$	$(-46 \pm 11) \times 10^4$	0.991	3

*Established from four concentrations assayed in duplicate

**Established at a concentration of 4 $\mu\text{g mL}^{-1}$

According to the above results, the conditions finally selected for the analysis of amphetamines in oral fluid were those indicated in Figure 126.

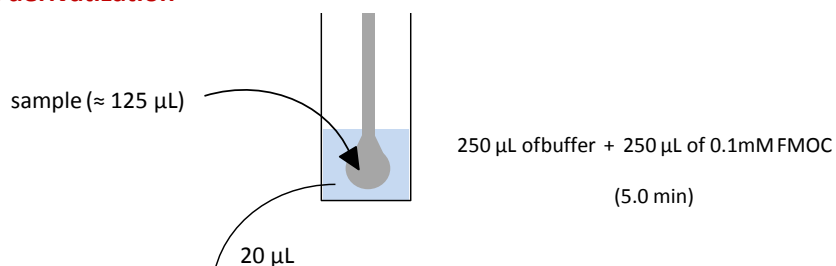
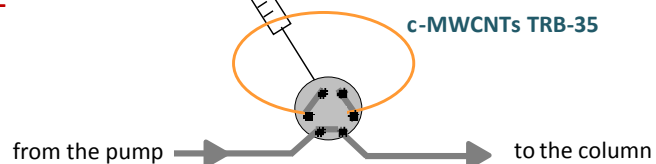
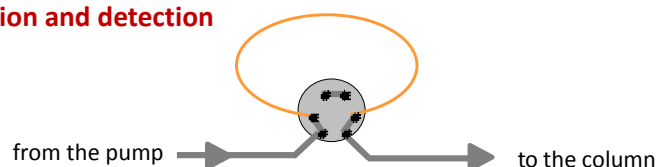
1) Extraction/derivatization**2) IT-SPME****3) Separation and detection**

Figure 126. Scheme of the extraction/derivatization IT-SPME-CapLC method used for the analysis of amphetamines in oral fluid. The extractive capillary was a c-MWCNT functionalized PDMS₆₅ capillary (40 cm length).

A small peak was observed at a retention time slightly lower than that of the EP-FMOc derivative. This peak was not detected when effecting the derivatization in solution; thus, this peak was due to a compound present in the cotton. Nevertheless, it could be differentiated from the peak corresponding to the EP derivative (See Figure 127).

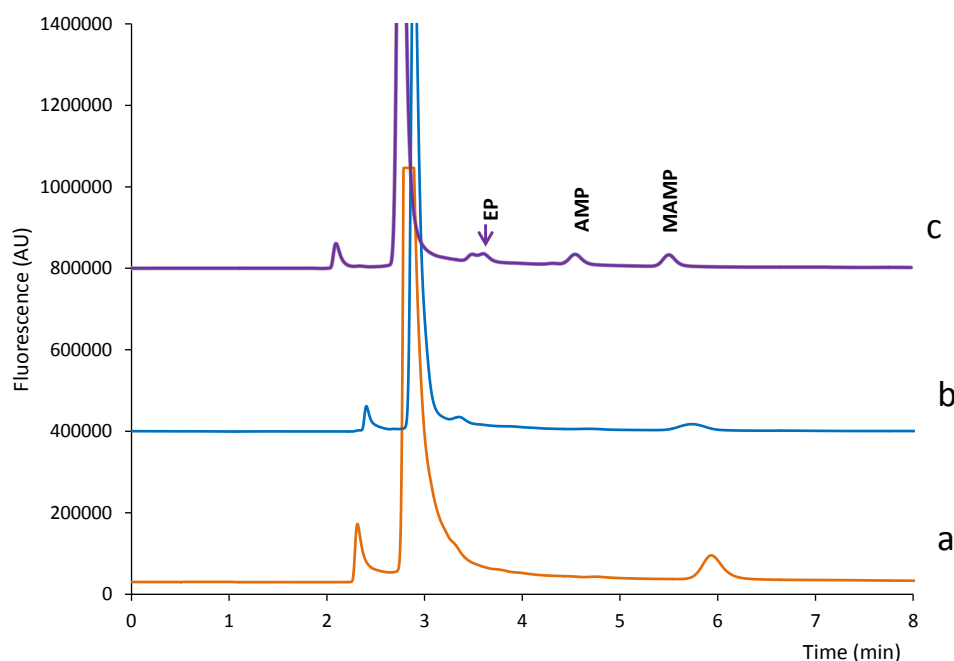


Figure 127. (a) Chromatograms obtained for the reaction mixture (250 μL of buffer and 250 μL of 0.1 mM FMOC), (b) the same reaction mixture after the introduction of a cotton swab for 5 min, and (c) after the introduction of a cotton swab impregnated with 125 μL of a standard solution of EP (2 $\mu\text{g mL}^{-1}$). For IT-SPME a c-MWCNTs functionalized PDMS₆₅ capillary (40 cm length) was used.

In Figure 128 are shown the chromatograms obtained for a sample of oral fluid and the same sample spiked with a mixture of the analytes. The chromatograms obtained for oral fluid were similar to those obtained for standard solutions subjected to the same extraction/derivatization procedure (Figure 127). It was then concluded that the selectivity provided by the c-MWCNTs coated PDMS₆₅ capillary was suitable. In addition, no significant differences were observed in the chromatograms obtained for samples obtained from different donors. LODs, established as the concentration of amphetamines that yielded a signal-to-noise ratio of 3, were 0.8 $\mu\text{g mL}^{-1}$ for EP, and 0.5 $\mu\text{g mL}^{-1}$ for AMP and MAMP. The precision was also satisfactory, being the interday coefficients of variation 6 % for EP and AMP, and 3 % for MAMP (n = 3). Finally, no additional cleaning of the extractive capillary with an organic solvent after each run was necessary as during the transfer and chromatographic separation steps the

capillary was flushed with an eluent containing a high percentage of acetonitrile (70 %).

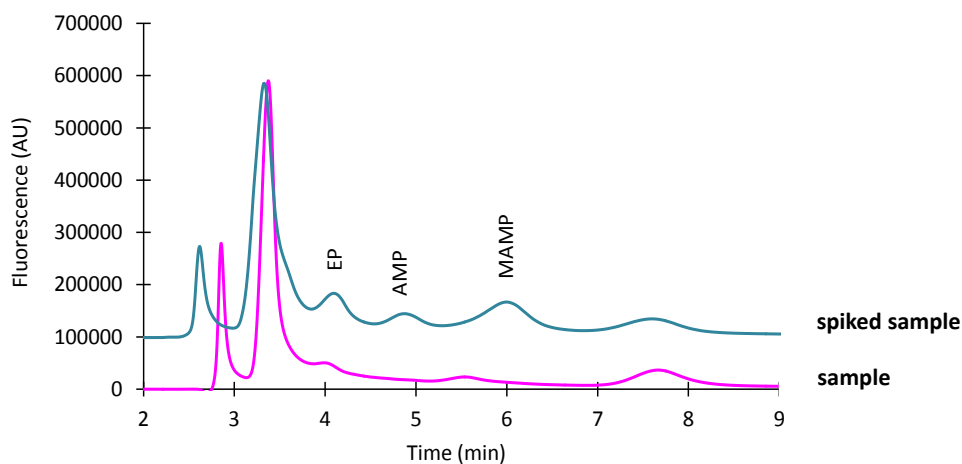


Figure 128. Chromatograms obtained with the proposed extraction/derivatization IT-SPME-CapLC method for an oral fluid sample, and the same sample spiked with the tested amphetamines ($8 \mu\text{g mL}^{-1}$, each).

Utility

Different strategies have been proposed for sample treatment prior to the chromatographic analysis of drugs in oral fluid. Extraction of the analytes into an organic solvent (toluene, butyl chloride, chloroform) has been the option traditionally used for the extraction of amphetamines (Drummer, O.H. *et al.*, 2007; Kankaanpää, A. *et al.*, 2004; Meng, P. and Wang, Y., 2010) often in combination with evaporation of the extracts to dryness in order to concentrate the extracts to be chromatographed. SPE followed by solvent evaporation has also been proposed (Concheiro, M. *et al.*, 2008). These methodologies allow the detection of the analytes at low ng mL^{-1} levels by GC, although the resulting procedures are labor-intensive. More recently, different methods have been reported that involve SPME with fibres (Djozan, D., Baheri, T., 2010; Djozan, D. *et al.*, 2011) again prior to GC; LODs of $14\text{--}27 \text{ ng mL}^{-1}$ were reported for MAMP. Very recently, microextraction with a C_{18} sorbent packed into the needle of a syringe has been proposed for the analysis of illicit drugs in oral fluid by LC-MS/MS (Montesano, C. *et al.*, 2015). In this case, samples were treated to precipitate the proteins, and

the supernatant was passed through the sorbent by repetitive aspirating/dispensing cycles, being the LOD reported for AMP 1 ng mL^{-1} .

Compared with previously described procedures, the main advantage of the present methodology is the simplicity. After sample collection, the only operations required are the immersion of the swabs into the derivatization solution and, after 5 min, the loading of an aliquot of the resulting solution into the IT-SPME device. The proposed method is also advantageous in terms of time of analysis and solvent and reagents consumption. Although the LODs are about one order of magnitude higher than those reported by other authors, the proposed method can be considered adequate for the measurement of amphetamines in oral fluid of abusers. For example, concentrations of amphetamine found in oral fluid samples during random tests programs were in the $0.3\text{--}8.8 \text{ }\mu\text{g mL}^{-1}$ range (Samyn, N. and van Haeren, C. 2000; Samyn, N. et al., 2002). Nevertheless, for other types of studies, more sensitive methodologies may be required.

Conclusions

The present study shows that IT-SPME is a valid option for the on-line extraction of amphetamines derivatized with FMOC, and for their subsequent separation by CapLC. The efficiencies of the IT-SPME have been examined for different PDMS-based extractive capillaries, as well as for the same capillaries after their functionalization with CNTs. The introduction of CNTs in the extractive coatings has a positive effect not only on the extraction efficiencies but also on the chromatographic profiles. In all instances, highest responses were obtained for PDMS₆₅ capillaries, which can be explained by a $\pi\text{--}\pi$ interaction mechanism. In this sense, the use of FMOC (which introduces two aromatic rings in the compounds to be extracted) may be advantageous over other derivatization reagents typically used for amphetamines (Herrez-Hernandez, R. et al., 1996). On the other hand, the chromatograms observed for PDMS₆₅ capillaries functionalized with c-SWCNTs and c-MWCNTs were quite similar, although the analytical responses obtained with the latter capillary were slightly higher. According to these results, a new approach has been described for the analysis of amphetamines derivatives using a PDMS₆₅ capillary functionalized with c-MWCNTs. The described approach combines the simplicity of in-valve IT-SPME with enhanced sensitivity, and can be considered an alternative for the analysis of

amphetamines. As an illustrative example of application, in the present study oral fluid samples ($\approx 125 \mu\text{L}$) collected with cotton swabs have directly been derivatized and processed by IT-SPME-CapLC. The proposed method is very simple and cost-effective, and provides suitable selectivity, sensitivity and reproducibility at low $\mu\text{g mL}^{-1}$ concentration levels, which are concentrations typically found in oral fluid of abusers.

4.3 METALLIC-BASED MATERIALS

4.3.1 MOF

4.3.1.1 Peptide MOF for enantioselective separation of chiral drugs

The discovery of chiral adsorbents that permit rapid separation of individual enantiomers is relevant in the pharmaceutical industry. In the present section, the application of a MOF is focused as chiral phase for SPE. The proposed 3D MOF is based on the tripeptide Gly-L-His-Gly (GHG) to engineer the chiral pockets in their structure for the separation of chiral polar drugs such as MAMP and EP enantiomers. Monte Carlo (MC) simulations have been used to reveal how intermolecular interactions between the drugs and the peptide backbone guide chiral recognition. Synthesis, theoretical simulations and characterization of the proposed MOF have been carried out with FuniMat Group (Instituto de Ciencia Molecular, Universidad de Valencia). Enantioselective separation has been evaluated by chromatographic analysis. For the first set of preliminary studies, the enantiomeric recognition of Cu(GHG) has been examined in solution and subsequently the enantioselective separation has been carried out with SPE by using Cu(GHG) as chiral phase.

Synthesis of Cu(GHG)

Cu(GHG) was synthesized by slow diffusion of GHG (*See Figure 129*) and Cu(II) acetate to produce prismatic, micrometric blue crystals by following a synthetic procedure recently reported (*Martí-Gastaldo, C. et al., 2015*). 24.2 mg of the peptide (90 μmol) were dissolved in 300 μL of an aqueous solution of $\text{Cu}(\text{OAc})_2 \cdot 2\text{H}_2\text{O}$ 0.3 M (90 μmol) in a 4 mL glass vial to produce a blue solution. The solution was manually stirred followed by sequential addition of 1.26 mL of absolute ethanol and 200 μL of water. The mixture was then left to stand in a temperature controlled chamber at 25°C for the formation of blue coloured prismatic crystals. After 48 hours, crystals were filtered, washed with absolute ethanol and stored at 4°C (75% yield, calculated for the metal).

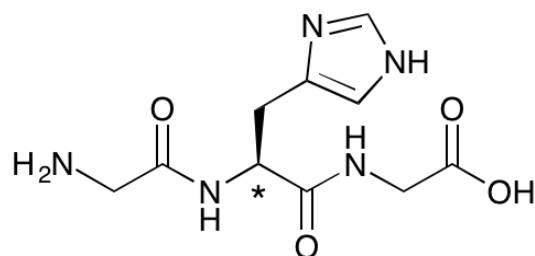


Figure 129. GHG structure.

Characterization of Cu(GHG)

Phase purity was studied by SEM (*Figure 130*), CHN, FTIR, thermogravimetric analysis and powder X-ray diffraction (PXRD).

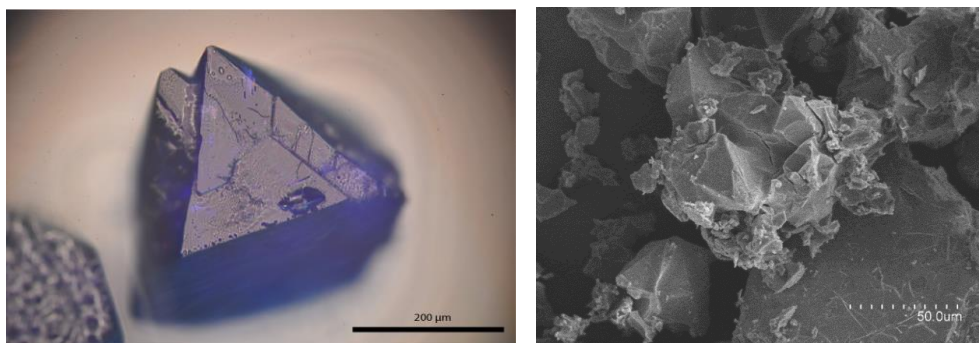


Figure 130. Microscopic (left) and SEM images (right) of as-made crystals of Cu(GHG). Particle morphologies and dimensions at an accelerating voltage of 20 keV.

Cu(GHG) crystallizes to produce an open 3D framework, built from the interconnection of 4-fold helicoidal Cu-peptide-Cu chains by μ 2-carboxylate bridges in C-terminal Gly (*Figure 131A*). Porosity arises from the interconnection of 1D empty channels that account for a solvent-accessible volume close to 60 % of the total volume. Use of peptides as metal connectors allows us to decorate the surface of the empty space with carboxylate, amide, amino, and imidazole groups pointing into the channels (*Figure 131B*). This renders chemically versatile channels featuring a manifold of interaction sites for modulating framework/guest interactions (*Figure 131C*).

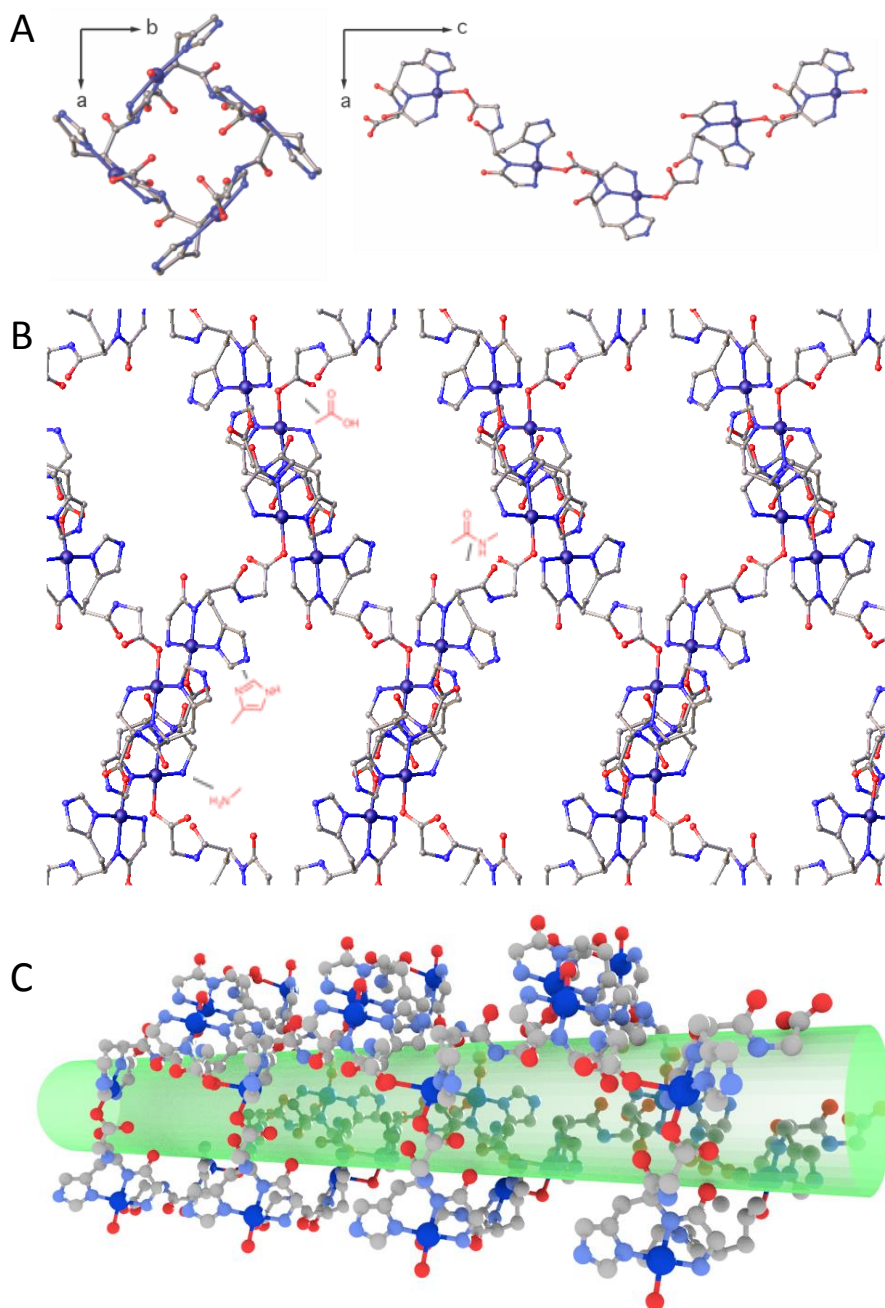


Figure 131. (A) Structure of helicoidal chains in Cu(GHG) MOF, (B) Functional groups in the peptidic backbone decorating the surface of the pores, (C) 1D channels in Cu(GHG) are surrounded by functional sites prone to establish supramolecular interactions.

Theoretical simulatons

The chiral recognition can potentially be triggered by preferential sorption in the chiral pockets of the MOF rather than interactions at the surface of the solid. MC simulations were used to gain a better understanding of the role played by the functional groups from the peptide in controlling preferential adsorption for more favorable binding sites. We simulated the adsorption of the two enantiomers (+,-) of MAMP and EP. The structure of Cu(GHG) (CCDC961607) was first prepared for the theoretical study by removal of solvent molecules occupying the pores. Most stable conformations of MAMP and EP enantiomers were explored by randomly changing the torsion angles.

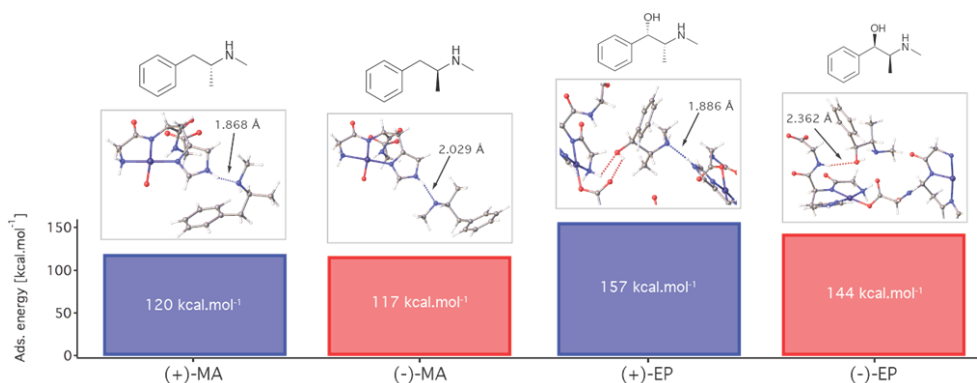


Figure 132. Representative MC binding geometries of (+,-) MAMP and EP enantiomers within the structure of Cu(GHG) and corresponding adsorption energies as absolute values calculated with respect to gas phase. Most relevant H-bonds in directing guest binding are annotated in each case.

Figure 132 summarizes the adsorption energies and preferential binding sites for the most representative host-guest adducts calculated. Adsorption of both MAMP enantiomers is preferentially directed by the formation of H-bonds between the amine and the imidazole group in His side chain. We have used discrete models of the MOF and quantumchemistry calculations to confirm that this interaction is energetically most favorable, at least 4 kcal mol⁻¹ stronger than those accessible by interaction with other functional groups in the pocket involving C-terminal and N-terminal Gly (Table 48).

Table 48. Summary of binding energies and H-bond lengths for MAMP-MOF interactions as estimated by quantum-chemistry calculations.

H-Bond	Binding Energy (kcal.mol ⁻¹)	Bond Length (Å)
(MAMP)-HN ⁺ HN ⁻ (imidazole; His)	15.0	1.977
(MAMP)-HN ⁺ H ₂ N ⁻ (amino, Gly; N-term)	10.9	2.054
(MAMP)-NH ⁺ O=C ⁻ (amide bond, Gly N-term)	6.3	2.149

Regarding enantiomeric recognition, (+)-MAMP is accommodated closer to the pocket for a stronger interaction via an imidazole H-bond. This elongates from 1.87 Å for (+)-MAMP to 2.03 Å when interacting with (-)-MAMP, due to small changes in the adsorption configurations of the enantiomers (*Figure 132*). The higher binding energy observed for (+)-MAMP mainly arises from stronger van der Waals interactions due to a better fit to the shape of the pocket. While the accuracy of the force-field model and the difficulty of replicating experimental solvation effects do not allow for quantitative prediction of chiral selectivities, our simulations suggest that more effective enantioselective recognition is expected for EP as result of cooperative supramolecular interactions.

As shown in *Figure 132*, adsorption of (-)-EP is solely directed by the formation of a weak elongated H-bond (2.36 Å) with the amide bond in C-terminal Gly. In contrast, (+)-EP combines short His-EP H-bonds (1.89 Å), equivalent to that with (+)-MAMP, with auxiliary bonds with the carboxylate and amino groups (2.09 and 2.40 Å) in the C-terminal and N-terminal Gly aa's of Cu(GHG) for more favorable adsorption. It is the strength and number of H-bonds-EP has two H-bonding groups capable of interacting synergically with the environment of the peptide MOF that translate into a bigger difference in adsorption energies close to 13 kcal mol⁻¹.

MC simulations suggest that Cu(GHG) might display stereoselectivity, in particular for EP enantiomers, associated with the control of non-covalent interactions over their binding geometries. This promising result prompted us to attempt actual separation experiments from solutions of the racemates. One of the key limitations of flexible MOFs is their poor mechanical robustness that results in collapse of the structure upon solvent removal. This is also the case for Cu(GHG), which displays sponge-like behavior with a crystalline-to-amorphous transformation after activation that can be reverted to the original state in the

presence of polar solvents. Though this is a key limitation for gas storage, which requires the porous material to be activated prior to gas sorption, chiral recognition is a dynamic process, and prior filling of the pores is not imperative since the solvent molecules occupying the pores can be progressively exchanged with the chiral guests in solution. Hence, all separation experiments were carried out by using non-evacuated, as-synthesized materials to preserve their structural integrity.

Enantioselective recognition in solution

First, the ability of Cu(GHG) to recognize selectively enantiomers from solution was studied by soaking 10 mg of fresh solid in racemic mixtures of MAMP and EP (40 $\mu\text{g mL}^{-1}$ in ethanol:water 75:25). Enantioselective recognition was evaluated chromatographically as a function of contact time (See Methodology Chapter for experimental details). As shown in Figure 133, adsorption of (-)-MAMP and (-)-EP can be considered negligible, whereas $30 \pm 3\%$ of (+)-MAMP and $37 \pm 3\%$ of (+)-EP are preferentially adsorbed after 4 and 2 h, respectively.

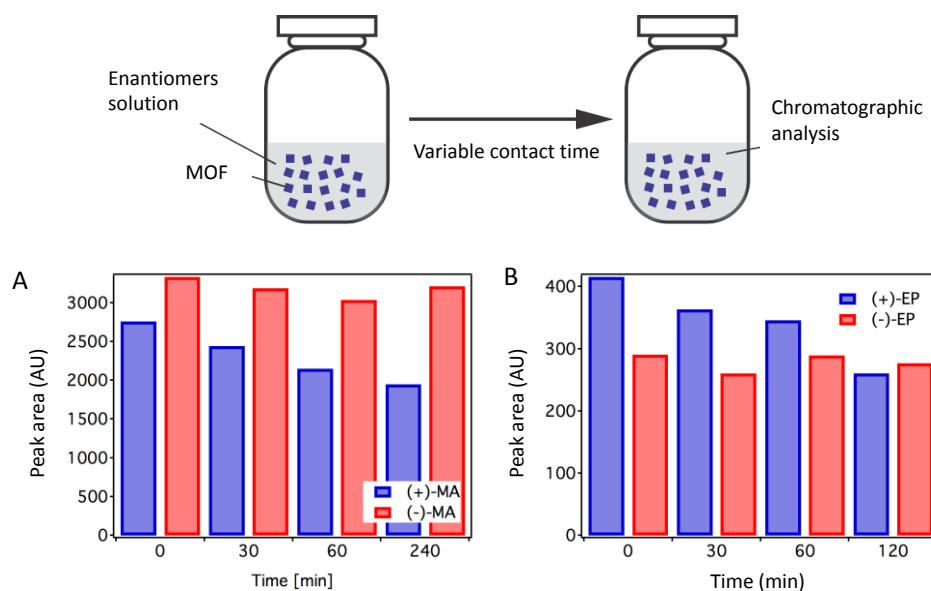


Figure 133. Evolution of the enantioselective recognition of Cu(GHG) for chiral drugs in ethanol:water 75:25 solution with contact time for (A) MAMP and (B) EP. Chiral adsorption was evaluated from chromatographic analysis of the supernatant solution.

For clarity, we have defined the enantioselective recognition of Cu(GHG) for (+)-MAMP and (+)-EP as the ratio between the difference of the peak areas for these enantiomers after 240 and 120 min (minimum signal intensity detected experimentally in each case) and the maximum at 0 min for free enantiomers in solution in absence of the MOF normalized to the peak area of this last. Experiments were repeated three times for confirming precision of the reported behavior, data are summarized in the *Table 49*.

Table 49. Experimental data used for calculation of enantioselective recognition capability of Cu(GHG).

Time (min)	Peak area (+)-MAMP		
	Test 1	Test 2	Test 3
0 (no MOF)	2828	2694	2750
240 (with MOF)	2092	1812	1914
Enantioselective recognition (%)	26.0	32.7	30.4
Average (%)	30		
Standard Deviation (s)	3		

Time (min)	Peak area (+)-EP		
	Test 1	Test 2	Test 3
0 (no MOF)	440	392	410
120 (with MOF)	288	234	267
Enantioselective recognition (%)	34.5	40.3	34.9
Average (%)	37		
Standard Deviation (s)	3		

We attribute the long recognition times to the highly polar mixture of solvents used. This will stabilize the chiral drugs in solution, preventing fast diffusion into the porous chiral medium for a slow recognition process with long equilibration times. This experiment agrees well with the MC simulations that support preferential interaction of (+)-enantiomers in the chiral pocket linked to specific conformations that enable H-bond formation with the histidine side chain. As described above, theoretical predictions are also consistent with more favorable separation of EP enantiomers over those of MAMP based on the energy differences for enantiomer interaction with Cu(GHG), which are higher for the former.

Control study

We also performed a control experiment by using a ground mixture of GHG and Cu(II) acetate in the same proportion present in the MOF. Individual components do not show measurable chiral recognition (*Figure 134*), suggesting that the periodic distribution of chiral channels in the MOF scaffold is key for enantiomeric separation.

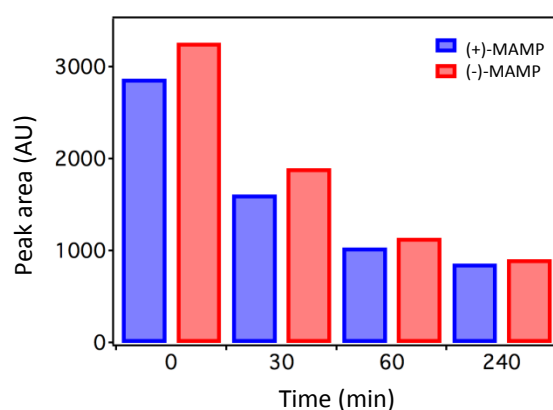


Figure 134. Control experiment to confirm the observed chiral recognition is specific to the MOF architecture rather than to any of its components. Below chromatograms for a physical mixture of GHG and Cu(II) acetate in the same proportion present in the MOF. Evolution of the peak areas for (+) and (-)-MAMP in a solution of the MOF components rules out measurable enantioselective recognition of any of the enantiomers. Inset in the right column highlights the signal specific to each enantiomer.

To confirm the stability of the solid in the experimental conditions, we collected UV/vis spectra of dispersions of Cu(GHG) at variable times. As shown in *Figure 135*, spectra remained constant and there is no signature of Cu(II) leaching that might account for partial dissolution. As for the MOF structure, PXRD of the solid after the experiment confirms the structure remains intact with only minor variations in the relative intensities of some Bragg's reflections ascribed to preferential orientation of the crystals or changes in the nature of the species occupying the pores.

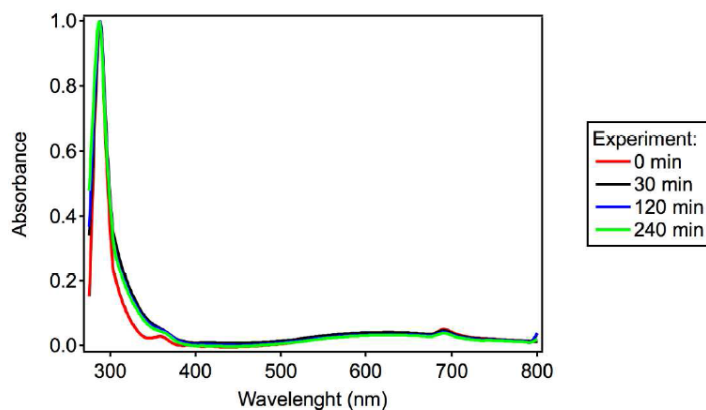


Figure 135. Time evolution of the UV-Vis spectra at room temperature of a dispersion of as-made 50 mg of Cu(GHG) in 500 μ L of EtOH:H₂O (25:75 v%) from 0 to 240 min. This set of conditions are equivalent to those used for studying the ability of Cu(GHG) to recognize selectively enantiomers from solution. The system remains constant and no signature of Cu(II) leaching –broad absorption band centered at 600 nm– can be observed, confirming the chemical integrity of the solid in these conditions.

Enantioselective separation with Cu(GHG)/SPE

Recent reports highlight the potential of chiral MOFs for the development of chiral stationary phases in the form of packed columns for HPLC enantioselective separation. However, the limited number of tests available suggests that the main limitations of MOFs as stationary phases are their poor stability and particle heterogeneity. This limits the range of mobile phases available, in particular for polar analytes, and makes it difficult to achieve efficient packing of the particles in the column, which relies on narrow distributions in size and shape for reproducible sorption/desorption kinetics. Lack of control over these variables can result in high retention times, low chromatographic performance, and energy-consuming separations. MOFs might be instead better fitted for SPE separation technologies. SPE enables isolation of the enantiomers rather than only providing a measure of the enantiomeric purity of a mixture. SPE can allow for more efficient chromatographic analysis by removal of interferences, increase of trace concentration, or sample simplification, but use of chiral MOFs in this context remains unexplored.

To illustrate this concept, 50 mg of Cu(GHG) were packed in a polypropylene SPE cartridge and a racemic mixture of (\pm)-EP in hexane:ethanol 75:25 at 0.25 mL min⁻¹ was eluted, followed by HPLC analysis of the resulting extract (Figure 136A). For the experimental setup see *Methodology Chapter (Section 3.3.1.1)*. We opted for EP rather than MAMP based on our preliminary results that suggested faster and more efficient recognition of the former. As shown in Figure 136B, comparison of the chromatograms of the sample before and after SPE/Cu(GHG) separation confirms the ability of the MOF to trap preferentially (+)-EP, in line with our theoretical predictions. While the peak area contribution for (-)-EP remains constant, there is a significant decrease for the (+)-form.

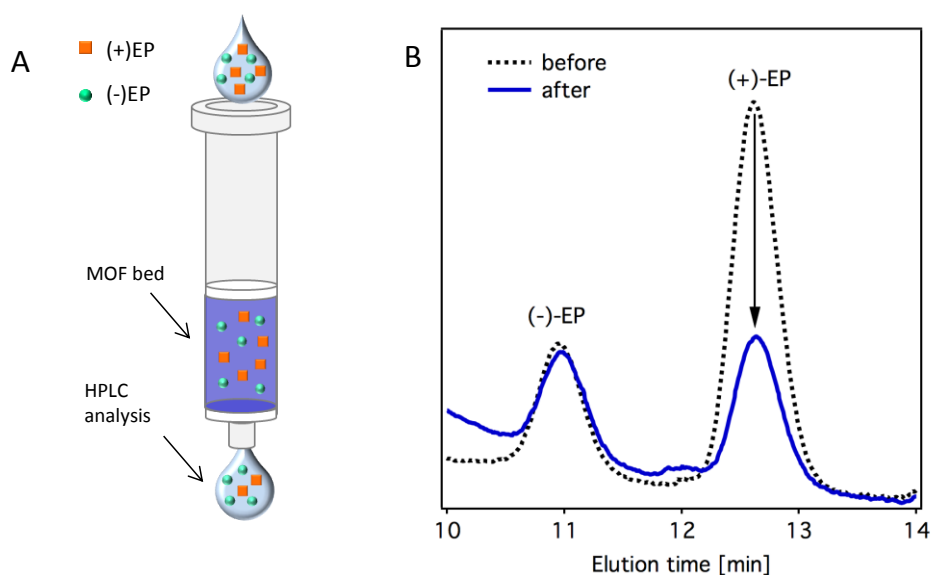


Figure 136. (A) SPE separation of EP in hexane:EtOH 75:25 by using Cu(GHG) as chiral bed. (B) HPLC chromatograms of EP racemate before (dashed line) and after (solid line) passing through the MOF bed.

Quantitatively, the chiral solid permits separating 54 ± 2 % of (+)-EP from equimolar mixtures of the enantiomers in 4 min with a satisfactory precision (RSD = 4 %) for the different cartridges tested (Table 50).

Table 50. Cartridge to cartridge precision.

Conditions	Peak area (+)-EP		
	Test 1	Test 2	Test 3
no MOF	68103	66451	69391
with MOF	30420	31873	30611
Enantioselective recognition (%)	55.3	52.0	55.9
Average (%)	54		
Standard Deviation (s)	2		
RSD (%)	4		

HPLC analysis of the solution desorbed from the MOF by elution with fresh solvent confirms that only (+)-EP enantiomers are retained in the separation, confirming enantioselectivity (Figure 137). Compared to SPE, direct soaking of the crystals in a racemic mixture of (\pm)-EP in hexane:EtOH 75:25 also leads to enantioselective separation of 44 % of (+)-EP in the same time (Figure 138). MOF cartridges can be used at least for two runs without significant loss of enantioselectivity.

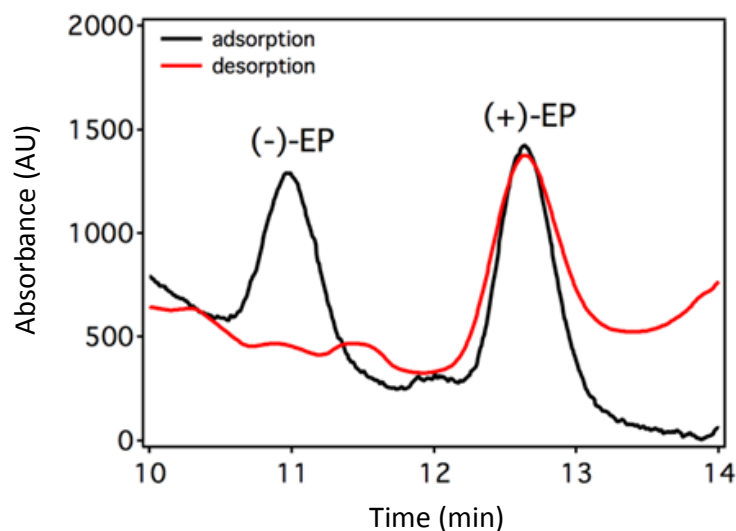


Figure 137. Comparison of HPLC chromatograms of a racemic mixture of (\pm)-EP in Hexane:EtOH 75:25 after passing through the MOF SPE cartridge (black line, adsorption) and after elution with fresh solvent (desorption). The presence of (-)-EP in the desorbed fraction is negligible whilst only (+)-EP can be detected in the chromatogram in good agreement with the reported enantioselectivity.

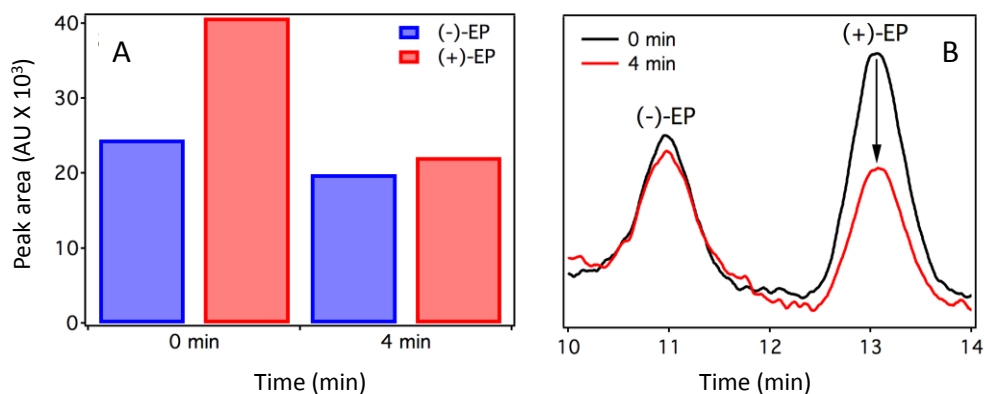


Figure 138. Control experiment by soaking as-made crystals of CuGHG in a racemic mixture of (\pm)-EP in hexane:EtOH 75:25. (A) Evolution of the peak areas for (-) and (+)-EP. Adsorption of (-)-EP can be considered negligible whilst close to 44 % of (+)-EP is preferentially adsorbed. (B) HPLC chromatograms of EP racemic solution in contact with the MOF before (0 min) and after 4 minutes

SEM (Figure 139) studies of the crystals in the MOF bed after separation experiments confirm that both the structure and the morphology of the solid remain unchanged. Hence, we ascribe loss of activity to an inefficient packing of the solid rather than to chemical degradation.

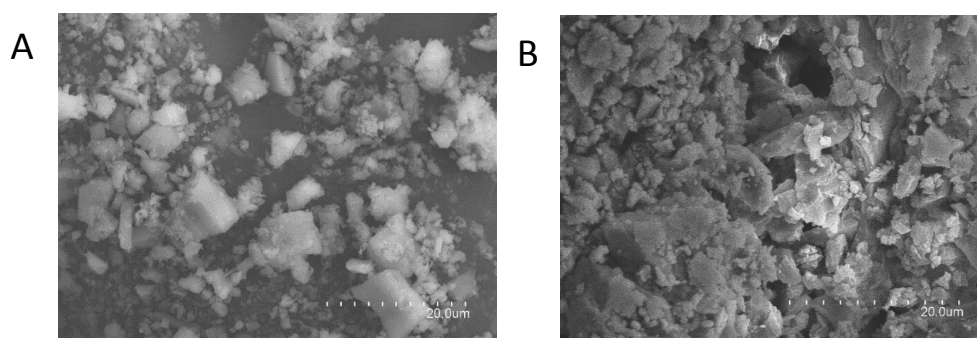


Figure 139. SEM pictures of Cu(GHG) before (A) and after (B) SPE separation, at an accelerating voltage of 20 keV. Crystals were metalized with a mixture of gold and palladium during 30 s.

Conclusions

Results suggest that Cu(GHG) offers high performance in terms of stereoselective recognition and time efficiency, for a high-speed chiral separation medium. Peptide MOFs are particularly well suited for enantioselective recognition. The chiral pockets in their structure can be manipulated for maximizing host–guest intermolecular interactions for a specific enantiomer simply by suitable choice of the peptide sequence. Cu(GHG) is capable of separating >50 % of (+)-EP from a racemic mixture in only 4 min when used as a chiral SPE cartridge. This is a promising result, considering the limited availability of SPE cartridges for chiral separation on the market. According to our theoretical simulations, stereoselectivity is driven by preferential non-covalent interactions with specific amino acids, particularly His, in the MOF backbone. This combination of theory and experiment holds great potential and might help in addressing the challenge of chiral recognition by producing more complex chemical environments in which supramolecular interactions can be finely tuned for maximizing enantiomeric resolution for particular drugs.

4.3.2 AgNPs and AuNPs

Metallic NPs as AuNPs and AgNPs have exceptional properties that make them suitable for different analytical applications. As explained in *Introduction Chapter*, metallic NP colloids exhibit different and strong colour in the visible region attributed to the SPR. The presence of some analytes induces UV plasmon band/visual changes. This strategy has been applied to colorimetric sensors development. Here, the AgNPs and AuNPs have been evaluated as candidates to develop a sulphur sensor based on plasmonic/visual changes due to thiol affinity. The interest in AgNPs is very high due to still outstanding plasmon activity compared with AuNPs. In addition, AgNPs has a molar extinction coefficient which is 100x greater, increasing sensitivity when using absorption spectroscopy. Thus, a rapid and portable sensor based on AgNPs immobilized on nylon has been designed for the in-situ detection of VSCs ($-S^2$, $-S$) which are the main causes of halitosis. The interaction between the thiol groups and AgNPs causes a color change from yellow to brown according to the concentration of sulphure compound. Quantification has been carried out by DR and DI analysis. Studies about sensor dependence of AgNPs size, batch-to-batch precision, AgNPs immobilization and their stability have supported this study. Indeed, the sensors have been tested in 10 healthy volunteers. From our point of view, the developed sensor is a potential commercial point-of-care to evaluate sulphure content for oral malodour due to its high sensitivity and low-cost.

4.3.2.1 Colorimetric sensor based on AgNPs for detecting volatile sulfur compounds

AgNPs vs AuNPs for sulphure detection

Firstly, AgNPs and AuNPs solutions were tested as candidates to detect sulphur compounds. As *Figure 140* shows, AuNPs remain red with an absorbance peak wavelength at 520 nm after sulphur addition while AgNPs dispersion change from yellow to orange/brown and the absorbance peak wavelength blue shift after the addition of Na_2S and CH_3SNa (*Figure 140*).

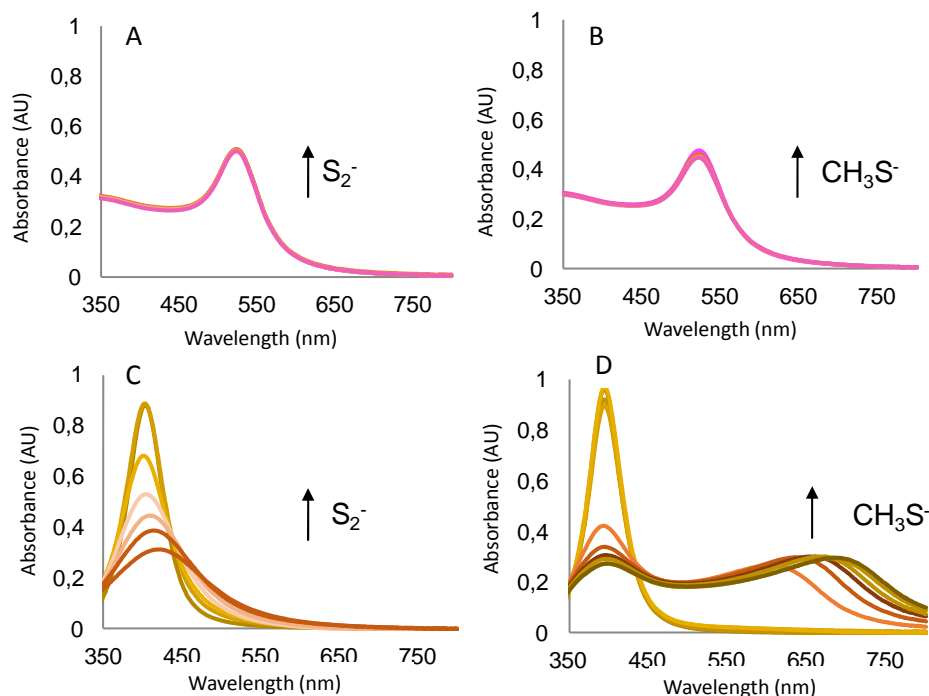


Figure 140. Absorption spectra of A, B) AuNP 20 nm in solution and C, D) AgNP 20 nm in solution registered 20 s by UV spectrophotometer after addition of A, C) Na_2S and B, D) CH_3SH in a range between 250 - 10000 $\mu g L^{-1}$.

The sensing mechanism of AgNPs vs AuNPs in presence of sulphur compounds is represented in Figure 141. The AgNP and AuNPs remain monodisperse due the presence of negative charge citrate absorbed on their surface to stabilized them by electrostatic repulsions. The citrate can be replaced or release by ligands with strong affinity, and then interact with the NPs surface. That is the situation which take place in presence of sulphur compounds ($-S^{-2}$ and $-SH$). Silver is readily sulphurized to form Ag_2S . Sulphidation of AgNPs has been reported in several studies (Elechiguerra, J.L. et al., 2005) that form Ag_2S -AgNP structure after Na_2S exposure, however the sulphidation mechanism and the structure and morphology of AgNPs still under study. The Ag_2S formation produce the destabilization of the monodisperse AgNP dispersion and their aggregation which explain the plasmon changes observed. In case of AuNPs, the $-S^{-2}$ and $-S^-$ acts as a ligand to bound the AuNPs for preserving them. Therefore, the absorbance peak of AuNPs at 520 nm still unchanged after Na_2S addition. Based

on the results, AgNPs were selected over AuNPs.

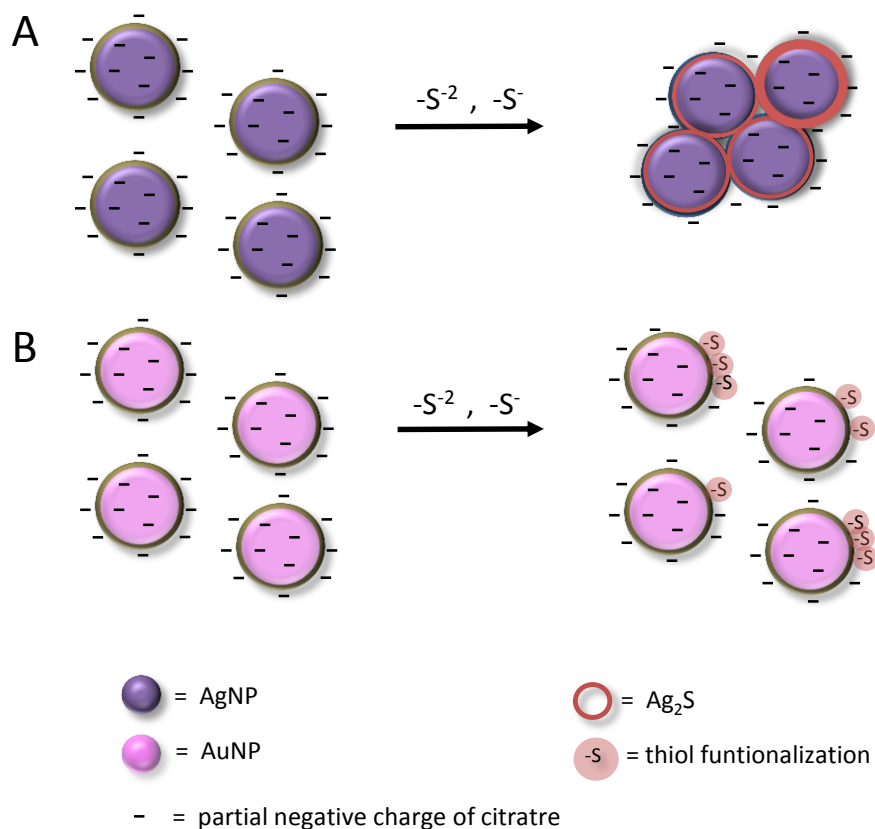


Figure 141. Schematic drawing of the A) AgNP aggregation and B) AuNPs functionalization by sulphur compounds.

Sensor optimization

Sensor is based on the immobilization of monodisperse sodium citrate-coated AgNPs (0.02 mg mL^{-1} , 10, 20 and 40 nm) on a support. Several immobilization supports were tested including cellulose, glass fiber and nylon. *Figure 142A-C* shows microscopic images of the different membranes before and after immobilization of AgNPs. Nylon immobilized higher amount of AgNPs because of the yellow intensity observed (*Figure 142D*), whereas silver aggregates were observed on the glass fiber.

The response of several sensors was tested using H_2S at 250 and 1000 $\mu\text{L m}^{-3}$ by DR and visual inspection (Figure 142D-F). Only nylon sensor showed a response as function of the concentration (Figure 142D). Thus, nylon was selected as support for developing the AgNPs-based sensor.

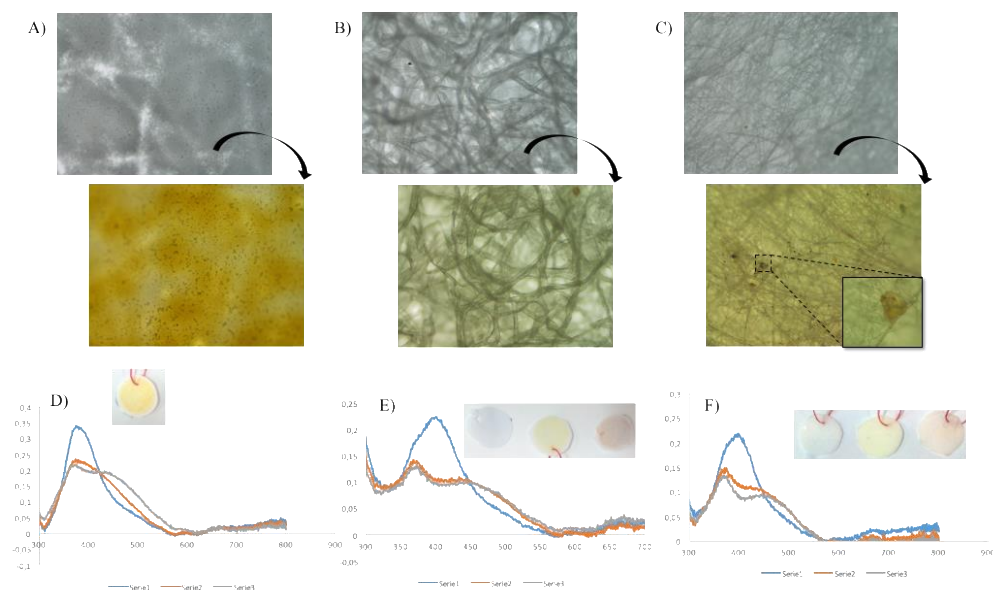


Figure 142. Microscopic images of different kinds of support for AgNP immobilization A) nylon, B) cellulose, C) glass fiber. The scale bar is 100 μm and inset c is 20 μm . Absorbance by DR of the AgNPs immobilized on D) nylon, E) cellulose, F) glass fiber and their response in presence of volatile H_2S (250 and 1000 $\mu\text{L m}^{-3}$). Inset AgNPs immobilized on the membrane and the response at 1000 $\mu\text{L m}^{-3}$.

Nylon membrane was analysed by Raman spectroscopy, showing a characteristic band at 1620 cm^{-1} of amide ($\text{C}=\text{O}$). The increase of the band indicates the bonding of AgNPs to nylon (Figure 143a-b). The shifted to higher wavenumber (from 1618 to 1622 cm^{-1}) and band decrease in presence of VSCs at high levels (Figure 143e-f) compared to the AgNPs nylon (Figure 143b) can be attributed to H_2S interaction on AgNPs surface producing the AgNPs aggregation. The LOD by Raman for S^{-2} was found at 1000 $\mu\text{L m}^{-3}$ in air.

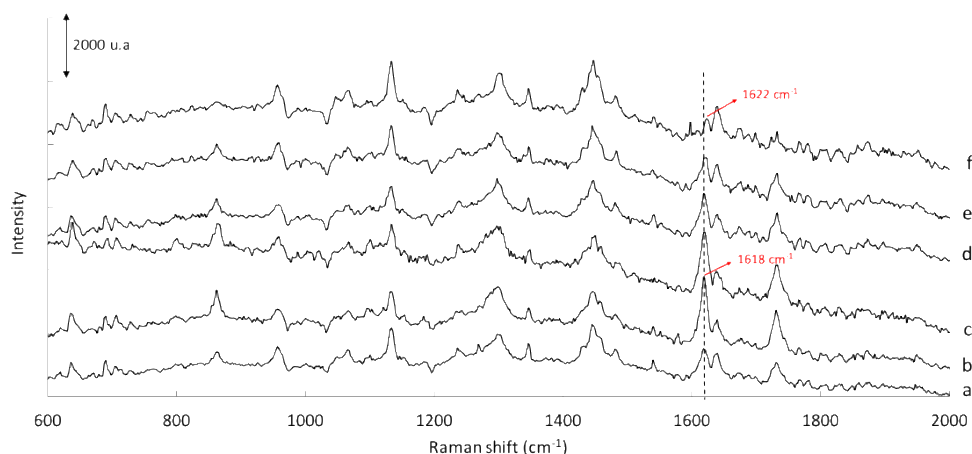


Figure 143. Raman spectra of a) nylon, b) AgNP-nylon and device response to sulphur compounds in c) 250, d) 500, e) 1000, f) 10000 $\mu\text{L m}^{-3}$ levels.

Once the nylon membrane was selected as optimum support and characterized, several porous sizes were studied. Similar AgNPs retention and sensitivity were obtained by using membranes of 0.22 and 0.47 μm , but preferably 0.47 μm . On the other hand, several citrate-AgNPs sizes were tested: 10, 20 and 40 nm. The size of NPs plays an important role in the aggregation with the analyte. Thus, the response of the three sizes of AgNP solution was studied as function of the Na_2S concentration (Figure 144). Color change from yellow to brownish was observed for the three sizes of AgNPs. Similar sensitivity was observed for 10 and 20 nm ($\text{LOD}=45 \mu\text{g L}^{-1}$), whereas 200 $\mu\text{g L}^{-1}$ of LOD was observed for 40 nm of AgNPs. As can be seen in Figure 144, a linear range between 250-10000 $\mu\text{g L}^{-1}$ was obtained by using AgNPs of 20 nm, whereas no satisfactory linear range was obtained by using AgNPs of 10 nm. Therefore, citrate-AgNPs of 20 nm were selected for fabricating nylon-based sensors.

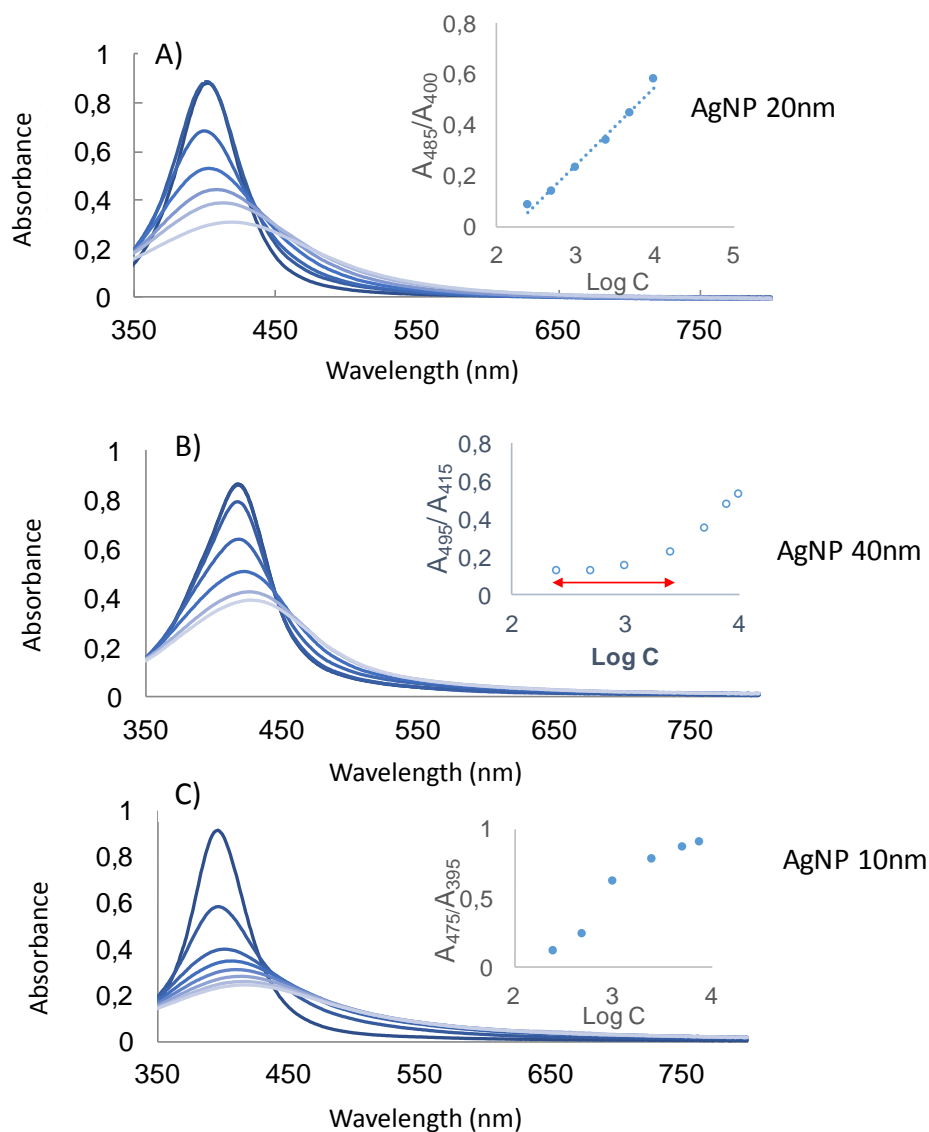


Figure 144. Absorption spectra of AgNPs of 20 nm (A), 40 nm (B) and 10 nm (C) in solution after addition of Na_2S concentrations. Inset: plot of corresponding absorbance ratios vs $\log [S^{2-}]$.

For immobilizing the AgNPs on the membrane, several techniques were tested including deposition, immersion and filtering. The sensors prepared by filtering required shorter time of operation and showed higher yellow color intensity indicating higher retention of NPs. Thus, sensors were fabricated by

filtering AgNPs of 20 nm through nylon membrane (See *Methodology Chapter* for more details).

Colorimetric responses of AgNPs-based sensor

The optimized sensors were tested for quantitative determination of H_2S , CH_3SH and $((\text{CH}_3)_2\text{S})$. The plasmon band at 415 nm decreased and a new band at 550 nm increased due to the aggregation as function of the concentration. The sensor color changed in presence of H_2S and CH_3SH but no in presence of $(\text{CH}_3)_2\text{S}$. *Figure 145* shows the A_{550}/A_{415} ratio vs logarithm of H_2S concentration in the range from 150 to $2500 \mu\text{L m}^{-3}$. The color of the sensor gradually changed from yellow to ochre, and finally to brown when increasing H_2S concentration. Visual inspection of the colored sensors allows a semiquantitative estimation of H_2S concentration (See *photograph inset the Figure 145*). For quantification, absorbance measurements by DR and color intensity measurements by DI were registered. The reaction time was also studied up to 60 min. The time of 10 min were selected as a compromise between the signal and analysis time.

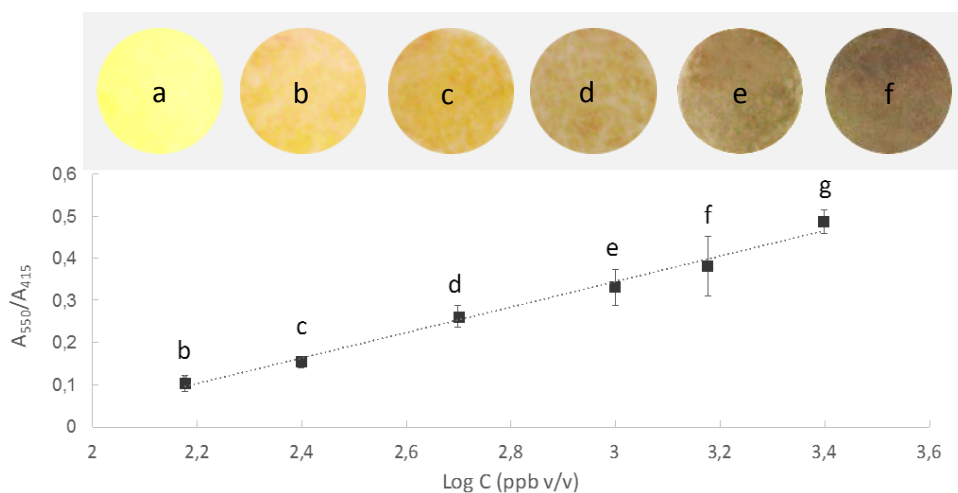


Figure 145. Photography of sensors and calibration curve by plotting A_{550}/A_{415} ratio vs logarithm of H_2S concentrations of 0 (a), 150 (b), 250 (c), 500 (d), 1000 (e), 1500 (f) and 2500 (g) $\mu\text{L m}^{-3}$.

Glycerol effect

After sampling, colored sensors were coated by glycerol (50 μL scattered with a spatula) in order to improve the color intensity and so the sensitivity. The absorbance measured was 2x greater and the color reminded for weeks. The coating by glycerol should be done after sampling maybe due to glycerol preserves AgNPs over aggregation in presence of VSCs.

Analytical permormance

Table 51 shows the calibration equations for sulphur quantification. A linear behavior of analytical signal (A_{550}/A_{415}) versus H_2S concentration was obtained at concentrations up to $2500 \mu\text{L m}^{-3}$. In addition, a linear behavior with lineal correlation of $R^2=0.991$ by using the other analytical signal from DI was also obtained with a calibration equation of $y=(253 \pm 3) + (-0.056 \pm 0.018) x$, where y is the red color intensity from RGB mode and x is the H_2S concentration. Satisfactory precision was evaluated for 20 sensors prepared in the same synthesis. No significative differences were obserbed from different synthesis. *Table 51* also shows the LOD and LOQ calculated as $3 s_{\text{blank}}/b$ and $10 s_{\text{blank}}/b$, respectively, where b is the slope of linear calibration curve and s_{blank} is the standard deviation of the absorbance of ten blanks.

Table 51. Analytical parameters obtained for H_2S determination by AgNPs-nylon based sensor proposed.

Linear range ($\mu\text{L m}^{-3}$)	Linearity $y=a+bx$ ($\text{m}^3 \mu\text{L}^{-1}$)			RSD (%) n=20	LOD ($\mu\text{L m}^{-3}$)	LOQ ($\mu\text{L m}^{-3}$)
	$a \pm s_a$	$b \pm s_b$	R^2			
250-2500	-0.58 ± 0.05	0.31 ± 0.02	0.990	10	45	150

Similar slopes were obtained by using AgNPs-based sensor with glycerol and AgNPs in solution. In spite of the difficulties of NPs synthesis, 3 different bathes of commercial AgNPs were tested and satisfactory precision was obtained. The selectivity was tested against volatile organic compounds interferents in human breath related to different diseases such as ethanol, acetone and ammonia. The sensors did not show colorimetric response for the interferents assayed.

An important limitation of AgNPs is their instability against external factors such as the light. However, this limitation is overcome thanks to the immobilization of AgNPs on nylon membranes. NPs remain stable for three months at room temperature.

Application to breath samples

The applicability of the sensor to detect halitosis was evaluated by analyzing the breath of 10 healthy volunteers. For this purpose, volunteers blew into plastic bags for air sampling containing the AgNPs-sensor. A quantitative analysis was performed by measuring the absorbance by DR and/or color coordinates from DI of sensors. *Figure 146A* shows the sulphur concentration found in samples. As can be seen, the concentration of the samples analyzed was below the concentration considered as persistent bad breath or severe halitosis. In addition, a study on the high-H₂S food intake was carried out. An example of which is the garlic. For this study, 4 volunteers were studied before and after taking a garlic sauce. *Figure 146B* shows the increase in levels of sulphur in breath after taking the garlic-based product.

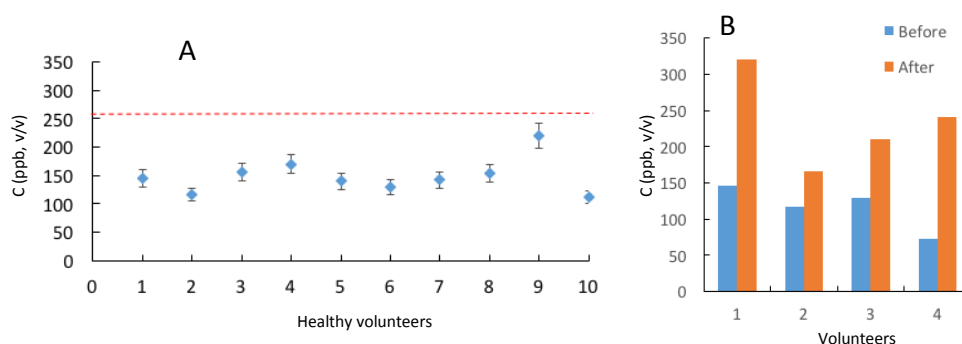


Figure 146. Sulphur concentration found in A) 10 healthy volunteers using AgNPs-based sensor and B) 4 volunteers before (blue bars) and after garlic consumption (orange bars). Average responses and standard deviation for $n = 3$.

For the recovery study, samples were spiked with the analyte at concentrations from 250 to 500 $\mu\text{L m}^{-3}$ by adding 0-100 μL of Na_2S 50 mg L^{-1} and phosphoric acid after blowing. Recovery values were from 98 to 117 % (See Table 52) indicating that matrix effect was not present under the experimental conditions.

Table 52. Recoveries of 2 spiked samples of healthy volunteers obtained by using DR and DI.

Spiked samples ($\mu\text{L m}^{-3}$)	Volunteer 1				Volunteer 2			
	DR		DI		DR		DI	
	Detection ($\mu\text{L m}^{-3}$)	Recovery (%)	Detection ($\mu\text{L m}^{-3}$)	Recovery (%)	Detection ($\mu\text{L m}^{-3}$)	Recovery (%)	Detection ($\mu\text{L m}^{-3}$)	Recovery (%)
0	145	-	151	-	116	-	115	-
250	392	99	367	91	429	117	349	96
300	506	113	475	105	464	111	421	101
500	666	103	601	92	672	109	637	103

Conclusions

A colorimetric sensor for the in-situ determination of VSCs ($\text{R-S}^- \text{ y S}^{-2}$) has been proposed. The developed sensor is based on the citrate capped-AgNPs immobilization on nylon membrane. This is a passive sensor which means that it is zero energy cost. The main advantages of the AgNPs-sensor are the easy and low cost fabrication by using non toxic reagents, as well as its easy of use and no trained personnel requirement. Moreover, the sensor is stable for three months at room temperature. The sensor provides satisfactory LOD of $45 \mu\text{L m}^{-3}$ by measuring the absorbance by DR in a short time (10 min). Furthermore, the method provided suitable linearity and precision. Therefore, the AgNPs-sensor can be considered as a viable clinical kit for on-site VSCs detection in human breath.

CHAPTER 5. GENERAL CONCLUSIONS

The present Thesis is focused on the study of new (nano)materials for the development and improvement of sustainable analytical methodologies for estimating several compounds in fields as diverse as environment, industry, forensic and medicine. The proposed methodologies have been based on the miniaturization and automatization following the new trends in Analytical Chemistry. Thus, the analytical methodologies developed in this Thesis have been aimed at two research lines:

- (i) Miniaturized sample pretreatment techniques and chromatography
- (ii) In-situ analytical sensors

Miniaturized sample pretreatment techniques and chromatography

One of the most important point in the sample pretreatment technique is the use of suitable extractive material. In this Thesis, C₁₈ material has been evaluated in MSPD for the disruption and clean-up, followed by the derivatization onto the dispersant blend of amphetamines in hair matrix. This method have allowed the rapid and simple estimation of AMP, MAMP, EP and MDMA in hair, with LODs of 0.25–0.75 ng mg⁻¹. MSPD is considered a cost-effective alternative to classical multi-step methods for sample pretreatment due to the analytical process is simplified and thus, the sample and solvent consumption is reduced. On the other hand, peptide-based MOF has been proposed as chiral phase in SPE for the enantioselective separation of (±)-MAMP and (±)-EP. Cu(GHG) MOF has been capable of separating >50 % of (+)-EP from a racemic mixture in only 4 min when it is used in a chiral SPE cartridge. This is a promising result, considering the limited availability of SPE cartridges for chiral separation on the market. SPE allows the isolation of the analytes prior the determination technique although it is not a miniaturized technique. According to the principles of Green Analytical Chemistry, a miniaturized and automated technique such as in valve IT-SPME has been used in this Thesis, where PDMS has been played an important role as extractive phase.

In-valve IT-SPME modality coupled to CapLC allows to carry out the preconcentration, clean-up and analysis of the sample in a one-step, which means an automatization of the analytical process. Thus, IT-SPME is governed by the minimization of solvents consumption and waste generation, energy-efficiency, as well as the reduction of sample handling and analysis time. In this sense, in-valve

IT-SPME-CapLC avoids the contamination of the sample and the loss of the analyte. In addition, improvements in the reliability of the analytical performance parameters, such as sensitivity, precision and accuracy can be achieved. The configuration proposed, in flow-through IT-SPME, is based on a polymeric-coated capillary column as injection loop of the valve where the analytes are adsorbed in order to be preconcentrated; and then desorbed and transferred to the chromatographic system by the mobile phase.

In this Thesis, in-valve IT-SPME-CapLC combined with DAD or FLD has been proposed to estimate DEHP in sediments and water, BAK in industrial biocide formulation, DPA deposited on shooter hands and amphetamine-like drugs in oral fluid.

The estimation of DEHP in sediments and water by combining MSPD using C_{18} as sorbent phase and IT-SPME-CapLC-DAD using $PDMS_{95}$ -based capillary column has been successfully carried out in less than 20 min. Satisfactory LODs of 270 and $90 \mu\text{g kg}^{-1}$ (for 0.1 and 0.3 g of sediment, respectively) were obtained to control environmental quality. Moreover, the reduction of sample and solvent consumption, as well as the extraction steps, can avoid the risk of DEHP contamination.

The versatility of IT-SPME-CapLC-DAD with $PDMS_{65}$ -based extractive phase for BAK homologues analysis in mixtures of biocides has been demonstrated. The proposed method has shown that the evaluation of matrix effect is required for analyzing BAK in mixtures of biocides. Different effects have been observed depending on the co-biocide type present (ADP and TMTDAC), ratio co-biocide/BAK homologue and total surfactant amount, these maybe due to the formation of mixed micelles. In all cases, C_{12} -homologue response was more affected than C_{14} -homologue response. Thus, the method proposed is a cost-effective way to control industrial processes where BAK is considered as unwanted compound in a formulation.

The estimation of DPA for forensic investigations has been successfully carried out by selecting the optimum $PDMS$ -based extractive phase for the capillary column. Satisfactory LOD of 3 ng of DPA has been achieved by using $PDMS_{65}$. The utility of the proposed method has been well tested by estimating the DPA collected by cotton swab from shooter hands and extracted by vortex-assisted conditions.

PDMS-based capillary columns have been functionalized with CNTs (MWCNTs and SWCNTs) in order to enhance the extraction capability. Nanostructured coatings offer high surface-to-volume ratio, thus increasing the extraction efficiency to extend the applicability of in-valve IT-SPME to those analytical problems in which the volume of sample is limited such as oral fluid. The presence of MWCNTs in the extractive coatings has enhanced the extraction efficiency and also has improved the chromatographic profiles, thus resulting in a reliable option for the analysis of amphetamines in saliva. Samples have been easily collected by a cotton swab and have directly been derivatized and processed by in-valve IT-SPME-CapLC-FLD. The proposed method is very simple and cost-effective, and provided suitable selectivity, precision and sensitivity at $\mu\text{g mL}^{-1}$ concentration levels (LODs of 0.5–0.8 $\mu\text{g mL}^{-1}$).

Satisfactory analytical parameters and application to samples have been obtained by IT-SPME-CapLC in the works described in this Thesis. These results have demonstrated the suitability of the IT-SPME-CapLC method to detect several analytes in different kinds of matrices in line with the Green Analytical Chemistry principles.

In-situ analytical sensors

The second approach of this Thesis has been the development of colorimetric sensors that allow the on-site analysis via visual inspection, spectroscopic techniques and/or DI processing. Following the current trends in technology, image analysis by smartphones is an emerging alternative to spectroscopic techniques for quantification purposes. The use of mobile phones with color image processing software allows an easy, rapid and cost-effective analysis without the requirement of highly trained personnel and expensive instrumentation.

In this Thesis, the developed sensors has been based on the derivatizing reagents (NQS and $\text{Co}(\text{SCN})_2$) embedding into PDMS-based support and on the other hand, the immobilization of AgNPs on nylon support. In both cases, analytes interact with the derivatizing reagents or the NPs in the solid sensor changing the color of the sensor. Absorbance by DR or color intensity by DI have been measured for quantitative purposes. Semiquantitative analysis can be performed

by visual inspection. In addition, electromechanical sensors such as screen-printing piezoelectric cantilevers have been also tested as sensors.

In this Thesis, in-situ sensors have been developed for estimating casein in wastewaters generated by the dairy industry, ADP in industrial products, amphetamine-like drugs and ketamine in illicit street pills/powders, as well as, VSCs from the breath.

A sensor based on PDMS/TEOS/SiO₂NPs/NQS to determine casein with good sensitivity and precision (LOD = 15 mg L⁻¹; RSD ≤ 12 %) has been also proposed. This sensor overcomes one of the main limitations of the conventionally used BCA assay, the degradation of the reagents. Taking into account the advantages of rapidity, simplicity and stability, the polymeric sensor is expected to have practical applications for in-situ determination of casein in effluents from dairy industries.

The sensor based on PDMS/TEOS/SiO₂NPs/NQS for estimating the biocide ADP in industrial formulations has achieved satisfactory LOD of 0.018 % (w/w) and precision (RSD ≤ 12 %). This sensor allows a green, robust, portable, cost-effective and rapid approach for controlling ADP, suggesting good prospects for its implementation in several industries.

A colorimetric kit based on PDMS/TEOS/SiO₂NPs/NQS sensor for the in-situ identification and determination of several kinds of amphetamine-type drugs (MDA, AMP, MAMP, MDMA) in illicit samples has been developed. Satisfactory LODs (0.002-0.005 g mL⁻¹) and RSD < 10 % have been achieved. In the same way of illicit drug samples, another kit based on PDMS/Co(SCN)₂ for estimating ketamine with a LOD of 30 µg and good precision (RSD < 10%) has been developed. Both kits are very useful tools for the instant screening of the most frequently used illicit drugs in roadside drug testing owing to its simplicity, rapidity, stability and portability, at a very low-cost. Uncertainty and delay times could be minimized through the development of this workplace test.

In respect of AgNPs-nylon based sensor, VSCs (-S⁻², -S⁻) have been satisfactory estimated with LODs of 45 µL m⁻³. This passive sensor does not require an external energy source and so, this energy cost is zero. The advantages such as stability, simplicity, rapidity (10 min) and low-cost make them a potential point-of-care testing for oral malodour as well as in atmospheres or enclosed areas.

Finally, screen-printing piezoelectric microcantilevers have been tested as gas sensors. New fabrication procedure, design and sintering aid composition have been studied. Satisfactory electromechanical properties have been achieved with 0.75% Li_2O_3 , 1.2% Bi_2O_3 and 1.05% CuO composition. The use of a polymeric commercial material for the sacrificial layer have been simplified the fabrication procedure due to it is removed during the firing step. Successful functionalization by MCF dispersion has been carried out ($8 \text{ Hz } \mu\text{g}^{-1}$ mass sensitivity). The low sensitivity (0.1 Hz ppm^{-1}) to humidity suggests a potential applicability as sensor to estimate VOCs for environmental purposes.

Therefore, the in-situ sensors proposed in this Thesis can be considered a suitable alternative to conventional instrumental methods. The immobilization of the reagents in PDMS and nylon has avoided the need to prepare solutions to carry out the reaction, as well as, expensive equipment has not required.

In conclusion, the (nano)materials studied in this Thesis has been covered two of the new trends in Analytical Chemistry:

- The development of analytical strategies that reduce the steps of the sample pretreatment and minimize the environmental impact.
- The development of rapid, simple and cost-effective sensors for on-site analysis.

The importance of (nano)materials to develop analytical methodologies have been demonstrated in this Thesis:

1. PDMS is an excellent extractive material as well as an optimal encapsulant of derivatizing reagents thanks to its coefficient partition, permeation and optical transparency.
2. C_{18} is a widely used sorbent material in MSPD due to its hydrophobicity and easy packing.
3. MCF silica is a material with a potential applicability as sensing layer for resonant microcantilevers owing to its high surface area.

4. CNTs functionalized on commercial capillary columns improve the extraction efficiencies and chromatographic profiles for analytes that interact through π - π stacking interaction.
5. The peptide MOF Cu(GHG) is a well-suited material for enantioselective recognition due to the preferential binding of one of the enantiomers due to stronger or additional H-bonds with the framework.
6. AgNPs can be used for colorimetric nylon-based sensor to sensitive detections.

Table 53 summarizes the applications and results obtained in this Thesis for the materials used.

Table 53. Summary of the application and results obtained in this Thesis for the materials used.

Material	PDMS as extractive phase	PDMS as sensor support	C ₁₈	MCF mesoporous silica	CNTs	MOF	AgNPs
Format	Capillary column coating	Film	SPE cartridge	Deposited layer on electrode	Capillary column coating	SPE cartridge	Immobilized on nylon
Sample preparation	IT-SPME	-	MSPD	-	IT-SPME	SPE	-
Separation technique	Cap-LC	-	HPLC	-	Cap-LC	HPLC	-
Detection technique	DAD	Absorbance (DR mode) and color intensity	FL	Impedance	FL	FL	Absorbance (DR mode) and color intensity
Matrix	Sediments/water ^a Industrial product ^b Hands ^c	Effluents ^d Industrial product ^e Illicit drug sample ^{f,g}	Hair	Air	Oral fluid	-	Human breath
Analyte	DEHP ^a BAK ^b DPA ^c	Casein ^d ADP ^e Amphetamine-like drugs ^f Ketamine ^g	AMP, MAMP, EP, MDMA	Humidity	AMP, MAMP, EP	MAMP, (±)-EP and (±)-MAMP	VSCs
Time	9 min ^a 12 min ^b <11 min ^c	10 min	20 min	15 min	10 min	4 min	10 min
LOD	8 µg L ^{-1,a} 0.03-0.006 µg mL ^{-1,b} 0.15 ng mL ^{-1,c}	15 mg L ^{-1,d} 0.018 % ^e 0.002-0.005 g mL ^{-1,f} 30 µg ^g	0.25-0.75 ng mg ⁻¹	-	0.5-0.8 µg mL ⁻¹	-	45 ppb (v/v)
Cost	+++	+	+++	++	+++	+++	+
Toxicity	no	no	yes	no	no	no	no
Portability	no	yes	no	yes	no	no	yes

^aMuñoz-Ortuño, M. et al., 2014; ^bPrieto-Blanco, M.C. et al., 2016; ^cArgente-García, A. et al.2018(draft paper), ^dMuñoz-Ortuño, M. et al., 2015; ^eArgente-García, A. et al., 2016a; ^fArgente-García, A. et al., 2016b; ^gArgente-García, A. et al., 2017

Future perspectives

IT-SPME-CapLC is an interesting approach thanks to the preconcentration, clean-up and analysis can be carried out in one step. Thus, waste generation, solvents consumption and costs are minimized. However, the extraction efficiencies are not enough quantitative. Thus, the research of MINTOTA group is directed towards the coating of capillary columns with nanomaterials, thanks to the project CTQ2014-53916P. Due to the extension of the use of nanomaterials, their study by LC is an emerging research field. In this context, MINTOTA group has studied AuNPs and AgNPs by Cap-LC (*González-Fuenzalida, R.A. et al., 2016a*). Following this work, the characterization of AuNPs with different end-capping is carried out by NanoLC, work in process.

On the other hand, the development of devices that allows an in-situ and green analysis without the need of trained personnel and expensive equipment are one of the goals of the nowadays chemistry. The development of analytical tools based on color modes is causing a revolution due to the costs are significantly minimized when a quantitative analysis is required. Thus, this technology could be implemented in resource-poor settings. Moreover, biodegradable materials from natural products (e.g. proteins, polysaccharides, etc.) are studied as supports for sensors developing thanks to PROMETEO 2016/109 project. From the results obtained, a project *“Valoritza i Transfereix 2016-2017”* of the University of Valencia entitled *“Proyecto piloto basado en el empleo de kits para la evaluación de la contaminación en entornos ambientales de diferente naturaleza”* has been developed. Several companies have collaborated to validate the in-situ sensors. Taking into account the interdisciplinary and knowledge transfer requirement, the research carried out in this Thesis has been applied to solve industrial, environmental, forensic and clinical problems. Some works of this Thesis has been carried out in collaboration with other research groups from different fields such as inorganic chemistry (FuniMmat Group, Instituto de Ciencia Molecular, Universidad de Valencia) and medicine (Project VLC-BIOMED 2016, B Programme, *“Desarrollo de un prototipo sensible para la detección de gas sulfhídrico que permita la identificación de nuevos fármacos cardioprotectores”*).

The study of more sustainable (nano)materials to improve or develop new analytical applications has been the key point of the present Thesis as well as one of the main goals of many future research.

REFERENCES

- Adarsh, N., Shanmugasundaram, M., Ramaiah, D., 2013. Efficient reaction based colorimetric probe for sensitive detection, quantification, and on-site analysis of nitrite ions in natural water resources. *Anal. Chem.* 85, 10008-10012.
- Aguilar, C., Janssen, H.G., Cramers, C.A., 2000. On-line coupling of equilibrium-sorptive enrichment to gas chromatography to determine low-molecular-mass pollutants in environmental water samples. *J. Chromatogr. A* 867, 207–218.
- Alagirisamy, N., Hardas, S., Jayaraman, S., 2010. Novel colorimetric sensor for oral malodour. *Anal. Chim. Acta* 661, 97–102.
- Alatrisme-Mondragon, F., Iranpour, R., Ahring, K.K., 2003. Toxicity of di-(2-ethylhexyl) phthalate on the anaerobic digestion of wastewater sludge. *Water Res.* 37, 1260-169.
- Alkadir, R.S.J., Ornatska, M., Andreescu, S., 2012. Colorimetric Paper Bioassay for the Detection of Phenolic Compounds. *Anal. Chem.* 84 (22), 9729–9737.
- Alula, M.T., Karamchand, L., Hendricks, N.R., Blackburn, J.M., 2018. Citrate-capped silver nanoparticles as a probe for sensitive and selective colorimetric and spectrophotometric sensing of creatinine in human urine. *Anal. Chim. Acta.* 1007, 40-49.
- Aminian, M., Nabatchian, F., Vaisi-Raygani, A., Torabi, M., 2013. Mechanism of Coomassie Brilliant Blue G-250 binding to cetyltrimethylammonium bromide: an interference with the Bradford assay. *Anal. Biochem.* 434, 287–291.
- Amou, T., Hinode, D., Yoshioka, M., Grenier, D., 2014. Relationship between halitosis and periodontal disease - associated oral bacteria in tongue coatings. *Int. J. Dent. Hyg.* 12(2), 145-51.
- Anastas, P.T., Warner, J.C., 1998. *Green Chemistry: Theory and Practice*, Green Chem. Theory Pract. Oxford Univ. Press, New York.

- Andrade, M.A., Lancas, F.M., 2017. Determination of ochratoxin A in wine by packed in-tube solid phase microextraction followed by high performance liquid chromatography coupled to tandem mass spectrometry. *J. Chromatogr. A* 1493, 41-48.
- Argente-García, A., Muñoz-Ortuño, M., Molins-Legua, C., Moliner-Martínez, M., Campíns-Falcó, P., 2016a. A solid Device based on doped hybrid composites for controlling the dosage of the biocide N-(3-aminopropyl)-N-dodecyl-1,3- propanediamine in industrial formulations. *Talanta* 147, 147–154.
- Argente-García, A., Jornet-Martínez, N., Herráez-Hernández, R., Campíns-Falcó, P., 2016b. A solid colorimetric sensor for the analysis of amphetamine-like street samples. *Anal. Chim. Acta* 943, 123-130.
- Argente-García, A., Moliner-Martínez, Y., López-García, E., Campíns-Falcó, P., Herráez-Hernández, R., 2016c. Application of Carbon Nanotubes Modified Coatings for the Determination of Amphetamines by In-Tube Solid-Phase Microextraction and Capillary Liquid Chromatography. *Chromatography* 3, 7-21.
- Argente-García, A., Moliner-Martínez, Y., Campíns-Falcó, P., Verdú-Andrés, J., Herráez-Hernández, R., 2016d. Determination of amphetamines in hair by integrating sample disruption, clean-up and solid phase derivatization. *J. Chromatogr. A*, 1447, 47–56.
- Argente-García, A., Jornet-Martínez, N., Herráez-Hernández, R., Campíns-Falcó, P., 2017. A passive solid sensor for in-situ colorimetric estimation of the presence of ketamine in illicit drug samples. *Sens. Actuator B* 253, 1137–1144.
- Argente-García, A., L. Hakobyan, Moliner-Martínez, Y., Herráez-Hernández, R., Campíns-Falcó, P., 2017. Sensitive on-line miniaturized method for estimating diphenylamine deposited on shooter hands as a forensic tool. *Submitted*.
- Arndt, J., Bell, S., Crookshanks, L., Lovejoy, M., Oleska, C., Tulley, T., Wolfe, D.,

2012. Preliminary evaluation of the persistence of organic gunshot residue. *Forensic Sci. Int.* 222(1-3), 137–145.
- Arthur, C.L., Pawliszyn, J., 1990. Solid phase microextraction with thermal desorption using fused silica optical fibers. *Anal. Chem.* 62, 2145– 2148.
- Ash, M., Ash, I., 2004. *Handbook of Preservatives*, Synapse InfoResources; Endicott, NY, USA.
- Asiabi, H., Yamini, Y., Seidi, S., Shamsayei, M., Safari, M., Rezaei, F., 2016a. On-line electrochemically controlled in-tube solid phase microextraction of inorganic selenium followed by hydride generation atomic absorption spectrometry. *Anal Chim Acta.* 922, 37-47.
- Asiabi, H., Yamini, Y., Seidi, S., 2016b. Preparation and evaluation of a novel molecularly imprinted polymer coating for selective extraction of indomethacin from biological samples by electrochemically controlled in-tube solid phase microextraction. *Anal. Chim. Acta* 913, 76-85.
- Aufartová, J., Torres-Padron, M.E., Sosa-Ferrera, Z., Solich, P., Santana-Rodriguez, J.J., 2012. Optimization of an in-tube solid-phase microextraction method coupled with HPLC for determination of some oestrogens in environmental liquid samples using different capillary columns, *Int. J. Environ. Anal. Chem.* 92, 382-396.
- Baciu, T., Borrull, F., Aguilar, C., Calull, M., 2015. Recent trends in analytical methods and separation techniques for drugs of abuse in hair. *Anal. Chim. Acta* 856, 1–26.
- Bahzadi, M., Noroozian, E., Mirzaei, M., 2013. A novel coating based on carbon nanotubes/poly-orthophenylenediamine composite for headspace solid-phase microextraction of polycyclic aromatic hydrocarbons. *Talanta* 108, 66–73.
- Bailey, M. J., Kirkby, K. J., Jeynes, C., 2009. Trace element profiling of gunshot residues by PIXE and SEM-EDS: a feasibility study. *X-Ray Spectrometry.* 38(3), 190–194.

- Bala, R., Mittal, S., Sharma, R.K., Wangoo, N., 2018. A supersensitive silver nanoprobe based aptasensor for low cost detection of malathion residues in water and food samples. *Spectrochim. Acta A* 196, 268-273.
- Bao, Y.Y., Xy, P.C., Cai, S.R., Yu, H.T., Li, X.X., 2018. Detection of volatile-organic-compounds (VOCs) in solution using cantilever-based gas sensors. *Talanta* 182, 148-155.
- Barker, S.A., 2007. Matrix solid phase dispersion (MSPD). *J. Biochem. Biophys. Methods.* 70, 151-162.
- Bassarab, P., Williams, D., Dean, J.R., Ludkin, E., Perry, J.J., 2011. Determination of quaternary ammonium compounds in seawater samples by solid-phase extraction and liquid chromatography–mass spectrometry. *J. Chromatogr. A* 1218, 673–677.
- Beck, J. S., Vartuli, J. C., Roth, W. J., Leonowicz, M. E., Kresge, C. T., Schmitt, K. D., Sheppard, E. W., 1992. A new family of mesoporous molecular sieves prepared with liquid crystal templates. *J. Am. Chem. Soc.* 114, 10834–10843.
- Belay, K., 2016. Advanced analytical microextraction techniques and their applications: A review, *J. Biol. Agric. Healthc.* 6, 13–20.
- Bernal Morales, E., Revilla Vázquez, A. L., 2004. Simultaneous determination of inorganic and organic gunshot residues by capillary electrophoresis. *J. Chromatogr. A*, 1061(2), 225–233.
- Betts, T.A., Tipple, C.A., Sepaniak, M.J., Datskos, P.G., 2000. Selectivity of chemical sensors based on micro-cantilevers coated with thin polymer films. *Anal. Chim. Acta* 422, 89–99.
- Biedermann-Brem, S., Biedermann, M., Pfenninger, S., Bauer, M., Altkofer, W., Rieger, K., Hauri, U., 2008. Plasticizers in PVC toys and childcare products:

- what succeeds the phthalates? market survey 2007. *Chromatographia* 68 (3), 227-234.
- Bin, L., Zhang, X.-X., Huang, H.-Y., Chen, L.-Q., Cui, J.-H., Liu, Y., Jin, H., Lee, B.-J., Cao, Q.-R., 2018. Effective deactivation of A549 tumor cells in vitro and in vivo by RGD-decorated chitosan-functionalized single-walled carbon nanotube loading docetaxel. *Int. J. Pharm.* 543, 8-20.
- Biondi, C.A.M., 2011. Applying the precautionary principle to consumer household cleaning product development. *J. Clean. Prod.* 19, 429–437.
- Bloch, E. D., Queen, W. L., Krishna, R., Zadrozny, J. M., Brown, C. M., Long, J. R., 2012. Hydrocarbon separations in a metal-organic framework with open iron(II) coordination sites. *Science* 335, 1606-1610.
- Bodas, D., Khan-Malek, C., 2007. Hydrophilization and hydrophobic recovery of PDMS by oxygen plasma and chemical treatment—an SEM investigation. *Sens. Actuators B Chem.* 123, 368–373.
- Boisen, A., Dohn, S., Keller, S., Schmid, S., and Tenje, M., 2011. Cantilever-like micromechanical sensors. *Rep. Prog. Phys.* 74(3), 36101-36132.
- Bolle, C.M., Beikler, T., 2012. Halitosis: the multidisciplinary approach. *Int. J. Oral. Sci.* 4(2), 55-63.
- Bouchaala, A., Nayfeh, A. H., Younis. M. I., 2016. Frequency shifts of micro and nanocantilever beam resonators due to added masses. *J. Dyn. Sys., Meas., Control.* 138, 91002-91011.
- Boudjiet, M.-T., Bertrand, J., Mathieu, F. Nicu, L., Mazenq, L., Leïchlé, T., Heinrich, S., Pellet, C., Dufour, I., 2015. Geometry optimization of uncoated silicon microcantilever-based gas density sensors. *Sens. Actuators, B.* 208, 600-607.
- Boyacı, E., Sparham, C., Pawliszyn, J., 2014. Thin-film microextraction coupled to LC-ESI-MS/MS for determination of quaternary ammonium compounds in water samples. *Anal. Bioanal. Chem.* 406, 409–420.

- Brozek-Mucha, Z., 2007. Comparison of cartridge case and airborne GSR-a study of the elemental composition and morphology by means of SEM-EDX. *X-Ray Spectrom.* 36(6), 398-407.
- Bu, Y., Feng, J., Sun, M., Zhou, C., Luo, C., 2016. Gold-functionalized stainless-steel wire and tube for fiber-in-tube solid-phase microextraction coupled to high-performance liquid chromatography for the determination of polycyclic aromatic hydrocarbons. *J. Sep. Sci.* 39, 932-938.
- Burleson, G. L., Gonzalez, B., Simons, K., Yu, J. C. C., 2009. Forensic analysis of a single particle of partially burnt gunpowder by solid phase microextraction-gas chromatography-nitrogen phosphorus detector. *J. Chromatogr. A*, 1216(22), 4679–4683.
- Cadiau, A., Adil, K., Bhatt, P. M., Belmabkhout, Y., Eddaoudi, M., 2016. A metal-organic framework-based splitter for separating propylene from propane. *Science* 353, 137-140.
- Caelen, I., Kalman, A., Wahlström, L., 2004. Biosensor-Based Determination of Riboflavin in Milk Samples. *Anal. Chem.* 76, 137–143.
- Camilleri, A.M., Caldicott, D., 2005. Underground pill testing, down under. *Forensic Sci. Int.* 151, 53-58.
- Campíns-Falcó, P., Verdú-Andrés, J., Sevillano-Cabeza, A., Molins-Legua, C., Herráez-Hernández, R., 2008. New micromethod combining miniaturized matrix solid phase dispersion and in-tube-in-valve solid phase microextraction for estimating polycyclic aromatic hydrocarbons in bivalves. *J. Chromatogr. A* 1211, 13-21.
- Campíns-Falcó, P., Herráez-Hernández, R., Verdú-Andrés, J., Cháfer-Pericas, C., 2009. Online determination of aliphatic amines in water using in-tube solid-phase microextraction- assisted derivatization in in-valve mode for processing large sample volumes in LC. *Anal. Bioanal. Chem.* 394, 557-565.
- Campíns-Falco, P., Verdú-Andrés, J., Sevillano-Cabeza, A., Herráez-Hernández, R., Molins-Legua, C., Moliner-Martínez, Y., 2010. In-tube solid phase

- microextraction coupled by in-valve mode to capillary LC-DAD: improving the detectability to multiresidue organic pollutants analysis in several whole waters. *J. Chromatogr. A* 1217, 2695-2702.
- Campíns-Falcó, P., Moliner-Martínez, Y., Herráez-Hernández, R., Molins-Legua, C., Verdú-Andrés, J., Jornet-Martínez, N., 2016. Passive sensor for in situ detection of amines in chemical industries. Patent 201300436.
- Capitán-Vallvey, L.F., López-Ruiz, N., Martínez-Olmos, A., Erenas, M.M., Palma, A.J., 2015. Recent developments in computer vision-based analytical chemistry: a tutorial review. *Anal. Chim. Acta* 899, 23-56.
- Capriotti, A. L., Cavaliere, C., Giansanti, P., Gubbiotti, R., Samperi, R., Laganà, A., 2010. Recent developments in matrix solid-phase dispersion extraction. *J. Chromatogr. A* 1217, 2521-2532.
- Cardinetti, B., Ciampini, C., D'Onofrio, C., Orlando, G., Gravina, L., Ferrari, Di Tullio, D., Torresi, L., 2004. X-ray mapping technique: A preliminary study in discriminating gunshot residue particles from aggregates of environmental occupational origin. *Forensic Sci. Int.* 143(1), 1–19.
- Cháfer-Pericas, C., Campíns-Falcó, P., Herráez-Hernández, R., 2004. Application of solid-phase microextraction combined with derivatization to the determination of amphetamines by liquid chromatography. *Anal. Biochem.* 333, 328-335.
- Cháfer-Pericás, C., Herráez-Hernández, R., Campíns-Falcó, P., 2006. On-fibre solid-phase microextraction coupled to conventional liquid chromatography versus in-tube solid-phase microextraction coupled to capillary liquid chromatography for screening analysis of triazines in water samples, *J. Chromatogr. A* 1125, 159-171.
- Cháfer-Pericás, C., Herráez-Hernández, R., Campíns-Falcó, P., 2007. In-tube solid-phase microextraction-capillary liquid chromatography as a solution for the screening analysis of organophosphorus pesticides in untreated environmental water samples. *J. Chromatogr. A* 1141,10-21.

- Cháfer-Pélicas, C., Campíns-Falcó, P., Prieto-Blanco, M. C., 2008. Automatic in-tube SPME and fast liquid chromatography: A cost-effective method for the estimation of dibutyl and di-2-ethylhexyl phthalates in environmental water samples. *Anal. Chim. Acta* 610, 268-273.
- Chai, F., Wang, C., Wang, T., Ma, Z., Su, Z., 2010. L-cysteine functionalized gold nanoparticles for the colorimetric detection of Hg²⁺ induced by ultraviolet light. *Nanotechnology* 21, 25501-25507.
- Chaler, R., Cantón, L., Vaquero, M., Grimalt, J.O., 2004. Identification and quantification of *n*-octyl esters of alkanolic and hexanedioic acids and phthalates as urban waste water markers in biota and sediments from estuarine areas. *J. Chromatogr. A* 1046, 203-210.
- Chang, J., Li, H., Hou, T., Li, F., 2016. Paper-based fluorescent sensor for rapid naked eye detection of acetylcholinesterase activity and organophosphorus pesticides with high sensitivity and selectivity, *Biosens. Bioelectron.* 86, 971–977.
- Chang, N., Gu, Z-Y., Wang, H-F., Yan, X-P., 2011. Metal-organic-framework-based tandem molecular sieves as a dual platform for selective microextraction and high-resolution gas chromatographic separation of n-alkanes in complex matrixes. *Anal. Chem.* 83(18), 7094-7101.
- Chang, Y.J., Chao, M.-R., Chen, S.-C., Chen, C.-H., Chang, Y.Z., 2014. A high-throughput method based on microwave-assisted extraction and liquid chromatography-tandem mass spectrometry for simultaneous analysis of amphetamines ketamine, opiates, and their metabolites in hair. *Anal. Bioanal. Chem.* 406, 2445–2455.
- Chaplan, C.A., Mitchell, H.T., Martinez, A.W., 2014. Paper-based standard addition assays, *Anal. Methods.* 6, 1296-1301.
- Chaudhary, M., Gupta, A., 2009. Microcantilever-based sensors. *Def. Sci. J.* 59(6), 634-641.

- Chaves, A.R., Silva, B.J., Lanças, F.M., Queiroz, M.E., 2011. Biocompatible in-tube solid-phase microextraction coupled with liquid chromatography-fluorescence detection for the determination of interferon $\alpha 2a$ in plasma samples. *J. Chromatogr. A* 1218, 3376-3381.
- Chaves, A.R., Queiroz, M.E.U., 2013a. Immunoaffinity in tube solid phase microextraction coupled with liquid chromatography with fluorescence detection for determination of interferon alpha in plasma samples. *J. Chromatogr. B Analyt. Technol. Biomed. Life Sci.* 928, 37-43.
- Chaves, A.R., Queiroz, M.E.C., 2013b. In-tube solid-phase microextraction with molecularly imprinted polymer to determine interferon alpha 2a in plasma sample by high performance liquid chromatography. *J. Chromatogr. A* 1318, 43-48.
- Chen, G.H, Chen, W.-Y., Yen, Y.-C., Wang, C.-W., Chang, H.-T., Chen, C.-F., 2014. Detection of Mercury(II) Ions Using Colorimetric Gold Nanoparticles on Paper-Based Analytical Devices. *Anal. Chem.* 86 (14), 6843–6849.
- Chen, W., Fang, X., Li, H., Cao, H., Kong, J., 2016. A simple paper-based colorimetric device for rapid mercury (II) assay. *Sci. Rep.* 6, 31948-31954.
- Chen, Y., Drogeb, S.T.J., Hermensa, J.L.M. 2012. Analyzing freely dissolved concentrations of cationic surfactant utilizing ion-exchange capability of polyacrylate coated solid-phase microextraction fibers. *J. Chromatogr. A* 1252, 15–22.
- Chen, Y.-C., Lee, I. L., Sung, Y.-M., Wu, S.-P., 2013. Colorimetric detection of Al^{3+} ions using triazole-ether functionalized gold nanoparticles. *Talanta* 117, 70-74.
- Chen, Y., Zilberman, Y., Mostafalu, P., Sonkusale, S.R., 2015. Paper based platform for colorimetric sensing of dissolved NH_3 and CO_2 . *Biosensors & Bioelectronics.* 67, 477-484.
- Cheng, W.-C., Ng, K.-M., Chan, K.-K., Mok, V.K.-K., Cheung, B.K.-L., 2007. Roadside detection of impairment under the influence of ketamine—

- evaluation of ketamine impairment symptoms with reference to its concentration in oralfluid and urine. *Forensic Sci. Int.* 170, 51–58.
- Chin, C.D., Linder, V., Sia, S.K., Daar, A.S., Thorsteinsdottir, H., Martin, D.K., 2007. Lab on-a-chip devices for global health: Past studies and future opportunities, *Lab Chip.* 7, 41–57.
- Choodum, A., Kanatharana, P., Womgniramaikul, W., 2015. A sol-gel colorimetric sensor for methamphetamine detection. *Sens. Actuat. B* 215, 553-560.
- Christodouleas, D.C., Nemiroski, A., Kumar, A.A., Whitesides, G.M., 2015. Broadly available imaging devices enable high-quality low-cost photometry, *Anal. Chem.* 87, 9170–9178.
- Chutipongtanate, S., Watcharatanyatip, K., Homvises, T., Jaturongkakul, K., Thongboonkerd, V., 2012. Systematic comparisons of various spectrophotometric and colorimetric methods to measure concentrations of protein, peptide and amino acid: detectable limits, linear dynamic ranges, interferences, practicality and unit costs. *Talanta* 98, 123–129.
- Clément, P., Del Castillo Perez, E., Gonzalez, O., Calavia, R., Lucat, C., Llobet, E., Debéda, H., 2016. Gas discrimination using screen-printed piezoelectric cantilevers coated with carbon nanotubes. *Sens. Actuators, B* 237, 1056–1065.
- Coffey, C.C., Pearce, T.A., 2010. Direct-reading Methods for Workplace Air Monitoring. *J. Chem. Health. Saf.* 17, 10-21.
- Commercial Pool Test kits. Walmart Web Portal. <https://www.walmart.com/c/kp/pool-test-kits> (accessed 02 May 2018).
- Cui, X-Y., Gu, Z-Y., Jiang, D-Q., Li, Y., Wang, H-F., Yan, X-P., 2009. In situ hydrothermal growth of metal-organic framework 199 films on stainless steel fibers for solid-phase microextraction of gaseous benzene homologues. *Anal. Chem.* 81(23), 9771-9777.

- Dalby, O., Butler, D., Birkett, J. W., 2010. Analysis of gunshot residue and associated materials - A review. *J. Forensic Sci.* 55(4), 924–943.
- Debéda, H., Lakhmi, R., Lucat, C., Dufour, I., 2013. Use of the longitudinal mode of screen-printed piezoelectric cantilevers coated with PEUT for toluene detection: Comparison with silicon cantilevers. *Sens. Actuators, B* 187, 198–203.
- Debéda, H., Lucat, C., 2014. Feasibility of screen-printed PZT microceramics for structural health monitoring applications. *Int. J. Appl. Ceram. Technol.*, 11 (3), 413–421.
- Debéda, H., Clément, P., Llobet, E., Lucat, C., 2015. One-step firing for electroded PZT thick films applied to MEMS. *Smart Mater. Struct.* 24, 25020-25028.
- Demoranville, T., Verkouteren, J.R., 2013. Measurement of drug facilitated sexual assault agents in simulated sweat by ion mobility spectrometry. *Talanta* 106, 375–380.
- Deng, H.-H., Weng, S.-H., Huang, S.-Lu, Zhang, L.-N., Liu, A.-L., Lin, X.-H., Chen, W., 2014. Colorimetric detection of sulfide based on target-induced shielding against the peroxidase-like activity of gold nanoparticles. *Anal. Chim. Acta.* 852, 218-222.
- Dev Satyanarayan, S.R., Demirci, A., Graves, R.E., Puri, V.M., 2014. Optimization and modeling of an electrolyzed oxidizing water based clean-in-place technique for farm milking systems using a pilot-scale milking system. *J. Food Eng.* 135, 1–10.
- Devlin, T.M., 1992. *The Textbook of Biochemistry*. 3rd ed. Wiley-Liss Inc. New York.
- Directive 2008/105/EC of the European Parliament and of the Council of 16 December 2008 on environmental quality standards in the field of water policy.

- Dittrich, P. S., Manz, A., 2006. Lab-on-a-chip: microfluidics in drug discovery. *Nat. Rev. Drug. Discov.* 5, 210–218.
- Dong, Y., Gao, W., Zhou, Q., Zheng, Y., You, Z., 2010. Characterization of the gas sensors based on polymer-coated resonant microcantilevers for the detection of volatile organic compounds. *Anal. Chim. Acta* 671(1), 85-91.
- Dou, B., Hu, Q., Li, J., Qiao, S., and Hao, Z., 2011. Adsorption performance of VOCs in ordered mesoporous silicas with different pore structures and surface chemistry. *J. Hazard. Mater.* 186 (2), 1615-1624.
- Drochioiu, G., Damoc, N.E., Przybylski, M., 2006. Novel UV assay for protein determination and the characterization of copper–protein complexes by mass spectrometry. *Talanta* 69, 556–564.
- Duerinck, T., Denayer, J. F. M., 2015. Metal-organic frameworks as stationary phases for chiral chromatographic and membrane separations. *Chem. Eng. Sci.* 124, 179-187.
- Eisert, R., Pawliszyn, J., 1997. Automated In-Tube Solid-Phase Microextraction Coupled to High-Performance Liquid Chromatography, *Anal. Chem.* 69, 3140–3147.
- El-Haj, B.M., Al-Amri, A.M., Hassan, M.H., Ali, H.S., Khadem, R.H.B., 2003. The use of cyclohexanone as a “derivatizing” reagent for the GC-MS detection of amphetamines and ephedrine in seizures and the urine. *Forensic Sci. Int.* 135, 16-26.
- Elechiguerra, J.L., Larios-López, L., Liu, C., García-Gutiérrez, D., Camacho-Bragado, A., Yacaman, M.J, 2005. Corrosion at the Nanoscale: The Case of Silver Nanowires and Nanoparticles. *Chem. Mater.*, 17 (24), 6042–6052.
- Endo, T., Yanagida, Y., Hatsuzawa, T., 2007. Colorimetric detection of volatile organic compounds using a colloidal crystal-based chemical sensor for environmental applications. *Sens. Actuator B-Chem.* 125, 589-595.

- Ercag, E., Uezer, A., Apak, R., 2009. Selective spectro photometric determination of TNT using a dicyclohexylamine-based colorimetric sensor. *Talanta* 78, 772-780.
- European Drug Report 2017: Trends and Developments, 2017. European Monitoring Centre for Drugs and Drug Addition, Lisbon. http://www.emcdda.europa.eu/publications/edr/trends-developments/2017_en (accessed 8 May 2018).
- Fang, Z.-L., Zheng, S.-R., Tan, J.-B., Cai, S.-L., Fan, J., Yan, X., Zhang, W.-G., 2013. Tubular metal–organic framework-based capillary gas chromatography column for separation of alkanes and aromatic positional isomers. *J. Chromatogr. A* 1285, 132-138.
- Farokhchah, A., Alizadeh, N., 2013. Determination of diphenylamine residue in fruit samples using spectrofluorimetry and multivariate analysis. *LWT - Food Sci. Technol.* 54(1), 6–12.
- Feng, J., Tian, Y., Wang, X., Luo, C., Sun, M., 2018. Basalt fibers functionalized with gold nanoparticles for in-tube solid-phase microextraction. *J. Sep. Sci.* 41(5), 1149-1155.
- Feng, X., Li, Y., Jing, R., Jiang, X., Tian, M., 2014. Detection of organophosphorous pesticides in soil sample with multiwalled carbon nanotubes coating spme fiber. *B. Environ. Contam. Tox.* 93, 769–774.
- Fernández-Amado, M., Prieto-Blanco, M.C., López-Mahía, P., Muniategui-Lorenzo, S., Prada-Rodríguez, D., 2016. A novel and cost-effective method for the determination of fifteen polycyclic aromatic hydrocarbons in low volume rain water samples. *Talanta* 155, 175-184.
- Fernández-Amado, M., Prieto-Blanco, M.C., López-Mahia, P., Muniategui-Lorenzo, S., Prada-Rodríguez, D., 2017. Ion-pair in-tube solid phase microextraction for the simultaneous determination of phthalates and their degradation products in atmospheric particulate matter. *J. Chromatogr. A* 1520, 35-47.

- Frankhauser-Noti, A., Grob, K., 2007. Blank problems in trace analysis of diethylhexyl and dibutyl phthalate: investigation of the sources, tips and tricks. *Anal. Chim. Acta* 582, 353-360.
- Freitas, S.S., Serafim, F.A.T., Lancas, F.M., 2018. Determination of target pesticide residues in tropical fruits employing Matrix Solid-Phase Dispersion (MSPD) extraction followed by high resolution gas chromatography. *J. Braz. Chem. Soc.* 29 (5), 1140-1148.
- Freudenmann, R.W., Spitzer, M., 2004. The neuropsychopharmacology and toxicology of 3,4-methylenedioxy-N-ethyl-amphetamine (MDEA). *CNS Drug Rev.* 10, 89-116.
- Gabrielson, J., Hart, M., Jarelöv, A., Kühn, I., McKenzie, D., Möllby, R. 2002, Evaluation of redox indicators and the use of digital scanners and spectrophotometer for quantification of microbial growth in microplates. *J. Microbiol. Methods* 50, 63–73.
- Gałaszka, A., Migaszewski, Z., Namieśnik, J., 2013. The 12 principles of green analytical chemistry and the SIGNIFICANCE mnemonic of green analytical practices, *TrAC-Trends Anal. Chem.* 50, 78–84.
- García-López, M., Canosa, P., Rodríguez, I., 2008. Trends and recent applications of matrix solid-phase dispersion. *Anal. Bioanal. Chem.* 391, 963-974.
- García-Romeo, D., Pellejero, I., Urbiztondo, M.A., Sese, J., Pina, M.P., Martínez, P.A., Calvo, B., Medrano, N., 2014. Portable low-power electronic interface for explosive detection using microcantilevers. *Sens. Actuator B-Chem.* 200, 31-38.
- Gary-Bobo, M., Hocine, O., Brevet, D., Maynadier, M., Raehm, L., Richeter, S., 2012. Cancer therapy improvement with mesoporous silica nanoparticles combining targeting, drug delivery and PDT. *Int. J. Pharm.* 423, 509-15.
- Ghrera, A.S., Pandey, C.M., Malhotra, B.D., 2018. Multiwalled carbon nanotube modified microfluidic-based biosensor chip for nucleic acid detection. *Sens. Actuator B-Chem.* 266, 329-336.

- Gibson, L. T., 2014. Mesosilica materials and organic pollutant adsorption: part A removal from air. *Chem. Soc. Rev.* 43, 5163–5172.
- Giorgetti, R., Marcotulli, D., Tagliabracci, A., Schifano, F., 2015. Effects of ketamine on psychomotor, sensory and cognitive functions relevant for driving ability. *Forensic Sci. Int.* 252, 127–142.
- Globig, D., Weickhardt, C., 2005. Fully automated in-tube solid-phase microextraction for liquid samples coupled to gas chromatography. *Anal. Bioanal. Chem.* 381, 656–659.
- González-Castro, M. I., Olea-Serrano, M. F., Rivas-Velasco, A.M., Medina-Rivero, E., Ordonez-Acevedo, L. G., De Leon-Rodriguez, A., 2011. Phthalates and Bisphenols Migration in Mexican Food Cans and Plastic Food Containers. *Bull Environ Contam Toxicol.* 86 (6), 627-631.
- González-Fuenzalida, R.A., Moliner-Martínez, Y., Prima-Garcia, H., Ribera, A., Campins-Falcó, P., Zaragoza, R.J., 2014. Evaluation of superparamagnetic silica nanoparticles for extraction of triazines in magnetic in-tube solid phase microextraction coupled to capillary liquid chromatography. *Nanomaterials* 4, 242-255.
- González-Fuenzalida, R.A., Moliner-Martínez, Y., Molins-Legua, C., Parada-Artigues, V., Verdú-Andrés, J., Campins-Falcó, P., 2016a. New tools for characterizing metallic nanoparticles: AgNPs, a case study. *Anal. Chem.* 88, 1485-1493.
- Gonzalez-Fuenzalida, R.A., Lopez-Garcia, E., Moliner-Martinez, Y., Campins-Falco, P., 2016b. Adsorbent phases with nanomaterials for in-tube solid-phase microextraction coupled on-line to liquid nanochromatography. *J. Chromatogr. A* 1432, 17-25.
- Gopinath, P. G., 2014. MEMS microcantilevers sensor modes of operation and transduction principles, *Int. J. Comput. Eng. Sci.* 4 (2), 1–11.

- Gou, Y., Pawliszyn, J., 2000. In-tube solid-phase microextraction coupled to capillary LC for carbamate analysis in water samples. *Anal. Chem.* 72, 2774-2779.
- Gjerde, H., Nordfjærn, T., Bretteville-Jensen, A.L., Edland-Gryt, M., Furuhaugen, H., Karinen, R., Øiestad, E.L., 2016. Comparison of drugs used by nightclub patrons and criminal offenders in Oslo Norway. *Forensic Sci. Int.* 265, 1–5.
- Green, R., Hauser, R., Calafat, A.M., Weuve, J., Schettler, T., Ringer, S., Huttner, K., Hu, H., 2005. Use of di(2-ethylhexyl) phthalate-containing medical products and urinary levels of mono(2-ethylhexyl) phthalate in neonatal intensive care unit infants. *Environ Health Perspect.* 113(9), 1222-12225.
- Grima, M., Butler, M., Hanson, R., Mohameden, A., 2012. Firework displays as sources of particles similar to gunshot residue. *Sci. Justice*, 52(1), 49–57.
- Guo, Y., Schutz, S., Vaghi, A., Li, Y.H., Guo, Z.Q., Chang, F.K., Barrettino, D., Wang, S.X., 2017. Stand-Alone Stretchable Absolute Pressure Sensing System for Industrial Applications. *Trans. Ind. Electron.* 64 (11), 8739-8746.
- Haddoub, R., Ferry, D., Marsal, P., Siri, O., 2011. Cobalt thiocyanate reagent revisited for cocaine identification on TLC, *New J. Chem.* 35, 1351–1354.
- Hakobyan, L., Pla-Tolós, J., Moliner-Martínez, Y., Molins-Legua, C., Ramos, J.R., Gordon, M., Ramirez-Gallego, P., Campins-Falcó, P., 2018. Determination of meropenem in endotracheal tubes by in-tube solid phase microextraction coupled to capillary liquid chromatography with diode array detection. *J. Pharm. Biomed. Anal.* 151, 170-177.
- Hamdi, K., Hébrant, M., Martin, P., Galland, B., Etienne, M., 2016. Mesoporous silica nanoparticle film as sorbent for in situ and real-time monitoring of volatile BTX (benzene, toluene and xylenes). *Sens. Actuator B-Chem.* 223, 904-913.
- Hatamie, A., Zargar, B., Jalali, A., 2014. Copper nanoparticles: A new colorimetric probe for quick, naked-eye detection of sulfide ions in water samples. *Talanta*, 121, 234-238.

- He, Y., Zhang, X., 2016. Ultrasensitive colorimetric detection of manganese (II) ions based on anti-aggregation of unmodified silver nanoparticles. *Sens. Actuators B Chem.* 222, 320-324.
- Herráez-Hernández, R., Campíns-Falcó, P., Sevillano-Cabeza, A., 1996a. On-line derivatization into precolumns for the analysis of drugs by liquid chromatography and column switching: determination of amphetamines in urine. *Anal. Chem.* 68, 734-739.
- Herráez-Hernández, R., Campíns-Falcó, P., Sevillano-Cabeza, A., 1996b. Determination of amphetamine and related compounds in urine using on-line derivatization in octadecyl silica columns with 9-fluorenylmethylchloroformate and liquid chromatography. *J. Chromatogr. B* 679, 69-78.
- Herráez-Hernández, R., Campíns-Falcó, P., Sevillano-Cabeza, A., Trümpler, I., 1997. Derivatization of amines in solid-phase extraction supports with 9-fluorenylmethyl chloroformate for liquid chromatography. *Anal. Chim. Acta* 344, 125-136.
- Herráez-Hernández, R., Campíns-Falcó, P., Verdú-Andrés, J., 2001. Sensitive determination of methylenedioxyated amphetamines by liquid chromatography. *Analyst* 126, 581-586.
- Herráez-Hernández, R., Campíns-Falcó, P., Verdú-Andrés, J., 2002. Enantiomeric separation of amphetamine and related compounds by liquid chromatography using precolumn derivatization with o-phthalaldehyde. *Chromatographia* 56, 559-565.
- Hosu, O., Ravalli, A., Lo Piccolo, G.M., Cristea, C., Sandulescu, R., Marrazza, G., 2017. Smartphone-based immunosensor for CA125 detection. *Talanta*. 166, 234-240.
- Huang, P.-C., Tien, C.-J., Sun, Y.-M., Hsieh, C.-Y., Lee, C.-C., 2008. Occurrence of phthalates in sediment and biota: relationship to aquatic factors and the biota-sediment accumulation factor. *Chemosphere* 73, 539-544.

- Hui, I., Hecheng, L., Ying, L., Dan, Z., Cheng, W., Heseng, C., Stepan, L., 2010. Distribution of phthalate esters in alluvial sediment: a case study at JiangHan Plain, Central China. *Chemosphere* 78, 382-388.
- Hung, C., Bai, H., 2008. Adsorption behaviors of organic vapors using mesoporous silica particles made by evaporation induced self-assembly method. *Chem. Eng. Sci.* 63(7), 1997-2005.
- Hunter, C.M., HP Niles, H.P., Vazquez, J., Kloos, C., Subramanyam, R., Williams, M.I., Cummins, D., Lenton, P.A., Majerus, G.J., 2005. Breath odor evaluation by detection of volatile sulfur compounds – correlation with organoleptic odor ratings. *Oral Diseases*.11, 48–50.
- Iijima, S., 1991. Helical microtubules of graphitic carbon. *Nature*. 354, 56-58.
- Illescas, J.F., Mosquera, M.J., 2011. Surfactant-synthesized PDMS/silica nanomaterials improve robustness stain resistance of carbonate stone. *Phys. Chem. C*. 115 (30), 14624–14634.
- Janzen, M.C., Ponder, J.B., Bailey, D.P., Ingison, C.K., Suslick, K.S., 2006. Colorimetric sensor Arrays for volatile organic compounds. *Anal. Chem.* 78, 3591–3600.
- Jia, M.Y., Wu, Q.S., Li, H., Zhang, Y., Guan, Y.F., Feng, L., 2015. The calibration of cellphone camera-based colorimetric sensor array and its application in the determination of glucose in urine, *Biosens. Bioelectron.* 74, 1029–1037.
- Jornet-Martínez, J., Muñoz-Ortuño, M., Moliner-Martínez, Y., Herráez- Hernández, R., Campíns-Falcó, P., 2014a. On-line in-tube solid phase microextraction-capillary liquid chromatography method for monitoring degradation products of di-(2-ethylhexyl) phthalate in water. *J. Chromatogr. A* 1347, 157-160.
- Jornet-Martínez, N., González-Béjar, M., Moliner- Martínez, Y., Campíns-Falcó, P., Pérez-Prieto, J., 2014b. Sensitive and selective plasmonic assay for spermine as biomarker in human urine. *Anal. Chem.* 86, 1347-1351.

- Jornet-Martínez, N., Antón-Soriano, C., Campíns-Falcó, P., 2015a. Estimation of the presence of unmetabolized dialkyl phthalates in untreated human urine by an on-line miniaturized reliable method, *Sci. Total Environ.* 532, 239-244.
- Jornet-Martínez, N., Serra-Mora, P., Moliner-Martínez, Y., Herráez-Hernández, R., Campíns-Falcó, P., 2015b. Evaluation of carbon nanotubes functionalized polydimethylsiloxane based coatings for in-tube solid phase microextraction coupled to capillary liquid chromatography. *Chromatography 2* (3), 515-528.
- Jornet-Martínez, N., Moliner-Martínez, Y., Herráez-Hernández, R., Molins-Legua, C., Verdú-Andrés, J., Campíns-Falcó, P., 2016a. Designing solid optical sensor for in situ passive discrimination of volatile amines based on a new one-step hydrophilic PDMS preparation. *Sens. Actuator B Chem.*, 223, 333-342.
- Jornet-Martínez, N., Campíns-Falcó, P., Hall, E.A.H., 2016b. Zein as biodegradable material for effective delivery of alkaline phosphatase and substrates in biokits and biosensors. *Biosens. Bioelectron.* 86, 14-19.
- Jornet-Martínez, N., Moliner-Martínez, Y., Molins-Legua, C., Campíns-Falcó, P., 2017. Trends for the Development of In Situ Analysis Devices. *Encyclopedia of Analytical Chemistry: Applications, Theory and Instrumentation*. JohnWiley & Sons, Ltd. Environment: water and waste
- Jose, D.A., Mishra, S., Ghosh, A., Shrivastav, A., Mishra, S.K., Das, A., 2007. Colorimetric sensor for ATP in aqueous solution. *Org. Lett.* 9, 1979–1982.
- Jothi, L., Jayakumar, N., Jaganathan, S.K., Nageswaran, G., 2018. Ultrasensitive and selective non-enzymatic electrochemical glucose sensor based on hybrid material of graphene nanosheets/graphene nanoribbons/nickel nanoparticle. *Mater. Res. Bull.* 98, 300-307.
- Kacmaz, S., Ertekin, K., Mercan, D., Oter, O., Cetinkaya, E., Celik, E., 2015. An ultra sensitive fluorescent nanosensor for detection of ionic copper. *Spectrochim. Acta A.* 135, 551-559.

- Kamizake, N.K.K., Gonçalves, M.M., Zaia, C.T.B.V., Zaia, D.A.M., 2003. Determination of total proteins in cow milk powder samples: a comparative study between the Kjeldahl method and spectrophotometric methods. *J. Food Compos. Anal.* 16, 507–516.
- Kangas, M.J., Burks, R.M., Atwater, J., Lukowicz, R.M., Williams, P., Holmes, A.E., 2016. Colorimetric sensor arrays for the detection and identification of chemical weapons and explosives. *Crit. Rev. Anal. Chem.* 47, 1–16.
- Kataoka, H., 2002. Automated sample preparation using in-tube solid-phase microextraction and its application – a review. *Anal. Bioanal. Chem.* 373, 31–45.
- Kataoka, H., Itano, M., Ishizaki, A., Saito, K., 2009. Determination of patulin in fruit juice and dried fruit samples by in-tube solid phase microextraction coupled with liquid chromatography-mass spectrometry. *J. Chromatogr. A* 1216, 3746-3750.
- Kataoka, H., Mizuno, K., Oda, E., Saito, A., 2016. Determination of the oxidative stress biomarker urinary 8-hydroxy-2-deoxyguanosine by automated on-line in-tube solid-phase microextraction coupled with liquid chromatography-tandem mass spectrometry. *J. Chromatogr. B* 1019, 140-146.
- Katsoulidis, A. P., Park, K. S., Antypov, D., Martí-Gastaldo, C., Miller, G. J., Warren, J. E., Robertson, C. M., Blanc, F., Darling, G. R., Berry, N. G., Purton, J. A., Adams, D. J., Rosseinsky, M. J., 2014. Guest-adaptable and water-stable peptide-based porous materials by imidazolate side chain control. *Angew. Chem., Int. Ed.* 53, 193-198.
- Khalid, N., Kobayashi, I., Nakajima, M., 2017. Recent la-on-chip developments for novel drug discovery. *9* (4), 1381-1398.
- Kilinc, N., Cakmak, O., Kosemen, A., Ermek, E., Ozturk, S., Yerli, Y., Ozturk, Z., Urey, H., 2014. Fabrication of 1D ZnO nanostructures on MEMS cantilever for VOC sensor application. *Sens. Actuator B-Chem.* 202, 357-364.

- Kosuge, K., Kubo, S., Kikukawa, N., Takemori, M., 2007. Effect of pore structure in mesoporous silicas on VOC dynamic adsorption/desorption performance. *Langmuir* 23, 3095-3102.
- Kralj, J.G., Munson, M.S., Ross, D., 2014. Total protein quantitation using the bicinchoninic acid assay and gradient elution moving boundary electrophoresis. *Electrophoresis* 35, 1887–1892.
- Kruk, M., Jaroniec, M., Ko, C.H., Ryoo, R., 2000. Characterization of the Porous Structure of SBA-15. *Chem. Mater.*, 2000, 12, 1961–1968.
- Kueseng, P., Pawliszyn, J., 2013. Carboxylated multiwalled carbonnanotubes/polydimethylsiloxane, a new coating for 96-blade solid-phase microextraction for determination of phenolic compounds in water. *J. Chromatogr. A* 1317, 199–202.
- Kusunoki, H., Okuma, K., Hamaguchi, I., 2012. Estimation of lactose interference in vaccines and a proposal of methodological adjustment of total protein determination by the Lowry method. *Jpn. J. Infect. Dis.* 65, 489–494.
- Kutzscher, C., Müller, P., Raschke, S., Kaskel, S., 2016. Chiral Linker Systems. *The Chemistry of Metal–Organic Frameworks: Synthesis, Characterization, and Applications*, Wiley: Weinheim 387–419.
- Lam, T., Devadhasan, J.P., Howse, R., Kim, J., 2017. A Chemically Patterned Microfluidic Paper-based Analytical Device (C- μ PAD) for Point-of-Care Diagnostics. *Sci Rep.* 7 (1), 1188-1198.
- Laza, D., Nys, B., Kinder, J. De, Kirsch-De Mesmaeker, A., & Moucheron, C., 2007. Development of a quantitative LC-MS/MS method for the analysis of common propellant powder stabilizers in gunshot residue. *Journal of Forensic Sciences*, 52(4), 842–850.
- Lee, B., Park, J.H., Byun, J.Y., Kim, J.H., Kim, M.G., 2018. An optical fiber-based LSPR aptasensor for simple and rapid in-situ detection of ochratoxin A. *Biosens Bioelectron.* 102, 504-509.

- Lee, J.N., Park, C., Whitesides, G.M., 2003. Solvent compatibility of poly(dimethylsiloxane)-based microfluidic devices. *Anal. Chem.* 75 (23), 6544-6554.
- Leuvering, J.H.W., Thal, P.J.H.M., Van der Waart, M., Schuurs, A.H.W.M., 1980. Sol Particle Immunoassay. *J. Immunoassay* 1, 77-91.
- Li, C., Lu, A., Wang, J., Li, J., Ping, H., Luan, Y., Chen, J., Ha, X., 2014. Determination of five sulfonylurea herbicides in environmental waters and soil by ultra high performance liquid chromatography with tandem mass spectrometry after extraction using grapheme. *J. Sep. Sci.* 37 (24), 3714-3721.
- Li, D., Xu, F., Liu, Z., Zhu, J., Zhang, Q., Shao, L., 2013. The effect of adding PDMS-OH and silica nanoparticles on sol-gel properties and effectiveness in stone protection. *Appl. Surf. Sci.* 266, 368-374.
- Li, Q., Wu, Z., Eng, D. F., Tu, B., Zhao, D. J., 2010. Hydro-thermal stability of mesostructured cellular silica foams. *J. Phys. Chem. C.* 114 (11) 2010, 5012-5019.
- Li, Q., Qiu, T., Hao, H., Zhou, H., Wang, T., Zhang, Y., Li, X., Huang, G., Cheng, J., 2012. Rapid and on-site analysis of illegal drugs on the nano-microscale using a deep ultraviolet-visible reflected optical fiber sensor. *Analyst* 137, 1596-1603.
- Li, T., Xu, J., Wu, J.-H., Feng, Y.-Q., 2009. Liquid-phase deposition of silica nanoparticles into a capillary for in-tube solid phase microextraction coupled with high-performance liquid chromatography, *J. Chromatogr. A* 1216, 2989-2995.
- Li, T., Yu, P., Lou, Y., 2015. Polydimethylsiloxane mixed-matrix membranes for dissolved oxygen removal from water, *J. Appl. Polym. Sci.* 41350, 1-9.
- Li, X., Lee, D.W., 2012. Integrated microcantilevers for high-resolution sensing and probing. *Meas. Sci. Technol.* 23, 22001-22042.

- Li, Y., Xu, H., 2015. Development of a novel graphene/polyaniline electrodeposited coating for on-line in-tube solid phase microextraction of aldehydes in human exhaled breath condensate, *J. Chromatogr. A* 1395, 23-31.
- Liana, D.D., Raguse, B., Justin Gooding, J., Chow, E., 2012. Recent advances in paper based sensors, *Sensors*. 12, 11505–11526.
- Liang, X., Liu, S., Wang, S., Guo, Y., Jiang, S., 2014. Carbon-based sorbents: carbon nanotubes. *J. Chromatogr. A* 1357, 53–67.
- Lim, S.H., Mix, S., Xu, Z., Taba, B., Budvytiene, I., Berliner, A.N., Queralto, N., Churi, Y.S., Huang, R.S., Eiden, M., Martino, R.A., Rhodes, P., Banaei, N., 2014. Colorimetric sensor array allows fast detection and simultaneous identification of sepsis-causing bacteria in spiked blood culture. *J. Clin. Microbiol.* 52, 592–598.
- Lin, Z.P., Ikononou, M.G., Jing, H., Mackintosh, C., Gobas, F.A.P.C., 2003. Determination of Phthalate Ester Congeners and Mixtures by LC/ESI-MS in Sediments and Biota of an Urbanized Marine Inlet. *Environ. Sci. Technol.* 37, 2100-2108.
- Lindsey, M.E., Meyer, M., Thurman, E.M., 2001. Analysis of trace levels of sulfonamide and tetracycline antimicrobials in groundwater and surface water using solid-phase extraction and liquid chromatography/mass spectrometry. *Anal. Chem.* 73 (19), 4640-4646.
- Ling, X., Zhang, W., Chen, Z., 2016. Electrochemically modified carbon fiber bundles as selective sorbent for online solid-phase microextraction of sulfonamides, *Microchim. Acta* 183, 813-820.
- Liu, C.C., Janmanchi, D., Wen, D.R., Oung, J.N. Mou, C.Y., Yu, S.S.F. Chan, S.I., 2018. Catalytic oxidation of light alkanes mediated at room temperature by a tricopper cluster complex immobilized in mesoporous silica nanoparticles(parallel to). *ACS Sustain. Chem. Eng.* 6(4), 5431-5440.

- Liu, Q., Shi, J., Sun, J., Wang, T., Zeng, L., Zhu, N., Jiang, G., 2011. Graphene-assisted matrix solid-phase dispersion for extraction of polybrominated diphenyl ethers and their methoxylated and hydroxylated analogs from environmental samples. *Anal. Chim. Acta.* 708, 61-68.
- Liu, S., Tong, Z., Mu, X., Liu, B., Du, B., Liu, Z., Gao, C., 2018. Detection of Abrin by Electrochemiluminescence Biosensor Based on Screen Printed Electrode. *Sensors* 18 (2), 357-379.
- Liu, X.-Y., Ji, Y.-S., Zhang, H.-X., Liu, M.-C., 2008. Highly sensitive analysis of substituted aniline compounds in water samples by using oxidized multiwalled carbon nanotubes as an in-tube solid phase microextraction medium, *J. Chromatogr. A* 1212, 10-15.
- Lledo-Fernandez, C., Banks, C.E., 2011. An overview of quantifying and screening drugs of abuse in biological samples: Past and present. *Anal. Methods* 3, 1227–1245.
- Lopez-Ruiz, N., Curto, V.F., Erenas, M.M., Benito-Lopez, F., Diamond, D., Palma, A.J., Capitan-Vallvey, L.F., 2014. Smartphone-based simultaneous pH and nitrite colorimetric determination for paper microfluidic devices. *Anal. Chem.* 86, 9554–9562.
- Löttersy, J.C., Ithuis, W.O., Veltink, P.H., Bergveld, P., 1997. The mechanical properties of the rubber elastic polymer polydimethylsiloxane for sensor applications. *J. Micromech. Microeng.* 7, 145–147.
- Lynch, J.M., Barbano, D.M., Fleming, J.R., 1998. Indirect and direct determination of the casein content of milk by Kjeldahl nitrogen analysis: collaborative study, *J. AOAC Int.* 81, 763–774.
- Ma, K., Rivera, J., Hirasaki, G.J., Biswal, S.B., 2011. Wettability control and patterning of PDMS using UV–ozone and water immersion. *J. Colloid Interface Sci.* , 2011, 363, 371.

- Ma, X.-M., Sun, M., Lin, Y., Liu, Y.-J., Luo, F., Guo, L.H., Qiu, B., Lin, Z.-Y., Chen, G.-N., 2018. Progress of visual biosensor based on gold nanoparticles. *Chinese J. Anal. Chem.* 46, 1-10.
- Ma, Y., Niu, H., Zhang, X., Cai, Y., 2011. One-step synthesis of silver/dopamine nanoparticles and visual detection of melamine in raw milk. *Analyst* 136, 4192-4196.
- Maddah, B., Alimardani, V., Moradifard, H., 2015. A simple colorimetric kit for determination of ketamine hydrochloride in water samples. *Anal. Methods* 7, 10364–10370.
- Manbohi, A., Ahmadi, S.H., 2015. In-tube magnetic solid phase microextraction of some fluoroquinolones based on the use of sodium dodecyl sulfate coated Fe₃O₄ nanoparticles packed tube. *Anal. Chim. Acta* 885, 114-121.
- Mansfield, E., Kar, A., Quinn, T.P., Hooker, S.A., 2010. Quartz crystal microbalances for microscale thermogravimetric analysis. *Anal. Chem.* 82 (24), 9977-9982.
- Marti-Gastaldo, C., Warren, J. E., Stylianou, K. C., Flack, N. L. O., Rosseinsky, M. J., 2012. enhanced stability in rigid peptide-based porous materials. *Angew. Chem. Int. Ed.* 51, 11044-11048.
- Martí-Gastaldo, C., Antypov, D., Warren, J. E., Briggs, M. E., Chater, P. A., Wiper, P.V., Miller, G.J., Khimyak, Y. Z., Darling, G.R., Berry, N.G., Rosseinsky, M.J., 2014. Side-chain control of porosity closure in single- and multiple-peptide-based porous materials by cooperative folding. *Nat. Chem.* 6, 343-351.
- Martí-Gastaldo, C., Warren, J. E., Briggs, M. E., Armstrong, J. A., Thomas, K. M., Rosseinsky, M. J., 2015. Sponge-Like behaviour in isorecticular Cu(Gly-His-X) peptide-based porous materials. *Chem. - Eur. J.* 2015, 21, 16027-16034.
- Martínez-Carballo, E., Sitka, A., González-Barreiro, C., Kreuzinger, N., Fürhacker, M., Scharf, S., Gans, O., 2007. Determination of selected quaternaryammonium compounds by liquid chromatography with mass

- spectrometry. Part I. Application to surface, waste and indirect discharge water samples in Austria. *Environ. Pollut.* 145, 489–496.
- Masià, A., Moliner-Martínez, Y., Muñoz-Ortuño, M., Picó, Y., Campíns-Falcó, P., 2013. Multiresidue analysis of organic pollutants by in-tube solid phase microextraction coupled to ultra-high performance liquid-chromatography-electrospray-tandem mass spectrometry, *J. Chromatogr. A* 1306, 1-11.
- Masson, J.F., 2017. Surface Plasmon Resonance Clinical Biosensors for Medical Diagnostics. *ACS Sens.* 2 (1), 16–30.
- Mauriz, E., Calle, A., Lechuga, L.M., Quintana, J., Montoya, A., Manclús, J.J., 2006. Real-time detection of chlorpyrifos at part per trillion levels in ground, surface and drinking water samples by a portable surface plasmon resonance immunosensor. *Anal. Chim. Acta.* 561, 40–47.
- Medesi, A., Greiner, T., Benkler, M., Megnin, C., Henemann, T., 2014. Low temperature sintering of PZT. *J. Phys.: Conf. Ser.* 557(1), 122132-122138.
- Mei, H., Quan, Y., Wang, W., Zhou, H., Liu, Z., Shi, H., & Wang, P., 2016 . Determination of diphenylamine in gunshot residue by HPLC-MS/MS. *J. Forensic Sci. Med.* 2(1), 18.
- Mei, M., Huang, X., Luo, Q., Yuan, D., 2016. Magnetism-enhanced monolith-based in-tube solid phase microextraction. *Anal. Chem.* 88, 1900-1907.
- Mei, M., Huang, X., 2017. Online analysis of five organic ultraviolet filters in environmental water samples using magnetism-enhanced monolith-based in-tube solid phase microextraction coupled with high-performance liquid chromatography. *J. Chromatogr. A* 1525, 1-9.
- Meng, L., Meng, P., Zhang, Q., Wang, Y., 2013. Fast screening of ketamine in biological samples based on molecularly imprinted photonic hydrogels. *Anal. Chim. Acta* 771, 86–94.

- Meng, P., Wang, Y., 2010. Small volume liquid extraction of amphetamines in saliva. *Forensic Sci. Int.* 197, 80–84.
- Meng, Q., Han, T., Wang, G., Zheng, N., Cao, C., Xie, S., 2014. Preparation of a natural dye doped Ormosil coating for the detection of formaldehyde in the optical gas sensor. *Sensor Actuat. B-Chem.* 196, 238-244.
- Míguez-Framil, M., Moreda-Piñeiro, A., Bermejo-Barrera, P., Álvarez-Freire, I., Tabernero, M.J., Bermejo, A.M., 2010. Matrix solid-phase dispersion on column clean-up/pre-concentration as a novel approach for fast isolation of abuse drugs from human hair. *J. Chromatogr. A* 1217 (41), 6342-6349.
- Míguez-Framil, M., Moreda-Piñeiro, A., Bermejo-Barrera, P., Cocho, J.A., Tabernero, M.J., Bermejo, A.M., 2011. Electrospray ionization tandem mass spectrometry for the simultaneous determination of opiates and cocaine in human hair. *Anal. Chim. Acta* 704, 123–132.
- Míguez-Framil, M., Cobarcos, P., Tabernero, M.J., Bermejo, A.M., Bermejo-Barrera, P., Moreda-Piñeiro, A., 2013. Matrix solid phase dispersion assisted enzymatic hydrolysis as a novel approach for cocaine and opiates isolation from human hair. *J. Chromatogr. A* 1316, 15–22.
- Mizuno, K., Kataoka, H., 2015. Analysis of urinary 8-isoprostane as an oxidative stress biomarker by stable isotope dilution using automated online in-tube solid-phase microextraction coupled with liquid chromatography-tandem mass spectrometry. *J. Pharm. Biomed. Anal.* 112 (82015), 36-42.
- Moliner-Martínez, Y., Campíns-Falcó, P., Herráez-Hernández, R., 2004. A method for the determination of dimethylamine in air by collection on solid support sorbent with subsequent derivatization and spectrophotometric analysis. *J. Chromatogr. A* 1059, 17–24.
- Moliner-Martínez, Y., Herráez-Hernández, R., Molins-Lagua, C., Campíns-Falcó, P., 2010. Improving analysis of apolar organic compounds by the use of a capillary titania-based column: application to the direct determination of faecal sterols, cholesterol and coprostanol in wastewater samples. *J. Chromatogr. A* 1217, 4682-4687.

- Moliner-Martínez, Y., Molins-legua, C., Verdú-Andrés, J., Herráez-Hernández, R., Campíns-Falcó, P., 2011. Advantages of monolithic over particulate columns for multiresidue analysis of organic pollutants by in-tube solid phase microextraction coupled to capillary liquid chromatography. *J. Chromatogr. A* 1218, 6256-6262.
- Moliner-Martínez, Y., González-Fuenzalida, R.A., Herráez-Hernández, R., Campíns-Falcó, P., Verdú-Andrés, J., 2012a. Cleaning sorbents used in matrix solid-phase dispersion with sonication: Application to the estimation of polycyclic aromatic hydrocarbons at ng/g levels in marine sediments. *J Chromatogr. A* 1263, 43– 50.
- Moliner-Martínez, Y., Prima-García, H., Ribera, A., Coronado, E., Campíns-Falcó, P., 2012b. Magnetic in-tube solid phase microextraction. *Anal. Chem.* 84, 7233-7240.
- Moliner-Martínez, Y., Vitta, Y., Prima-Garcia, H., Gonzalez-Fuenzalida, R.A., Ribera, A., Campíns-Falcó, P., Coronado, E., 2014a. Silica supported Fe_3O_4 magnetic nanoparticles for magnetic solid-phase extraction and in-tube solid phase microextraction: application to organophosphorous compounds. *Anal. Bioanal. Chem.* 406, 2211-2215.
- Moliner-Martínez, Y., Muñoz-Ortuño, M., Herráez-Hernández, R., Campíns-Falcó, P., 2014b. Rapid analysis of effluents generated by the dairy industry for fat determination by preconcentration in nylon membranes and attenuated total reflectance infrared spectroscopy measurement. *Talanta* 119, 11–16.
- Moliner-Martínez, Y., Herráez-Hernández, R., Verdú-Andrés, J., Molins-Legua, C., Campíns-Falcó, P., 2015a. Recent advances of in-tube solid-phase microextraction, *Trends Anal. Chem.* 71, 205-213.
- Moliner-Martínez, Y., Serra-Mora, P., Verdú-Andrés, J., Herráez-Hernández, R., Campíns-Falcó, P., 2015b. Analysis of polar triazines and degradation products in waters by in-tube solid-phase microextraction and capillary chromatography: an environmentally friendly method, *Anal. Bioanal. Chem.* 407, 1485-1497.

- Mondin, A., Bogialli, S., Venzo, A., Favaro, G., Badocco, D., Pastore, P., 2014. Characterization and quantification of N-(3-aminopropyl)-N-dodecyl-1,3-propanediamine biocide by NMR, HPLC/MS and titration techniques. *Chemosphere* 95, 379–386.
- Monoudis, P.N., Tsakalof, A., Karapanagiotis, I., Zubirtikudis, I., Pnyiotou, C., 2009. Fabrication of super-hydrophobic surfaces for enhanced stone protection. *Surf. Coat. Technol.* 203, 1322–1328.
- Morelato, M., Beavis, A., Ogle, A., Doble, P., Kirkbride, P., Roux, C., 2012. Screening of gunshot residues using desorption electrospray ionisation-mass spectrometry (DESI-MS). *Forensic Sci. Int.*, 217(1-3), 101–106.
- Morris, J.A., 2007. Modified cobalt thiocyanate presumptive color test for ketamine hydrochloride. *J. Forensic Sci.* 52, 84–87.
- Mullet, W.M., Levens, K., Borlak, J., Wu, J.C., Pawliszyn, J., 2002. Automated in-tube solid phase microextraction coupled with HPLC for the determination of N-nitrosamines in cell cultures. *Anal. Chem.* 74, 1695-1701.
- Muñoz-Ortuño, M., Moliner-Martínez, Y., Cogollos-Costa, S., Herráez-Hernández, R., Campíns-Falcó, P., 2012. A miniaturized method for estimating di-(2-ethylhexyl)phthalate in bivalves as bioindicators. *J. Chromatogr. A* 1260, 169-173.
- Muñoz-Ortuño, M., Argente-García, A., Moliner-Martínez, Y., Verdú-Andrés, J., Herráez-Hernández, R., Picher, M.T., Campíns-Falcó, P., 2014. A cost-effective method for estimating di(2-ethylhexyl)phthalate in coastal sediments. *J. Chromatogr. A.* 1324, 57– 62.
- Muñoz-Ortuño, M., Argente-García, A., Moliner-Martínez, Y., Molins-Legua, C., Campíns-Falcó, P., 2015. Polydimethylsiloxane composites containing 1,2-naphthoquinone-4-sulphonate as unique dispositive for estimation of casein in effluents from dairy industries. *Anal. Chim. Acta* 873, 31–37.

- Musile, G., Wang, L., Bottoms, J., Tagliarob, F., McCord, B., 2015. The development of paper microfluidic devices for presumptive drug detection. *Anal. Methods*. 7, 8025–8033.
- Navarro-Sánchez, N., Argente-García, A., Moliner-Martínez, Y., Roca-Sanjuán, D., Antypov, D., Campíns-Falcó, P., Rosseinsky, M.J., Martí-Gastaldo, C., 2017. Peptide Metal–Organic Frameworks for enantioselective separation of chiral drugs. *J. Am. Chem. Soc.* 139, 4294–4297.
- Nazari, A.M., Miri, A.K., Shinozaki, D.M., 2016. Mechanical characterization of nanoclay-filled PDMS thin films. *Polym. Test.* 52, 85–88.
- Net, S., Delmont, A., Sempéré, R., Paluselli, A., Ouddane, B., 2015. Reliable quantification of phthalates in environmental matrices (air, water, sludge, sediment and soil): A review. *Sci. Total Environ.* 515, 162-180.
- Ngom, B., Guo, Y., Wang, X., Bi, D., 2010. Development and application of lateral flow test strip technology for detection of infectious agents and chemical contaminants: a review. *Anal. Bioanal. Chem.*, 397, 1113-1135.
- Nguyen, T.A.H., Pham, T.N.M., Ta, T.T., Nguyen, X.T., Nguyen, T.L., Le, T.H.H., Koenka, I.J., Saiz, J., Hauser, P.C., Mai, T.D., 2015. Screening determination of four amphetamine-type drugs in street-grade illegal tablets and urine samples by portable capillary electrophoresis with contactless conductivity detection. *Sci. Justice* 55, 481-486.
- Nightingale, A.M., Beaton, A.D., Mowlem, M.C., 2015. Trends in microfluidic systems for in situ chemical analysis of natural waters. *Sensors Actuators B Chem.* 221, 1398–1405.
- Niu, H., Wang, S., Zhou, Z., Ma, Y., Ma, X., Cai, Y., 2014. Sensitive Colorimetric Visualization of Perfluorinated Compounds Using Poly(ethylene glycol) and Perfluorinated Thiols Modified Gold Nanoparticles. *Anal. Chem.* 86 (9), 4170–4177.
- Nonaka, Y., Saito, K., Hanioka, N., Narimatsu, S., Kataoka, H., 2009. Determination of aflatoxins in food samples by automated on-line in-tube solid-phase

- microextraction coupled with liquid chromatography-mass spectrometry, *J. Chromatogr. A* 1216, 4416-4422.
- Nowack, N., Krug, H. F., Height, M., 2011. 120 Years of nanosilver history: implications for policy makers. *Environmental Science and Technology* 45, 1177–1183.
- Nugent, P., Burd, S. D., Forrest, K., Pham, T., Ma, S., Space, B., Wojtas, L., Eddaoudi, M., Zaworotko, M.J., 2013. Porous materials with optimal adsorption thermodynamics and kinetics for CO₂ separation. *Nature*, 495, 80-84.
- Oelschlaeger, C., Willenbacher, N., 2012. Mixed wormlike micelles of cationic surfactants: effect of the cosurfactant chain length on the bending elasticity and rheological properties. *Colloid Surf. A* 406, 31–37.
- Oftedal, O.T., Eisert, R., Barrel, G.K., 2014. Comparison of analytical and predictive methods for water protein, fat, sugar, and gross energy in marine mammal milk. *J. Dairy Sci.* 97, 4713–4732.
- Ogirala, T., Eapen, A., Salvante, K.G., Rapaport, T., Nepomnaschy, P.A., Parameswaran, A.M., 2017. Smartphone-based colorimetric ELISA implementation for determination of women's reproductive steroid hormone profiles, *Med. Biol. Eng. Comput.* 55(10), 1735-1741.
- On, D. T., Kaliaguine, S., 2003. Zeolite-Coated Mesostructured Cellular Silica Foams, *J. Am. Chem. Soc.* 125 (3), 618-619.
- Oncescu, V., O'Dell, D., Erickson, D., 2013. Smartphone based health accessory for colorimetric detection of biomarkers in sweat and saliva, *Lab Chip.* 13, 3232–8.
- Oommen, Z., Pierce, S. M., 2006. Lead-free primer residues: A qualitative characterization of Winchester WinClean™, Remington/UMC LeadLess™, Federal BallisticClean™, and Speer Lawman Clean Fire™ handgun ammunition. *J. Forensic Sci.* 51(3), 509–519.

- Ornatska, M., Sharpe, E.M., Andreescu, D., Andreescu, S., 2011. Paper bioassay based on ceria nanoparticles as colorimetric probes. *Anal.Chem.* 83, 4273–4280.
- Pandey, S.K., Kim, K.H., Tang, K.T., 2012. A review of sensor-based methods for monitoring hydrogen sulfide. *TrAC - Trends Anal. Chem.* 32, 87–99.
- Park, I.S., Heo, E., Nam, Y.S., Lee, C.W., Kim, J.M., 2012. Colorimetric detection of aliphatic primary amines and a molecular logic gate based on a photochromic phenoxyquinone derivative. *J. Photochem. Photobiol. AChem.* 238, 1–6.
- Park, Y.W., Juárez, J., Ramos, M., Haenlein, G.F.W., 2007. Physico-chemical characteristics of goat and sheep milk. *Small Ruminant Res.* 68, 88–113.
- Pena-Pereira, F., Villar-Blanco, L., Lavilla, I., Bendicho, C., 2018. Test for arsenic speciation in waters based on a paper-based analytical device with scanometric detection. *Anal. Chim. Acta.* 1011, 1-10.
- Peng, L.Q., Yi, L., Yang, Q.C., Cao, Jun., Du, L.J., Zhang, Q.D., 2017. Graphene nanoplatelets based matrix solid-phase dispersion microextraction for phenolic acids by ultrahigh performance liquid chromatography with electrochemical detection. *Sci. Rep.* 7, 7496-7508.
- Peng, X.-T., Shi, Z.-G., Feng, Y.-Q., 2011. Rapid and high-throughput determination of cationic surfactants in environmental water samples by automated on-line polymer monolith microextraction coupled to high performance liquid chromatography–mass spectrometry. *J. Chromatogr. A* 1218, 3588–3599
- Pérez-López, B., Merkoçi, A., 2011. Magnetic nanoparticles modified with carbon nanotubes for electrocatalytic magnetoswitchable biosensing applications. *Adv. Funct. Mater.* 21, 255-260.
- Peters, K.L., Corbin, I., Kaufman, L.M., Zreibe, K., Blanes, L., McCord, B.R., 2015. Simultaneous colorimetric detection of improvised explosive compounds

- using microfluidic paper-based analytical devices (μ PADs). *Analytical Methods*, 7, 63- 70.
- Picó, Y., Molto, J.C., Manes, J., Font, G., 1994. Solid-phase techniques in the extraction of pesticides and related-compounds from foods and soils. *J Microcolumn*. 6, 331–59.
- Picó, Y., Fernández, M., Ruiz, M.J., Font, G., 2007. Current trends in solid-phase-based extraction techniques for the determination of pesticides in food and environment. *J. Biochem. Biophys. Methods*. 70, 117–131.
- Pierri, G., Kottoni, D., Simone, P., Villani, C., Pepe, G., Campiglia, P., Dugo, P., Gasparri, F., 2013. Analysis of bovine milk caseins on organic monolithic columns: an integrated capillary liquid chromatography–high resolution mass spectrometry approach for the study of time-dependent casein degradation. *J. Chromatogr. A* 1313, 259–269.
- Piette, V., Parmentier, F., 2002. Analysis of illicit amphetamine seizures by capillary zone electrophoresis. *J. Chromatogr. A* 979, 345-352.
- Pla-Tolós, J., Moliner-Martínez, Y., Molins-Legua, C., Herráez-Hernández, R., Verdú-Andrés, J., Campíns-Falcó, P., 2015, Selective and sensitive method based on capillary liquid chromatography with in-tube solid phase microextraction for determination of monochloramine in water. *J. Chromatogr. A* 1388, 17-23.
- Pla-Tolós, J., Serra-Mora, P., Hakobyan, L., Molins-Legua, C., Moliner-Martínez, Y., Campíns-Falcó, P., 2016a. A sustainable on-line CapLC method for quantifying antifouling agents like irgarol-1051 and diuron in water samples: estimation of the carbon footprint. *Sci. Total Environ*. 569-570, 611-618.
- Pla-Tolós, J., Moliner-Martínez, Y., Molins-Legua, C., Campíns-Falcó, P., 2016b. Colorimetric biosensing dispositive based on reagentless hybrid biocomposite: application to hydrogen peroxide determination, *Sens. Actuators B Chem*. 231, 837-846.

- Pla-Tolós, J., Moliner-Martinez, Verdú-Andrés, J., Casanova-Cháfer, J., Molins-Legua, C., Campins-Falcó, P., 2016c. New optical paper sensor for in situ measurement of hydrogen sulphide in waters and atmospheres. *Talanta* 156-157, 79-86.
- Pla-Tolós, J., Moliner-Martínez, Y., Molins-Legua, C., Campins-Falcó, P., 2018. Solid glucose biosensor integrated in a multi-well microplate coupled to a camera-based detector: Application to the multiple analysis of human serum samples. *Sens. Actuators, B.* 258, 331-341.
- Prieto-Blanco, M.C., López-Mahía, P., Prada-Rodríguez, D., 1999. Analysis of residual products in benzalkonium chloride by high-performance liquid chromatography. *J. Chromatogr. Sci.* 37, 295–299.
- Prieto-Blanco, M.C., Cháfer-Pericás, C., López-Mahía, P., Campins-Falcó, P., 2008. Automated on-line in tube solid-phase microextraction-assisted derivatization coupled to liquid chromatography for quantifying residual dimethylamine in cationic polymers. *J. Chromatogr. A* 1188, 118-123.
- Prieto-Blanco, M. C., López-Mahía, P., Campins-Falcó, P., 2009a. In-tube solid-phase microextraction and liquid chromatography using monolithic column for the selective determination of residual ethylenediamine in industrial cationic polymers. *Analytical Chemistry* 81, 5827–5832.
- Prieto-Blanco, M.C., López-Mahía, P., Prada-Rodríguez, D., 2009b. Analysis of residual products in benzyl chloride used for the industrial synthesis of quaternary compounds by liquid chromatography with diode-array detection. *J. Chromatogr. Sci.* 47, 121–126.
- Prieto-Blanco, M.C., López-Mahía, P., Campins-Falcó, P., 2011. On-line analysis of carbonyl compounds with derivatization in aqueous extracts of atmospheric particulate PM₁₀ by in-tube solid phase microextraction coupled to capillary liquid chromatography. *J. Chromatogr. A* 1218, 4834-4839.
- Prieto-Blanco, M.C., Moliner-Martinez, Y., Lopez-Mahia, P., Campins-Falcó, P., 2012. Ion pair in-tube solid-phase microextraction and capillary liquid

- chromatography using titania-based column: application to the specific lauralkonium chloride determination in water. *J. Chromatogr. A* 124, 55-59.
- Prieto-Blanco, M.C., Moliner-Martínez, Y., Campíns-Falcó, P., 2013a. Combining poly(dimethyldiphenylsiloxane) and nitrile phases for improving the separation and quantification of benzalkonium chloride homologues: in-tube solid phase microextraction- capillary liquid chromatography-diode array detection-mass spectrometry for analyzing industrial samples. *J. Chromatogr. A* 1297, 226-230.
- Prieto-Blanco, M.C., Moliner-Martínez, Y., López-Mahia, P., Campíns-Falcó, P., 2013b, Determination of carbonyl compounds in particulate matter PM_{2.5} by in-tube solid phase microextraction coupled to capillary liquid chromatography/mass spectrometry. *Talanta* 115, 876-880.
- Prieto-Blanco, M.C., Jornet-Martínez, N., Moliner-Martínez, Y., Molins-Legua, C., Herráez-Hernández, R., Verdú Andrés, J., Campíns-Falcó, P., 2015. Development of a Polydimethylsiloxane-Thymol/Nitroprusside Composite Based Sensor Involving Thymol Derivatization for Ammonium Monitoring in Water Samples, *Sci. Total Environ.* 150, 503–504.
- Prieto-Blanco, M.C., Argente-García, A., Campíns-Falcó, P., 2016. A capillary liquid chromatography method for benzalkonium chloride determination as a component or contaminant in mixtures of biocides. *J. Chromatogr. A* 1431, 176–183.
- Pyrzyska, K., 2011. Carbon nanotubes as sorbent in the analysis of pesticides. *Chemosphere* 83, 1407–1413.
- Qin, Y., Wang, Y., Wang, H., Gao, J., Qu, Z., 2013. Effect of morphology and pore structure of SBA-15 on toluene dynamic adsorption/desorption performance. *Procedia Environ. Sci.* 18, 366-371.
- Quan-Min, L., Zhan-Jun, Y., 2007. Spectrophotometric determination of aminomethylbenzoic acid using sodium 1,2-naphthoquinone-4-sulfonate

- as the chemical derivative chromogenic reagent. *Spectrochim. Acta Part A* 66, 656-661.
- Rabone, J., Yue, Y. F., Chong, S., Stylianou, K., Bacsa, J., Bradshaw, D., Darling, G.R., Berry, N. G., Khimyak, Y. Z., Ganin, A. Y., Wiper, P., Claridge, J. B., Rosseinsky, M. J., 2010. An adaptable peptide-based porous material. *Science* 329, 1053-1057.
- Ramirez-Palomino, P., Fernandez-Romero, J.M., Gomez-Hens, A., 2014. Rapid chromatographic determination of caseins in milk with photometric and fluorimetric detection using a hydrophobic monolithic column. *Food Chem.* 142, 249–254.
- Ramos, L., 2012. Critical overview of selected contemporary sample preparation techniques. *J. Chromatogr. A* 1221, 84-98.
- Ravelo-Pérez, L.M., Herrera-Herrera, A.V., Hernández-Borges, J., Rodríguez-Delgado, M.A., 2010. Carbon nanotubes: Solid-phase extraction. *J. Chromatogr. A* 1217(16), 2618-2641.
- Ridgway, K., Lalljie, S.P.D., Smith, R.M., 2007. Sample preparation techniques for the determination of trace residues and contaminants in foods. *J. Chromatogr. A* 1153, 36–53.
- Roda, A., Michelinia, E., Zangheria, M., Fuscoa, M.D., Calabria, D., Simonc, P., 2016. Smartphone-based biosensors: a critical review and perspectives. *TrAC Trends Anal.Chem.* 79, 317-325.
- Rosolina, S. M., Carpenter, T.S., Xue, Z.L., 2016. Bismuth-Based, Disposable Sensor for the Detection of Hydrogen Sulfide Gas. *Anal. Chem.* 88 (3), 1553–1558.
- Saha, K., Agasti, S.S., Kim, C., Li, X., Rotello, V.M., 2012. Gold nanoparticles in chemical and biological sensing. *Chem. Rev.* 112, 2739.
- Sachdev, D., Kumar, V., Maheshwari, P.H., Pasricha, R., Deepthi, Baghel, N., 2016. Silver based nanomaterial, as a selective colorimetric sensor for visual detection of post harvest spoilage in onion. *Sensor Actuat. B* 228, 471-479.

- Saito, K., Yagi, K., Ishizaki, A., Kataoka, H., 2010. Determination of anabolic steroids in human urine by automated in-tube solid-phase microextraction coupled with liquid chromatography-mass spectrometry, *J. Pharm. Biomed. Anal.* 52, 727-733.
- Saito, K., Ikeuchi, R., Kataoka, H., 2012. Determination of ochratoxins in nuts and grain samples by in-tube solid-phase microextraction coupled with liquid chromatography-mass spectrometry, *J. Chromatogr. A* 1220, 1-6.
- Salako, N.O., Philip, L., 2011. Comparison of the use of the Halimeter and the Oral Chroma™ in the assessment of the ability of common cultivable oral anaerobic bacteria to produce malodorous volatile sulfur compounds from cysteine and methionine. *Med Princ Pract.* 20 (1), 75-79.
- Salehnia, F., Hosseini, M., Ganjalnia, M.R., 2018. Enhanced electrochemiluminescence of luminol by an in situ silver nanoparticle-decorated graphene dot for glucose analysis. *Anal. Methods* 10, 508-514.
- Santos Barreto, A., de Cassia de Silva Andrade, P., Meira Farias, J., Menezes Filho, A., Fernandes de Sa, G., Alves Junior, S., 2018. Characterization and application of a lanthanide-based metal-organic framework in the development and validation of a matrix solid-phase dispersion procedure for pesticide extraction on peppers (*Capsicum annum* L.) with gas chromatography-mass spectrometry. *J Sep Sci.* 41 (7), 1593-1599.
- Saraz, J.A.O., Tinoco, I.F.F., Gates, R.S., Rocha, K.S.O., Marín, L.Z., 2015. A simple methodology to measure ammonia flux generated in naturally ventilated poultry houses, *Rev. Colomb. Ciencias Pecu.* 28, 3–12.
- Saroj, S., Rajput, S.J., 2018. Tailor made pH sensitive polyacrylic acid functionalized mesoporous silica nanoparticles for efficient and controlled delivery of anticancer drug Etoposide. *Drug Dev. Ind. Pharm.* 44 (7), 1198-1211.
- Scherperel, G., Reid, G. E., Waddell Smith, R., 2009. Characterization of smokeless powders using nanoelectrospray ionization mass spectrometry (nESI-MS). *Anal. Bioanal. Chem.* 394(8), 2019–2028.

- Schettler, T., 2006. Human exposure to phthalates via consumer products. *Int. J. Androl.* 29, 134-139.
- Schliemann, S., Zahlten, A., Krautheim, A., Elsner, P., 2010. Occupational allergic contact dermatitis caused by N-(3-aminopropyl)-N-dodecylpropane-1,3-diamine in a surface disinfectant. *Contact Dermat.* 63, 290–291.
- Schmidt-Winkel, P., Lukens, W.W., Zhao, D., Yang, P., Chmelka, B.F., Stucky, G.D., 1999. Mesocellular Siliceous Foams with Uniformly Sized Cells and Windows. *J. Am. Chem. Soc.* 21 (1), 254-255.
- Schneider, R.C., Kovar, K.A., 2003. Analysis of ecstasy tablets: comparison of reflectance and transmittance near infrared spectroscopy. *Forensic Sci. Int.* 134, 187-197.
- Seethapathy, S., Górecki, T., 2012. Applications of polydimethylsiloxane in analytical chemistry: A review. *Anal. Chim. Acta* 750, 48-62.
- Selvam P., Bhatia, S.K., Sonwane, C.G., 2001. Recent advances in processing and characterization of periodic mesoporous MCM-41 silicate molecular sieves. *Ind. Eng. Chem. Res.* 40, 3237-61.
- Serra-Mora, P., Jornet-Martínez, N., Moliner-Martínez, Y., Campins-Falcó, P., 2017. In tube-solid phase microextraction-nano liquid chromatography: Application to the determination of intact and degraded polar triazines in waters and recovered struvite. *J. Chromatogr. A* 1513, 51-58.
- Sharma, S., Tolley, L.T., Tolley, H.D., Plistil, A., Stearns, S.D., Lee, M.L., 2015. Hand-portable liquid chromatographic instrumentation. *J. Chromatogr. A* 1421, 38–47.
- Shamsayei, M., Yamini, Y., Asiabi, H., Safari, M., 2018. On-line packed magnetic in tube solid phase microextraction of acidic drugs such as naproxen and indomethacin by using $\text{Fe}_3\text{O}_4@\text{SiO}_2$ @layered double hydroxide nanoparticles with high anion exchange capacity. *Microchim. Acta.* 185(3), 192-202.

- Sheikhaleh, A., Abedi, K., Jafari, K., 2017. An Optical MEMS Accelerometer Based on a Two-Dimensional Photonic Crystal Add-Drop Filter. *J. Light. Technol.* 35 (14), 3029-3034.
- Shih, Y.H., Wang, K.Y., Singco, B., Lin, C.H., Huang, H.Y., 2016. Metal Organic Framework-Polymer Composite as a Highly Efficient Sorbent for Sulfonamide Adsorption and Desorption: Effect of Coordinatively Unsaturated Metal Site and Topology. *Langmuir* 32 (44), 11465-11473.
- Shrivastava, K., Nirmalkar, N., Thakur, S.S., Deb, M.K., Shinde, S.S., Shankar, R., 2018. Sucrose capped gold nanoparticles as a plasmonic chemical sensor based on non-covalent interactions: Application for selective detection of vitamins B1 and B6 in brown and white rice food samples. *Food Chem.* 250, 14-21.
- Sicard, C., Glen, C., Aubie, B., Wallace, D., Jahanshahi-Anbuhi, S., Pennings, K., Daigger, G.T., Pelton, R., Brennan, J.D., Filipe, C.D.M., 2015. Tools for water quality monitoring and mapping using paper-based sensors and cell phones. *Water Res.* 70, 360–369.
- Smith, J.E., Griffin, D.K., Leny, J.K., Hagen, J.A., Chávez, J.L., Kelley-Loughnane, N., 2014. Colorimetric detection with aptamer-gold nanoparticle conjugates coupled to an android-based color analysis application for use in the field. *Talanta*. 121, 247-255.
- Smith, J.P., Sutcliffe, O.B., Banks, C.E., 2015. An overview of recent developments in the analytical detection of new psychoactive substances (NPSs). *Analyst* 140, 4932–4948.
- Smith, P.A., 2012. Person-portable gas chromatography: rapid temperature program operation through resistive heating of columns with inherently low thermal mass properties. *J. Chromatogr. A* 1261, 37–45.
- Soga, T., Jimbo, Y., Suzuki, K., Citterio, D., 2013. Inkjet-Printed Paper-Based Colorimetric Sensor Array for the Discrimination of Volatile Primary Amines. *Anal. Chem.* 85 (19), 8973–8978.

- Song, X.Y., Ha, W., Chen, J., Shi, Y.P., 2014. Application of beta-cyclodextrin-modified, carbon nanotubereinforced hollow fiber to solid-phase microextraction of plant hormones. *J. Chromatogr. A* 1374, 23–30.
- Souza, I.D., Melo, L.P., Jardim, I.C.S.F., Monteiro, J.C.S., Nakano, A.M.S., Queiroz, M.E.C., 2016. Selective molecularly imprinted polymer combined with restricted access material for in-tube SPME/UHPLC-MS/MS of parabens in breast milk samples. *Anal. Chim. Acta* 932, 49-59.
- Souza Caldas, S., Meira Soares, B., Abreu, F., Braga Castro, I., Fillmann, G., Gilberto Primel, E., 2018. Antifouling booster biocide extraction from marine sediments: a fast and simple method based on vortex-assisted matrix solid-phase extraction. *Environ. Sci. Pollut. Res. Int.* 25, 7553-7565.
- Srinives, S., Sarkar, T., Mulchandani, A., 2014. Primary amine-functionalized polyaniline nanothin film sensor for detecting formaldehyde. *Sens. Actuator B-Chem.* 194, 255-259.
- Stankova, N.E., Atanasov, P.A., Nikov, R.G., Nikov, R.G., Nedyalkov, N.N., Stoyanchoy, T.R., Fukata, N., Kolev, K.N., Valova, E.I., Georgieva, J.S., Armyanov, S.A., 2015. Optical properties of polydimethylsiloxane (PDMS) during nanosecond laser processing. *Appl. Surf. Sci.* 374, 96–103.
- Stassi, S., Cauda, V., Fiorilli, S., Ricciardi, C., 2015. Surface area enhancement by mesoporous silica deposition on microcantilever sensors for small molecule detection. *J. Mater. Chem. C* 3, 12507-12513.
- Steinhauer, T., Kulozik, U., Gebhardt, R., 2014. Structure of milk protein deposits formed by casein micelles and β -lactoglobulin during frontal microfiltration. *J. Memb. Sci.* 468, 126-132.
- Stewart, M.E., Anderton, C.R., Thompson, L.B., Maria, J., Gray, S.K., Rogers, J.A., Nuzzo, R.G., 2008. Nanostructured plasmonic sensors, *Chem. Rev.* 108, 494–521.
- Stumr, F., Gabrovská, D., Rvsova, J., Hanak, P., Plicka, J., Tomkova, K., Dvorska, P., Cuhra, P., Kubik, M., Barsova, S., Karsulinova, L., Bulawova, H., Brychta, J.,

- Yman, I.M., 2010. ELISA kit for casein determination: interlaboratory study. *J. AOAC Int.* 93, 676–682.
- Su, K., Zou, Q., Hu, N., Wang, P., 2015. High-sensitive and high-efficient biochemical analysis method using a bionic electronic eye in combination with a smartphone-based colorimetric reader system, *Sensors Actuators B Chem.* 216, 134–140.
- Su, K., Qiu, X., Fang, F., Zou, Q., Wang, P., 2017. An improved efficient biochemical detection method to marine toxins with a smartphone-based portable system-Bionic e-Eye, *Sensors Actuators, B Chem.* 238, 1165–1172.
- Suarez, F.L., Furnel, J.K., Springfield, J., Levittl, M.D., 2000. Morning Breath Odor: Influence of Treatments on Sulfur Gases. *J Dent Res* 79(10), 1773-1777.
- Sun, M., Feng, J., Bu, Y., Luo, C., 2015. Nanostructured-silver-coated polyetheretherketone tube for online in-tube solid-phase microextraction coupled with high-performance liquid chromatography. *J. Sep. Sci.* 38, 3239-3246.
- Tabernerero, M.J., Felli, M.L., Bermejo, A.M., Chiarotti, M., 2009. Determination of ketamine and amphetamines in hair by LC/MS/MS. *Anal. Bioanal. Chem.* 395, 2547–2557.
- Tamayo, A., Rubio, J., 2010. Structure modification by solvent addition into TEOS/PDMS hybrid materials. *J. Non-Cryst Solids* 356, 1742–1748.
- Tan, F., S.H., Nguyen, N.T., Chua, Y.C., Kang, G.T., 2010. Oxygen plasma treatment for reducing hydrophobicity of a sealed polydimethylsiloxane microchannel. *Biomicrofluidics* 4, 32204-32212.
- Tan, F., Zhao, C., Li, L., Liu, M., He, X., Gao, J., 2015. Graphene oxide based in-tube solid-phase microextraction combined with liquid chromatography tandem mass spectrometry for the determination of triazine herbicides in water. *J. Sep. Sci.* 38, 2312-2319.

- Tangerman, A., Winkel, E.G., 2007. Intra- and extra-oral halitosis: finding of a new form of extra-oral blood-borne halitosis caused by dimethyl sulphide. *J Clin. Periodontol.* 34(9), 748-55.
- Tangerman, A., Winkel, E.G., 2008. The portable gas chromatograph OralChroma™: a method of choice to detect oral and extra-oral halitosis. *J Breath Res.* 2(1), 17010- 17017.
- Tarifa, A., Almirall, J. R., 2015. Fast detection and characterization of organic and inorganic gunshot residues on the hands of suspects by CMV-GC-MS and LIBS. *Sci. Justice* 55(3), 168-175.
- Tezel, U., 2009. Fate and effect of quaternary ammonium compounds in biological systems, PhD Thesis, Georgia Institute of Technology. Atlanta, GA.
- Timberlake, K.C., 1992. *Chemistry*, 5th ed. Haper-Collins Publishers Inc. New York.
- Tong, Y., Wu, Z., Yang, C., Yu, J., Zhang, X., Yang, S., Wen, Y., 2001. Determination of diphenylamine stabilizer and its nitrated derivatives in smokeless gunpowder using a tandem MS method. *The Analyst* 126(4), 480–484.
- Tomita, M., Nakashima, M.N., Wada, M., Nakashima, K , 2007. Sensitive determination of MDMA and its metabolite MDA in rat blood and brain microdialysates by HPLC with fluorescence detection. *Biomed. Chromatogr.* 21 (10), 1016-1022.
- Tsai, C.H., Xu, M.Z., Kunal, P., Trewyn, B.G., 2018. Aerobic oxidative esterification of primary alcohols over Pd-Au bimetallic catalysts supported on mesoporous silica nanoparticles. *Catal. Today* 306, 81-88.
- Tsujikawa, K., Kuwayama, K., Miyaguchi, H., Kanamori, T., Iwata, Y.T., Yoshida, T., Inoue, H., 2008. Development of an on-site screening system for amphetamine-type stimulant tablets with a portable attenuated total reflection fourier transform infrared spectrometer. *Anal. Chim. Acta* 608, 95-103.

- Turner, C., 2013. Sustainable analytical chemistry-more than just being green, *Pure Appl. Chem.* 85, 2217-2229.
- USEPA, 1991. National Primary Drinking Water Regulations: Federal Register, Part 12, 40 CFR Part 141, US Environmental Protection Agency.
- Valcarcel, M., Cardenas, S., Simonet, B.M., Moliner-Martínez, Y., Lucena, R., 2008. Carbon nanostructures as sorbent materials in analytical processes. *TrAC-Trend. Anal. Chem.* 27, 34-43.
- Vashist, S.K., Van Oordt, T., Schneider, E.M., Zengerle, R., Von Stetten, F., Luong, J.H.T., 2014. A smartphone-based colorimetric reader for bioanalytical applications using the screen-based bottom illumination provided by gadgets. *Biosens. Bioelectron.* 67, 248-255.
- Vashist, S.K., Marion Schneider, E., Zengerle, R., Von Stetten, F., Luong, J.H.T., 2015. Graphene-based rapid and highly-sensitive immunoassay for C-reactive protein using a smartphone-based colorimetric reader, *Biosens. Bioelectron.* 66, 169-176.
- Verkouteren, J.R., Staymates, J.L., 2010. Reliability of ion mobility spectrometry for qualitative analysis of complex, multicomponent illicit drug samples. *Forensic Sci. Int.* 206, 190-196.
- Vidal Giné, C., Ventura Vilamala, M., Fornís Espinosa, I., Gil Lladanosa, C., Calzada Álvarez, N., Fitó Fruitós, A., Rodríguez Rodríguez, J., Domingo Salvany, A., de la Torre Fornell, R., 2016. Crystals and tablets in the Spanish ecstasy market 2000-2014: are they the same or different in terms of purity and adulteration? *Forensic Sci. Int.* 263, 164-168.
- Vitta, Y., Moliner-Martinez, Y., Campíns-Falcó, P., Cuervo, A.F., 2010. An in-tube SPME device for the selective determination of chlorophyll a in aquatic systems, *Talanta* 82, 952-956.
- Vogliardi, S., Tucci, M., Stocchero, G., Ferrara, S.D., Favretto, D., 2015. Sample preparation methods for determination of drugs of abuse in hair samples: a review. *Anal. Chim. Acta* 857, 1-27.

- Wada, M., Ikeda, R., Kuroda, N., Nakashima, K., 2010. Analytical methods for abused drugs in hair and their applications. *Anal. Bioanal. Chem.* 397, 1039–1067.
- Wada, M., Sugimoto, Y., Crabtree, B.L., Evans, C., Montgomery, J.H., Ikeda, R., Kuroda, N., Nakashima, N., 2013. Simultaneous determination of amphetamine-typesimulabnts in abusers' hair: clinical usefulness of hair analysis in prehospitalization for abusers. *Forensic Toxicol.* 31, 2–8.
- Waddell-Smith, R.J.H., 2007. A review of recent advances in impurity profiling of illicit MDMA samples. *J. Forensic Sci.* 52, 1297–1304.
- Wallace, J. S., 2008. *Chemical Analysis of Firearms, Ammunition, and Gunshot Residue. International Forensic Science and Investigation.* CRC Press, 320.
- Wan, Y., Zhao, D. Y., 2007. On the Controllable Soft-Templating Approach to Mesoporous Silicates. *Chem. Rev.* 107 (7), 2821–2860.
- Wang, F., Gu, Z., Lei, W., Wang, W., Xia., Hao, Q., 2014. Graphene quantum dots as a fluorescent sensing platform for highly efficient detection of copper(II) ions. *Sens. Actuator B-Chem.* 190, 516-522.
- Wang, J-X., Jiang, D-Q., Gu, Z-Y., Yan, X-P., 2006. Multiwalled carbon nanotubes coated fibers for solid phase microextraction of polybrominated diphenyl ethers in water and milk samples before gas chromatography with electron-capture detection. *J. Chromatogr. A* 1137(1), 8-14.
- Wang, L.Y., Huo, M.F., Chen, Y., Shi, J.L., 2018. Iron-engineered mesoporous silica nanocatalyst with biodegradable and catalytic framework for tumor-specific therapy. *Biomaterials.* 163, 1-13.
- Wang, R., Li, W., Chen, Z., 2018. Solid phase microextraction with poly(deep eutectic solvent) monolithic column online coupled to HPLC for determination of non-steroidal anti-inflammatory drugs. *Anal. Chim. Acta* 1018, 111-118.

- Wang, S., Hu, S., Xu, H., 2015. Analysis of aldehydes in human exhaled breath condensates by in- tube SPME-HPLC. *Anal. Chim. Acta* 900, 67-75.
- Wang, T., Tong, J., Sun, M., Chen, L., 2011. Fast and selective extraction of chloramphenicol from soil by matrix solid-phase dispersion using molecularly imprinted polymer as dispersant. *J. Sep. Sci.* 34, 1886-1892.
- Wang, T., Chen, Y., Ma, J., Hu, M., Li, U., Fang, J., Gao, H., 2014. A novel ionic liquid-modified organic-polymer monolith as the adsorbent for in-tube solid phase microextraction of acidic food additives. *Anal. Bioanal. Chem.* 406, 4955-4963.
- Wang, T., Chen, Y., Ma, J., Qian, Q., Jin, Z., Zhang, L., Zhang, Y., 2016. Attapulgite nanoparticles-modified monolithic column for hydrophilic in-tube solid-phase microextraction of cyromazine and melamine. *Anal. Chem.* 88, 1535-1541.
- Wang, T., Chen, Y., Ma, J., Jin, Z., Chai, M., Xiao, X., Zhang, L., Zhang, Y., 2018. A polyethyleneimine-modified attapulgite as a novel solid support in matrix solid-phase dispersion for the extraction of cadmium traces in seafood products. *Talanta*. 180, 254-259.
- Wang, X., Ma, Q., Li, M., Chang, C., Bai, Y., Feng, Y., Liu, H., 2013. Automated and sensitive analysis of 28-epihomobrassinolide in *Arabidopsis thaliana* by on-line polymer monolith microextraction coupled to liquid chromatography-mass spectrometry. *J. Chromatogr. A* 1317, 121-128.
- Wang, X., Li, X., Li, Ze., Zhang, L., Bai, Y., Liu, H., 2014. Online coupling of in-tube solid-phase microextraction with direct analysis in real time mass spectrometry for rapid determination of triazine herbicides in water using carbon-nanotubes-incorporated polymer monolith. *Anal. Chem.* 86 (10), 4739-4747.
- Wardencki, W., 2000. Sulfur Compounds: Gas Chromatography. *Encyclopedia of Separation Science*. Poland, 4285.

- Warren, J. E., Perkins, C. G., Jelfs, K. E., Boldrin, P., Chater, P. A., Miller, G.J., Manning, T.D., Briggs, M.E., Stylianou, K.C., Claridge, J.B., Rosseinsky, M.J., 2014. Shape selectivity by guest-driven restructuring of a porous material. *Angew. Chem.* 53, 4592-4596.
- Wen, X. L., Jiang, L. C., Jing, H., Xi, L., Shu, T., 2008. Multi-residues of organic pollutants in surface sediments from littoral areas of the Yellow Sea, China. *Mar. Pollut. Bull.* 56, 1091-1103.
- Weyerman, C., Mimoune, Y., Anglada, F., Massonet, G., Esseiva, P., Buzzini, P., 2011. Applications of a transportable Raman spectrometer for the in situ detection of controlled substances at border controls, *Forensic Sci. Int.* 209, 21-28.
- Wu, F., Wang, J., Zhao, Q., Jiang, N., Lin, X., Xie, Z., Li, J., Zhang, Q., 2016. Detection of trans-fatty acids by high performance liquid chromatography coupled with in-tube solid-phase microextraction using hydrophobic polymeric monolith. *J Chromatogr. B Analyt. Technol. Biomed. Life Sci.* 1040, 214-221.
- Wu, J.C., Pawliszyn, J., 2001. Polypyrrole coated capillary coupled to HPLC for in-tube solid phase microextraction and analysis of aromatic compounds in aqueous samples, *Anal. Chem.* 73, 55-63.
- Wu, S., Cai, C., Cheng, J., Cheng, M., Zhou, H., Deng, J., 2016. Polydopamine/dialdehyde starch/chitosan composite coating for in-tube solid-phase microextraction and in situ derivation to analysis of two liver cancer biomarkers in human blood, *Anal. Chim. Acta* 935, 113-120.
- Wu, Z.X., Guo, F., Huang, L., Wang, L., 2018. Electrochemical nonenzymatic sensor based on cetyltrimethylammonium bromide and chitosan functionalized carbon nanotube modified glassy carbon electrode for the determination of hydroxymethanesulfinate in the presence of sulfite in foods. *Food Chem.* 259, 213-218.

- Xu, B., Cheng, S., Wang, X., Wang, D., Xu, L., 2015. Novel polystyrene/antibody nanoparticle-coated capillary for immunoaffinity in-tube solid-phase microextraction. *Anal Bioanal Chem.* 407(10), 2771-5.
- Xu, H., Wu, J., Chen, C.H., Zhang, L., Yang, K.L., 2010. Detecting hydrogen sulfide by using transparent polymer with embedded CdSe/CdS quantum dots. *Sens. ActuatorB – Chem.* 143, 535–538.
- Xu, J., Zheng, J., Tian, J., Zhu, F., Zeng, F., Su, C., Ouyang, G., 2013. New materials in solid-phase microextraction. *Trends Analyt. Chem.* 47, 68-83.
- Xu, P.C., Guo, S.B., Yu, H.T., Li, X.X., 2014. Mesoporous Silica Nanoparticles (MSNs) for Detoxification of Hazardous Organophorous Chemicals. *Small* 10 (12), 2404-2412.
- Xu, T., Xu, P., Zheng, D., Yu, H., Li, X., 2016. Metal–organic frameworks for resonant-gravimetric detection of trace-level xylene molecules. *Anal. Chem.* 88, 12234–12240.
- Yambem, S.D., Timm, J., Weiss, M., Pandey, A.K., Marschall, R., 2017. Sulfonated mesoporous silica as proton exchanging layer in solid-state organic transistor. *Adv. Electron. Mater.* 3 (12), 1700316.
- Yarbakht, M., Nikkhah, M., 2015. Unmodified gold nanoparticles as a colorimetric probe for visual methamphetamine detection. *J. Exp. Nanosci.*, 11(7), 593-601.
- Ying, L.-L., Ma, Y.-C., Xu, B., Wang, X.-H., Dong, L.-Y., Wang, D.-M., Liu, K., Xu, L., 2017. Poly(glycidylmethacrylate) nanoparticle-coated capillary with oriented antibody immobilization for immunoaffinity in-tube solid phase microextraction: Preparation and characterization. *J. Chromatogr. A* 1509, 1-8.
- Yuan, S.-Y., Huang, I.-C., Chang, B.-V., 2010. Biodegradation of dibutyl phthalate and di-(2-ethylhexyl) phthalate and microbial community changes in mangrove sediment. *J. Hazar. Mat.* 184, 826-831.

- Zarejousheghani, M., Moeder, M., Borsdorf, H., 2013. A new strategy for synthesis of an in-tube molecularly imprinted polymer-solid phase microextraction device: Selective off-line extraction of 4-nitrophenol as an example of priority pollutants from environmental water samples. *Analytica Chimica Acta* 798, 48-55.
- Zhang, B.-T., Zheng, X., Li, H.-F., Lin, J.-M. 2013. Application of carbon-based nanomaterials in sample preparation: a review. *Anal. Chim. Acta* 784, 1–17.
- Zhang, C., Suslick, K.S., 2007. Colorimetric sensor array for soft drink analysis. *J. Agric. Food Chem.* 55, 237–242.
- Zhang, H.-Y., Pan, H.-Q., Zhang, B.-L., Tang, J.-L., 2012. Microcantilever sensors for chemical and biological applications in liquid. *Chin. J. Anal. Chem.* 40(5), 801–808.
- Zhang, J., Zhang, W., Bao, T., Chen, Z., 2015. Polydopamine-based immobilization of zeolitic imidazolate framework-8 for in-tube solid-phase microextraction. *J. Chromatogr. A* 1388, 9-16.
- Zhang, S., Jia, K., Wang, S., 2010. Determination of b-Carotene in Corn by in tube SPME coupled to micro-LC. *Chromatographia* 72 (11), 1231-1233.
- Zhang, W.P., Zhang, J., Bao, T., Zhou, W., Meng, J.W., Zheng, Z.L., 2013. Universal multilayer assemblies of graphene in chemically resistant microtubes for extraction. *Anal. Chem.* 85, 6846-6854.
- Zhang, X.F., Liu, Z.G., Shen, W., Gurunathan, S., 2016. Silver Nanoparticles: Synthesis, Characterization, Properties, Applications, and Therapeutic Approaches. *Int. J. Mol. Sci.* 17(9), 1534.
- Zhang, Z., Chen, Z., Wang, S., Qu, C., Chen, L., 2014. On-Site Visual Detection of Hydrogen Sulfide in Air Based on Enhancing the Stability of Gold Nanoparticles. *ACS Appl. Mater. Interfaces* 6 (9), 6300-6307.

- Zhao, W., Ali, M.M., Aguirre, S.D., Brook, M.A., Li, Y., 2008. Paper-based bioassays using gold nanoparticle colorimetric probes. *Anal. Chem.* 80 (22), 8431–8437.
- Zheng, M.-M., Ruan, G.-D., Feng, Y.-Q., 2009. Evaluating polymer monolith in-tube solid phase microextraction coupled to liquid chromatography/quadrupole time of flight mass spectrometry for reliable quantification and confirmation of quinolone antibacterials in edible animal food. *J. Chromatogr. A* 1216, 7510-7519.
- Zheng, M.-M., Wang, S.T., Hu, W.K., Feng, Y.Q., 2010. In tube solid-phase microextraction based on hybrid silica monolith coupled to liquid chromatography-mass spectrometry for automated analysis of ten antidepressants in human urine and plasma. *J. Chromatogr. A* 1217, 7493-7501.
- Zhu, K.Y., Leung, K.W., Ting, A.K.L., Wong, Z.C.F., Ng, W.Y.Y., Choi, R.C.Y., Dong, T.T.X., Wang, T., Lau, D.T.W., Tsim, K.W.K., 2012. Microfluidic chip based nano liquid chromatography coupled to tandem mass spectrometry for the determination of abused drugs and metabolites in human hair. *Anal. Bioanal. Chem.* 402, 2805–2815.

ANNEX

A1. Abbreviations

A1. ABBREVIATIONS

aa	Aminoacid
$a \pm s_a$	Ordinate \pm standard deviation of ordinate
ACN	Acetonitrile
ADP	N-(3-aminopropyl)-N-dodecyl-1,3-propanediamine
AFM	Atomic Force Microscopy
AgNPs	Silver nanoparticles
AMP	Amphetamine
APTS	(3-Aminopropyl)triethoxysilane
AuNPs	Gold nanoparticles
$b \pm s_b$	Slope \pm standard deviation of slope
BAK	Benzalkonium Chloride
BCA	Bicinchoninic acid
CapLC	Capillary Liquid Chromatography
CIP	Cleaning In Place
CMC	Critical Micellar Concentration
CMYK	Cyan Magent Yellow Key
c-MWCNTs	Carboxylated multi-wall carbon nanotubes
CNTs	Carbon nanotubes
CSPs	Chiral stationary phases
c-SWCNTs	Carboxylated single-wall carbon nanotubes
DAD	Diode Array Detection
DART-MS	Direct analysis in real time mass spectrometry
DCC	Dicyclohexylcarbodiimide
DEHP	Di(2-ethylhexyl)phthalate
DEP	Diethylphthalate
DBP	Dibutylphthalate
DI	Digital image
DPA	Diphenylamine
DR	Diffuse reflectance
ECHA	European Chemical Agency
EDTA	Ethylenediamine-tetraacetic acid
EDX	Energy-dispersive X-ray spectroscopy
EEUU	United States
e.g.	For example (“ <i>exempli gratia</i> ”)
EMCDDA	European Monitoring Centre for Drugs and Drug Addiction
EP	Ephedrine
EQS	Environmental Quality Standards
ETH ^T 4001	4-(N,N-dioctylamino)-4'-trifluoroacetylazobenzene
EU	European Union
FLD	Fluorescence Detector
FMOC	9-Fluorenylmethyl chloroformate
FMOC-L-Pro	9-Fluorenylmethyl chloroformate-L-proline
FTIR-ATR	Fourier transform infrared-attenuated total reflectance
GC	Gas Chromatography

GHG	Glycine-L-Histidine-Glycine
GHS	Globally harmonized system of classification and labelling of chemicals
GIMP	GNU Image Manipulation Program
GSRs	Gunshot residues
HG-AAS	Hybrid generation atomic absorption spectrometry
HPLC	High Performance Liquid Chromatography
HRP	Horseradish peroxidase enzyme
HS	Head space
HSV	Hue Saturation Value
i.d.	Internal diameter
IMS	Ion mobility spectrometry
IGSRs	Inorganic gunshot residues
IT-SPME	In-tube solid phase microextraction
LC	Liquid chromatography
LPE	Liquid phase extraction
LOD	Limit of detection
LOQ	Limit of quantification
MAMP	Methamphetamine
MC	Monte Carlo
MEHP	Mono-ethylhexylphthalate
MEMS	Microelectromechanical systems
MCF	Mesoporous cellular foam
MCM	Mobile composition of matter
MDA	3,4-methylenedioxyamphetamine
MDEA	3,4-methylenedioxyethylamphetamine
MDMA	3,4-methylenedioxymetamphetamine
MIPs	Molecularly imprinted polymers
MOF	Metal-organic framework
MTEOS	methyltriethoxysilane
MS	Mass spectrometry
MSPD	Matrix solid phase dispersion
MWCNTs	Multiwall carbon nanotubes
NanoLC	Nano liquid chromatography
NPs	Nanoparticles
NQS	1,2-Naphthoquinone-4-sulphonate
NTA	Nitrilotriacetic acid
PAHs	Polycyclic aromatic hydrocarbon
PBS	Phosphate buffered saline
PDMS	Polydimethylsiloxane
PCB	Printed circuit board
PEEK	Polyether ether ketone
PEG	Polyethylene glycol
PR	Preconcentration rates
PVC	Polyvinylchloride
PXRD	Powder Xray diffraction
PZT	Lead Zirconate Titanate

QAC	Quaternary Ammonium Compounds
RD	Real Decreto
RGB	Red Green Blue
RSD	Relative standard deviation
SBA	Santa Barbara Amorphous
SEM	Scanning Electron Microscopy
SiO ₂ NPs	Silicon dioxide nanoparticles
SPE	Solid phase extraction
SPME	Solid phase microextraction
SPR	Surface plasmon resonance
SWCNTs	Single-wall carbon nanotubes
TEM	Transmission Electron Microscopy
TEOS	Tetraethylortosilicate
TMB	3,3,5,5-tetramethylbencidine
TMOS	Tetramethylortosilicate
TMTDAC	Trimethyl-tetradecylammonium chloride
UAE	Ultrasound-assisted extraction
UNODC	United Nations Office on Drugs and Crime
UV-Vis	Ultraviolet Visible
USEPA	United States Environmental Protection Agency
VAE	Vortex-assisted extraction
VOCs	Volatile organic compounds
VSCs	Volatile sulphure compounds
v/v	volume/volume
w/w	weight/weight
w/v	weight/volume
3D	Three-dimensional

A2. Figure List

A2. FIGURE LIST

Figure 1. Scheme of the SPE procedure	7
Figure 2. Evolution of the number of citations on Web of Science for matching the search items “IT-SPME” OR “In-tube SPME” OR “In-tube solid phase microextraction”	9
Figure 3. Schematic representation of configurations used for IT-SPME-LC: A) draw/eject cycle mode, B) flow-through in-valve IT-SPME and C) flow-through with an additional pumping system.....	11
Figure 4. Percentage of studies using several materials as extractive phases for the last five years. Data from Web of Science matching the search terms “IT-SPME” OR “In-tube solid phase microextraction” OR “In-tube SPME”.....	14
Figure 5. Schematic representation of in-line, on-line and off-line analytical methods and their relationship with in situ analysis	22
Figure 6. Number of citations on Web of Science for matching the following search term “in situ analysis” AND “sensors” in the 1998-2017 period.....	24
Figure 7. Number of citations on Web of Science for matching the following search term “smartphone sensor” OR “smartphone reader” OR “smartphone photometr” in the 2012-2017 period.....	25
Figure 8. Microcantilever-based sensor.....	30
Figure 9. Principle of micro-cantilever-based sensors for chemical detection: static and dynamic mode.....	31
Figure 10. Summary of piezoelectric effect a) after polarization, b) output voltage of same polarity as material due to a compressive stress, c) output voltage of opposite polarity as material due to a tensile stress, d) applied voltage of same polarity as material produce a contraction of material and e) applied voltage of same polarity as material produce a expansion of material	33
Figure 11. Print cycle of the screen-printing procedure. The screen is located just above the substrate (1). Then, the mesh of the screen is brought into line contact with the squeegee and scanned across the screen (2). The mesh should peel away from the surface immediately behind the squeegee, leaving all the ink that was in the mesh deposited onto the printing surface (3).....	34
Figure 12. Chemical structure of PDMS	36
Figure 13. Number of citations on Web of Science for matching the following search terms: “PDMS” OR “Polydimethylsiloxane” AND “extractive phase” between 2013 and 2017 (March 2018).....	37
Figure 14. Chemical structure of bondesil C ₁₈	40

Figure 15. Schematic representation of MWCNTs coating.....	43
Figure 16. Illustration of the excitation of localized SPR where electrons in the metallic NP are driven into oscillation due to coupling with incident light; d is the diameter of sphere and λ is the wavelength of the light	44
Figure 17. Surface plasmon band of spherical AgNPs of 15-20 nm.....	45
Figure 18. Evolution of number of citations about AgNPs from the year 2008 in the web of science by searching “AgNPs” OR “Silver nanoparticles” in the field of “Title”.....	46
Figure 19. Schematic picture of the AgNPs aggregation in presence of sulphure compounds (See Section 4.3.2.1)	48
Figure 20. A) Porous structure and B) Crystalline structure of Cu(GHG) MOF.....	49
Figure 21. Structure of the phthalate analyzed in this thesis, DEHP	51
Figure 22. Structure of several biocides studied in this Thesis.....	54
Figure 23. Structure of casein (data from PubChem)	56
Figure 24. Structure of the amphetamine-like drugs studied in this Thesis.....	57
Figure 25. Structures of chiral A) MAMP and B) EP.....	60
Figure 26. Structure of ketamine	61
Figure 27. Structure of DPA	63
Figure 28. A) Cary 60 Fiber Optic UV-Vis spectrophotometer and B) Remote fiber optic DR accessory	83
Figure 29. Cary 630 ATR-FTIR spectrophotometer	84
Figure 30. Horiba-MTB RAMAN spectrophotometer.....	84
Figure 31. Impedancemeter HP4194A.....	85
Figure 32. HPLC-FLD System A) Jasco and B) Hewlett-Packar	87
Figure 33. CapLC-DAD system for isocratic mode.....	88
Figure 34. CapLC system with binary capillary pump	88
Figure 35. CapLC-FLD system in isocratic mode.....	89
Figure 36. Nikon light microscope	90
Figure 37. SEM A) Hitachi S-4100 and B) Philips XL 30 ESEM.....	91
Figure 38. Dektak 150 profilometer.....	91
Figure 39. A) Scheme of the experimental setup used for SPE enantioseparation and B) Picture of the actual polypropylene SPE tube after incorporation of the chiral MOF bed.....	92
Figure 40. Scheme of A) Sampling by scrubbing the shooter hand with cotton swab and B) Standard solution preparation for the VAE	93

Figure 41. Scheme of A) MSPD for the determination of DEHP in sediments, B) MSPD/solution derivatization (b.1) and Integrated MSPD/solid support derivatization (b.2) for the determination of amphetamines in hair.....	95
Figure 42. In-valve IT-SPME coupled to LC with six port valve A) In load position and B) In inject position.....	96
Figure 43. Procedure of PDMS/TEOS/SiO ₂ NPs-NQS sensors fabrication	98
Figure 44. Procedure of PDMS-Co(SCN) ₂ sensors fabrication	99
Figure 45. Procedure of the AgNPS immobilization on nylon membrane.....	100
Figure 46. A) Turbula mixer and B) three-roll mill (EXAKT 80S).....	101
Figure 47. A) Stencil for PZT printing; B) Screen with emulsion with patterns on mesh for gold, sacrificial and dielectric printings; C) Mask with pattern of disks and fiducials for reveling; D) Screen copy unit Variocop S for insolation.....	102
Figure 48. Procedure of mesh revelation.....	103
Figure 49. A) Overall view of DEK Horizon 03iX screen printing platform and B) view of the print cycle.....	104
Figure 50. A) Furnace and B) Time-temperature profile in the firing process	105
Figure 51. Polarization equipment AET	106
Figure 52. Scheme of the reaction between amphetamines tested and A) FMOC B) FMOC-L-Pro and DCC	109
Figure 53. Procedure to obtain the colorimetric response of polymeric sensors..	111
Figure 54. Sensor hanged up into static dilution bottle to generate gaseous standard.....	112
Figure 55. A) Gas chamber connected to impedancemeter and gas generator (Inset: top view of cantilever on alumina substrate bonded on PCB support and B) Vapor generator.....	113
Figure 56. FTIR-ATR spectra obtained for C ₁₈ used as solid phase in the MSPD procedure, sediment, MSPD mixture and MSPD mixture after extraction with acetonitrile.....	123
Figure 57. Chromatograms at 230 nm obtained for a sediment sample (A), sediment sample spiked with 47.62 ppb (B), and 69.77 ppb (C) of DEHP (concentrations in the extracts). The spikes were realized before MSPD treatment. Inset corresponds to DEHP spectrum	125
Figure 58. Photographs of the proportions according to particle sizes (A, B, C, D, and E corresponding to bigger than 0.4, 0.4, 0.3, 0.2, and 0.1 mm, respectively) for different types of sediments: (1) sediment sample obtained from coast zone, (2) sediment sample obtained from transition zone, and (3) sediment sample obtained from a port zone.....	127

- Figure 59.** Absorbance ratio Si-O/C-O for the sediments assayed (see also Figure 58 and Table 23) 128
- Figure 60.** A) Effect of acetonitrile (ACN) percentage on the retention of C₁₂-BAK (first peak) and C₁₄-BAK (second peak) homologues at 0.5 µg mL⁻¹ using short C₁₈ column. Flow rate = 10 µL min⁻¹, B) Comparative separation of BAK homologues (at 0.5 µg mL⁻¹) on C₁₈ and nitrile capillary column. Conditions of mobile phase and flow rate: 85% ACN and 20 µL min⁻¹ for C₁₈ column; 65% ACN and 10 µL min⁻¹ for nitrile column 131
- Figure 61.** Effect of BAK concentration on extraction efficiency of each homologue when water is used as sample solvent. Conditions: nitrile column, ACN:acetate buffer (65:35), flow rate = 10 µL min⁻¹, 1000 µL for BAK 0.5 and 5 µg mL⁻¹, and 100 µL for BAK 50 µg mL⁻¹ 133
- Figure 62.** Percentage response of each homologue in simultaneous IT-SPME of BAK and ADP with respect of the response in individual BAK extraction (% s-BAK/i-BAK), at several relations of concentration of ADP and BAK (a) 1 (BAK 50 µg mL⁻¹ and ADP 50 µg mL⁻¹), (b) 2 (BAK 50 µg mL⁻¹ and ADP 100 µg mL⁻¹), (c) 3 (BAK 50 µg mL⁻¹ and ADP 200 µg mL⁻¹), (d) 40 (BAK 5 µg mL⁻¹ and ADP µg mL⁻¹), (e) 60 (BAK 0.5 µg mL⁻¹ and ADP 30 µg mL⁻¹). Optimized conditions for nitrile column were employed..... 135
- Figure 63.** IT-SPME of 0.5 µg mL⁻¹ of BAK in water and simultaneous IT-SPME of 0.5 µg mL⁻¹ of BAK in presence of 30 µg mL⁻¹ of ADP by using (A) Nitrile column, acetonitrile:acetate buffer (65:35), Flow rate = 10 µL min⁻¹ (B) Short C₁₈ column, acetonitrile:acetate buffer (85:25), Flow rate = 20 µL min⁻¹ 136
- Figure 64.** Effect of TMTDAC on extraction efficiency of C₁₂-BAK and C₁₄-BAK. Mixtures of 1.5 µg mL⁻¹ BAK with 1.5 and 30 µg mL⁻¹ TMTDAC. Conditions: Short C₁₈ column, ACN:acetate buffer (85:25), Flow rate = 20 µL min⁻¹ 137
- Figure 65.** Effect of ADP on extraction efficiency of BAK. Mixtures of 1.5 µg mL⁻¹ BAK with 1.5, 15 and 30 µg mL⁻¹ of DPA from biocide product (sample DC1). Conditions: Short C₁₈ column, acetonitrile:acetate buffer (85:25), Flow rate = 20 µL min⁻¹ 139
- Figure 66.** Comparison of peak areas obtained for standard solution (3 µL of 10 µg mL⁻¹ in 2 mL of water, 15 ng mL⁻¹) with different (A) sample collectors (B) solvents to wet cotton swab (at 10 ng mL⁻¹): dry (a), water(b), acetone (c) and ethanol (d), together with normalized spectra (inset) of DPA (black dashed line) and unknown compound (black solid line), (C) extraction modalities and (D) extraction time... 143

- Figure 67.** Chromatograms of blanks (dashed lines) and standard solution of 5 ng mL⁻¹ DPA (solid lines) obtained with different extraction solvents: water (a), 90:10 water: ethanol (b) and 90:10 water: acetonitrile (c) 144
- Figure 68.** Effect of (A) acetonitrile percentage and mobile phase flow (800 µL at 7 ng mL⁻¹, PDMS₆₅, 30 cm); (B) nature of the extractive phase (800 µL at 5 ng mL⁻¹, capillary length 30 cm, optimum mobile phase); (C) capillary length (800 µL, 5 ng mL⁻¹, PDMS₆₅, optimum mobile phase) and (D) sample volume processed (5 ng mL⁻¹, PDMS₆₅, capillary length 90 cm, optimum mobile phase) on the DPA retention in IT-SPME 145
- Figure 69.** Chromatograms obtained for sample 2A (black solid line) and blank of non-shooter hand (black dashed line). The inserts correspond to the matching of the spectra of DPA found (blue line) in reference to the library of the standard (red line) 150
- Figure 70.** Visual and microscopically (10x magnification) inspection of cotton swab after sampling a non-shooter hand (A) and after sampling a shooter hand, sample 2A (B) 152
- Figure 71.** SEM image (a) and EDX spectra of inorganic gunshot residue found on swab sample (sample 2A) after shooting (b) 153
- Figure 72.** SEM images (left) and EDX spectra (right) of spherical particles found on tapes used to collect GSR after shooting a gun: sample 21K.2 (A), sample 22K.7(B), sample 25N.4(C), sample 21K.4 (D) and sample 24 M.6 (E) 154
- Figure 73.** SEM images (left) and EDX spectra (right) of non-spherical particles found on tapes used to collect GSR after shooting a gun: sample 22K.2 (A), sample 25N.3 (B), sample 21K.1 (C), sample 25N.2 (D)..... 155
- Figure 74.** (A) SEM image, (B) overlay X-ray map of singles X-ray of Sb (C); Pb (D) and Ba (E) of particle found on a tape used to collect GSR on hands 157
- Figure 75.** Optimization of sensor composition and temperature conditions. (A) TEOS percentage: 50% (a1) 60% (a2), (B) Proportion of SiO₂NPs: 0.1% (b1) and 1% (b2), (C) NQS percentage: 0.05% (c1), 0.1% (c2), 0.2% (c3). (D) Sensor at two different temperatures: (d1) room temperature, (d2) 100 °C for 10 min. Blue columns represent the signals of blanks and red columns show the signals of the sensor with casein stock solutions 162
- Figure 76.** Sensor absorbance obtained for different amino acids at a concentration level of 0.01 M. Blue line: signal from sensor at room temperature for 18 h. Red line: sensor heated for 10 min in a water bath 163
- Figure 77.** (A) Kinetic study. Red line: blank, Blue line: signal in presence of casein 1 g L⁻¹ and (B) Optimization of the sample amount for determination of casein 164

- Figure 78.** Spectra and images of the NQS–PDMS sensors at different concentration levels of casein. (A) Blank, (B) 15 mg L⁻¹ (C) 50 mg L⁻¹, (D) 750 mg L⁻¹ and (E) 2000 mg L⁻¹ 165
- Figure 79.** Intraday precision of DR method obtained from the values of the absorbance at 590 nm for different casein concentration..... 166
- Figure 80.** Images of PDMS-NQS sensors at different concentration levels of casein, (a) Blank, (b) 15, (c) 50, (d) 750 and (e) 2000 mg L⁻¹ 169
- Figure 81.** Optimization of sensor: (A) photographs of devices without (a1, a2) and with 0.1% (w/w) NPs (a3, a4), before (left) and after (right) exposition of 1% (w/w) ADP during 20 min. Sensors prepared with PDMS/TEOS (50/50, w/w) and 0.1% (w/w) of NQS. (B) Effect of different amounts of PDMS/TEOS and NPs (containing 0.1% (w/w) of NQS). (C) Photographs of sensors with PDMS/TEOS (50/50, w/w), 0.1% (w/w) of NPs and different NQS amounts (c1, c2) 0.2 (c3, c4) 0.1, (c5, c6) 0.05% (w/w), blanks (left) and exposed to 0.5% (w/w) ADP during 5 min. (D) Effect of the NQS amount on the analytical response 172
- Figure 82.** 5x5 μm AFM topographic maps and corresponding height profiles along the marked lines: (A) Composite of 50/50 TEOS/PDMS and 0.1 % (w/w) of NPs. Color scale from 0 to 120 nm. The embedded nanoparticles are visible at the surface. (B) Composite of 50/50 TEOS/PDMS without NPs. Color scale from 0 to 10 nm; (C) SEM image of composite chosen which contains 50/50 TEOS/PDMS and 0.1 % (w/w) NPs..... 174
- Figure 83.** Variation of device response for 0.5% (w/v) of ADP as function of the reaction time. The analytical signal was obtained in DR mode at 600 nm. Devices studied had optimum composition 175
- Figure 84.** Spectra of the stability of NQS in aqueous solution over time under dark (blue lines) and light (red lines) storage. Responses are quantified as the absorbance at 380 nm of NQS 2.4 x 10⁻⁴ mol L⁻¹. Inset: Photography of responses of NQS solution against light at a) 5 min, b) 7 days, c) 0 min, d) 30 days..... 176
- Figure 85.** Microscopic photographs of (A) device of a blank, (B) device after 3 min and (C) after 6 min of 0.5 % (w/v) ADP contact at 100x magnification. 176
- Figure 86.** Stability of sensor under two storage conditions over time (sensors in the dark and exposed to light) without ADP contact. Average responses and standard deviation for n=3..... 177
- Figure 87.** (A) Stability of sensor responses under two storage conditions over time (in the dark and exposed to sunlight). Absorbance measurements of sensors just synthesized and after 8 days, 1 month and 8 months of being synthesized at 0.1 % (w/v) of ADP. Average responses and Standard deviation for n=3. (B) Stability of

colored sensor after reaction between NQS-ADP (0.1% (w/v)). Absorbance measurements correspond to sensors just colored and colored after spending 30 min, 3 and 4 months for n=8 assays. Inset: photographs of colored composites after (b1) 30 min (b2) 4 months..... 178

Figure 88. (A) Reaction scheme of ADP with NQS, together with a picture of the derivatization procedure. (B) Left: spectra of ADP response at different concentrations to get her with the photographs of sensors (b1) Blank, (b2) 0.015%, (b3) 0.05 %, (b4) 0.1%, (b5) 0.2 %, (b6) 0.5% and (b7) 1% (w/v) of ADP. Right: calibration curve and linear plot (inset) of colored sensors at 600 nm of absorbance. Stoichiometry 2:1 (NQS:ADP) 179

Figure 89. Optimization of sensor composition. (A) Effect of different weight ratios of PDMS/TEOS on the analytical response, (B) Photographic images of sensors containing 50/50 (left) and 40/60 (right) of PDMS/TEOS (w/w) exposed to AMP (b1, b2) and MAMP (b3, b4) and blanks (b5, b6) and (C) Microscopic photographs at 10x magnification obtained with for PDMS sensors (c1), PDMS/TEOS 50:50 (w/w) sensors (c2), and PDMS:TEOS 40/60 (w/w) sensors (c3). Conditions: 0.01 g mL⁻¹ of AMP and MAMP, 10 min of exposure, sensors with 0.1 % NQS and 0.1 % NPs 186

Figure 90. Absorbance at 525 for AMP and MDA (primary amines) and 600 nm for MAMP and MDMA (secondary amines) recorded against a reagent blank at different reaction times. Conditions: sensor composition of 0.1 % NQS, 0.1 % NPs, 50/50 PDMS/TEOS; analyte concentration of 0.01 g mL⁻¹..... 187

Figure 91. Photographic image of the analysis by the colorimetric kit (composed by a vial with basic buffer, NQS-polymeric sensors and powder/pill drug) for AMP (above) and MAMP (down), together with absorbance spectra at different concentrations a) blank, b) 0.005, c) 0.01, d) 0.03 and f) 0.05 g·mL⁻¹ of AMP (A) and MAMP (B). Inset: photographic image of sensors containing previous concentration levels. Optimal conditions..... 188

Figure 92. Stability of the sensors. Responses are expressed as the absorbance of sensors after their immersion into a buffer solution containing 0.01 g mL⁻¹ of MAMP or into the buffer (blanks). Average responses and standard deviation for n=3 191

Figure 93. A) Chromatograms obtained for a blank (water), a standard solution of MDMA (16.5 mg mL⁻¹), a street samples containing MDMA (S3), and samples containing mixtures of MDMA and MAMP (S4: (27.4 ± 0.6) % of MDMA and (46 ± 4) % of MAMP; S5: (65 ± 5) % of MDMA and (5.1 ± 0.2) % of MAMP; S6: (17 ± 1) %

of MDMA and (34 ± 1) % of MAMP). B) FTIR-ATR spectra obtained for a street sample (S1) and for pure MDMA 192

Figure 94. Microscopic photographs of: (A) a sensor containing 0.6 % of reagent in PDMS (w, w). (B) Sensors containing 0.3% of reagent in PDMS (w/w) during (down) reaction and 30 min after reaction (up) exposure to a blank (left) and to a solution of ketamine $25000 \mu\text{g mL}^{-1}$ (right); (C) detail of reagent particle in a sensor containing 0.3% of reagent in PDMS (w/w) (left), a sensor exposed to a blank (center) and a sensor exposed to a solution of ketamine $25000 \mu\text{g mL}^{-1}$ for 15 min (right) 197

Figure 95. Effect of the percentage of reagent in PDMS sensors on the absorbances (625 nm) for a blank and for a solution of ketamine ($700 \mu\text{g mL}^{-1}$); time of exposure, 10 min. Inset: Photographic images of sensors containing 0.3% of reagent exposed to (a) a solution of ketamine, (b) a blank; sensors containing 0.9% of reagent exposed to (c) a solution of ketamine and (d) a blank. Concentration of ketamine, $1000 \mu\text{g mL}^{-1}$; time of exposure, 10 min; time until measurement, 5 min 199

Figure 96. Effect on the absorbances measured for a blank and a solution of ketamine ($500 \mu\text{g mL}^{-1}$) of: (A) the time of reaction, and (B) the time elapsed between reaction and measurement. In (A) the absorbance was measured immediately after the removal of the sensor from the sample; in (B) the reaction time was of 10 min. The conditions selected as optima were: reaction time, 10 min; time until absorbance measurement, 5 min 201

Figure 97. Results obtained for sample S1: (A) sensor absorbance spectra registered for a blank, for a standard solution of ketamine ($500 \mu\text{g mL}^{-1}$) and for the sample solution; insert: sensor images obtained for a blank and for the sample solution; (B) FTIR-ATR spectra obtained for the sample, pure ketamine and pure caffeine; (C) left: chromatograms obtained for a standard solution of ketamine ($50 \mu\text{g mL}^{-1}$) and for the sample solution; right: normalized spectra of ketamine and suspected ketamine in the sample. The sample solution in (C) was a dilution 1:10 of the sample in (A) 204

Figure 98. Chromatograms obtained for aqueous solutions and for hair samples treated by the ultrasound-assisted alkaline digestion method: (a) blank (water), (b) blank hair, (c) an standard solution of the amphetamines ($0.5 \mu\text{g mL}^{-1}$, each compound), and (d) a spiked hair sample (25 ng mg^{-1} , each compound) 209

Figure 99. Photographs of: (a) a hair sample (25 mg), (b) the blend obtained after grinding the sample with 400 mg of the C_{18} phase, and (c) the blend transferred to an extraction tube 212

- Figure 100.** Photographs obtained with the optical microscope of: (a) C_{18} sorbent ground for 5 min, (b) a hair sample, and (c) the blend obtained after grinding the sample and the C_{18} dispersant for 5 min. Ratio sample to dispersant, 1:16..... 212
- Figure 101.** Chromatograms obtained for hair samples spiked with the analytes (25 ng mg^{-1}) treated by MSPD/solution derivatization method using in the washing step: (a) 2.0 mL of water, (b) 2.0 mL of carbonate buffer, and (c) 4.0 mL of carbonate buffer as washing solvents. 213
- Figure 102.** Effect of the derivatization conditions on the analyte responses obtained with the integrated MSPD/solid support derivatization method: (a) reaction time, (b) pH of the buffer, and (c) concentration of the Fmoc solution. Tested for a sample containing 20 ng mg^{-1} of each analyte..... 215
- Figure 103.** Chromatograms obtained by the three approaches tested: (a) hair sample spiked with 100 ng mg^{-1} of each analyte treated by the ultrasound-assisted alkaline digestion/solution derivatization method, (b) hair sample spiked with 25 ng mg^{-1} of each analyte treated by the MSPD/solution derivatization method, and (c) hair sample spiked with 10 ng mg^{-1} of each analyte treated by the integrated MSPD/solid phase derivatization method..... 216
- Figure 104.** Chromatograms obtained with the integrated MSPD/solid support derivatization method for: drug-free hair sample (a), and for hair samples spiked to contain the analytes at concentrations of (b) 2 ng mg^{-1} , (c) 10 ng mg^{-1} and (d) 20 ng mg^{-1} 217
- Figure 105.** Chromatograms obtained for: (A) a real hair sample positive for MAMP and for a blank hair sample spiked with 2 ng mg^{-1} of each analyte, and (B) the real hair sample and the same sample fortified with 20 ng mg^{-1} of each analyte; the dark zones in (b) indicate the elution windows for the target compounds 220
- Figure 106.** Design of disk fabricated in this work..... 223
- Figure 107.** Fabrication steps of disk A) screen-printing of sacrificial layer, B) screen-printing of bottom gold electrode, C) Screen-printing of PZT layer, D) Screen-printing of top gold electrode E) Sacrificial layer elimination after firing, F) Poling of PZT wired disk (cross view), together with photographs of the top view of the disk step by step..... 224
- Figure 108.** Microscopic images at x6 of top view of disk before (A) and after firing (B), aligned disk before (C) and after firing (D). Disks fabricated with formula reported in (Debéda, H. et al., 2013) 225
- Figure 109.** Real photographs and scheme of the top view of fabrication steps of the cantilevers A) Screen-printing of anchor pad B) Screen-printing of the sacrificial layer C) Screen-printing of the bottom gold electrode D) Screen-printing of the

cantilever E) Screen printing of the top gold electrode, F) Sacrificial layer elimination after firing G) Poling of wired cantilever with the cross view	226
Figure 110. A) Design of the cantilever, B) Photography of cantilever before firing and C) Photography of cantilever after firing, fabricated in this work on Al ₂ O ₃ substrate	227
Figure 111. Pictures of thickness profile before firing of A) PZT anchor-Sacrificial layers on Al ₂ O ₃ with different print gap of anchor, B) Different print order of anchor and sacrificial layer	229
Figure 112. Microscopic images of A,B) first layer of bottom gold electrode, C,D) cantilevers before firing. Left: green dielectric anchor on AlN, Right: PZT anchor on Al ₂ O ₃	230
Figure 113. Optical microscope pictures of cantilevers after firing on Al ₂ O ₃ (A) and AlN (B)	231
Figure 114. 3D profile analysis of the cross-section axis of A) Disks (two formulas) and B) Cantilever (first batch) with formula A (Debéda, H. et al., 2013), before firing.....	231
Figure 115. Graphic of A) Conductance, B) Z , C) Susceptance and D) Impedance phase measurements of disks fabricated with two formulas A (Debéda,H. et al., 2013) and B (Medesi, A. et al., 2014) and commercial disk.....	232
Figure 116. Equations used for the calculation of K_{eff} and Q_{mv} where f_m is the frequency at the minimum impedance (Z), f_M is the frequency at the maximum impedance, f_r is the resonance frequency at G maximum, $\Delta f = f_2 - f_1$ is the width of peak, where f_1 is the frequency at the maximum B and f_2 is the frequency at the minimum B.....	233
Figure 117. Microscopic photography of the functionalized cantilever by MCF mesoporous silica.....	234
Figure 118. A) Spectrum of the conductance for the first longitudinal mode before and after deposition of mesoporous silica layer and B) Relative resonant frequency shifts as a function of humidity.....	235
Figure 119. Chromatograms obtained for a standard solution containing AMP, MAMP and EP (8.0 $\mu\text{g mL}^{-1}$, each) using a percentage of acetonitrile in the mobile phase of: (A) 50 % and (B) 70 %, using an unmodified PDMS ₆₅ extractive capillary (30 cm length) for IT-SPME	248
Figure 120. Chromatograms obtained for a standard solution containing AMP, MAMP and EP (8 $\mu\text{g mL}^{-1}$, each) with PDMS ₆₅ extractive capillaries of different length	239

- Figure 121.** Peak areas obtained for a standard solution of the amphetamines tested ($8 \mu\text{g mL}^{-1}$, each) with different extractive capillaries: unmodified PDMS₉₅ (36 cm), unmodified PDMS₆₅ (40 cm), c-SWCNTs functionalized PDMS₉₅ (36 cm), c-SWCNTs functionalized PDMS₆₅ (40 cm) and c-MWCNTs functionalized PDMS₆₅ (40 cm) 240
- Figure 122.** Chromatograms obtained for a standard solution of the amphetamines tested ($8 \mu\text{g mL}^{-1}$ each) with the unmodified PDMS₉₅ and the c-SWCNTs functionalized PDMS₉₅ capillaries 241
- Figure 123.** Chromatograms obtained for a standard solution of the amphetamines tested ($8 \mu\text{g mL}^{-1}$ each) with the unmodified PDMS₆₅ and the c-MWCNTs functionalized PDMS₆₅ capillaries 242
- Figure 124.** Chromatograms obtained for a standard solution of the amphetamines tested ($8 \mu\text{g mL}^{-1}$, each) with the c-SWCNTs and the c-MWCNTs functionalized PDMS₆₅ capillaries 243
- Figure 125.** Peak areas obtained for different concentrations of the amphetamines tested within the $2\text{--}10 \mu\text{g mL}^{-1}$ concentration range with different extractive capillaries 244
- Figure 126.** Scheme of the extraction/derivatization IT-SPME CapLC method used for the analysis of amphetamines in oral fluid. The extractive capillary was a c-MWCNT functionalized PDMS₆₅ capillary (40 cm length) 257
- Figure 127.** (a) Chromatograms obtained for the reaction mixture (250 μL of buffer and 250 μL of 0.1 mM FMOC), (b) the same reaction mixture after the introduction of a cotton swab for 5 min, and (c) after the introduction of a cotton swab impregnated with 125 μL of a standard solution of EP ($2 \mu\text{g mL}^{-1}$). For IT-SPME a c-MWCNTs functionalized PDMS₆₅ capillary (40 cm length) was used 248
- Figure 128.** Chromatograms obtained with the proposed extraction/derivatization IT-SPME CapLC method for an oral fluid sample, and the same sample spiked with the tested amphetamines ($8 \mu\text{g mL}^{-1}$, each) 249
- Figure 129.** Glycyl-L-histidylglycine (GHG) 253
- Figure 130.** Microscope (left) and SEM images (right) of as-made crystals of Cu(GHG) at an accelerating voltage of 20 keV 253
- Figure 131.** (A) Structure of helicoidal chains in Cu(GHG) MOF, (B) Functional groups in the peptidic backbone decorating the surface of the pores, (C) 1D channels in Cu(GHG) are surrounded by functional sites prone to establish supramolecular interactions 254
- Figure 132.** Representative MC binding geometries of (+,-) MAMP and EP enantiomers within the structure of Cu(GHG) and corresponding adsorption

- energies as absolute values calculated with respect to gas phase. Most relevant H-bonds in directing guest binding are annotated in each case. 255
- Figure 133.** Evolution of the enantioselective recognition of Cu(GHG) for chiral drugs in ethanol:water 75:25 solution with contact time for (A) MAMP and (B) EP. Chiral adsorption was evaluated from chromatographic analysis of the supernatant solution..... 257
- Figure 134.** Control experiment to confirm the observed chiral recognition is specific to the MOF architecture rather than to any of its components. Below chromatograms for a physical mixture of GHG and Cu(II) acetate in the same proportion present in the MOF. Evolution of the peak areas for (+) and (-)-MAMP in a solution of the MOF components rules out measureable enantioselective recognition of any of the enantiomers. Inset in the right column highlights the signal specific to each enantiomer..... 259
- Figure 135.** Time evolution of the UV-Vis spectra at room temperature of a dispersion of as-made 50 mg of Cu(GHG) in 500 μ L of EtOH:H₂O (25:75 v%) from 0 to 240 min. This set of conditions are equivalent to those used for studying the ability of Cu(GHG) to recognize selectively enantiomers from solution. The system remains constant and no signature of Cu(II) leaching –broad absorption band centered at 600 nm- can be observed, confirming the chemical integrity of the solid in these conditions..... 260
- Figure 136.** (A) SPE separation of EP in hexane:EtOH 75:25 by using Cu(GHG) as chiral bed. (B) HPLC chromatograms of EP racemate before (dashed line) and after (solid line) passing through the MOF bed..... 261
- Figure 137.** Comparison of HPLC chromatograms of a racemic mixture of (\pm)-EP in Hexane:EtOH 75:25 after passing through the MOF SPE cartridge (black line, adsorption) and after elution with fresh solvent (desorption). The presence of (-)-EP in the desorbed fraction is negligible whilst only (+)-EP can be detected in the chromatogram in good agreement with the reported enantioselectivity 262
- Figure 138.** Control experiment by soaking as-made crystals of CuGHG in a racemic mixture of (\pm)-EP in hexane:EtOH 75:25. (A) Evolution of the peak areas for (-) and (+)-EP. Adsorption of (-)-EP can be considered negligible whilst close to 44% of (+)-EP is preferentially adsorbed. (B) HPLC chromatograms of EP racemic solution in contact with the MOF before (0 min) and after 4 minutes 263
- Figure 139.** SEM pictures of Cu(GHG) before (A) and after (B) SPE separation at an accelerating voltage of 20 keV. Crystals were metalized with a mixture of gold and palladium during 30 s..... 263

- Figure 140.** Absorption spectra of A, B) AuNP 20 nm in solution and C, D) AgNP 20 nm in solution after addition of A, C) Na_2S and B, D) CH_3SH in a range between 250 - 10000 $\mu\text{g L}^{-1}$ 269
- Figure 141.** Schematic drawing of the A) AgNP aggregation and B) AuNPs functionalization by sulphur compound..... 270
- Figure 142.** Microscopic images of different kinds of support for AgNP immobilization A) nylon, B) cellulose, C) glass fiber. The scale bar is 100 μm and inset c is 20 μm . Absorbance by DR of the AgNPs immobilized on D) nylon, E) cellulose, F) glass fiber and their response in presence of volatile H_2S (250 and 1000 ppb). Inset AgNPs immobilized on the membrane and the response at 1000 $\mu\text{L m}^{-3}$ 268
- Figure 143.** Raman spectra of a) nylon, b) AgNP-nylon and device response to sulphur compounds in c) 250, d) 500, e) 1000, f) 10000 $\mu\text{L m}^{-3}$ levels. 269
- Figure 144.** Absorption spectra of AgNPs of 20 nm (A), 40 nm (B) and 10 nm (C) after addition of Na_2S concentrations. Inset: plot of corresponding absorbance ratios vs $\log [\text{S}^2]$ 270
- Figure 145.** Photography of sensors and calibration curve by plotting A_{550}/A_{415} ratio vs logarithm of H_2S concentrations of 0 (a), 150 (b), 250 (c), 500 (d), 1000 (e), 1500 (f) and 2500 (g) $\mu\text{L m}^{-3}$ 271
- Figure 146.** A) Sulphur concentration found in A) 10 healthy volunteers using AgNPs-based sensor and B) 4 volunteers before (blue bars) and after garlic consumption (orange bars)..... 273

A3. Table List

A3. TABLE LIST







Table 1. Operative values for IT-SPME-CapLC and IT-SPME-NanoLC	15
Table 2. Summary of applications of IT-SPME described in the literature between 2013-2018	16-17
Table 3. Summary of analytical parameters (precision, LODs and recoveries) for different applications of IT- SPME.....	19
Table 4. Summary of in-situ sensors described in the literature between the years 2013-2018	20-21
Table 5. Summary of characteristics of some current methods for in situ analysis	23
Table 6. Features of different type of solid supports	28
Table 7. Summary of cantilever resonant modes in terms of the simple harmonic oscillator model, where L is the length, t is the thickness, E is the Young's modulus, w is the width, λ_n is the eigenvalue (n is a positive integer) and m is the cantilever mass	32
Table 8. Summary of resonant microcantilevers coated with different sensitive layers reported.....	35
Table 9. Examples of PDMS-based colorimetric sensors reported in the literature between 2010-2018	38
Table 10. Characteristics of SBA-15, MCM-41 and MCF-types mesoporous silica. MCM: Mobile Composition of Matter, SBA: Santa Barbara Amorphous, MCF: Mesoporous Cellular Foam (Beck, J. S. et al., 1992; Kruk, M. et al., 2000; Selvam, P. et al., 2001)	41
Table 11. Selected examples of plasmonic assays.....	47
Table 12. Summary of reagents and chemicals used in this Thesis, with their suppliers and GHS pictograms, where  = Flammable (GHS02);  = Corrosive (GHS05);  = Toxic (GHS06);  =Harmful (GHS07);  =Health hazard (GHS08);  = Environmental hazard (GHS09).....	79-81
Table 13. Spectrometric techniques and experimental details used in the present Thesis.....	85-86
Table 14. Summary of the chromatographic techniques used in this Thesis.....	90
Table 15. Composition, size and curing time of the developed sensors. Optimum sensor highlighted in blue	97
Table 16. Compositions of the different PDMS- Co(SCN) ₂ tested sensors.....	99
Table 17. Summary of materials and screen characteristics used to fabricate disks and cantilevers.....	103

Table 18. Main characteristics of the chromatographic works described in this Thesis.....	107
Table 19. Conditions for derivatization procedures of this Thesis	110
Table 20. Experimental conditions used in several works of this Thesis based on polymeric sensors.....	110
Table 21. Samples per analytes studied	118
Table 22. Some figures of merit to detect DEHP in sediments by MSPD and IT-SPME-CapLC-DAD.....	124
Table 23. Comparison of the composition of the three kind of sediment assayed according to size of particle after sieving	126
Table 24. Precision and addition curves of BAK in presence of ADP from the raw material LONZABAC and from DECTOCIDE with the two chromatographic columns tested	132
Table 25. Mixtures of BAK and ADP or TMTDAC	134
Table 26. Characteristics of capillary columns employed in IT-SPME.....	146
Table 27. Analytical data for DPA determination by IT-SPME-CapLC-DAD; a : ordinate, b : slope, s_a and s_b : standard deviation of the ordinate and slope, respectively, R^2 : determination coefficient.....	149
Table 28. Samples and quantification results from hands determined by optimized extraction procedure followed by in-tube SPME-CapLC-DAD. *tape lift kit samples quantified by regression equation 14 times lower than regression equation by cotton swab.....	151
Table 29. Summary of shape, surface and elemental composition of GRS particles founded on tape lift kit from shooter hands	156
Table 30. Analytical parameters obtained for casein determination in dairy sewages by the three methods assayed	167
Table 31. Found concentrations of casein mg L^{-1} obtained by the three quantification methods (bichinonic acid assay, and the two methods of measurement for the colorimetric sensor (GIMP and diffuse reflection) in different samples	169
Table 32. Figures of merits obtained with the different measure approaches for the ADP determination with the proposed NQS-sensor, and comparison with the figures of merit obtained with C_{18} -solid-support derivatization	181
Table 33. Concentration of ADP found in the analysed samples obtained with the NQS-sensor by DR and DI. Comparison with the results obtained with C_{18} Solid-Support derivatization.....	182

Table 34. Comparison of different properties of the procedures assayed. More +: better option	183
Table 35. Analytical data for the determination of AMP, MAMP, MDA and MDMA by using diffuse reflectance values. Absorbances measured at 525 nm and 600 nm for secondary and primary amines, respectively, in DR mode. Concentrations expresses in g mL^{-1}	189
Table 36. Analytical data for the determination of AMP, MAMP, MDA and MDMA by using color intensity of the DI. Concentrations expresses in g mL^{-1}	189
Table 37. Composition of the ecstasy street samples obtained by the sensor-based approaches and by the LC reference method. (*) Sum of the percentages of MDMA and MAMP expressed as MDMA	194
Table 38. Analytical data obtained by using the developed sensors.....	202
Table 39. Comparison of the results obtained for the drug street samples with the developed sensors and the LC reference method ($n = 3$)	205
Table 40. Analytical parameters of the methods tested	210
Table 41. Accuracy and precision of the proposed integrated MSPD/solid phase derivatization method.....	218
Table 42. Weight percentages and mass of each component in 40 g of piezoelectric powder	222
Table 43. Thickness measurements of anchor and sacrificial layers for cantilever fabrication. On average of 200 μm was employed for each measurement by the profilometer	228
Table 44. Comparison of K_{eff}	233
Table 45. Preconcentration rates (PRs) values found for the extractive capillaries tested	240
Table 46. Response vs concentration linearity data	245
Table 47. Linearity and reproducibility achieved with the proposed extraction-derivatization-IT-SPME-CapLC method for AMP, MAMP and EP within the 1–10 $\mu\text{g mL}^{-1}$ (2–10 $\mu\text{g mL}^{-1}$ for EP) concentration interval (values obtained with the c-MWCNTs coated PDMS ₆₅ capillary of 40 cm length)	246
Table 48. Summary of binding energies and H-bond lengths for MAMP-MOF interactions as estimated by quantum-chemistry calculations	256
Table 49. Experimental data used for calculation of enantioselective recognition capability of Cu(GHG).....	258
Table 50. Cartridge to cartridge precision	262
Table 51. Analytical parameters obtained for H ₂ S determination by AgNPs-nylon based sensor proposed.....	272

Table 52. Recoveries of 2 spiked samples of healthy volunteers obtained by using DR and DI 274

Table 53. Summary of the application and results obtained in this Thesis for the materials used..... 283

A4. PhD contributions to publications

1. M. Muñoz-Ortuño, **A. Argente-García**, Y. Moliner-Martínez, J. Verdú-Andrés, R. Herráez-Hernández, M.T. Picher, P. Campíns-Falcó, *A cost-effective method for estimating di (2-ethylhexyl) phthalate in sediments*, Journal of Chromatography A. 1324 (2014) 57-62. Impact factor (JCR 2018): 3.981. **Contribution 50%**
2. M. Muñoz-Ortuño, **A. Argente-García**, Y. Moliner-Martínez, C. Molins-Legua, P. Campíns-Falcó, *Polydimethylsiloxane composites containing 1,2-naphthoquinone 4-sulphonate as unique dispositive for estimation of casein in effluents from dairy industries*, Analytica Chimica Acta. 873 (2015) 31-37. Impact factor (JCR 2018): 4.950. **Contribution 50%**.
3. **A. Argente-García**, M. Muñoz-Ortuño, C. Molins-Legua, Y. Moliner-Martínez, P. Campíns-Falcó, *A solid device based on doped hybrid composites for controlling the dosage of the biocide N-(3-aminopropyl)-N-dodecyl-1,3-propanediamine in industrial formulations*, Talanta. 147 (2016) 147-154. Impact factor (JCR 2018): 4.162. **Contribution 100%**.
4. M.C. Prieto-Blanco, **A. Argente-García**, P. Campíns-Falcó, *A capillary liquid chromatography method for benzalkonium chloride determination as a component or contaminant in mixtures of biocides*, Journal of Chromatography A, 1431 (2016) 176-183. Impact factor (JCR 2018): 3.981.
5. **Argente-García**, Y. Moliner-Martínez, E. López-García, P. Campíns-Falcó, R. Herráez-Hernández, *Application of Carbon Nanotubes Modified Coatings for the Determination of Amphetamines by In-Tube Solid-Phase Microextraction and Capillary Liquid Chromatography*, Chromatography, 3 (2016) 7-21. **Contribution 100%**.
6. **Argente-García**, Y. Moliner-Martínez, P. Campíns-Falcó, J. Verdú-Andrés, R. Herráez-Hernández, *Determination of amphetamines in hair by integrating sample disruption, clean-up and solid phase derivatization*, Journal of Chromatography A. 1447 (2016) 47-56. Impact factor (JCR 2018): 3.981. **Contribution 100%**.
7. **Argente-García**, N. Jornet-Martínez, C. Molins-Legua, Y. Moliner-Martínez, P. Campíns-Falcó, *A solid colorimetric sensor for the analysis of amphetamine-like street samples*, Analytica Chimica Acta. 943 (2016) 123-130. Impact factor (JCR 2018): 4.950. **Contribution 100%**.
8. J. Navarro-Sánchez, **A. Argente-García**, Y. Moliner-Martínez, D. Roca-Sanjuán, Dmytro Antypov, P. Campíns-Falcó, Matthew J. Rosseinsky, C. Martí-Gastaldo, *Peptide Metal–Organic Framework for Enantioselective*

- Separation of Chiral Drugs*, Journal of the American Chemical Society. 139 (2017) 4292-4297. Impact factor (JCR 2018): 13.858. **Contribution 50%.**
9. **Argente-García**, N. Jornet-Martínez, R. Herráez-Hernández, P. Campíns-Falcó, *A passive solid sensor for in-situ colorimetric estimation of the presence of ketamine in illicit drug samples*, Sensors and Actuators B. 253 (2017) 1137-1144. Impact factor (JCR 2018): 5.401. **Contribution 100%.**
 10. **Argente-García**, L. Hakobyan, C. Guillem, P. Campíns-Falcó, *A new method for estimating diphenylamine in gunshot residues as a new tool for identifying both, inorganic and organic ones, in the same sample*. Submitted. **Contribution 50%.**
 11. Y. Moliner-Martínez, **A. Argente-García**, R. Herráez-Hernández, J. Verdú-Andrés, C. Molins-Legua, P. Campíns-Falcó, *Environmental Applications of Instrumental Chemical Analysis, Determination of organic pollutants in environmental samples*, Part II, **Chapter 14**, Mahmood Barbuooti. Apple Academic Press. CRCpress, a Taylor & Francis Group, 471-532, 2015, ISBN 9781771880619. **Contribution 100%.**
 12. **Argente-García**, N. Jornet-Martínez, C. Molins-Legua, Y. Moliner-Martínez, J. Verdú-Andrés, R. Herráez-Hernández, P. Campíns-Falcó, *Sensor colorimétrico basado en nanopartículas de plata para la determinación de compuestos volátiles de sulfuro*, **Patent 201600440**, Presentation data: 24/05/2016. **Contribution 100%.**

